## Targeted epigenetic therapy in inflammatory bowel disease

Elfiky, A.M.I.M.

**Publication date**
2023
**Document Version**
Final published version

# Targeted Epigenetic Therapy in Inflammatory Bowel Disease

Ahmed Elfiky

# Targeted Epigenetic Therapy in Inflammatory Bowel Disease

Ahmed Elfiky

Cover idea and design:

Lay-out and thesis printing: Proefschrift-AIO.nl

ISBN: 978-94-93353-19-0

# Targeted Epigenetic Therapy in Inflammatory Bowel Disease

ACADEMISCH PROEFSCHRIFT

ter verkrijging van de graad van doctor
aan de Universiteit van Amsterdam
op gezag van de Rector Magnificus
prof. dr. ir. P. P. C. C. Verbeek
ten overstaan van een door het College voor
Promoties ingestelde commissie, in
het openbaar te verdedigen
in de Aula der Universiteit

op vrijdag 13 oktober 2023, te 11.00 uur

door

**Ahmed Mohamed Ibrahim Metwalli Elfiky**
geboren te Gharbeya

***Promotiecommissie***

| | | |
|---|---|---|
| **Promotor:** | prof. dr. W.J. de Jonge | AMC-UvA |
| **Copromotores:** | dr. M.J. Bell | GlaxoSmithKline |
| | dr. S.E.M. Heinsbroek | AMC-UvA |
| **Overige leden:** | prof. dr. M.P.J. de Winther | AMC-UvA |
| | dr. J.E.J. Guikema | AMC-UvA |
| | prof. dr. R.P.J. Oude Elferink | AMC-UvA |
| | prof. dr. P.J. Verschure | Universiteit van Amsterdam |
| | prof. dr. F. van Wijk | Universiteit Utrecht |

Faculteit der Geneeskunde

# Table of contents

## Thesis Outline

Despite the availability of multiple therapeutic options for inflammatory bowel disease (IBD), non-responsiveness remains a significant issue, highlighting the need for new therapies. In the current dissertation, we explore the potential of epigenetic medicines in IBD. The first wave of epigenetic drugs lack specificity and have wide range of toxicities that limit clinical translation of their potent anti-inflammatory properties. Therefore more selective epigenetic therapies are required.

**In chapter 1**, we summarize the recent advances of developing new targeted epigenetic therapies that tackle the problem of specificity and improve the safety profile of targeting epigenetics. We reviewed endeavours to develop class-, isoform- and domain-specific histone deacetylases (HDAC) and bromodomain containing proteins (BCPs) inhibitors, along with drug design technologies for cell specific targeting. We highlighted the promises and limitations of these strategies in inflammation mediated diseases, including IBD. **In chapters 2 and 3**, we investigated the potentials of specific targeting of mononuclear myeloid cells (MMCs) using esterase sensitive motif (ESM) tagged HDAC and BET inhibitors in both *in vitro* and *in vivo* models. This technology allows ESM-tagged compounds to be retained in CES1 enzyme expressing cells. We explored the CES1 expression in IBD patients and demonstrated exclusive expression in MMCs in peripheral blood and locally inflamed intestinal tissues and highlighted enrichment of CES1-expressing MMCs in inflamed tissue environment. We demonstrated specific accumulation of ESM-HDAC528 in monocytes and macrophages, along with augmented anti-inflammatory potency. We showed efficacy of ESM-HDAC528 in preclinical murine models of IBD. Similarly, we demonstrated enhanced anti-inflammatory potency of ESM-iBET in monocytes and highlighted multiple IBD relevant inflammatory pathways targeted by ESM-iBET in monocytes. **In chapter 4**, we pinpointed an overlooked role of CES1 enzyme in modulating DCs phenotype and inflammatory response. CES1 inhibition promoted a more inflammatory dendritic cell (DCs) phenotype, with stronger phagocytic capacity and Th17 induction, meanwhile, transgenic human CES1 overexpression was associated with attenuated DCs inflammatory response and conferred protection against colitis development in T cell colitis model. We further characterized the underlying metabolomics and functional metabolic changes upon CES1 inhibition in DCs. **In chapter 5**, we explored the potential of a newly developed domain-specific BET inhibitor (GSK620), that selectively targets bromodomain 2 (BD2), a recently identified inflammation specific target. We demonstrated a modest clinical efficacy of both pan-BET and BD2-specific inhibitors in T cell transfer colitis model, with sustained intestinal inflammation despite markedly reduced systemic

inflammation. In **chapter 6**, we made use of single cells omics technologies to explore determinants of response/non-response to vedolizumab, a clinically available IBD biologic that targets α4β7 integrin. We identified altered peripheral blood myeloid cells compartment in response to vedolizumab, with a significant reduction of circulating plasmacytoid DCs and altered classical monocytes phenotype. In this study, we highlighted the potential of single cells omics to explore responsiveness to the currently available and upcoming IBD therapies for better personalized medicine practice.

Collectively, this thesis highlights the potential of the newly developed targeted epigenetic medicines in IBD. These novel therapeutic strategies of targeting the immune epigenome tackle the tolerability issues observed with earlier generations of epigenetic medicines and therefore help to translate their potent anti-inflammatory properties into a safer and effective drug options. These provide a novel therapeutic avenues to the IBD treatment landscape that faces a lot of challenges with high nonresponsive rates to current medications.

# 1

# Chapter 1

## General Introduction

**Selective Targeting of Epigenetic Readers and Histone Deacetylases in Autoimmune and Inflammatory Diseases: Recent Advances and Future Perspectives**

Mohammed Ghiboub[†], **Ahmed M. I. Elfiky**[†], Menno P. J. de Winther, Nicola R. Harker, David F. Tough and Wouter J. de Jonge

[†] Equally Contributing First authors

Journal of Personalized Medicine, 2021.

## Abstract

Histone deacetylases (HDACs) and bromodomain-containing proteins (BCPs) play a key role in chromatin remodeling. Based on their ability to regulate inducible gene expression in the context of inflammation and cancer, HDACs and BCPs have been the focus of drug discovery efforts, and numerous small-molecule inhibitors have been developed. However, dose-limiting toxicities of the first generation of inhibitors, which typically target multiple HDACs or BCPs, have limited translation to the clinic. Over the last decade, an increasing effort has been dedicated to designing class-, isoform-, or domain-specific HDAC or BCP inhibitors, as well as developing strategies for cell-specific targeted drug delivery. Selective inhibition of the epigenetic modulators is helping to elucidate the functions of individual epigenetic proteins and has the potential to yield better and safer therapeutic strategies. In accordance with this idea, several in vitro and in vivo studies have reported the ability of more selective HDAC/BCP inhibitors to recapitulate the beneficial effects of pan-inhibitors with less unwanted adverse events. In this review, we summarize the most recent advances with these strategies, discussing advantages and limitations of these approaches as well as some therapeutic perspectives, focusing on autoimmune and inflammatory diseases.


**Keywords:** epigenetics; histone deacetylases; bromodomain; inhibitor; esterase sensitive motif; autoimmune and inflammatory diseases

# Introduction

The human immune system requires complex mechanisms of regulation to avoid the induction of inappropriate responses, and defects in this regulation result in inflammatory and autoimmune diseases [1,2]. Epigenetics refers to mechanisms that modify cellular and organismal phenotypes without altering the DNA sequence and are linked to modified patterns of gene expression [3]. The critical role of epigenetic mechanisms in regulating gene expression in the immune system is well established, and the dysregulation of epigenetic control contributes to the development of a variety of human diseases [4,5]. Three main mechanisms are commonly ascribed to contribute to epigenetic regulation: [1] RNA interference via noncoding RNAs that modify mRNA translation; [2] DNA methylation, and [3] histone post-translational modification [6–8]. All of them can modify the structure of chromatin—the ordered structure of DNA and histones—and ultimately the accessibility of DNA to the transcriptional machinery [6–8].

Histones are modified in a dynamic way by enzymes that add or erase a wide range of post-translational modifications, including acetyl or methyl groups, to a variety of different amino acids [9]. These modifications can directly affect the interaction between histones and DNA—for example, by changing the charge of the histone—and can also serve as recognition marks for epigenetic "reader" proteins; both of these processes alter DNA accessibility to transcription factors (TFs) (**Figure. 1**) [9]. Enzymes that add or remove histone marks have been referred to as epigenetic "writers" or "erasers", respectively [9]. Among the wide diversity of possible epigenetic targets, this review will focus on histone deacetylase (HDAC) enzymes and bromodomain (BD)-containing proteins (BCPs), remodelers of histone tails, which play a central role in regulating inducible gene expression involved in immune response [10,11]. HDAC enzymes are examples of epigenetic erasers that remove an acetyl group from histone tails, which then limits the accessibility to DNA at these sites [12]. BCPs are a large family of epigenetic readers that can bind acetylated histones to facilitate recruitment and interactions of TFs [13]. The most extensively studied families of BCPs are BD and extra-terminal domain (BET) proteins, consisting of four individual proteins: BRD2, BRD3, BRD4, and BRDT [14].

Numerous small-molecule inhibitors targeting these proteins have been developed based on preclinical work, suggesting the potential to achieve therapeutic benefit in various human disorders [15,16]. Because of their reported strong anti-proliferative and anti-oncogenic properties, several inhibitors of these epigenetic targets have been investigated in cancer clinical trials, with some HDAC inhibitors FDA approved

for certain malignancies [17]. In addition, HDAC inhibitors (HDACi) and BET protein inhibitors (I-BET) have shown strong efficacy in preclinical models of several inflammatory and autoimmune diseases, such as models of inflammatory bowel disease (IBD) and rheumatoid arthritis (RA) [18–26]. Although several epigenetic inhibitors are being investigated in human trials, relatively few have progressed into clinical practice and thus far exclusively in the cancer field, largely due to the toxicity profile of these compounds [17,27]. Since these first-generation inhibitors typically target multiple members of the HDAC or BET family, unwanted effects may be linked to a broad impact on transcriptional activity that extends to off-target pathways [28,29].

Recently, increasing effort has been dedicated to developing inhibitors that can achieve a higher degree of selectivity in targeting the epigenetic modulators, which may alleviate safety issues that hold back their translation into clinical use [30,31]. Different strategies are being adopted to tackle this challenge: (1) designing isoform-specific or domain-specific inhibitors that can target only single proteins or individual domains in multi-domain proteins; (2) developing a targeted approach that can selectively deliver the drug to the relevant proinflammatory cell types that fuel the inflammation in the disease of interest [32]. In this review, we gather the most recent updates regarding these different strategies and we discuss their potential in paving the way towards the next wave of epigenetic drugs, focusing on inflammatory and autoimmune diseases.

## Methods

To give an overview of existing selective small-molecule inhibitors targeting HDACs and BCPs and gather the most relevant advances in this direction with focus on their use in inflammatory and autoimmune disease models, we performed a literature review in Medline (PubMed) using "HDAC", "bromodomain"," inhibitor", "selective", "isoform", "class", '' esterase sensitive motif" ''autoimmune diseases", and ''inflammatory diseases" as keywords. Reference lists of existing (systematic) reviews of this topic were searched for additional relevant literature. All included articles were in English. There were no specific inclusion or exclusion criteria for this review. The most referenced articles were selected and are described in the review, with an overview of study characteristics and results shown in **Table 1**. The figure illustrations were created in BioRender.com.

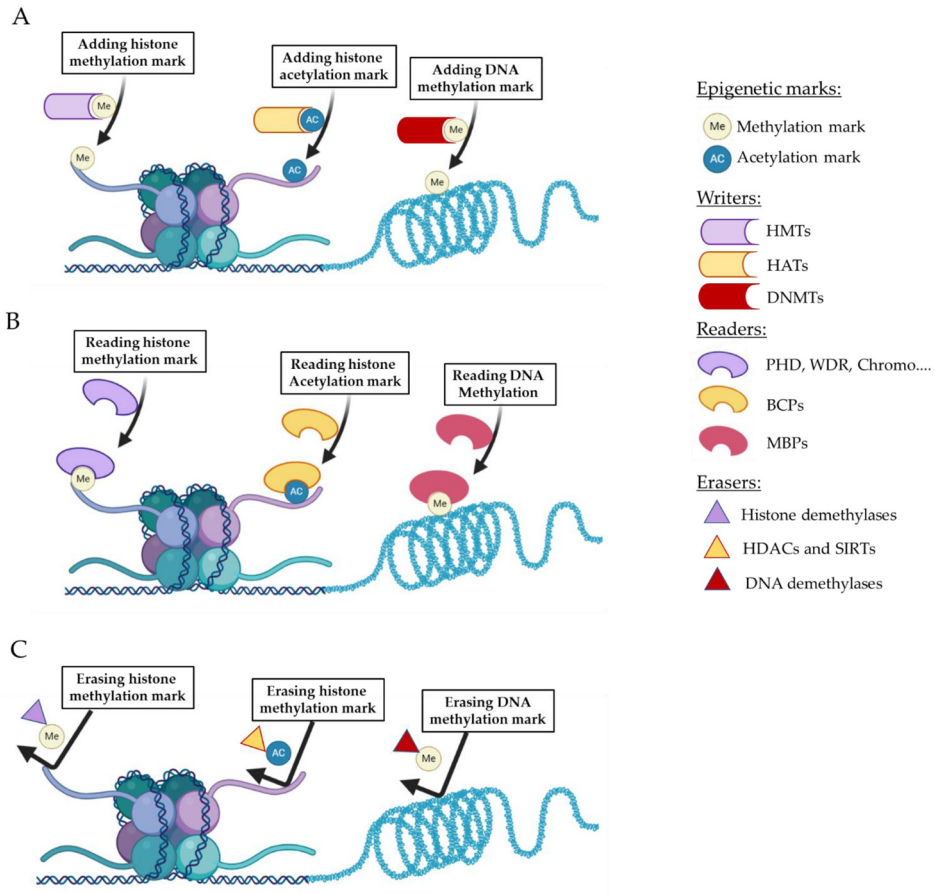


**Figure 1. DNA methylation and histone modifications.** Post-translational modifications of histones and DNA methylation provide a fine-tuned mechanism for regulating chromatin structure and dynamics. Panel (**A**) depicts methylation and acetylation of histone tails that involve the addition of methyl group (Me) and acetyl group (AC), respectively. These processes are catalyzed by the epigenetic writers; histone methyl transferases (HMTs) and histone acetylases (HATs), respectively. DNA methylation is catalyzed by the epigenetic writers DNA methyltransferases (DNMTs), including DNMT1, DNMT3a, and DNMT3b, which add a methyl group on to the 5-carbon of the cytosine ring. Panel (**B**) illustrates examples of epigenetic readers that possess specialized domains that recognize specific covalent histone or DNA modifications and respond to upstream signals. Such crosstalk generates a different binding platform for the recruitment of other regulatory proteins, ultimately controlling the chromatin accessibility to transcription factors and gene transcription, such as plant homeodomain (PHD), WD40-repeat (WDR) proteins, and chromo domains that recognize histone methylation marks, bromodomian-containing proteins (BCPs) that recognize histone acetylation marks, and the methyl-CpG-binding proteins (MBPs) that recognize methylation of DNA. Panel (**C**) shows examples of epigenetic eraser proteins that can remove modifications from DNA or histones to regulate gene expression.

## Advances in HDAC Selective Targeting in Autoimmune and Inflammatory Diseases

In humans, the HDAC enzymes family comprises 18 members divided into 4 classes: class I HDACs (HDACs 1–3 and 8), class IIa HDACs (HDACs 4, 5, 7, and 9), class IIb HDACs (HDACs 6 and 10), class III sirtuins (Sirt1–7), and class IV HDACs (HDAC11) [12,33,34]. While histone acetyltransferases (HAT) add acetyl groups to lysine residues, thereby permitting TFs binding and subsequent gene expression, histone deacetylases (HDACs) erase histone acetyl residues, leading to chromatin compaction, generally resulting in gene repression [33,34]. However, in contrast to the common role of HDACs for gene repression, treatment with HDAC inhibitors typically leads to a reduction rather than increase in pro-inflammatory gene expression by immune cells [35]. This may be due to global histone hyperacetylation induced by HDACi, which results in over-recruitment of epigenetic readers (in steady state, there is an equilibrium between acetylation and deacetylation) [35]. As a consequence, a large pool of epigenetic readers will be sequestrated nonspecifically, reducing the availability of readers for recruitment to newly induced promoters. This subsequently limits the binding of TFs and gene expression induction at these sites, rendering cells less responsive to external inflammatory stimuli [35], as described in **Figure 2**. HDAC inhibition was also suggested to reduce cytokine expression by promoting mRNA decay. For instance, Grabiec et al. have shown that pan-HDACi can disrupt IL-6 production in RA fibroblast-like synoviocytes (FLS) by accelerating its mRNA breakdown [36].

HDAC enzymes are key regulators of diverse cellular functions, including the inflammatory response, and their dysregulation has been strongly associated with multiple inflammatory diseases [37]. Current research aims to dissect the biological functions of each individual HDAC with attempts to develop class- or isoform-selective HDACi that can maintain similar anti-inflammatory potency of pan-HDACi while providing a better safety profile [38]. A summary of some of the main selective class or isoform inhibitors of HDACs that have been tested in ex vivo and in vivo animal models of inflammatory and autoimmune diseases is provided in **Table 1**. An approach for drug delivery to specific cell types has also been developed to limit the off-target activity associated with pan-HDACi.

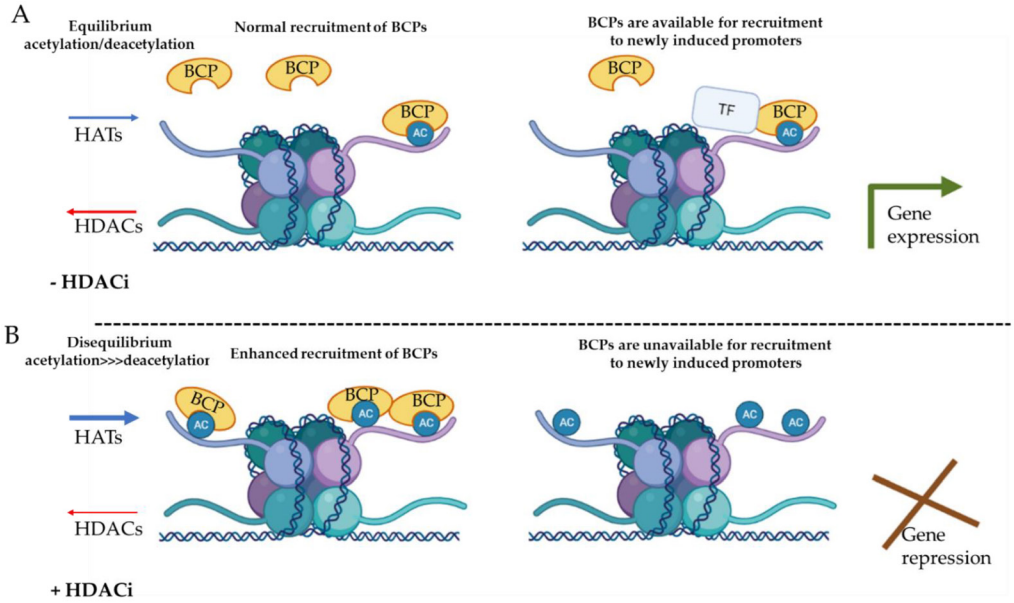


**Figure 2. Possible mechanism for inhibition of inflammatory gene expression by HDACi.** (**A**) In steady state, there is an equilibrium between acetylation (AC) and deacetylation, which maintains a pool of epigenetic readers available for recruitment to newly induced promoters, recruitment of transcription factors (TF), and induction of gene expression. (**B**) Histone deacetylase (HDACs) inhibition increases acetylation of histones that sequester the epigenetic readers, such the bromodomain-containing proteins (BCPs), preventing their recruitment to newly induced promoters.

## Class-Specific HDACi

### *Class I-Specific HDACi*

Entinostat (MS-275) [39] and Tacedinaline (CI994) [40] are the first potent selective inhibitors of class I HDACs and have shown therapeutic potential by ameliorating inflammation in preclinical models of various inflammatory and autoimmune diseases, including RA [41], Chronic Obstructive Pulmonary Disease (COPD) [42], pancreatitis [19], inflammation associated with angiotensin II-induced hypertension [43], liver fibrosis [44], and lipopolysaccharide-induced acute kidney injury (LPS-AKI) [45]. These beneficial preclinical outcomes were accompanied by a marked reduction in multiple proinflammatory cytokines and leukocyte infiltration [46]. Entinostat treatment reduced cytokine production and suppressed osteoclastic bone resorption in vitro (osteoclast generated from human monocytes), suggesting therapeutic potential in RA and periodontitis [41]. This was borne out by the efficacy of Entinostat in collagen antibody-induced arthritis model where it strongly reduced inflammatory cells infiltration and improved disease score [46]. Notably, Entinostat

showed a superior clinical efficacy to pan-HDACi (SAHA) in this model [46]. Similarly, Entinostat was able to significantly affect expression of proinflammatory cytokines in precision-cut lung slices and robustly attenuated inflammatory expression of CXCL1 and neutrophil influx in the lungs in an in vivo mice model of smoking-induced airway inflammation, while the pan-HDACi (SAHA) was without effect in this model [42].

Loh et al. also provided evidence for the importance of class I HDAC inhibition, showing that Entinostat, but not inhibitors of class IIa (PG100) and IIb HDAC (PG50) enzymes, potently suppressed chronic hepatic inflammation and fibrosis in mice [44]. Entinostat has been shown to reduce $CD68^+$ macrophage infiltration into aortic tissue in an angiotensin II-induced hypertension murine model [43]. In Cerulein-induced acute and chronic pancreatitis, Entinostat reduced the infiltration of inflammatory immune cells, including macrophages and T cells, and directly disrupted macrophage activation [47]. In terms of safety profiles, although no human clinical data are available yet for inflammatory and autoimmune diseases, the class I HDACi Reminostat exhibited an improved safety profile over pan-HDACi in clinical trials in cancer patients showing no cardiac-related toxicities [48,49]. Two class I HDACis; Etinostat and Mocetinostat, initially exhibited cardiac-related events in early studies. However, further evaluation found that the cardiac events were not related to Mocetinostat [50], while for Entinostat cardiac events were attributed to disparities in drug pharmacokinetics compared with preclinical models, which was mitigated upon redesigning the treatment regimens [51,52]. However, a recent trial for metastatic urethral cancer reported pericardial effusion for one patient that was believed to be Mocetinostat-related [53]. Thus, while class I HDACi appears to have fewer side effects than pan-HDACi, adverse events are still apparent, although some caution should be used in interpreting these events in patients with advanced cancer.

***Class II-Specific HDACi***

TMP195 (TFMO 2) is a selective, first-in-class, class IIa HDAC inhibitor reported by Lobera et al. [54]. TMP195 exhibited a potent effect on monocyte and macrophage activation in vitro, reducing CCL2 protein secretion and increasing the production of CCL1 by monocyte-derived macrophages and modifying human monocyte responses to the colony-stimulating factors CSF-1 and CSF-2 in vitro [55]. In an LPS acute injury in vivo model, TMP195 inhibited multiple proinflammatory cytokines/chemokines and accumulation of inflammatory cells in the injured kidney [56]. The reno-protective effects of TMP195 observed in this model suggest that targeting class IIa HDACs might be a novel therapeutic strategy for treating renal inflammation, although further investigation of this hypothesis is required.

## Isoform-Specific HDACi

Genetic depletion of individual HDACs has demonstrated that these proteins mediate specific and unique functions [57], suggesting therapeutic relevance for selective isoform targeting. While achieving this is a challenge due to conserved structural similarity between HDAC isoforms [12], HDACi has been reported with selectivity for HDAC1, HDAC2, HDAC3 [33,58–61], HDAC8 [62,63], HDAC6 [64], HDAC11 [65], SIRT1, and SIRT2 [66,67]. However, caution should be taken in interpreting the specificity of the effects of these published inhibitors given the variability of available HDAC assays and the residual dose-dependent effects on other isoforms (**Table 1**).

### *HDAC3 Inhibitors*

Inhibitors with a high degree of reported selectivity toward HDAC3, including RGFP966, MI192, and ITF3100, have been shown to efficiently attenuate inflammatory responses [33,58,59,68] and to restore LPS tolerance in inflammatory macrophages in vitro [33]. RGFP966 has demonstrated efficacy in preclinical models of diabetes [69], osteoarthritis (OA) [70], and allergy [71] via modulating inflammatory pathways. In diabetic mouse models, RGFP-966 was shown to prevent diabetes-associated liver damage, cerebral ischemia, and cardiomyopathy [72–74]. Zhang et al. found that RGFP966 could inhibit the expression of inflammatory markers of OA in rats [70]. Interestingly and unlike pan-HDACi, HDAC3 inhibitor MI192 was able to inhibit the inflammatory response in peripheral blood mononuclear cells (PBMCs) of RA patients but not in PBMCs of healthy control [68]. In line with these observations, inhibition of HDAC3 by the small molecule ITF3100 in RA FLS largely recapitulated the effects of pan-HDACi in suppressing inflammatory gene expression [75]. No effect of HDAC1/2 or HDAC8 inhibition was observed in RA FLS. These data suggest the potential for a clinically relevant advantage of the selective targeting of HDAC3 in RA [75].

### *HDAC6 Inhibitors*

HDAC6 has been extensively studied in various inflammatory settings, and several small-molecule inhibitors have been designed and reported to be selective, such as BML-281 (CAY10603) [76], Ricolinostat (ACY-1215) [77], CKD-506 [78], Tubastatin A [79], and ACY-738 [80]. HDAC6 inhibition has shown efficiency in multiple preclinical models of inflammatory and autoimmune diseases, including IBD [81–83], RA [84,85], systemic lupus erythematosus (SLE) [78,86], multiple sclerosis [87], lung inflammatory diseases [88,89], allograft rejection [90], skin inflammatory diseases [91], sepsis [92], and acute liver injury [93]. HDAC6 inhibition has been reported to control immune cell recruitment and to modulate T and B cell differentiation [78,83,94]. In a DSS colitis model, $CD19^+$ B cell influx into the inflamed colon was reduced in mice treated with BML-281 [83]. In addition, CKD-506 inhibits NF-κB signaling in

intestinal epithelial cells and macrophages and ameliorates murine colitis [81]. LTB2 treatment significantly alleviated DSS-induced colitis in mice [82]. Similarly, in a preclinical murine model of SLE, ACY-738 and CKD-506 were able to modulate both B cell and T cell differentiation, restoring aberrant B cell development and enhancing the frequency of splenic Tregs [78,94]. In addition, in this model, HDAC6 inhibition significantly reduced inflammatory cytokines such as IL-17 and TNF-α and increased TGF-β in serum [78,94]. In experimental autoimmune encephalomyelitis (EAE), ACY-738 delayed disease onset and reduced disease severity [87]. BML-281 blocks inflammatory signaling and caspase-1 activation in the LPS-induced acute lung injury mice model [89].

HDAC6 inhibition impairs effector CD8 T-cell functions during skin inflammation using murine CD8 T cell-related skin disease models, including contact hypersensitivity (CHS) and experimental graft-versus-host disease (GVHD)-like disease [91]. ACY-1215 prevented the development of CHS and GVHD-like disease in vivo by modulating CD8 T cell activation and functions, abrogating the induction of effector T cells from naive CD8 T cells [91]. Tubastatin A downregulated Th17 cell function and suppressed acute lung allograft rejection via the HIF-1α/RORγt pathway in mice [95]. Notably, this effect was observed only with HDAC6 inhibition but not in HDAC1i-, HDAC3i-, HDAC4i-, and HDAC8i-treated recipients [95]. In a murine model of RA, CKD-506 suppressed monocyte/macrophage inflammatory responses, improved Treg function, and ameliorated arthritis severity [84]. Similarly, Tubastatin A showed significant inhibition of IL-6 in paw tissues of arthritic mice in a collagen-induced arthritis model [96].

Although there are no human clinical studies as yet in inflammatory and autoimmune disease patients, similarly to class I HDACi in patients with cancer, HDAC6 inhibitors exhibit an improved safety profile compared with pan-HDACi [50]. For instance, Ricolinostat has shown no drug-related cardiac events in two clinical trial conducted for multiple myeloma patients either alone or in combination with other drugs [97,98]. Life-threatening cardiac arrhythmias are one of the most limiting factors for the use of pan-HDACi in clinical trials [50]. Pan-HDACi is thought to exert this cardiotoxic effect via inhibition of hERG ion channels either directly [99] or indirectly mediated by transcriptional changes that affect ion channel trafficking [100]. Interestingly selective inhibition of HDAC6 was found to stabilize hERG channel expression, which suggests an application for HDAC6 inhibition in long QT syndrome type 2 treatment [101]. To date, seven registered clinical trials are running for other HDAC6 inhibitors, which will help us to better characterize the safety profile of HDAC6 inhibition.

***HDAC8 Inhibitors***

Some inhibitors of HDAC8 that have been recently reported have shown a marked anti-inflammatory potential in some preclinical models of inflammatory and autoimmune diseases such as sepsis [63], neuro-inflammation [102], and asthma [100]. WK2-16 [102] and PCI-34051 [103] are reported to be the most selective HDAC8 inhibitors. WK2-16 reduced IL-6, TNF-α, and MPP8 expression in both sepsis and LPS-induced neuro-inflammation murine models [63,102] via inhibition of STAT-1/-3 and Akt activation in the absence of an effect on NF-κB or MAPK signaling pathways [63,102]. PCI-34051 was reported to alleviate airway inflammation in a preclinical model of asthma by disrupting HDAC8 interaction with Galectin-3, a protein involved in inflammation and pathogenesis of asthma [104].

***Other Isoform-Specific Inhibitors***

Santacruzamate A (CAY10683) is a potent HDAC2 inhibitor, with >3600-fold selectivity over other HDACs [105]. Fang-Zhou et al. have demonstrated that Santacruzamate A could suppress neuro-inflammatory responses and TLR4/NF-κB signaling pathways in an animal model of LPS-induced neuro-inflammation [106]. Other HDAC isoforms are reported to regulate the inflammatory response, including HDAC5 [107] and HDAC10 [108], but as of now there are no specific inhibitors to these isoforms. SIS17 is described as a highly selective HDAC11 inhibitor; however, no data are available on studies with this molecule in preclinical models [109].

Finally, selective inhibitors have been developed for some members of the SIRT family (HDAC class III), including EX-527 and AK 7 that target SIRT1 and SIRT2, respectively [66,67]. Although SIRT1 and SIRT2 are implicated in several inflammatory diseases such as RA and IBD, no data are reported for the use of EX-527 and AK 7 in vitro or in vivo models of inflammation.

## Cell-Specific Targeted Drug Delivery of Pan-HDACi

Mononuclear myeloid cells play a key role in the pathogenesis of multiple inflammatory diseases but are also critically required for tissue homeostasis and healing [110,111]. Because of the anti-inflammatory activity of HDACi in monocytes/macrophages, selective targeting of these cells could represent an attractive approach for retaining efficacy while minimizing adverse events linked to HDACi in other cell types. A strategy to do so has been developed based on the expression pattern of carboxylesterase 1 (CES1) enzyme (also known as serine esterase 1), which in humans is predominantly expressed in hepatocytes and cells of the mononuclear myeloid lineage, such as monocytes and macrophages, with very little expression reported outside these two sources, mainly in adipose tissue, kidney, and heart

[112,113]. CES1 plays a key role in hydrolyzing ester- and amide-bond-containing xenobiotics and drugs [114].

Esterase sensitive motif (ESM) technology has been employed to selectively target CES1-expressing cells. Small-molecule inhibitors are tagged with the ESM motif, the ESM-tagged inhibitors enter cells, and when CES1 is expressed, the ESM motif is hydrolyzed into an acid [32] as described in **Figure 3**. In acid form, the compound is less able to cross the plasma membrane, thus increasing retention and therefore potency in CES1 expressing cells [32] (**Figure. 3**). Such targeted molecules have shown efficacy in a preclinical model of RA in which transgenic mice that express human CES1 under the CD68 promotor were generated to allow human CES1 expression in mononuclear myeloid cells [32]. ESM-HDACi achieved clinical improvement at doses as low as 1 mg/kg compared with 100 mg/kg of conventional pan-HDACi (SAHA) needed to achieve a similar clinical response [32]. ESM-HDACi was tolerated up to 30 mg/kg in vivo dosing [32].

In a phase 1 clinical study, ESM-HDACi proved to be safe and well tolerated while showing efficient and sustainable accumulation in blood monocytes [115]. This sparked the interest to further explore this strategy in other inflammatory disease models. In both acute DSS colitis [116] and acute peritonitis [117] models, ESM-HDACi impaired the differentiation of monocyte in inflamed tissue, which translated into modestly improved colitis [116]. Exploring this strategy in a variety of inflammatory disease models may identify the best application of this approach given the complex role of these cells in mediating the inflammatory response in different diseases [118,119]. In addition, using ESM technology with more selective HDAC inhibitors (class or isoform specific) would provide better therapeutic potential.

## Advances in Selective Targeting of BCPs

BCPs are group of epigenetic readers that recognize acetylated lysine residues on histone tails and play a role in modulating DNA accessibility to TFs and the transcriptional machinery [120]. Disturbance in BCP function has been reported as a key contributor to a large variety of diseases [15]. In humans, if we exclude splice variants, there are around 56 BDs and 42 BCPs characterized [121]. Based on sequence homology, BCPs are classified into eight different subgroups [120], as described in **Figure 4**. BCPs are tractable to small-molecule antagonists that prevent protein–protein interaction between BCPs and acetylated histones and transcription factors [122]. Although numerous compounds targeting BCPs (primarily BET family

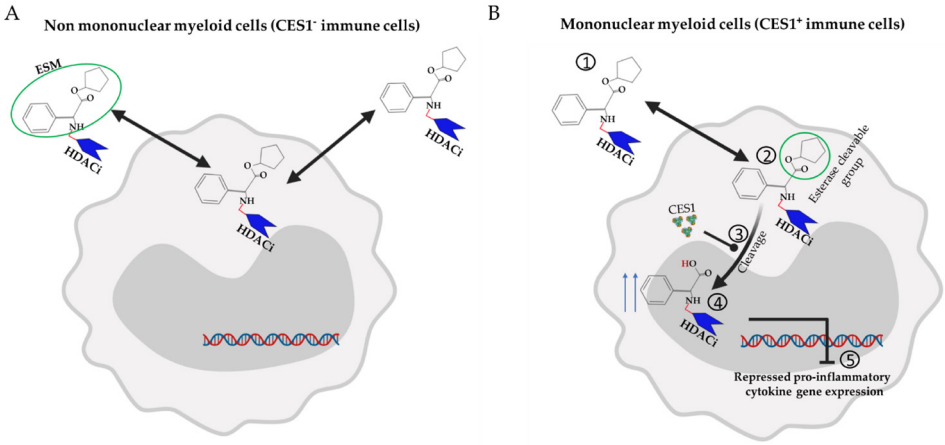


**Figure 3. Selective targeting of myeloid cells with HDACi.** CES-1 expression in humans is restricted to hepatocytes and cells of the mononuclear myeloid lineage, such as monocytes and macrophages. (**A**) When ESM-HDACi enters into CES-1-negative cells such as T and B cells, the compound freely diffuses out of the cells; lack of retention of the HDACi minimizes the pharmacological effect. (**B**) After entry of ESM-HDACi into CES-1-positive cells ①, esters are selectively hydrolyzed by the CES-1 enzyme ②, generating charged acids ③ that are less able to cross the membrane. This leads to intracellular retention of HDACi ④ and enhanced pharmacological effect (e.g., histone hyperacetylation and repression of proinflammatory genes) ⑤.

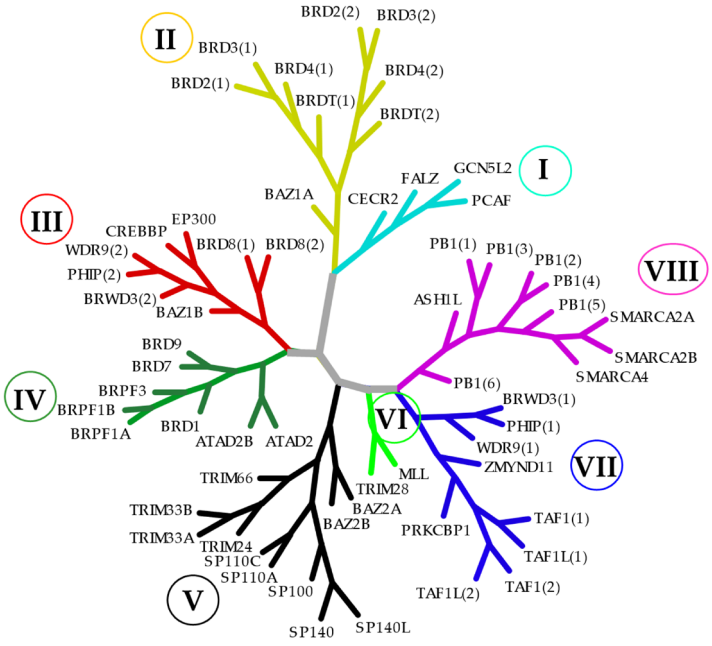


**Figure 4. Phylogenetic tree of the human bromodomain-containing protein subgroups.** On the basis of sequence homology, BCPs are classified into eight different subgroups (families). The distinct families are indicated by Roman numbers (I–VIII) in circles and illustrated with different colors.

BCPs) have displayed promising therapeutic potential in preclinical models of cancer and autoimmunity/inflammation, these compounds have not yet been approved by FDA [123]. The majority of BCP inhibitors lack selectivity for individual BCPs or a specific domain, and as BCPs regulate the expression of a plethora of genes and can be ubiquitously expressed, therapeutic translation into the clinic has been restricted by multiple adverse events [121]. To reduce the breadth of effects observed with first-generation BCP inhibitors, efforts have been made to achieve better selectivity amongst BRDs, as well as to develop specific cell type delivery of small molecules targeting BCPs. Three main advances in this direction are discussed below. A summary of some of the main tested selective domain or isoform inhibitors of BCPs in ex vivo and in vivo animal models of inflammatory and autoimmune diseases are described in **Table 1**.

**Table 1.** Summary of some of the main tested selective inhibitors of HDACs and BCPs in ex vivo and in vivo models of inflammatory and autoimmune diseases.

| Inhibitors | Targets | Degree of Selectivity in Cell Free Assay | Preclinical Models of Inflammatory and Autoimmune Diseases | Key Findings |
|---|---|---|---|---|
| Entinostat (MS-275) [39] | Class I HDAC | IC50s of 243, 453, and 248 nM for HDAC1, HDAC2, and HDAC3, respectively. | Collagen antibody-induced arthritis (mouse and rat) [46] | While pan-HDACi (SAHA) could not inhibit the onset of arthritis, Entinostat displayed strong antirheumatic activities. |
| | | | Cigarette smoke-induced airway inflammation (mouse) [42] | While Entinostat attenuated inflammatory expression and neutrophil influx in the lungs, pan-HDACi (SAHA) was without effect. |
| | | | Thioacetamide-induced hepatic inflammation (mouse) [44] | Entinostat but not class IIa and IIb HDACi suppressed chronic hepatic inflammation and fibrosis. |
| | | | Cerulein-induced acute and chronic pancreatitis (mouse) [47] | Reduced infiltration of inflammatory immune cells. |
| Tacedinaline (CI994) [40] | Class I HDAC | IC50s of 0.9, 0.9, 1.2, and >20 μM for human HDAC 1, 2, 3, and 8, respectively | Titanium particle-induced calvarial osteolysis (mouse) [124] | Tacedinaline inhibited osteoclastogenesis through targeting NF-κB and the downstream c-Fos/NFATc1 signaling pathway. |
| TMP195 (TFMO 2) [54] | Class IIa HDAC | IC50s of 59, 60, 26, and 15 nM for HDAC4, HDAC5, HDAC7, and HDAC9, respectively. 100-fold selectivity over other HDACs (IC50s >10 μM) | Lipopolysaccharide-induced acute kidney injury (mouse) [56] | TMP195 inhibited multiple proinflammatory cytokines/chemokines and reduced the accumulation of inflammatory immune cells in the injured kidney. |
| RGFP966 [125] | HDAC3 | IC50 of 0.08 μM inhibits HDAC3 > 200-fold selectivity over other HDACs | Diabetic models (mouse) [72–74] | RGFP966 prevented diabetes-associated liver damage, -cerebral ischemia and – cardiomyopathy. |
| | | | Osteoarthritis model (rat) [70] | RGFP966 inhibited the expression of inflammatory markers via modulating HDAC3/ NF-kB pathway. |
| MI192 [68] | HDAC3 | IC50s of 16 and 30 nM, for HDAC2 and HDAC3, respectively. | Ex vivo-stimulated human peripheral blood mononuclear cells (PBMCs) of RA patients [68] | Unlike pan-HDACi, MI192 inhibited inflammatory response in PBMC of RA patients but not in PBMCs of healthy control. |
| Santacruzamate A (CAY10683) [105] | HDAC2 | IC50 of 119 pM for HDAC2 and with >3600-fold selectivity over other HDACs. | LPS-induced neuro-inflammation (mouse) [106] | Santacruzamate A suppressed neuro-inflammatory responses and TLR4/NF-κB signaling pathways. |

**Table 1.** Continued

| Inhibitors | Targets | Degree of Selectivity in Cell Free Assay | Preclinical Models of Inflammatory and Autoimmune Diseases | Key Findings |
|---|---|---|---|---|
| Tubastatin A [79] | HDAC6 | IC50 of 15 nM for HDAC6. It is selective against all the other HDACs (1000-fold) except HDAC8 (57-fold). | Orthotopic lung transplantation model (mouse) [95] | Tubastatin A downregulated Th17 cell function and suppressed acute lung allograft rejection. Notably, this effect was observed only with HDAC6 inhibition but not with HDAC1i-, HDAC3i-, HDAC4i-, and HDAC8i-treated mice. |
| | | | Collagen-induced arthritis (mice) [96] | Tubastatin A reduced IL-6 in paw tissues of arthritic mice. |
| ACY-738 [80] | HDAC6 | IC50 of 1.7 nM for HDAC6 and 60- to 1500-fold selectivity over class I HDACs | Model of systemic lupus erythematosus (SLE) (mouse) [94] | ACY-738 modulated both B cell and T cell differentiation, restored the aberrant B cell development and enhanced the frequency of splenic Tregs. |
| | | | Experimental autoimmune encephalomyelitis model (mouse) [87] | ACY-738 delayed disease onset and reduced disease severity. |
| BML-281 (CAY10603) [76] | HDAC6 | IC50s of 2 pM; for HDAC6. *BML-281* also inhibits HDAC1, HDAC2, HDAC3, HDAC8, and HDAC10, with IC50s of 271, 252, 0.42, and 90.7 nM. | DSS-induced colitis (mouse) [83] | $CD19^+$ B cell influx into inflamed colon was reduced in mice treated with BML-281. |
| | | | LPS-induced acute lung injury (mouse) [89] | BML-281 blocks inflammatory signaling and caspase-1 activation. |
| LTB2 [82] | HDAC6 | IC50 value of 3.9 nM | DSS-induced colitis (mouse) [82] | LTB2 prevented DSS-induced colitis. |
| Ricolinostat (ACY-1215) [77] | HDAC6 | IC50 of 5 nM for HDAC6. Ricolinostat also inhibits HDAC1, HDAC2, and HDAC3 with IC50s of 58, 48, and 51 nM, respectively. | Contact hypersensitivity (CHS) and experimental graft-versus-host disease (GVHD)-like disease (mouse) [91] | Ricolinostat prevented the development of CHS and GVHD-like disease by modulating CD8 T cell activation and functions; abrogated the induction of effector T cells from naive CD8 T cells |

**Table 1.** Continued

| Inhibitors | Targets | Degree of Selectivity in Cell Free Assay | Preclinical Models of Inflammatory and Autoimmune Diseases | Key Findings |
|---|---|---|---|---|
| CKD-506 [78] | HDAC6 | IC50 of around 5 nM. IC50 values for HDAC1, HDAC2, HDAC7, and HDAC8 were in the range of 2000–5000 nM. | DSS- and adoptive T cell transfer-induced colitis (mouse) [81]. | CKD-506 ameliorated weight loss, disease activity, and histopathologic score and downregulated proinflammatory cytokines production. |
| | | | Model of SLE (mouse) [78] | CKD-506 modulate both B cell and T cell differentiation, restoring the aberrant B cell development and enhancing frequency of splenic Tregs |
| | | | Adjuvant-induced arthritis (mouse) [84] | Suppresses monocytes/macrophages inflammatory responses, improves Treg function, and ameliorates arthritis severity. |
| WK2-16 [102] | HDAC8 | - | Sepsis and LPS-induced neuro-inflammation (mouse) [63,102] | WK2-16 was able to reduce IL-6, TNF-α and MPP8. |
| PCI-34051 [103] | HDAC8 | IC50 of 10 nM for HDAC8 and with 200-fold selectivity over HDAC1 and 6 and more than 1000-fold selectivity over HDAC2, 3, and 10. | Ovalbumin-induced asthma (mice) [104] | PCI-34051 alleviated airway inflammation and disrupted HDAC8 interaction with Galectin-3, a protein involved in inflammation and pathogenesis of asthma. |
| ESM-HDAC528 [32] | Pan-HDAC | Selective accumulation of pan-HDACi in $CES1^+$ cells. | Arthritis model [32] | ESM-HDAC528 achieved clinical improvement at lower dose of 1 mg/kg compared with 100 mg/kg of conventional pan-HDACi (SAHA) |
| | | | DSS-induced colitis [116] | ESM-HDACi impaired monocytes differentiation in the inflamed tissue, and this was translated into modest improved colitis |
| ZL0420 and ZL0454 [126,127] | BRD4 | For ZL0420, an IC50 of 27 nM against BRD4 BD1 and 32 nM against BRD4 BD2, and for ZL0454, an IC50 of 49 and 32 nM for BD1 and BD2. | TLR3-mediated acute airway inflammation (mice) [126] | The infiltration of neutrophils into the airway fluids and cytokine expression in the lung tissue were more effectively blocked by BRD4 inhibitors than pan-I-BET; (+)-JQ1 or RVX-208 |
| GSK761 [4] | SP140 | IC50 value of 77.79 ± 8.27 nM | $CD14^+$ macrophages isolated from Crohn's disease colonic tissues [4] | GSK761 reduced the spontaneous secretion of proinflammatory cytokines by macrophages |

| Inhibitors | Targets | Degree of Selectivity in Cell Free Assay | Preclinical Models of Inflammatory and Autoimmune Diseases | Key Findings |
|---|---|---|---|---|
| I-BRD9 [128,129] | BRD9 | pIC50 of 7.3 for BRD9, with pIC50 of 5.3 against BRD4. | Nur77 knockout-induced obesity (mice) [130] | Combining I-BRD9 with calcipotriol regulated the gut microbiota and improved intestinal mucosal barrier function. |
| GSK046 (iBET-BD2) [131] | BD2 of BET proteins | IC50s of 264 nM (BRD2 BD2), 98 nM (BRD3 BD2), 49 nM (BRD4 BD2), and 214 nM (BRDT BD2). | Models of RA and psoriasis (mouse) [131] | Immunomodulatory effects. |
| GSK778 (iBET-BD1) [131] | BD1 of BET proteins | IC50s of 75 nM (BRD2 BD1), 41 nM (BRD3 BD1), 41 nM (BRD4 BD1), and 143 nM (BRDT BD1), respectively | Cancer model (mouse) [131] | GSK778 phenocopied the effects of pan-BET inhibitors in cancer models. |

## Domain-Selective Targeting (BD1 or BD2 Targeting)

The BET protein family of BCPs comprise the ubiquitously expressed BRD2, BRD3, and BRD4 and the testis-restricted BRDT, all of which harbor two highly conserved tandem bromodomains, BD1 and BD2, allowing them to recognize acetylated lysines [131,132]. BET proteins are well recognized as drug targets for multiple human diseases [131]. Most potent and selective BCP inhibitors reported target all eight BDs of the BET family (i.e., BD1 and BD2 in BRD2, 3, 4 and T), and include I-BET762 [133], (+)-JQ1 [134], I-BET151 [122], and I-BET726 [135]. These compounds display similar affinities to BD1 and BD2 [131]. Such compounds have been utilized to demonstrate the function of these proteins in selectively regulating expression of genes with high therapeutic interest for several human inflammatory diseases [21,131,136]. Recent reports studying the molecular mechanisms of BET protein binding demonstrate differential binding of BD1 and BD2 to different targets [136,121]. These mechanistic studies suggest a model where BD1 is essential for BET protein binding to di-acetylated nucleosomes, while BD2 is more relevant to binding to TFs and protamines [136,121]. Therefore, selective inhibition of either BD1 or BD2 binding might promote different functional consequences that allow for more selectivity in functional effect and an improved safety profile to be explored in different diseases settings [136,121].

BD1 and BD2 have high sequence similarity within the acetyl–lysine binding site but exhibit distinct recognition patterns of acetylated histone peptide targets [137]. Accordingly, BD1 and BD2 of BRD4 can both recognize acetylated H4 peptide [137]. However, only BD1 has been shown to specifically recognize N-terminal-acetylated H4 peptides in a sequence-dependent manner, while BD2 is more promiscuous [131]. In addition, BD1 favors binding to di-acetylated residues on histone H4, particularly H4 K5ac/K8ac, whereas BD2 is more permissive and can accommodate a variety of di-acetylated peptides [131]. Importantly, despite the ability of BD2 to bind acetylated histones in vitro, biochemical studies have indicated that BD1 of the BET proteins is mainly responsible for chromatin binding [137,138]. This suggests that selective inhibition of BD1 or BD2 would be expected to yield distinct subsets of effects other than observed with pan-BET inhibitors [139]. Emerging data with domain-selective inhibitors are providing support for this idea.

ABBV-744 is a BET inhibitor that shows preferential inhibition of the BD2 domain [140]. ABBV-744 has demonstrated a robust activity in prostate cancer xenografts and exhibited fewer platelet and gastrointestinal toxicities compared with the dual-bromodomain BET inhibitors (DbBi) [140]. Recently, Gilan et al. described the development of GSK778 (iBET-BD1) and GSK046 (iBET-BD2), the first highly selective

small-molecule inhibitors of BET-BD1 and BET-BD2, respectively [131]. This advance has helped to highlight more distinct roles of BD1 and BD2 (**Figure. 5**). iBET-BD1 showed a selectivity of ≥130-fold for BRD4 BD1, and iBET-BD2 showed selectivity of ≥130-fold for BRD4 BD2 [131]. In this study, iBET-BD1 was able to replicate the effects of pan-BET inhibitor I-BET151 in human cancer cell lines, such as inducing cell cycle arrest and clonogenic capacity [131]. Notably, the effects of iBET-BD2 were less pronounced in this setting [131]. This was explained by the ability of iBET-BD1 to reduce the chromatin binding of all BET proteins, including BRD4, which is known to be critical for maintaining oncogenic and homeostatic transcriptional programs, while iBET-BD2 failed to interfere with BRD 2, 3, or 4 binding in an in vitro THP-1 homeostatic model. Interestingly, in the context of inflammatory stimulus-induced in vitro models, iBET-BD2 was able to strongly reduce BRD2 and BRD3 binding while only sparing BRD4 binding and was able to inhibit the IFNγ-induced transcriptional program [131]. Despite no effects on cancer cell proliferation or survival, iBET-BD2, like iBET-BD1, exerted immunomodulatory effects by decreasing the expression of proinflammatory cytokines in in vitro assay [131]. These mechanistic studies of BET BD1/BD2 functionality indicate a model where BD1 binding is sufficient to maintain homeostatic and oncogenic gene transcription programs, while both BD1 and BD2 binding is required to promote an inflammatory transcriptional response (**Figure. 5**). This observation implies that selective inhibition of BD2 could be a promising strategy for treatment of inflammatory diseases with a potential for an improved safety profile. Indeed, iBET-BD2 was shown to provide efficacy in animal models of RA and psoriasis [131]. Overall, these findings of differential functions for BD1 and BD2 (**Figure. 5**) indicate a therapeutic rationale founded on distinct BET BD-selective targeting in cancer and immuno-inflammatory diseases.

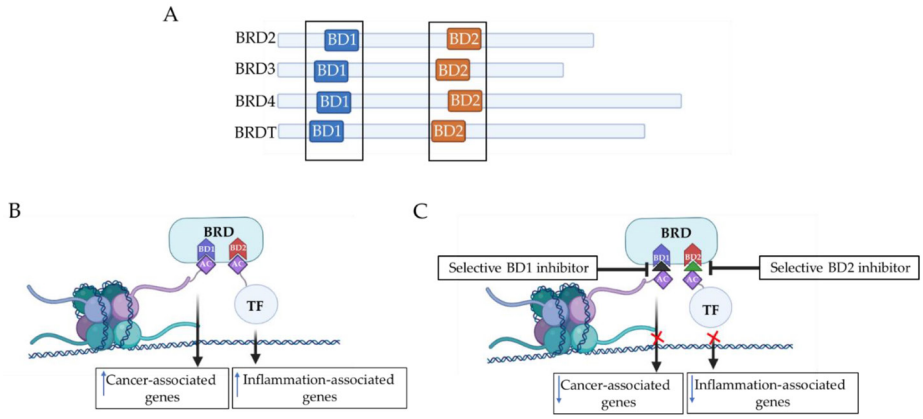


**Figure 5. Selective domain targeting of BD1 and BD2.** (**A**) BET proteins family of BCPs comprise the ubiquitously expressed BRD2, BRD3, and BRD4 and BRDT, which all harbor two highly conserved tandem bromodomains, BD1 and BD2, allowing them to recognize acetylated lysine. (**B**) BD1 and BD2 have distinct functions. BD1 binding is sufficient to maintain homeostatic and oncogenic gene transcription programs, while BD2 binding is required to promote an inflammatory transcriptional response. (**C**) Domain-selective inhibitors for BD1 and BD2 show preferential effects on different types of cellular functions [141].

## Selective Targeting of Single BCP

### *BRD4 Inhibitors*

Important advances in new technologies and tools such as assay kits for screening inhibitors, Targetome, BromoMELT, BromoScan assay, and others, have revolutionized the discovery of series of diverse small molecules that selectively target a single BCP. These include ZL0420 and ZL0454, potent selective inhibitors of BRD4 [126,127]. ZL0420 has reported IC50 values of 27 nM against BRD4 BD1 and 32 nM against BRD4 BD2, while ZL0454 shows IC50 value of 49 and 32 nM for BD1 and BD2, respectively [126,127]. These molecules have been utilized to explore the potential of selective targeting of BRD4 in airway inflammation, based on reports of a critical role for BRD4 in NF-κB-mediated epithelial–mesenchymal transition in an in vitro model of airway epithelial cell culture and in in vivo murine models of pulmonary fibrosis and TLR3-mediated acute airway inflammation [27]. Intranasal administration of poly(I:C) induced a substantial increase of total cells and neutrophils into the airway fluids, and cytokine expression in the lung tissue [126]. These changes were more effectively blocked by BRD4 inhibitors than by pan-I-BET; (+)-JQ1 or RVX-208 [126]. In another study, MS436, a compound that preferentially targets the first bromodomain of BRD4, blocked the transcriptional activity of BRD4 in the NF-κB-directed production of nitric oxide and IL-6 [142]. In addition to the small molecules inhibiting BET BD protein–protein interactions described above, molecules able to

degrade BET proteins based on PROTAC technology have been developed. Notably, some of these have been reported to have BET isoform selectivity, such dBET57 [143] and QCA570 [144], which have been reported to selectively degrade BRD4. To date, however, no in vivo studies with these molecules are reported.

***SP140 Inhibitor***

The development of inhibitors targeting BCPs proteins other than BET in inflammatory and autoimmune diseases are rare, although some advances have been reported. Another BCP with reported therapeutic potentials is speckled 140 KDa (SP140), which belongs to the SP100 family of proteins that also includes SP100, SP110, and SP140 L [4]. Genetic and epigenetic alterations in the SP140 locus have been strongly associated with autoimmune and inflammatory diseases, including Crohn's disease (CD) and multiple sclerosis [145,146]. SP140 is predominantly expressed in immune cells, suggesting an interesting therapeutic potential [4]. Ghiboub et al. have described the first selective small-molecule inhibitor of SP140 (GSK761). GSK761 was shown to compete with the N-terminal tail of histone H3 for interactions with the SP140 BRD-PHD module [4]. GSK761 decreased the differentiation of monocytes into inflammatory macrophages and LPS-induced inflammatory activation, whilst inducing the generation of $CD206^+$ regulatory macrophages that mark anti-TNF remission induction in CD patients. Notably, ex vivo treatment of $CD14^+$ macrophages isolated from CD intestinal mucosa with GSK761 inhibited the spontaneous expression of cytokines, including *TNF* [4]. While this study identifies SP140 as a druggable epigenetic reader and potential therapeutic target for CD, GSK761 however shows poor in vivo pharmacokinetics, potentially restricting its use in vivo [4].

***BRD9 Inhibitors***

BRD9 is part of the SWI/SNF remodeling BAF complex [147], and selective BRD9 inhibitors, I-BRD9 and BI-7273, have been described [128,129]. Evidence for the importance of BRD9 in immune function has come from studies in the T cell transfer colitis model, where T effector cells were co-transferred with either BRD9-depleted or normal Treg cells [148]. Notably, BRD9-deficient Tregs, unlike control Tregs, failed to prevent colitis development in recipient mice. [148]. As BRD9-deficient Tregs were also defective in the context of tumor immunity, the authors suggested that small-molecule drugs could be useful to fight cancer. Interestingly, a study by Qingqing Lv et al. showed that calcipotriol combined with I-BRD9 can regulate the gut microbiota, improve intestinal mucosal barrier function, and reduce LPS absorption into the blood [130].

***CREB Inhibitor***

The BCP cyclic AMP response element-binding protein (CREB) is a transcriptional coactivator of many different transcription factors and plays an essential role in regulating the immune response [149], including mediating TNF-α and IL-10 production in macrophages and controlling cytokine expression by Th1 (IL-2 and IFN-γ) and Th2 cells (IL-4 and IL-13) through the regulation of IFN-γ production [149]. Dysregulation of CREB has been associated with several immune-mediated diseases [149–151]. For instance, CREB was shown to play a role in synovial cell hyperfunction in patients with RA [151] and intestinal barrier dysfunction in IBD [150]. Thus, targeting CREB selectively may yield therapeutic benefits for inflammatory diseases. PF-CBP1 and KG-501 have been reported as potent selective inhibitors of CREB by Eugene L et al. [152] and Jennifer L et al. [153], respectively. These compounds target specifically the BD in CREB protein [152,153]. PF-CBP1 demonstrated strong potential to reduce proinflammatory cytokines in human macrophages in vitro [152]. Notably, the authors observed several other genes that were affected by PF-CBP1 but not by pan-BET inhibitor, including REL, RELB, CCL2, CCL3, MRC1, and NFKBIA [152]. These data highlight the effects of CBP pharmacological inhibition on specific and distinct molecular targets and suggest that CBP inhibitors could be used to investigate therapeutic opportunities in inflammation that possess a molecular etiology mechanistically different to BET-associated inflammation.

***4BRPF Inhibitors***

BRD and plant homeodomain finger-containing (BRPF) family proteins consist of three members: BRPF1, BRPF2 (BRD1), and BRPF3 [154]. Julia et al. have reported three potent and selective inhibitors: one (PFI-4) with high selectivity for the BRPF1B isoform and two pan-BRPF bromodomain inhibitors (OF-1, NI-57) [155]. Intriguingly, the inhibitors impaired RANKL-induced differentiation of primary murine bone marrow cells and human primary monocytes into bone-resorbing osteoclasts by specifically repressing transcriptional programs required for osteoclastogenesis [155].

## Cell-Specific Targeted Drug Delivery of I-BET

As discussed above, the ESM technology can be used to preferentially target small-molecule inhibitors to myeloid cells. GlaxoSmithKline (GSK) has utilized this approach to generate myeloid-targeted ESM-I-BET compounds [156]. However, no preclinical data are available yet for these compounds [156].

## Conclusions/Perspectives

While progress is being made regarding the development of more isoform/domain-selective HDAC and BCP inhibitors, further pre- and clinical studies of these molecules are required to better characterize their efficacy and safety profiles. Although new HDAC and BCP inhibitors display high affinity towards specific classes, isoforms, or domains, most still retain residual effects on one or more other epigenetic enzymes, as described in the Table 1. Thus, efforts should continue towards developing new isoform/domain-selective inhibitors with improved specificity to avoid potential off-target effects. Meanwhile, two valuable approaches for future studies can help improve safety and guide applications into the inflammatory disease field. The first approach would involve examining individual HDAC and BCP expressions in different inflammatory diseases, as reviewed for IBD here [157]. This may better identify the relevant individual HDAC/BCP for each disease setting and guide selective inhibitor design to target the relevant isoform/domain for each disease. A second approach would involve conducting transcriptional analysis studies that compare the impact of individual isoform/domain knockdowns/inhibitions in different in vitro and in vivo systems. This can help to identify targets that show efficient modulation of inflammatory pathways without impacting other central/homeostatic pathways upon their inhibition. Results from such studies can guide the development and application of further selective HDAC/BCP inhibitors in inflammatory and autoimmune diseases.

**Author Contributions:** Conceptualization, W.J.d.J., M.G. and A.M.I.F.; writing—original draft preparation, M.G., D.F.T., N.R.H. and A.M.I.F.; review and editing, W.J.d.J., D.F.T., N.R.H. and M.P.J.d.W.; supervision, W.J.d.J.; Figure preparation, M.G. All authors have read and agreed to the published version of the manuscript.

**Funding:** M.G. and A.M.I.F. are funded by European Union's Horizon 2020 research and innovation program under Grant Agreement No. ITN-2014-EID-641665. W.J.d.J. is funded by Dutch Ministry of Economic Affairs, LSH-TKI, and Health Holland.

**Institutional Review Board Statement:** Not applicable.

**Informed Consent Statement:** Not applicable.

**Data Availability Statement:** Not applicable

**Conflicts of Interest:** The authors declare no conflict of interest.

**Abbreviations:** HDAC: histone deacetylase; BD: bromodomain; BRD: *BET* bromodomain-containing protein; IC50: half-maximal inhibitory concentration; SP140: speckled 140 KDa, CES1: carboxylesterase 1; BCP: Bromodomain containing protein.

# References


1. Kondilis-Mangum, H.D.; Wade, P.A. Epigenetics and the adaptive immune response. *Mol. Asp. Med.* **2013**, *34*, 813–825, doi:10.1016/j.mam.2012.06.008.
2. Lang, K.S.; Burow, A.; Kurrer, M.; Lang, P.A.; Recher, M. The role of the innate immune response in autoimmune disease. *J. Autoimmun.* **2007**, *29*, 206–212, doi:10.1016/j.jaut.2007.07.018.
3. Chen, Z.; Li, S.; Subramaniam, S.; Shyy, J.Y.; Chien, S. Epigenetic Regulation: A New Frontier for Biomedical Engineers. *Annu. Rev. Biomed. Eng.* **2017**, *19*, 195–219.
4. Ghiboub, M.; Koster, J.; Craggs, P.D.; Li Yim, A.Y.F.; Shillings, A.; Hutchinson, S.; Bingham, R.P.; Gatfield, K.; Hageman, I.L.; Yao, G.; et al. Modulation of macrophage inflammatory function through selective inhibition of the epigenetic reader protein SP140. *bioRxiv* **2020**, doi:10.1101/2020.08.10.239475.
5. Shanmugam, M.K.; Sethi, G. Role of epigenetics in inflammation-associated diseases. *Subcell Biochem.* **2013**, *61*, 627–657.
6. Holoch, D.; Moazed, D. RNA-mediated epigenetic regulation of gene expression. *Nat. Rev. Genet.* **2015**, *16*, 71–84, doi:10.1038/nrg3863.
7. Zeng, Y.; Chen, T. DNA Methylation Reprogramming during Mammalian Development. *Genes* **2019**, *10*, 257, doi:10.3390/genes10040257.
8. Bannister, A.J.; Kouzarides, T. Regulation of chromatin by histone modifications. *Cell Res.* **2011**, *21*, 381–395, doi:10.1038/cr.2011.22.
9. Araki, Y.; Mimura, T. The Histone Modification Code in the Pathogenesis of Autoimmune Diseases. *Mediat. Inflamm.* **2017**, *2017*, 1–12, doi:10.1155/2017/2608605.
10. Hull, E.E.; Montgomery, M.R.; Leyva, K.J. HDAC Inhibitors as Epigenetic Regulators of the Immune System: Impacts on Cancer Therapy and Inflammatory Diseases. *Biomed Res. Int.* **2016**, *2016*, 1–15, doi:10.1155/2016/8797206.
11. Morgado-Pascual, J.L.; Rayego-Mateos, S.; Tejedor, L.; Suarez-Alvarez, B.; Ruiz-Ortega, M. Bromodomain and Extraterminal Proteins as Novel Epigenetic Targets for Renal Diseases. *Front. Pharm.* **2019**, *10*, 1315–1315, doi:10.3389/fphar.2019.01315.
12. Seto, E.; Yoshida, M. Erasers of Histone Acetylation: The Histone Deacetylase Enzymes. *Cold Spring Harb. Perspect. Biol.* **2014**, *6*, a018713, doi:10.1101/cshperspect.a018713.
13. Ferri, E.; Petosa, C.; McKenna, C.E. Bromodomains: Structure, function and pharmacology of inhibition. *Biochem. Pharm.* **2016**, *106*, 1–18, doi:10.1016/j.bcp.2015.12.005.
14. Filippakopoulos, P.; Knapp, S. Targeting bromodomains: Epigenetic readers of lysine acetylation. *Nat. Rev. Drug Discov.* **2014**, *13*, 337–356, doi:10.1038/nrd4286.
15. Muller, S.; Filippakopoulos, P.; Knapp, S. Bromodomains as therapeutic targets. *Expert Rev. Mol. Med.* **2011**, *13*, e29, doi:10.1017/s1462399411001992.
16. Hancock, W.W.; Akimova, T.; Beier, U.H.; Liu, Y.; Wang, L. HDAC inhibitor therapy in autoimmunity and transplantation. *Ann. Rheum. Dis.* **2012**, *71* (Suppl. 2), i46–i54, doi:10.1136/annrheumdis-2011-200593.
17. Singh, A.K.; Bishayee, A.; Pandey, A.K. Targeting Histone Deacetylases with Natural and Synthetic Agents: An Emerging Anticancer Strategy. *Nutrients* **2018**, *10*, 731, doi:10.3390/nu10060731.
18. Glauben, R.; Batra, A.; Fedke, I.; Zeitz, M.; Lehr, H.A.; Leoni, F.; Mascagni, P.; Fantuzzi, G.; Dinarello, C.A.; Siegmund, B. Histone Hyperacetylation Is Associated with Amelioration of Experimental Colitis in Mice. *J. Immunol.* **2006**, *176*, 5015–5022, doi:10.4049/jimmunol.176.8.5015.

19. Nadeem, A.; Al-Harbi, N.O.; Al-Harbi, M.M.; El-Sherbeeny, A.M.; Ahmad, S.F.; Siddiqui, N.; Ansari, M.A.; Zoheir, K.M.; Attia, S.M.; Al-Hosaini, K.A.; et al. Imiquimod-induced psoriasis-like skin inflammation is suppressed by BET bromodomain inhibitor in mice through RORC/IL-17A pathway modulation. *Pharm. Res.* **2015**, *99*, 248–257, doi:10.1016/j.phrs.2015.06.001.
20. Rudman, M.D.; Choi, J.S.; Lee, H.E.; Tan, S.K.; Ayad, N.G.; Lee, J.K. Bromodomain and extraterminal domain-containing protein inhibition attenuates acute inflammation after spinal cord injury. *Exp. Neurol.* **2018**, *309*, 181–192, doi:10.1016/j.expneurol.2018.08.005.
21. Copsel, S.N.; Lightbourn, C.O.; Barreras, H.; Lohse, I.; Wolf, D.; Bader, C.S.; Manov, J.; Kale, B.J.; Shah, D.; Brothers, S.P.; et al. BET Bromodomain Inhibitors Which Permit Treg Function Enable a Combinatorial Strategy to Suppress GVHD in Pre-clinical Allogeneic HSCT. *Front. Immunol.* **2019**, *9*, 3104, doi:10.3389/fimmu.2018.03104.
22. Friedrich, M.; Gerbeth, L.; Gerling, M.; Rosenthal, R.; Steiger, K.; Weidinger, C.; Keye, J.; Wu, H.; Schmidt, F.; Weichert, W.; et al. HDAC inhibitors promote intestinal epithelial regeneration via autocrine TGFβ1 signalling in inflammation. *Mucosal Immunol.* **2019**, *12*, 656–667, doi:10.1038/s41385-019-0135-7.
23. Cui, S.-N.; Chen, Z.-Y.; Yang, X.-B.; Chen, L.; Yang, Y.-Y.; Pan, S.-W.; Wang, Y.-X.; Xu, J.-Q.; Zhou, T.; Xiao, H.-R.; et al. Trichostatin A modulates the macrophage phenotype by enhancing autophagy to reduce inflammation during polymicrobial sepsis. *Int. Immunopharmacol.* **2019**, *77*, 105973, doi:10.1016/j.intimp.2019.105973.
24. Ali, M.N.; Choijookhuu, N.; Takagi, H.; Srisowanna, N.; Huynh, M.N.N.; Yamaguchi, Y.; Oo, P.S.; Kyaw, M.T.H.; Sato, K.; Yamaguchi, R.; et al. The HDAC Inhibitor, SAHA, Prevents Colonic Inflammation by Suppressing Pro-inflammatory Cytokines and Chemokines in DSS-induced Colitis. *Acta Histochem. Cytochem.* **2018**, *51*, 33–40, doi:10.1267/ahc.17033.
25. Jahagirdar, R.; Attwell, S.; Marusic, S.; Bendele, A.; Shenoy, N.; McLure, K.G.; Gilham, D.; Norek, K.; Hansen, H.C.; Yu, R.; et al. RVX-297, a BET Bromodomain Inhibitor, Has Therapeutic Effects in Preclinical Models of Acute Inflammation and Autoimmune Disease. *Mol. Pharm.* **2017**, *92*, 694–706, doi:10.1124/mol.117.110379.
26. Schilderink, R.; Bell, M.; Reginato, E.; Patten, C.; Rioja, I.; Hilbers, F.W.; Kabala, P.A.; Reedquist, K.A.; Tough, D.F.; Tak, P.P.; et al. BET bromodomain inhibition reduces maturation and enhances tolerogenic properties of human and mouse dendritic cells. *Mol. Immunol.* **2016**, *79*, 66–76, doi:10.1016/j.molimm.2016.09.010.
27. Yan, L.; Wang, F.; Xiaoxue, C.; Wang, J.; Zhao, Y.; Li, Y.; He, B. Zinc-dependent Deacetylase (HDAC) Inhibitors with Different Zinc Binding Groups. *Curr. Topics Med. Chem.* **2019**, *19*, 223–241.
28. Subramanian, S.; Bates, S.E.; Wright, J.J.; Espinoza-Delgado, I.; Piekarz, R.L. Clinical Toxicities of Histone Deacetylase Inhibitors. *Pharmaceuticals* **2010**, *3*, 2751–2767, doi:10.3390/ph3092751.
29. van Veggel, M.; Westerman, E.; Hamberg, P. Clinical Pharmacokinetics and Pharmacodynamics of Panobinostat. *Clin. Pharm.* **2018**, *57*, 21–29, doi:10.1007/s40262-017-0565-x.
30. Pervaiz, M.; Mishra, P.; Günther, S. Bromodomain Drug Discovery—The Past, the Present, and the Future. *Chem. Rec.* **2018**, *18*, 1808–1817, doi:10.1002/tcr.201800074.
31. Andrieu, G.; Belkina, A.C.; Denis, G.V. Clinical trials for BET inhibitors run ahead of the science. *Drug Discov. Today Technol.* **2016**, *19*, 45–50, doi:10.1016/j.ddtec.2016.06.004.
32. Needham, L.A.; Davidson, A.H.; Bawden, L.J.; Belfield, A.; Bone, E.A.; Brotherton, D.H.; Bryant, S.; Charlton, M.H.; Clark, V.L.; Davies, S.J.; et al. Drug Targeting to Monocytes and Macrophages Using Esterase-Sensitive Chemical Motifs. *J. Pharm. Exp.* **2011**, *339*, 132–142, doi:10.1124/jpet.111.183640.
33. Ghiboub, M.; Zhao, J.; Yim, A.Y.F.L.; Schilderink, R.; Verseijden, C.; van Hamersveld, P.H.P.; Duarte, J.M.; Hakvoort, T.B.M.; Admiraal, I.; Harker, N.R.; et al. HDAC3 Mediates the Inflammatory Response and LPS Tolerance in Human Monocytes and Macrophages. *Front. Immunol.* **2020**, *11*, 550769, doi:10.3389/fimmu.2020.550769.

34. Park, S.-Y.; Kim, J.-S. A short guide to histone deacetylases including recent progress on class II enzymes. *Exp. Mol. Med.* **2020**, *52*, 204–212, doi:10.1038/s12276-020-0382-4.

35. Marié, I.J.; Chang, H.-M.; Levy, D.E. HDAC stimulates gene expression through BRD4 availability in response to IFN and in interferonopathies. *J. Exp. Med.* **2018**, *215*, 3194–3212, doi:10.1084/jem.20180520.

36. Grabiec, A.M.; Korchynskyi, O.; Tak, P.P.; Reedquist, K.A. Histone deacetylase inhibitors suppress rheumatoid arthritis fibroblast-like synoviocyte and macrophage IL-6 production by accelerating mRNA decay. *Ann. Rheum. Dis.* **2011**, *71*, 424–431, doi:10.1136/ard.2011.154211.

37. Tang, J.; Yan, H.; Zhuang, S. Histone deacetylases as targets for treatment of multiple diseases. *Clin. Sci.* **2013**, *124*, 651–662, doi:10.1042/cs20120504.

38. Cao, F.; Zwinderman, M.R.; Van Merkerk, R.; Ettema, P.E.; Quax, W.J.; Dekker, F.J. Inhibitory selectivity among class I HDACs has a major impact on inflammatory gene expression in macrophages. *Eur. J. Med. Chem.* **2019**, *177*, 457–466, doi:10.1016/j.ejmech.2019.05.038.

39. Saito, A.; Yamashita, T.; Mariko, Y.; Nosaka, Y.; Tsuchiya, K.; Ando, T.; Suzuki, T.; Tsuruo, T.; Nakanishi, O. A synthetic inhibitor of histone deacetylase, MS-27-275, with marked in vivo antitumor activity against human tumors. *Proc. Natl. Acad. Sci. USA* **1999**, *96*, 4592–4597, doi:10.1073/pnas.96.8.4592.

40. Moradei, O.M.; Mallais, T.C.; Frechette, S.; Paquin, I.; Tessier, P.E.; Leit, S.M.; Fournel, M.; Bonfils, C.; Trachy-Bourget, M.-C.; Liu, J.; et al. Novel Aminophenyl Benzamide-Type Histone Deacetylase Inhibitors with Enhanced Potency and Selectivity. *J. Med. Chem.* **2007**, *50*, 5543–5546, doi:10.1021/jm701079h.

41. Cantley, M.D.; Fairlie, D.P.; Bartold, P.M.; Marino, V.; Gupta, P.K.; Haynes, D.R. Inhibiting histone deacetylase 1 suppresses both inflammation and bone loss in arthritis. *Rheumatology* **2015**, *54*, 1713–1723, doi:10.1093/rheumatology/kev022.

42. Leus, N.G.J.; Bosch, T.V.D.; van der Wouden, P.E.; Krist, K.; Ourailidou, M.E.; Eleftheriadis, N.; Kistemaker, L.E.M.; Bos, S.; Gjaltema, R.A.F.; Mekonnen, S.A.; et al. HDAC1-3 inhibitor MS-275 enhances IL10 expression in RAW264.7 macrophages and reduces cigarette smoke-induced airway inflammation in mice. *Sci. Rep.* **2017**, *7*, 45047, doi:10.1038/srep45047.

43. Ryu, Y.; Kee, H.J.; Sun, S.; Seok, Y.M.; Choi, S.Y.; Kim, G.R.; Kee, S.-J.; Pflieger, M.; Kurz, T.; Kim, H.-S.; et al. Class I histone deacetylase inhibitor MS-275 attenuates vasoconstriction and inflammation in angiotensin II-induced hypertension. *PLoS ONE* **2019**, *14*, e0213186, doi:10.1371/journal.pone.0213186.

44. Loh, Z.; Fitzsimmons, R.L.; Reid, R.C.; Ramnath, D.; Clouston, A.; Gupta, P.K.; Irvine, K.M.; Powell, E.E.; Schroder, K.; Stow, J.L.; et al. Inhibitors of class I histone deacetylases attenuate thioacetamide-induced liver fibrosis in mice by suppressing hepatic type 2 inflammation. *Br. J. Pharm.* **2019**, *176*, 3775–3790, doi:10.1111/bph.14768.

45. Zhang, H.; Zhang, W.; Jiao, F.; Li, X.; Zhang, H.; Wang, L.; Gong, Z. The Nephroprotective Effect of MS-275 on Lipopolysaccharide (LPS)-Induced Acute Kidney Injury by Inhibiting Reactive Oxygen Species (ROS)-Oxidative Stress and Endoplasmic Reticulum Stress. *Med. Sci. Monit.* **2018**, *24*, 2620–2630, doi:10.12659/msm.906362.

46. Lin, H.-S.; Hu, C.-Y.; Chan, H.-Y.; Liew, Y.-Y.; Huang, H.-P.; Lepescheux, L.; Bastianelli, E.; Baron, R.; Rawadi, G.; Clément-Lacroix, P. Anti-rheumatic activities of histone deacetylase (HDAC) inhibitors in vivo in collagen-induced arthritis in rodents. *Br. J. Pharm.* **2007**, *150*, 862–872, doi:10.1038/sj.bjp.0707165.

47. Bombardo, M.; Saponara, E.; Malagola, E.; Chen, R.; Seleznik, G.M.; Haumaitre, C.; Quilichini, E.; Zabel, A.; Reding, T.; Graf, R.; et al. Class I histone deacetylase inhibition improves pancreatitis outcome by limiting leukocyte recruitment and acinar-to-ductal metaplasia. *Br. J. Pharm.* **2017**, *174*, 3865–3880, doi:10.1111/bph.13984.

48. Walewski, J.; Paszkiewicz-Kozik, E.; Borsaru, G.; Hellmann, A.; Janikova, A.; Warszewska, A.; Mais, A.; Ammendola, A.; Herz, T.; Krauss, B.; et al. Resminostat in patients with relapsed or refractory Hodgkin lymphoma: Results of the phase II SAPHIRE study. *Leuk. Lymphoma* **2019**, *60*, 675–684, doi:10.1080/10428194.2018.1492122.
49. Kitazono, S.; Fujiwara, Y.; Nakamichi, S.; Mizugaki, H.; Nokihara, H.; Yamamoto, N.; Yamada, Y.; Inukai, E.; Nakamura, O.; Tamura, T. A phase I study of resminostat in Japanese patients with advanced solid tumors. *Cancer Chemother. Pharm.* **2015**, *75*, 1155–1161, doi:10.1007/s00280-015-2741-8.
50. Boumber, Y.; Younes, A.; Garcia-Manero, G. Mocetinostat (MGCD0103): A review of an isotype-specific histone deacetylase inhibitor. *Expert Opin. Investig. Drugs* **2011**, *20*, 823–829, doi:10.1517/13543784.2011.577737.
51. Knipstein, J.; Gore, L. Entinostat for treatment of solid tumors and hematologic malignancies. *Expert Opin. Investig. Drugs* **2011**, *20*, 1455–1467, doi:10.1517/13543784.2011.613822.
52. Ruiz, R.; Raez, E.L.; Rolfo, C. Entinostat (SNDX-275) for the treatment of non-small cell lung cancer. *Expert Opin. Investig. Drugs* **2015**, *24*, 1101–1109, doi:10.1517/13543784.2015.1056779.
53. Giannopoulou, A.F.; Velentzas, A.D.; Konstantakou, E.G.; Avgeris, M.; Katarachia, S.A.; Papandreou, N.C.; Kalavros, N.I.; Mpakou, V.E.; Iconomidou, V.; Anastasiadou, E.; et al. Revisiting Histone Deacetylases in Human Tumorigenesis: The Paradigm of Urothelial Bladder Cancer. *Int. J. Mol. Sci.* **2019**, *20*, 1291, doi:10.3390/ijms20061291.
54. Lobera, M.; Madauss, K.P.; Pohlhaus, D.T.; Wright, Q.G.; Trocha, M.; Schmidt, D.R.; Baloglu, E.; Trump, R.P.; Head, M.S.; Hofmann, G.A.; et al. Selective class IIa histone deacetylase inhibition via a nonchelating zinc-binding group. *Nat. Chem. Biol.* **2013**, *9*, 319–325, doi:10.1038/nchembio.1223.
55. Guerriero, J.L.; Sotayo, A.; Ponichtera, H.E.; Castrillon, J.A.; Pourzia, A.L.; Schad, S.; Johnson, S.F.; Carrasco, R.D.; Lazo, S.; Bronson, R.T.; et al. Class IIa HDAC inhibition reduces breast tumours and metastases through anti-tumour macrophages. *Nat. Cell Biol.* **2017**, *543*, 428–432, doi:10.1038/nature21409.
56. Zhang, W.; Guan, Y.; Bayliss, G.P.; Zhuang, S. Class IIa HDAC inhibitor TMP195 alleviates lipopolysaccharide-induced acute kidney injury. *Am. J. Physiol. Physiol.* **2020**, *319*, F1015–F1026, doi:10.1152/ajprenal.00405.2020.
57. Yanginlar, C.; Logie, C. HDAC11 is a regulator of diverse immune functions. *Biochim. Biophys. Acta* **2018**, *1861*, 54–59, doi:10.1016/j.bbagrm.2017.12.002.
58. Janczura, K.J., Volmar, C.H.; Sartor, G.C.; Rao, S.J.; Ricciardi, N.R.; Lambert, G.; Brothers, S.P.; Wahlestedt, C. Inhibition of HDAC3 reverses Alzheimer's disease-related pathologies in vitro and in the 3xTg-AD mouse model. *Proc. Natl. Acad. Sci. USA* **2018**, *115*, E11148–E11157.
59. Leus, N.G.; van der Wouden, P.E.; van den Bosch, T.; Hooghiemstra, W.T.; Ourailidou, M.E.; Kistemaker, L.E.; Bischoff, R.; Gosens, R.; Haisma, H.J.; Dekker, F.J. HDAC 3-selective inhibitor RGFP966 demonstrates anti-inflammatory properties in RAW 264.7 macrophages and mouse precision-cut lung slices by attenuating NF-κB p65 transcriptional activity. *Biochem. Pharmacol.* **2016**, *108*, 58–74.
60. Zhang, L.; Chen, Y.; Jiang, Q.; Song, W.; Zhang, L. Therapeutic potential of selective histone deacetylase 3 inhibition. *Eur. J. Med. Chem.* **2019**, *162*, 534–542, doi:10.1016/j.ejmech.2018.10.072.
61. Cao, F.; Zwinderman, M.R.; Dekker, F.J. The Process and Strategy for Developing Selective Histone Deacetylase 3 Inhibitors. *Molecules* **2018**, *23*, 551, doi:10.3390/molecules23030551.
62. Huang, W.-J., Wang, Y.-C.; Chao, S.-W.; Yang, C.-Y.; Chen, L.-C.; Lin, M.-H.; Hou, W.-C.; Chen, M.-Y.; Lee, T.-L.; Yang, P.; et al. Synthesis and biological evaluation of *ortho*-aryl N-hydroxycinnamides as potent histone deacetylase (HDAC) 8 isoform-selective inhibitors. *ChemMedChem* **2012**, *7*, 1815–1824.
63. Jan, J.-S.; Chou, Y.-C.; Cheng, Y.-W.; Chen, C.-K.; Huang, W.-J.; Hsiao, G. The Novel HDAC8 Inhibitor WK2-16 Attenuates Lipopolysaccharide-Activated Matrix Metalloproteinase-9 Expression in Human Monocytic Cells and Improves Hypercytokinemia in vivo. *Int. J. Mol. Sci.* **2017**, *18*, 1394, doi:10.3390/ijms18071394.

64. Ran, J.; Zhou, J. Targeted inhibition of histone deacetylase 6 in inflammatory diseases. *Thorac. Cancer* **2019**, *10*, 405–412, doi:10.1111/1759-7714.12974.

65. Kutil, Z.; Mikešová, J.; Zessin, M.; Meleshin, M.; Nováková, Z.; Alquicer, G.; Kozikowski, A.; Sippl, W.; Bařinka, C.; Schutkowski, M. Continuous Activity Assay for HDAC11 Enabling Reevaluation of HDAC Inhibitors. *ACS Omega* **2019**, *4*, 19895–19904, doi:10.1021/acsomega.9b02808.

66. Solomon, J.M.; Pasupuleti, R.; Xu, L.; McDonagh, T.; Curtis, R.; DiStefano, P.S.; Huber, L.J. Inhibition of SIRT1 Catalytic Activity Increases p53 Acetylation but Does Not Alter Cell Survival following DNA Damage. *Mol. Cell. Biol.* **2006**, *26*, 28–38, doi:10.1128/mcb.26.1.28-38.2006.

67. Chen, X.; Wales, P.; Quinti, L.; Zuo, F.; Moniot, S.; Hérisson, F.; Rauf, N.A.; Wang, H.; Silverman, R.B.; Ayata, C.; et al. The Sirtuin-2 Inhibitor AK7 Is Neuroprotective in Models of Parkinson's Disease but Not Amyotrophic Lateral Sclerosis and Cerebral Ischemia. *PLoS ONE* **2015**, *10*, e0116919, doi:10.1371/journal.pone.0116919.

68. Gillespie, J.; Savic, S.; Wong, C.; Hempshall, A.; Inman, M.; Emery, P.; Grigg, R.; McDermott, M.F. Histone deacetylases are dysregulated in rheumatoid arthritis and a novel histone deacetylase 3-selective inhibitor reduces interleukin-6 production by peripheral blood mononuclear cells from rheumatoid arthritis patients. *Arthritis Rheum.* **2012**, *64*, 418–422, doi:10.1002/art.33382.

69. Lei, L.; Bai, G.; Wang, X.; Liu, S.; Xia, J.; Wu, S.; Huan, Y.; Shen, Z. Histone deacetylase 3-selective inhibitor RGFP966 ameliorates impaired glucose tolerance through β-cell protection. *Toxicol. Appl. Pharm.* **2020**, *406*, 115189, doi:10.1016/j.taap.2020.115189.

70. Zhang, H.; Ji, L.; Yang, Y.; Wei, Y.; Zhang, X.; Gang, Y.; Lu, J.; Bai, L. The Therapeutic Effects of Treadmill Exercise on Osteoarthritis in Rats by Inhibiting the HDAC3/NF-KappaB Pathway in vivo and in vitro. *Front Physiol.* **2019**, *10*, 1060.

71. Zhang, W.; Sun, X.; Ba, G.; Tang, R.; Lin, H. RGFP966, a selective HDAC3 inhibitor, ameliorates allergic and inflammatory responses in an OVA-induced allergic rhinitis mouse model. *Int. Immunopharmacol.* **2021**, *93*, 107400, doi:10.1016/j.intimp.2021.107400.

72. Zhang, J.; Xu, Z.; Gu, J.; Jiang, S.; Liu, Q.; Zheng, Y.; Freedman, J.H.; Sun, J.; Cai, L. HDAC3 inhibition in diabetic mice may activate Nrf2 preventing diabetes-induced liver damage and FGF21 synthesis and secretion leading to aortic protection. *Am. J. Physiol. Metab.* **2018**, *315*, E150–E162, doi:10.1152/ajpendo.00465.2017.

73. Zhang, M.-J.; Zhao, Q.-C.; Xia, M.-X.; Chen, J.; Chen, Y.-T.; Cao, X.; Liu, Y.; Yuan, Z.-Q.; Wang, X.-Y; Xu, Y. The HDAC3 inhibitor RGFP966 ameliorated ischemic brain damage by downregulating the AIM2 inflammasome. *FASEB J.* **2019**, *34*, 648–662, doi:10.1096/fj.201900394rrr.

74. Xu, Z.; Tong, Q.; Zhang, Z.; Wang, S.; Zheng, Y.; Liu, Q.; Qian, L.-B.; Chen, S.-Y.; Sun, J.; Cai, L. Inhibition of HDAC3 prevents diabetic cardiomyopathy in OVE26 mice via epigenetic regulation of DUSP5-ERK1/2 pathway. *Clin. Sci.* **2017**, *131*, 1841–1857.

75. Angiolilli, C.; Kabala, P.A.; Grabiec, A.M.; I.M. van Baarsen, I.M.; Ferguson, B.S.; García, S.; Fernandez, B.M.; McKinsey, T.A.; Tak, P.P.; Fossati, G.; et al. Histone deacetylase 3 regulates the inflammatory gene expression programme of rheumatoid arthritis fibroblast-like synoviocytes. *Ann. Rheum. Dis.* **2017**, *76*, 277–285.

76. Kozikowski, A.P.; Tapadar, S.; Luchini, D.N.; Kim, K.H.; Billadeau, D.D. Use of the Nitrile Oxide Cycloaddition (NOC) Reaction for Molecular Probe Generation: A New Class of Enzyme Selective Histone Deacetylase Inhibitors (HDACIs) Showing Picomolar Activity at HDAC6. *J. Med. Chem.* **2008**, *51*, 4370–4373, doi:10.1021/jm8002894.

77. Santo, L.; Hideshima, T.; Kung, A.L.; Tseng, J.-C.; Tamang, D.; Yang, M.; Jarpe, M.; van Duzer, J.H.; Mazitschek, R.; Ogier, W.C.; et al. Preclinical activity, pharmacodynamic, and pharmacokinetic properties of a selective HDAC6 inhibitor, ACY-1215, in combination with bortezomib in multiple myeloma. *Blood* **2012**, *119*, 2579–2589, doi:10.1182/blood-2011-10-387365.

78. Choi, E.W.; Song, J.W.; Ha, N.; Choi, Y.I.; Kim, S. CKD-506, a novel HDAC6-selective inhibitor, improves

renal outcomes and survival in a mouse model of systemic lupus erythematosus. *Sci. Rep.* **2018**, *8*, 17297, doi:10.1038/s41598-018-35602-1.

79. Butler, K.V.; Kalin, J.; Brochier, C.; Vistoli, G.; Langley, B.; Kozikowski, A.P. Rational Design and Simple Chemistry Yield a Superior, Neuroprotective HDAC6 Inhibitor, Tubastatin, A. *J. Am. Chem. Soc.* **2010**, *132*, 10842–10846, doi:10.1021/ja102758v.
80. Jochems, J.; Boulden, J.; Lee, B.G.; Blendy, J.A.; Jarpe, M.; Mazitschek, R.; van Duzer, J.H.; Jones, S.; Berton, O. Antidepressant-Like Properties of Novel HDAC6-Selective Inhibitors with Improved Brain Bioavailability. *Neuropsychopharmacology* **2014**, *39*, 389–400, doi:10.1038/npp.2013.207.
81. Lee, J.W.; Lee, S.-M.; Chun, J.; Im, J.P.; Seo, S.-K.; Ha, N.; Y.; Choi, Y.I.; Kim, J.S. Novel Histone Deacetylase 6 Inhibitor CKD-506 Inhibits NF-κB Signaling in Intestinal Epithelial Cells and Macrophages and Ameliorates Acute and Chronic Murine Colitis. *Inflamm. Bowel Dis.* **2020**, *26*, 852–862.
82. Liu, T.; Wang, R.; Xu, H.; Song, Y.; Qi, Y. A Highly Potent and Selective Histone Deacetylase 6 Inhibitor Prevents DSS-Induced Colitis in Mice. *Biol. Pharm. Bull.* **2017**, *40*, 936–940, doi:10.1248/bpb.b16-01023.
83. Do, A.; Reid, R.C.; Lohman, R.-J.; Sweet, M.J.; Fairlie, D.P.; Iyer, A. An HDAC6 Inhibitor Confers Protection and Selectively Inhibits B-Cell Infiltration in DSS-Induced Colitis in Mice. *J. Pharm. Exp.* **2017**, *360*, 140–151, doi:10.1124/jpet.116.236711.
84. Park, J.K.; Jang, Y.J.; Oh, B.R.; Shin, J.; Bae, D.; Ha, N.; Choi, Y.I.; Youn, G.S.; Park, J.; Lee, E.Y.; et al. Therapeutic potential of CKD-506, a novel selective histone deacetylase 6 inhibitor, in a murine model of rheumatoid arthritis. *Arthritis Res.* **2020**, *22*, 1–9, doi:10.1186/s13075-020-02258-0.
85. Vishwakarma, S.; Iyer, L.R.; Muley, M.; Singh, P.K.; Shastry, A.; Saxena, A.; Kulathingal, J.; Vijaykanth, G.; Raghul, J.; Rajesh, N.; et al. Tubastatin, a selective histone deacetylase 6 inhibitor shows anti-inflammatory and anti-rheumatic effects. *Int. Immunopharmacol.* **2013**, *16*, 72–78, doi:10.1016/j.intimp.2013.03.016.
86. Ren, J.; Panther, E.; Liao, X.; Grammer, A.C.; Lipsky, P.E.; Reilly, C.M. The Impact of Protein Acetylation/Deacetylation on Systemic Lupus Erythematosus. *Int. J. Mol. Sci.* **2018**, *19*, 4007, doi:10.3390/ijms19124007.
87. Lopresti, P. The Selective HDAC6 Inhibitor ACY-738 Impacts Memory and Disease Regulation in an Animal Model of Multiple Sclerosis. *Front. Neurol.* **2019**, *10*, doi:10.3389/fneur.2019.00519.
88. Ren, Y.; Su, X.; Kong, L.; Li, M.; Zhao, X.; Yu, N.; Kang, J. Therapeutic effects of histone deacetylase inhibitors in a murine asthma model. *Inflamm. Res.* **2016**, *65*, 995–1008, doi:10.1007/s00011-016-0984-4.
89. Liu, L.; Zhou, X.; Shetty, S.; Hou, G.; Wang, Q.; Fu, J. HDAC6 inhibition blocks inflammatory signaling and caspase-1 activation in LPS-induced acute lung injury. *Toxicol. Appl. Pharm.* **2019**, *370*, 178–183, doi:10.1016/j.taap.2019.03.017.
90. Ellis, J.D.; Neil, D.A.; Inston, N.G.; Jenkinson, E.; Drayson, M.T.; Hampson, P.; Shuttleworth, S.J.; Ready, A.R.; Cobbold, M. Inhibition of Histone Deacetylase 6 Reveals a Potent Immunosuppressant Effect in Models of Transplantation. *Transplantation* **2016**, *100*, 1667–1674, doi:10.1097/tp.0000000000001208.
91. Tsuji, G.; Okiyama, N.; Villarroel, V.A.; Katz, S.I. Histone deacetylase 6 inhibition impairs effector CD8 T-cell functions during skin inflammation. *J. Allergy Clin. Immunol.* **2015**, *135*, 1228–1239, doi:10.1016/j.jaci.2014.10.002.
92. Li, Y.; Zhao, T.; Liu, B.; Halaweish, I.; Mazitschek, R.; Duan, X.; Alam, H.B. Inhibition of histone deacetylase 6 improves long-term survival in a lethal septic model. *J. Trauma Acute Care Surg.* **2015**, *78*, 378–385, doi:10.1097/ta.0000000000000510.
93. Zhang, W.-B.; Zhang, H.-Y.; Jiao, F.-Z.; Wang, L.-W.; Zhang, H.; Gong, Z.-J. Histone deacetylase 6 inhibitor ACY-1215 protects against experimental acute liver failure by regulating the TLR4-MAPK/NF-κB

pathway. *Biomed. Pharmacother.* **2018**, *97*, 818–824.

94. Regna, N.L.; Vieson, M.D.; Luo, X.M.; Chafin, C.B.; Puthiyaveetil, A.G.; Hammond, S.E.; Caudell, D.L.; Jarpe, M.B.; Reilly, C.M. Specific HDAC6 inhibition by ACY-738 reduces SLE pathogenesis in NZB/W mice. *Clin. Immunol.* **2016**, *162*, 58–73, doi:10.1016/j.clim.2015.11.007.
95. Zhou, W.; Yang, J.; Saren, G.; Zhao, H.; Cao, K.; Fu, S.; Pan, X.; Zhang, H.; Wang, A.; Chen, X. HDAC6-specific inhibitor suppresses Th17 cell function via the HIF-1α pathway in acute lung allograft rejection in mice. *Theranostics* **2020**, *10*, 6790–6805, doi:10.7150/thno.44961.
96. Lee, J.; Hong, E.C.; Jeong, H.; Hwang, J.W.; Kim, H.; Bae, E.-K.; Ahn, J.K.; Choi, Y.-L.; Han, J.; Cha, H.-S.; et al. A novel histone deacetylase 6-selective inhibitor suppresses synovial inflammation and joint destruction in a collagen antibody-induced arthritis mouse model. *Int. J. Rheum. Dis.* **2015**, *18*, 514–523, doi:10.1111/1756-185x.12501.
97. Yee, A.J.; Bensinger, W.I.; Supko, J.G.; Voorhees, P.M.; Berdeja, J.G.; Richardson, P.G.; Libby, E.N.; Wallace, E.E.; Birrer, E.N.; Burke, J.N.; et al. Ricolinostat plus lenalidomide, and dexamethasone in relapsed or refractory multiple myeloma: A multicentre phase 1b trial. *Lancet Oncol.* **2016**, *17*, 1569–1578, doi:10.1016/s1470-2045(16)30375-8.
98. Vogl, D.T.; Raje, N.; Jagannath, S.; Richardson, P.; Hari, P.; Orlowski, R.; Supko, J.G.; Tamang, D.; Yang, M.; Jones, S.S.; et al. Ricolinostat, the First Selective Histone Deacetylase 6 Inhibitor, in Combination with Bortezomib and Dexamethasone for Relapsed or Refractory Multiple Myeloma. *Clin. Cancer Res.* **2017**, *23*, 3307–3315, doi:10.1158/1078-0432.ccr-16-2526.
99. Shultz, M.D.; Cao, X.; Chen, C.H.; Cho, Y.S.; Davis, N.R.; Eckman, J.; Fan, J.; Fekete, A.; Firestone, B.; Flynn, J.; et al. Optimization of the in Vitro Cardiac Safety of Hydroxamate-Based Histone Deacetylase Inhibitors. *J. Med. Chem.* **2011**, *54*, 4752–4772, doi:10.1021/jm200388e.
100. Kopljar, I.; Gallacher, D.J.; De Bondt, A.; Cougnaud, L.; Vlaminckx, E.; Wyngaert, I.V.D.; Lu, H.R. Functional and Transcriptional Characterization of Histone Deacetylase Inhibitor-Mediated Cardiac Adverse Effects in Human Induced Pluripotent Stem Cell-Derived Cardiomyocytes. *Stem Cells Transl. Med.* **2016**, *5*, 602–612, doi:10.5966/sctm.2015-0279.
101. Li, P.; Ninomiya, H.; Kurata, Y.; Kato, M.; Miake, J.; Yamamoto, Y.; Igawa, O.; Nakai, A.; Higaki, K.; Toyoda, F.; et al. Reciprocal Control of hERG Stability by Hsp70 and Hsc70 With Implication for Restoration of LQT2 Mutant Stability. *Circ. Res.* **2011**, *108*, 458–468, doi:10.1161/circresaha.110.227835.
102. Lin, F.-L.; Yen, J.-L.; Kuo, Y.-C.; Kang, J.-J.; Cheng, Y.-W.; Huang, W.-J.; Hsiao, G. HADC8 Inhibitor WK2-16 Therapeutically Targets Lipopolysaccharide-Induced Mouse Model of Neuroinflammation and Microglial Activation. *Int. J. Mol. Sci.* **2019**, *20*, 410.
103. Balasubramanian, S.; Ramos, J.; Luo, W.; Sirisawad, M.; Verner, E.; Buggy, J.J. A novel histone deacetylase 8 (HDAC8)-specific inhibitor PCI-34051 induces apoptosis in T-cell lymphomas. *Leukemia* **2008**, *22*, 1026–1034, doi:10.1038/leu.2008.9.
104. Zuberi, R.I.; Hsu, D.K.; Kalayci, O.; Chen, H.-Y.; Sheldon, H.K.; Yu, L.; Apgar, J.R.; Kawakami, T.; Lilly, C.M.; Liu, F.-T. Critical Role for Galectin-3 in Airway Inflammation and Bronchial Hyperresponsiveness in a Murine Model of Asthma. *Am. J. Pathol.* **2004**, *165*, 2045–2053, doi:10.1016/s0002-9440(10)63255-5.
105. Pavlik, C.M.; Wong, C.Y.B.; Ononye, S.; Lopez, D.D.; Engene, N.; McPhail, K.L.; Gerwick, W.H.; Balunas, M.J. Santacruzamate A, a Potent and Selective Histone Deacetylase Inhibitor from the Panamanian Marine Cyanobacterium cf. Symploca sp. *J. Nat. Prod.* **2013**, *76*, 2026–2033, doi:10.1021/np400198r.
106. Jiao, F.-Z.; Wang, *Y.;* Zhang, H.-Y.; Zhang, W.-B.; Wang, L.-W.; Gong, Z.-J. Histone Deacetylase 2 Inhibitor CAY10683 Alleviates Lipopolysaccharide Induced Neuroinflammation through Attenuating TLR4/NF-κB Signaling Pathway. *Neurochem. Res.* **2018**, *43*, 1161–1170.
107. Poralla, L.; Stroh, T.; Erben, U.; Sittig, M.; Liebig, S.; Siegmund, B.; Glauben, R. Histone deacetylase 5 regulates the inflammatory response of macrophages. *J. Cell. Mol. Med.* **2015**, *19*, 2162–2171, doi:10.1111/jcmm.12595.

108. Liao, W.; Sun, J.; Liu, W.; Li, W.; Jia, J.; Ou, F.; Su, K.; Zheng, Y.; Zhang, Z.; Sun, Y. HDAC10 upregulation contributes to interleukin 1β-mediated inflammatory activation of synovium-derived mesenchymal stem cells in temporomandibular joint. *J. Cell. Physiol.* **2019**, *234*, 12646–12662, doi:10.1002/jcp.27873.

109. Son, S.I.; Cao, J.; Zhu, C.-L.; Miller, S.P.; Lin, H. Activity-Guided Design of HDAC11-Specific Inhibitors. *ACS Chem. Biol.* **2019**, *14*, 1393–1397, doi:10.1021/acschembio.9b00292.

110. Oishi, Y.; Manabe, I. Macrophages in inflammation, repair and regeneration. *Int. Immunol.* **2018**, *30*, 511–528, doi:10.1093/intimm/dxy054.

111. Koh, T.J.; DiPietro, L.A. Inflammation and wound healing: The role of the macrophage. *Expert Rev. Mol. Med.* **2011**, *13*, e23, doi:10.1017/s1462399411001943.

112. Lian, J.; Nelson, R.; Lehner, R. Carboxylesterases in lipid metabolism: From mouse to human. *Protein Cell* **2018**, *9*, 178–195, doi:10.1007/s13238-017-0437-z.

113. Satoh, T.; Hemmerlein, B.; Zschunke, F.; Radzun, H.J. In situ Detection of Human Monocyte/Macrophage Serine Esterase-1 mRNA Expression in Human Tissues. *Pathobiology* **1999**, *67*, 158–162, doi:10.1159/000028066.

114. Imai, T. Human Carboxylesterase Isozymes: Catalytic Properties and Rational Drug Design. *Drug Metab. Pharm.* **2006**, *21*, 173–185, doi:10.2133/dmpk.21.173.

115. Ossenkoppele, G.J.; Lowenberg, B.; Zachee, P.; Vey, N.; Breems, D.; van de Loosdrecht, A.A.; Davidson, A.H.; Wells, G.; Needham, L.; Bawden, L.; et al. A phase I first-in-human study with tefinostat-a monocyte/macrophage targeted histone deacetylase inhibitor-in patients with advanced haematological malignancies. *Br. J. Haematol.* **2013**, *162*, 191–201, doi:10.1111/bjh.12359.

116. Elfiky, A.; Ghiboub, M.; van Hamersveld, H.P.; Welting, O.; van den Berg, I.; Rahman, S.; de Winther, M.; Becker, M.; Wildenberg, M.E.; Furze, R.; et al. Mo1104 Mononuclear Myeloid Cell Targeted Histone Deactylase (HDAC) Inhibitor Demonstrates Potent Activity in Monocytes and Impairs Colon Monocytes to Macrophage Differentation During Acute DSS Colitis. *Gastroenterology* **2020**, *158*, 789–790, doi:10.1016/s0016-5085(20)32645-7.

117. Luque-Martin, R.; van den Bossche, J.; Furze, R.C.; Neele, A.E.; van der Velden, S.; Gijbels, M.J.J.; van Roomen, C.P.P.A.; Bernard, S.G.; de Jonge, W.J.; Rioja, I.; et al. Targeting Histone Deacetylases in Myeloid Cells Inhibits Their Maturation and Inflammatory Function with Limited Effects on Atherosclerosis. *Front. Pharm.* **2019**, *10*, 1242, doi:10.3389/fphar.2019.01242.

118. Fan, X.; Zhang, H.; Cheng, Y.; Jiang, X.; Zhu, J.; Jin, T. Double Roles of Macrophages in Human Neuroimmune Diseases and Their Animal Models. *Mediat. Inflamm.* **2016**, *2016*, 1–13, doi:10.1155/2016/8489251.

119. Liu, Y.-C.; Zou, X.-B.; Chai, Y.-F.; Yao, Y.-M. Macrophage Polarization in Inflammatory Diseases. *Int. J. Biol. Sci.* **2014**, *10*, 520–529, doi:10.7150/ijbs.8879.

120. Fujisawa, T.; Filippakopoulos, P. Functions of bromodomain-containing proteins and their roles in homeostasis and cancer. *Nat. Rev. Mol. Cell Biol.* **2017**, *18*, 246–262.

121. Meslamani, J.; Smith, S.G.; Sanchez, R.; Zhou, M.-M. Structural features and inhibitors of bromodomains. *Drug Discov. Today: Technol.* **2016**, *19*, 3–15, doi:10.1016/j.ddtec.2016.09.001.

122. Dawson, M.A.; Prinjha, R.K.; Dittmann, A.; Giotopoulos, G.; Bantscheff, M.; Chan, W.-I.; Robson, S.C.; Chung, C.-W.; Hopf, C.; Savitski, M.M.; et al. Inhibition of BET recruitment to chromatin as an effective treatment for MLL-fusion leukaemia. *Nat. Cell Biol.* **2011**, *478*, 529–533, doi:10.1038/nature10509.

123. Cochran, A.G.; Conery, A.R.; Sims, R.J. Bromodomains: A new target class for drug development. *Nat. Rev. Drug Discov.* **2019**, *18*, 609–628, doi:10.1038/s41573-019-0030-7.

124. Guo, D.; Hong, D.; Wang, P.; Wang, J.; Chen, L.; Zhao, W.; Zhang, L.; Yao, C.; Chu, B.; Chen, S.; et al. Histone deacetylase inhibitor CI-994 inhibits osteoclastogenesis via suppressing NF-κB and the

downstream c-Fos/NFATc1 signaling pathways. *Eur. J. Pharmacol.* **2019**, *848*, 96–104.

125. Malvaez, M.; McQuown, S.C.; Rogge, G.A.; Astarabadi, M.; Jacques, V.; Carreiro, S.; Rusche, J.R.; Wood, M.A. HDAC3-selective inhibitor enhances extinction of cocaine-seeking behavior in a persistent manner. *Proc. Natl. Acad. Sci. USA* **2013**, *110*, 2647–2652, doi:10.1073/pnas.1213364110.
126. Liu, Z.; Tian, B.; Chen, H.; Wang, P.; Brasier, A.R.; Zhou, J. Discovery of potent and selective BRD4 inhibitors capable of blocking TLR3-induced acute airway inflammation. *Eur. J. Med. Chem.* **2018**, *151*, 450–461, doi:10.1016/j.ejmech.2018.04.006.
127. Tian, B.; Liu, Z.; Litvinov, J.; Maroto, R.; Jamaluddin, M.; Rytting, E.; Patrikeev, I.; Ochoa, L.; Vargas, G.; Motamedi, M.; et al. Efficacy of Novel Highly Specific Bromodomain-Containing Protein 4 Inhibitors in Innate Inflammation–Driven Airway Remodeling. *Am. J. Respir. Cell Mol. Biol.* **2019**, *60*, 68–83, doi:10.1165/rcmb.2017-0445oc.
128. Theodoulou, N.H.; Bamborough, P.; Bannister, A.J.; Becher, I.; Bit, R.A.; Che, K.H.; Chung, C.-W.; Dittmann, A.; Drewes, G.; Drewry, D.H.; et al. Discovery of I-BRD9, a Selective Cell Active Chemical Probe for Bromodomain Containing Protein 9 Inhibition. *J. Med. Chem.* **2016**, *59*, 1425–1439, doi:10.1021/acs.jmedchem.5b00256.
129. Martin, L.J.; Koegl, M.; Bader, G.; Cockcroft, X.-L.; Fedorov, O.; Fiegen, D.; Gerstberger, T.; Hofmann, M.H.; Hohmann, A.F.; Kessler, D.; et al. Structure-Based Design of an in vivo Active Selective BRD9 Inhibitor. *J. Med. Chem.* **2016**, *59*, 4462–4475, doi:10.1021/acs.jmedchem.5b01865.
130. Lv, Q.; Yang, A.; Shi, W.; Chen, F.; Liu, Y.; Liu, Y.; Wang, D. Calcipotriol and iBRD9 reduce obesity in Nur77 knockout mice by regulating the gut microbiota, improving intestinal mucosal barrier function. *Int. J. Obes.* **2020**, *44*, 1052–1061, doi:10.1038/s41366-020-0564-0.
131. Gilan, O.; Rioja, I.; Knezevic, K.; Bell, M.J.; Yeung, M.M.; Harker, N.R.; Lam, E.Y.N.; Chung, C.-W.; Bamborough, P.; Petretich, M.; et al. Selective targeting of BD1 and BD2 of the BET proteins in cancer and immunoinflammation. *Science* **2020**, *368*, 387–394, doi:10.1126/science.aaz8455.
132. Taniguchi, Y. The Bromodomain and Extra-Terminal Domain (BET) Family: Functional Anatomy of BET Paralogous Proteins. *Int. J. Mol. Sci.* **2016**, *17*, 1849, doi:10.3390/ijms17111849.
133. Nicodeme, E.; Jeffrey, K.L.; Schaefer, U.; Beinke, S.; Dewell, S.; Chung, C.-W.; Chandwani, R.; Marazzi, I.; Wilson, P.; Coste, H.; et al. Suppression of inflammation by a synthetic histone mimic. *Nat. Cell Biol.* **2010**, *468*, 1119–1123, doi:10.1038/nature09589.
134. Filippakopoulos, P.; Qi, J.; Picaud, S.; Shen, Y.; Smith, M.C.; Fedorov, O.; Morse, E.M.; Keates, T.; Hickman, T.T.; Felletar, I.; et al. Selective inhibition of BET bromodomains. *Nature* **2010**, *468*, 1067–1073, doi:10.1038/nature09504.
135. Wyce, A.; Ganji, G.; Smitheman, K.N.; Chung, C.-W.; Korenchuk, S.; Bai, Y.; Barbash, O.; Le, B.; Craggs, P.D.; McCabe, M.T.; et al. BET Inhibition Silences Expression of MYCN and BCL2 and Induces Cytotoxicity in Neuroblastoma Tumor Models. *PLoS ONE* **2013**, *8*, e72967, doi:10.1371/journal.pone.0072967.
136. Chan, C.H.; Fang, C.; Qiao, Y.; Yarilina, A.; Prinjha, R.K.; Ivashkiv, L.B. BET bromodomain inhibition suppresses transcriptional responses to cytokine-Jak-STAT signaling in a gene-specific manner in human monocytes. *Eur. J. Immunol.* **2015**, *45*, 287–297, doi:10.1002/eji.201444862.
137. Miller, T.C.R.; Simon, B.; Rybin, V.; Grötsch, H.; Curtet, S.; Khochbin, S.; Carlomagno, T.; Müller, C.W. A bromodomain–DNA interaction facilitates acetylation-dependent bivalent nucleosome recognition by the BET protein BRDT. *Nat. Commun.* **2016**, *7*, 13855, doi:10.1038/ncomms13855.
138. Baud, M.G.J.; Lin-Shiao, E.; Cardote, T.; Tallant, C.; Pschibul, A.; Chan, K.-H.; Zengerle, M.; Garcia, J.R.; Kwan, T.T.-L.; Ferguson, F.M.; et al. A bump-and-hole approach to engineer controlled selectivity of BET bromodomain chemical probes. *Science* **2014**, *346*, 638–641, doi:10.1126/science.1249830.
139. Shi, J.; Wang, E.; Milazzo, J.P.; Wang, Z.; Kinney, J.B.; Vakoc, C.R. Discovery of cancer drug targets by CRISPR-Cas9 screening of protein domains. *Nat. Biotechnol.* **2015**, *33*, 661–667, doi:10.1038/nbt.3235.

140. Faivre, E.J.; McDaniel, K.F.; Albert, D.H.; Mantena, S.R.; Plotnik, J.P.; Wilcox, D.; Zhang, L.; Bui, M.H.; Sheppard, G.S.; Wang, L.; et al. Selective inhibition of the BD2 bromodomain of BET proteins in prostate cancer. *Nat. Cell Biol.* **2020**, *578*, 306–310, doi:10.1038/s41586-020-1930-8.

141. Filippakopoulos, P.; Knapp, S. Next-generation epigenetic inhibitors. *Science* **2020**, *368*, 367–368, doi:10.1126/science.abb5060.

142. Zhang, G.; Plotnikov, A.N.; Rusinova, E.; Shen, T.; Morohashi, K.; Joshua, J.; Zeng, L.; Mujtaba, S.; Ohlmeyer, M.; Zhou, M.-M. Structure-Guided Design of Potent Diazobenzene Inhibitors for the BET Bromodomains. *J. Med. Chem.* **2013**, *56*, 9251–9264, doi:10.1021/jm401334s.

143. Nowak, R.P.; DeAngelo, S.L.; Buckley, D.; He, Z.; Donovan, K.A.; An, J.; Safaee, N.; Jedrychowski, M.P.; Ponthier, C.M.; Ishoey, M.; et al. Plasticity in binding confers selectivity in ligand-induced protein degradation. *Nat. Chem. Biol.* **2018**, *14*, 706–714, doi:10.1038/s41589-018-0055-y.

144. Qin, C.; Hu, Y.; Zhou, B.; Fernandez-Salas, E.; Yang, C.-Y.; Liu, L.; McEachern, D.; Przybranowski, S.; Wang, M.; Stuckey, J.; et al. Discovery of QCA570 as an Exceptionally Potent and Efficacious Proteolysis Targeting Chimera (PROTAC) Degrader of the Bromodomain and Extra-Terminal (BET) Proteins Capable of Inducing Complete and Durable Tumor Regression. *J. Med. Chem.* **2018**, *61*, 6685–6704, doi:10.1021/acs.jmedchem.8b00506.

145. Yim, A.Y.F.L.; Duijvis, N.W.; Zhao, J.; de Jonge, W.J.; D'Haens, G.R.A.M.; Mannens, M.M.A.M.; Mul, A.N.P.M.; Velde, A.A.T.; Henneman, P. Peripheral blood methylation profiling of female Crohn's disease patients. *Clin. Epigenetics* **2016**, *8*, 1–13, doi:10.1186/s13148-016-0230-5.

146. Franke, A., McGovern, D.P.B.; Barrett, J.C.; Wang, K.; Radford-Smith, G.L.; Ahmad, T.; Lees, C.W.; Balschun, T.; Lee, J.; Roberts, R.; et al. Genome-wide meta-analysis increases to 71 the number of confirmed Crohn's disease susceptibility loci. *Nat. Genet.* **2010**, *42*, 1118–1125.

147. Sima, X.; He, J.; Peng, J.; Xu, Y.; Zhang, F.; Deng, L. The genetic alteration spectrum of the SWI/SNF complex: The oncogenic roles of BRD9 and ACTL6A. *PLoS ONE* **2019**, *14*, e0222305, doi:10.1371/journal.pone.0222305.

148. Loo, C.-S.; Gatchalian, J.; Liang, Y.; Leblanc, M.; Xie, M.; Ho, J.; Venkatraghavan, B.; Hargreaves, D.C.; Zheng, Y. A Genome-wide CRISPR Screen Reveals a Role for the Non-canonical Nucleosome-Remodeling BAF Complex in Foxp3 Expression and Regulatory T Cell Function. *Immunity* **2020**, *53*, 143–157.e8, doi:10.1016/j.immuni.2020.06.011.

149. Wen, A.Y.; Sakamoto, K.M.; Miller, L.S. The Role of the Transcription Factor CREB in Immune Function. *J. Immunol.* **2010**, *185*, 6413–6419, doi:10.4049/jimmunol.1001829.

150. Zhang, S.; Xu, W.; Wang, H.; Cao, M.; Li, M.; Zhao, J.; Hu, Y.; Wang, Y.; Li, S.; Xie, Y.; et al. Inhibition of CREB-mediated ZO-1 and activation of NF-κB-induced IL-6 by colonic epithelial MCT4 destroys intestinal barrier function. *Cell Prolif.* **2019**, *52*, e12673.

151. Takeba, Y.; Suzuki, N.; Wakisaka, S.; Takeno, M.; Kaneko, A.; Asai, T.; Sakane, T. Involvement of cAMP responsive element binding protein (CREB) in the synovial cell hyperfunction in patients with rheumatoid arthritis. *Clin. Exp. Rheumatol.* **2000**, *18*, 47–55.

152. Chekler, E.L.P.; Pellegrino, J.A.; Lanz, T.A.; Denny, R.A.; Flick, A.C.; Coe, J.; Langille, J.; Basak, A.; Liu, S.; Stock, I.A.; et al. Transcriptional Profiling of a Selective CREB Binding Protein Bromodomain Inhibitor Highlights Therapeutic Opportunities. *Chem. Biol.* **2015**, *22*, 1588–1596, doi:10.1016/j.chembiol.2015.10.013.

153. Best, J.L.; Amezcua, C.A.; Mayr, B.; Flechner, L.; Murawsky, C.M.; Emerson, B.; Zor, T.; Gardner, K.H.; Montminy, M. Identification of small-molecule antagonists that inhibit an activator: Coactivator interaction. *Proc. Natl. Acad. Sci. USA* **2004**, *101*, 17622–17627, doi:10.1073/pnas.0406374101.

154. Igoe, N.; Bayle, E.D.; Tallant, C.; Fedorov, O.; Meier, J.C.; Savitsky, P.; Rogers, C.; Morias, Y.; Scholze, S.; Boyd, H.; et al. Design of a Chemical Probe for the Bromodomain and Plant Homeodomain Finger-Containing (BRPF) Family of Proteins. *J. Med. Chem.* **2017**, *60*, 6998–7011, doi:10.1021/acs.

jmedchem.7b00611.

155. Meier, J.C.; Tallant, C.; Fedorov, O.; Witwicka, H.; Hwang, S.-Y.; Van Stiphout, R.G.; Lambert, J.-P.; Rogers, C.; Yapp, C.; Gerstenberger, B.S.; et al. Selective Targeting of Bromodomains of the Bromodomain-PHD Fingers Family Impairs Osteoclast Differentiation. *ACS Chem. Biol.* **2017**, *12*, 2619–2630, doi:10.1021/acschembio.7b00481.

156. Brown, J.A., Jones, K.L.; Prinjha, R.K.; Witherington, J. Covalent conjugates of bet inhibitors and alpha amino acid esters. U.S. Patent 15/559,518, 22 September2016.

157. Felice, C.; Lewis, A.; Armuzzi, A.; Lindsay, J.O.; Silver, A. Review article: Selective histone deacetylase isoforms as potential therapeutic targets in inflammatory bowel diseases. *Aliment. Pharm.* **2014**, *41*, 26–38, doi:10.1111/apt.13008.

# 2

# Chapter 2

## Carboxylesterase-1 Assisted Targeting of HDAC Inhibitors to Mononuclear Myeloid Cells in Inflammatory Bowel Disease

**Ahmed M. I. Elfiky**, Mohammed Ghiboub, Andrew Y. F. Li Yim, Ishtu L. Hageman, Jan Verhoeff, Manon de Krijger, Patricia H. P. van Hamersveld, Olaf Welting, Iris Admiraal, Shafaque Rahman, Juan J. Garcia-Vallejo, Manon E. Wildenberg, Laura Tomlinson, Richard Gregory, Inmaculada Rioja, Rab K. Prinjha, Rebecca C. Furze, Huw D. Lewis, Palwinder K Mander, Sigrid E. M. Heinsbroek, Matthew J. Bell, Wouter J. de Jonge

Journal of Crohn's and Colitis, 2021

## Abstract

**Background and Aims:** Histone deacetylase inhibitors (HDACi) exert potent anti-inflammatory effects. Because of the ubiquitous expression of HDACs, clinical utility of HDACi is limited by off-target effects. Esterase-sensitive motif (ESM) technology aims to deliver ESM-conjugated compounds to human mononuclear myeloid cells, based on their expression of carboxylesterase 1 (CES1). This study aims to investigate utility of an ESM-tagged HDACi in inflammatory bowel disease (IBD).

**Methods:** CES1 expression was assessed in human blood, *in vitro* differentiated macrophage and dendritic cells, and Crohn's disease (CD) colon mucosa, by mass cytometry, quantitative polymerase chain reaction (PCR), and immunofluorescence staining, respectively. ESM-HDAC528 intracellular retention was evaluated by mass spectrometry. Clinical efficacy of ESM-HDAC528 was tested in dextran sulphate sodium (DSS)-induced colitis and T cell transfer colitis models using transgenic mice expressing human *CES1* under the *CD68* promoter.

**Results:** *CES1* mRNA was highly expressed in human blood $CD14^+$ monocytes, *in vitro* differentiated and lipopolysaccharide (LPS)-stimulated macrophages, and dendritic cells. Specific hydrolysis and intracellular retention of ESM-HDAC528 in $CES1^+$ cells was demonstrated. ESM-HDAC528 inhibited LPS-stimulated IL-6 and TNF-α production 1000 times more potently than its control, HDAC800, in $CES1^{high}$ monocytes. In healthy donor peripheral blood, CES1 expression was significantly higher in $CD14^{++}CD16^-$ monocytes compared with $CD14^+CD16^{++}$ monocytes. In CD-inflamed colon, a higher number of mucosal $CD68^+$ macrophages expressed CES1 compared with non-inflamed mucosa. *In vivo,* ESM-HDAC528 reduced monocyte differentiation in the colon and significantly improved colitis in a T cell transfer model, while having limited potential in ameliorating DSS-induced colitis.

**Conclusions:** We demonstrate that monocytes and inflammatory macrophages specifically express CES1, and can be preferentially targeted by ESM-HDAC528 to achieve therapeutic benefit in IBD.


**Key Words:** HDAC inhibitor; CES1; IBD

## Introduction

Histone deacetylases (HDAC) are a family of 18 epigenetic enzymes that regulate histone and non-histone acetylation by erasing acetyl groups from lysine residues, leading to a chromatin remodeling and altered gene expression [1]. Several studies report a fundamental role of HDAC in regulating cell survival and inflammatory response [2], and therefore various HDAC inhibitors have been developed and investigated in, for instance, fields of cancer and inflammatory diseases. Several randomised clinical trials have been conducted in the oncology field, and four HDACi have been Food and Drug Administration (FDA)-approved for some malignancies like multiple melanoma, cutaneous T cell lymphoma, and peripheral T cell lymphoma [3,4]. Also, however, trial outcomes revealed a wide range of adverse events associated with HDACi [5] with treatment discontinuation as a result [6].

In immune-related diseases, HDACi treatment inhibits inflammatory responses both *in vitro* and *in vivo* [7,8]. Furthermore, in patients receiving HDACi, low plasma levels of pro-inflammatory cytokines were reported, and isolated immune cells from these patients were also less responsive to inflammatory stimuli [9–11]. In preclinical models of several inflammatory diseases including IBD, HDACi have demonstrated promising therapeutic benefits [12–18]. However, clinical translation is limited due to their off-target activity and wide toxicity profile, including life-threatening cardiac arrhythmias, bone marrow suppression effects, and gastrointestinal and hepatic toxicities [19–22].

As histone acetylation drives gene expression in a cell-specific manner, selective targeting strategies of relevant immune cells is a highly attractive approach. In this regard, a targeted drug delivery technology has been developed to selectively retain inhibitors tagged with an esterase-sensitive motif (ESM) in mononuclear myeloid cells, based on their expression of the carboxylesterase 1 (CES1) enzyme [23]. This technology is of interest in immune-related diseases where these cell subsets play a role in driving the pathology, and such an approach can minimise off-target effects. Murine models are designed to investigate this approach through transgenic human CES1 expression, which allow human CES1 to be expressed predominantly in mononuclear myeloid cells, driven by *CD68* promoter. These models have shown promising results; in an arthritis model, ESM-HDAC528 has improved the outcome of the disease at a 100-fold lower dose compared with non-targeted compound, SAHA [23].

We reasoned that this approach is likely to have a therapeutic benefit in inflammatory bowel disease (IBD). First, HDACi ameliorates colitis in preclinical models and second,

IBD is an immune-driven pathology where mononuclear myeloid cells, including inflammatory macrophages, are enriched in Crohn's disease (CD) colon mucosa [24] and are believed to perpetuate mucosal inflammation [25]. Furthermore, a recent report suggests that a unique mononuclear phagocyte cytokine/chemokine network is linked to anti-TNF-α resistance in CD [26]. In the current study, we demonstrate anti-inflammatory effects of ESM-HDAC528 in monocytes and macrophages, reflecting their differential *CES1* expression. In preclinical models of IBD, ESM- HDAC528 showed clinical efficacy in the T cell transfer colitis model, and in the dextran sulphate sodium (DSS)-induced colitis, ESM-HDAC528 attenuated monocytes-to-macrophages maturation in the colon and blunted response to inflammatory stimuli in peritoneal macrophages.

## Materials and Methods

### Compounds

ESM-HDAC528 and its non-hydrolysable HDAC800 control were provided by GlaxoSmithKline (Stevenage, UK).

### Animals

The human CES1 transgenic mouse (*CES1/Es1e$^{lo}$*) was generated as described earlier [23,27].The transgenic mouse (*CES1/Es1e$^{lo}$*/Rag$^{-/-}$) was generated by cross-breeding human CES1 transgenic mouse (*CES1/Es1e$^{lo}$*) with the immunodeficient RAG$^{-/-}$ mouse. All animal studies were ethically reviewed and carried out in accordance with European Directive 2010/63/EEC, the guidelines of the Ethical Animal Research Committee of the University of Amsterdam, and the GSK Policy on the Care, Welfare and Treatment of Animals.

### Murine colitis models

For DSS-induced colitis, *CES1/Es1e$^{lo}$* mice were given 2% dextran sulphate sodium (DSS; TdB Consultancy) for 7 days, followed by 2 days of normal drinking water. Simultaneously, mice received daily intraperitoneal (IP) injections of 1 or 3 or 10 mg/kg of ESM- HDAC528 or vehicle until sacrifice. For T cell transfer colitis; *CES1/ Es1e$^{lo}$*/Rag$^{-/-}$ mice received IP injection of CD4$^{+}$CD45Rb$^{high}$ cells, isolated from spleens of C57BL/6 WT mice. Three weeks later; mice received daily IP injections of 3 mg/kg of ESM-HDAC528 or vehicle for another 4 weeks until sacrifice.

### Human clinical samples

The human biological samples were sourced ethically and their re- search use was in accord with the terms of the informed consents under an IRB/EC approved protocol or approval of the accredited Medical Ethics Committee at the Amsterdam UMC, University of Amsterdam.

### Cytokine measurement

Cytokines were measured using either mouse inflammation CBA kit (BD Bioscience), Meso Scale Discovery (MSD) plates or enzyme-linked immunosorbent assay (ELISA) kits (R&D systems), according to the manufacturer's protocol.

### Flow cytometry analysis

All samples were acquired using a FACS Fortessa (BD Biosciences) and analysed using FlowJo software (Treestar Inc., Ashland, OR).

### Mass cytometry analysis

Samples were acquired on a CyTOF Helios mass cytometer. Data were normalised using bead normalisation.[28] Deconvolution of pooled samples was performed by processing flow cytometry standard (FCS) files with the standard single-cell debarcoding algorithm for CyTOF data [29]. Analysis were performed using R Studio. Clusters of phenotypically similar cells were identified using the FlowSOM-package [30].

### Quantitative real-time polymerase chain reaction

RNA was isolated using RNeasy mini kit (Qiagen) and cDNA was synthesised using cDNA synthesis kit (Qiagen) following the manufacturer's protocol. Quantitative polymerase chain reaction (PCR) was performed on a QuantStudio Flex 7 (Applied Biosystems) or a LightCycler 480 II (Roche Applied Science).

### Immunofluorescence

Paraffin sections, prepared from surgically resected colons of CD patients undergoing colectomy at Amsterdam University Medical Center, were stained for CD68 (clone PG-M1, Dako), CES1 (poly- clonal, Novus Biologicals), and DAPI

### In vitro human monocyte and macrophage assays

Freshly isolated $CD14^+$ monocytes or GM-CSF differentiated macrophages were pre-incubated for 1 h with ESM-HDAC528 or HDAC800, then stimulated with 1 ng/mL lipopolysaccharide (LPS) for 24 h. Supernatants were collected for cytokine analysis and cells were used for ATP bioluminescence assay.

### Mass spectrometry assay

Cell lysate samples were extracted using protein precipitation and directly injected onto the HPLC-MS/MS system. Analysis was con- ducted by reverse-phase HPLC-MS/MS. Nominal MRM transitions for HDAC800, hydrolysed ESM-HDAC528, and parent ESM- HDAC528 were 391 to 178, 335 to 178, and 403 to 178, respectively.

### Statistical analysis

The significance of the differences was analysed using Student's t test, a Mann-Whitney U test, and one-way or two-way analysis of variance (ANOVA), as indicated; *p*-values <0.05 were considered significant.

## Results

### ESM-HDAC528 is hydrolysed by CES1 and accumulates in human blood-derived CD14+ monocytes

ESM-targeted drug delivery technology depends on the expression and hydrolysing activity of CES1 in target cells, where an ESM-tagged compound is hydrolysed and retained [23] (**Figure. 1A**). First, we aimed to validate this technology using human monocytes as a model of CES1-expressing cells. Monocytes were incubated with ESM- HDAC528 or non-hydrolysable HDAC800 control compound; then both parent ester and hydrolysed acid of the compounds were measured intracellularly and in the supernatant (**Figure. 1B**). Monocytes retained little HDAC800, with no hydrolysed acid formed, whereas ESM-HDAC528 was retained more strongly, with efficient hydrolysed acid generation intracellularly. Concurrently, ESM-HDAC528 parent ester was more consumed over time by monocytes compared with HDAC800 parent ester, as measured in the supernatant, reflecting the enhanced take-up and consumption of the ESM-tagged compound. ESM-HDAC528 hydrolysed acid was gradually detected as well in the supernatant over time, indicating some active efflux activity (**Figure. 1B**).

### In vitro differentiated inflammatory macrophages and dendritic cells show high CES1 expression

Next, we aimed to profile *CES1* gene expression within *in vitro* monocytes-derived macrophages and dendritic cells (DCs) subsets, to address their potential to retain ESM-HADC528. *CES1* was found to be highly expressed in human monocytes, and its expression reduced upon differentiation into macrophages or immature DCs (imDCs) (**Figure. 1C**). However, an upregulation of *CES1* expression was observed in mature DCs (mDCs) upon LPS-primed maturation (**Figure. 1C**).

Furthermore, we aimed to validate the ability of macrophages and DC subsets to generate and retain the hydrolysed acids from ESM parent ester. Both macrophages and DCs showed efficient ESM-HDAC528 acid hydrolysis and intracellular retention following incubation with ESM-HDAC528 (**Figure. 1D and E**). Interestingly, mDCs did not show better ability to hydrolyse and retain ESM-HDAC528 compared with the imDCs (**Figure. 1E**), despite the upregulation of *CES1* mRNA levels seen upon LPS maturation of DCs (**Figure. 1C**). These data demonstrate the efficient CES1-mediated ESM-HDAC528 retention in mononuclear myeloid cell subsets, as well as the differential *CES1* gene expression among these cell populations.

## ESM-HDAC528 shows an enhanced anti- inflammatory effect in human blood monocytes compared with monocytes-derived macrophages

We next hypothesised that the observed differences in *CES1* expression among mononuclear myeloid cell subsets might be reflected in differential ESM-HDAC528 anti-inflammatory potency. Both human blood $CD14^{+}$ monocytes and *in vitro* differentiated macrophages from matched donors were incubated with serial dilutions of ESM-HDAC528 or HDAC800, and then stimulated with LPS. ESM-HDAC528 compromised adenosine triphosphate (ATP) production in monocytes culture at 9.7 nM compared with 156.2 nM in macrophages (**Figure. 1F–H**). Meanwhile, the same doses of HDAC800 treatment did not affect ATP production either in monocytes or in macrophages (**Figure. 1F–H**). In monocytes, ESM-HDAC528 strongly downregulated LPS-induced IL-6 and TNF-α production at low doses compared with HDAC800 control compound (**Figure. 1G**). This enhanced anti-inflammatory potency of ESM-HDAC528 was also observed in macrophages (**Figure. 1I**) but to a much lesser extent compared with donor-matched monocytes. The enhanced potency of ESM-HDAC528 over HDAC800 confirms the augmented effect of the ESM-HDAC528, mediated by CES1 activity.

## CES1 expression profiles in peripheral blood cells of healthy donors demonstrates higher expression in classical $CD14^{++}CD16^{-}$ monocytes compared with non-classical $CD14^{+}CD16^{++}$ monocytes.

We next aimed to explore CES1 expression in peripheral blood. Peripheral blood mononuclear cells (PBMCs) were isolated from healthy donors and analysed by flow cytometry for CES1 expression (**Figure. S1**, available as Supplementary data). Monocytes subsets were further characterised by CD14 and CD16 expression pattern (**Figure. 2A**) into classical monocytes ($CD14^{++}CD16^{-}$), intermediate monocytes ($CD14^{++}$ $CD16^{+}$), and non- classical monocytes ($CD14^{+}$ $CD16^{++}$). CES1 was specifically and highly expressed in monocytes, with no CES1 expression detected in $CD3^{+}$ T and $CD19^{+}$ B cells (**Figure. 2B**).

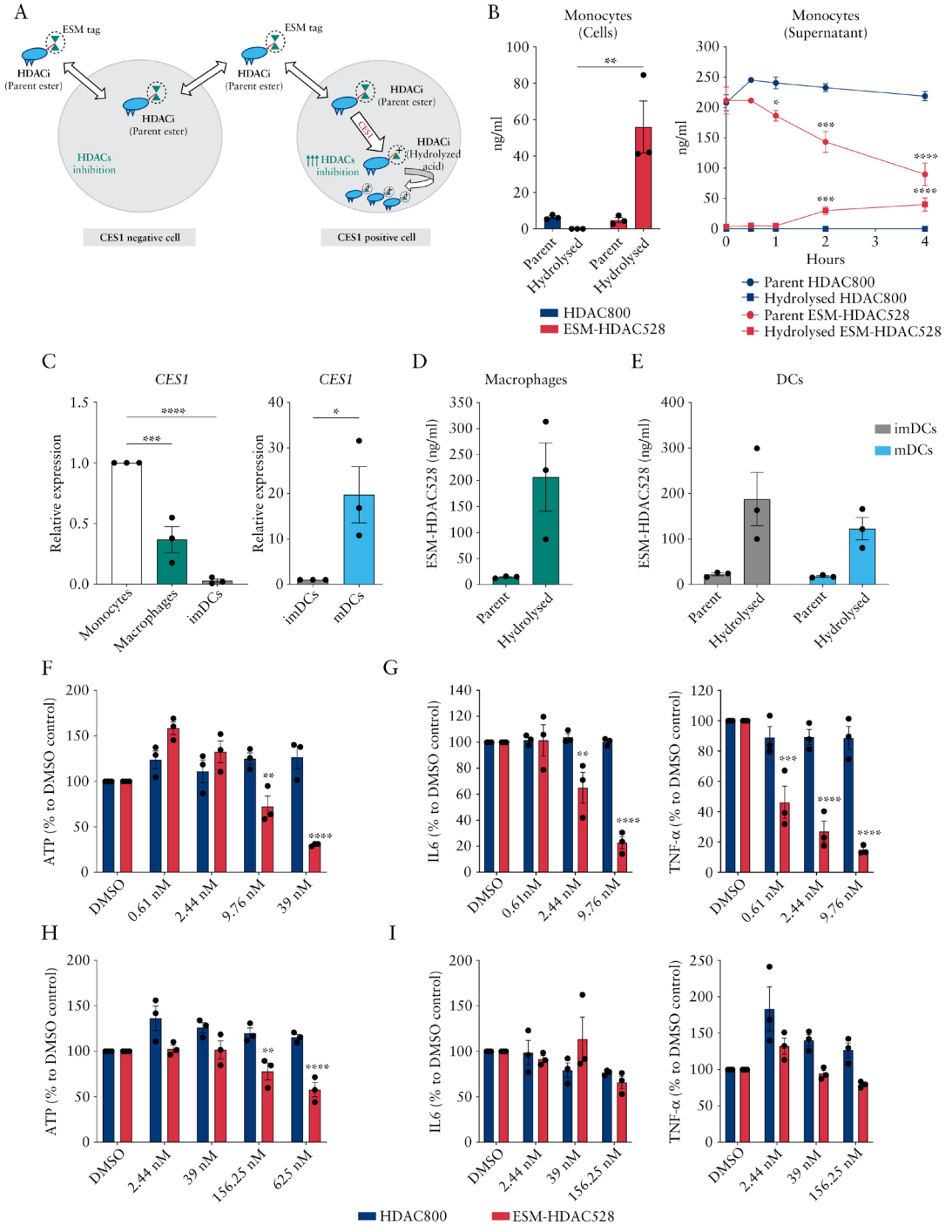
A
ESM tag
HDACi
(Parent ester)
HDACi
(Parent ester)
HDACs
inhibition
CES1 negative cell
ESM tag
HDACi
(Parent ester)
HDACi
(Parent ester)
CES1
HDACs
inhibition
HDACi
(Hydrolyzed
acid)
CES1 positive cell
B
Monocytes
(Cells)
ng/ml
Parent
Hydrolysed
Parent
Hydrolysed
HDAC800
ESM-HDAC528
Monocytes
(Supernatant)
ng/ml
Hours
Parent HDAC800
Hydrolysed HDAC800
Parent ESM-HDAC528
Hydrolysed ESM-HDAC528
C
CES1
Relative expression
Monocytes
Macrophages
imDCs
CES1
Relative expression
imDCs
mDCs
D
Macrophages
ESM-HDAC528 (ng/ml)
Parent
Hydrolysed
E
DCs
ESM-HDAC528 (ng/ml)
imDCs
mDCs
Parent
Hydrolysed
Parent
Hydrolysed
F
ATP (% to DMSO control)
DMSO
0.61 nM
2.44 nM
9.76 nM
39 nM
G
IL6 (% to DMSO control)
DMSO
0.61nM
2.44 nM
9.76 nM
TNF-α (% to DMSO control)
DMSO
0.61 nM
2.44 nM
9.76 nM
H
ATP (% to DMSO control)
DMSO
2.44 nM
39 nM
156.25 nM
62.5 nM
I
IL6 (% to DMSO control)
DMSO
2.44 nM
39 nM
156.25 nM
TNF-α (% to DMSO control)
DMSO
2.44 nM
39 nM
156.25 nM
HDAC800
ESM-HDAC528

**< Figure 1. Profiling ESM-HDAC528 accumulation and anti-inflammatory effect in mononuclear myeloid cell subsets.** (**A**) Schematic diagram of ESM technology for CES1-based targeted drug delivery to mononuclear myeloid cells; ESM-tagged HDACi (parent ester) can freely move in and out $CES1^-$ cells but, once it enters $CES1^+$ cells, it is hydrolysed by CES1 to the ESM-HDACi (hydrolysed acid) form of the compound which cannot leave the cells and is retained intracellularly, causing augmented HDACs inhibition. (**B**) Monocytes were incubated for 4 h with ESM-HDAC528 or non-hydrolysable HDAC800; the parent ester and hydrolysed acid of both compounds were measured both intracellularly and in the supernatant by LC-MS/MS. **(C)** *CES1* mRNA expression in $CD14^+$ monocytes, monocyte- differentiated macrophages and dendritic cells (imDCs), and LPS-polarised dendritic cells (mDCs). (**D** and **E**) Macrophages imDCs or mDCs were all incubated with ESM-HDAC528 for 4 h; the intracellular parent ester and its hydrolysed acid concentrations were measured by LC-MS/MS. (**F** and **G**) $CD14^+$ isolated monocytes or (**H** and **I**) macrophages differentiated from the same donors were pre-incubated with ESM-HDAC528 or HDAC800 and stimulated for 1 day with LPS, and then ATP production, IL-6, and TNF-α secretion were measured. Data are represented as mean with SEM of three donors, two technical replicates for each. In (**B,** right panel), parent or hydrolysed forms of HDAC800 and ESM-HDAC528 were compared. In (**F** to **I**), similar doses of ESM-HDAC528 and HDAC800 treatment were compared. Statistical testing was performed using two-way ANOVA test (**B, E, F, G, H, I**) or one-way ANOVA or Student's t test (**C**); *$p \leq 0.05$, **$p \leq 0.01$, *** $p \leq 0.001$, **** $p \leq 0.0001$. SEM, standard error of the mean.

In the monocyte population, non-classical monocytes showed significantly less CES1 expression compared with both classical and intermediate monocytes as identified by both frequency of $CES1^+$ cells and geometric mean of intensity of CES1 expression (**Figure. 2B**). Next, using mass cytometry, we further investigated differential CES1 expression in healthy donor PBMCs in more detail. Clusters of phenotypically similar cells were identified and shown in tSNE plots (**Figure. 2C**), the CES1 expression pattern was shown to localise among monocyte populations clusters (**Figure. 2D**). The heterogeneity of monocyte populations was further dissected, showing the expression pattern of monocyte-related markers among the monocyte population (**Figure. 2F**). Interestingly, we could identify a $CD14^-CD16^-$ population that expressed CD2 and α4β7 markers that have previously been linked to a DC precursor population [31, 32]. This $CD2^+$ $\alpha4\beta7^+$ DC precursor population expressed a similar level of CES1 as did non-classical monocytes, and both express significantly less CES1 compared with classical and intermediate monocytes (**Figure. 2E**). In conclusion, CES1 profiling in peripheral blood shows predominantly high CES1 expression among classical and intermediate monocyte populations and relatively less expression in non-classical monocytes.

## CES1-expressing macrophages are enriched in inflamed CD intestinal mucosa

Next, we addressed the CES1 expression in intestinal mucosa in both healthy and inflamed conditions. In CD colon mucosa, immunofluorescent staining for CES1 and the pan-macrophage marker CD68 was performed in macroscopically inflamed and non-inflamed areas. CES1 was found to be expressed in a proportion of $CD68^+$ cells in both inflamed and non-inflamed mucosa (**Figure. 3A**).

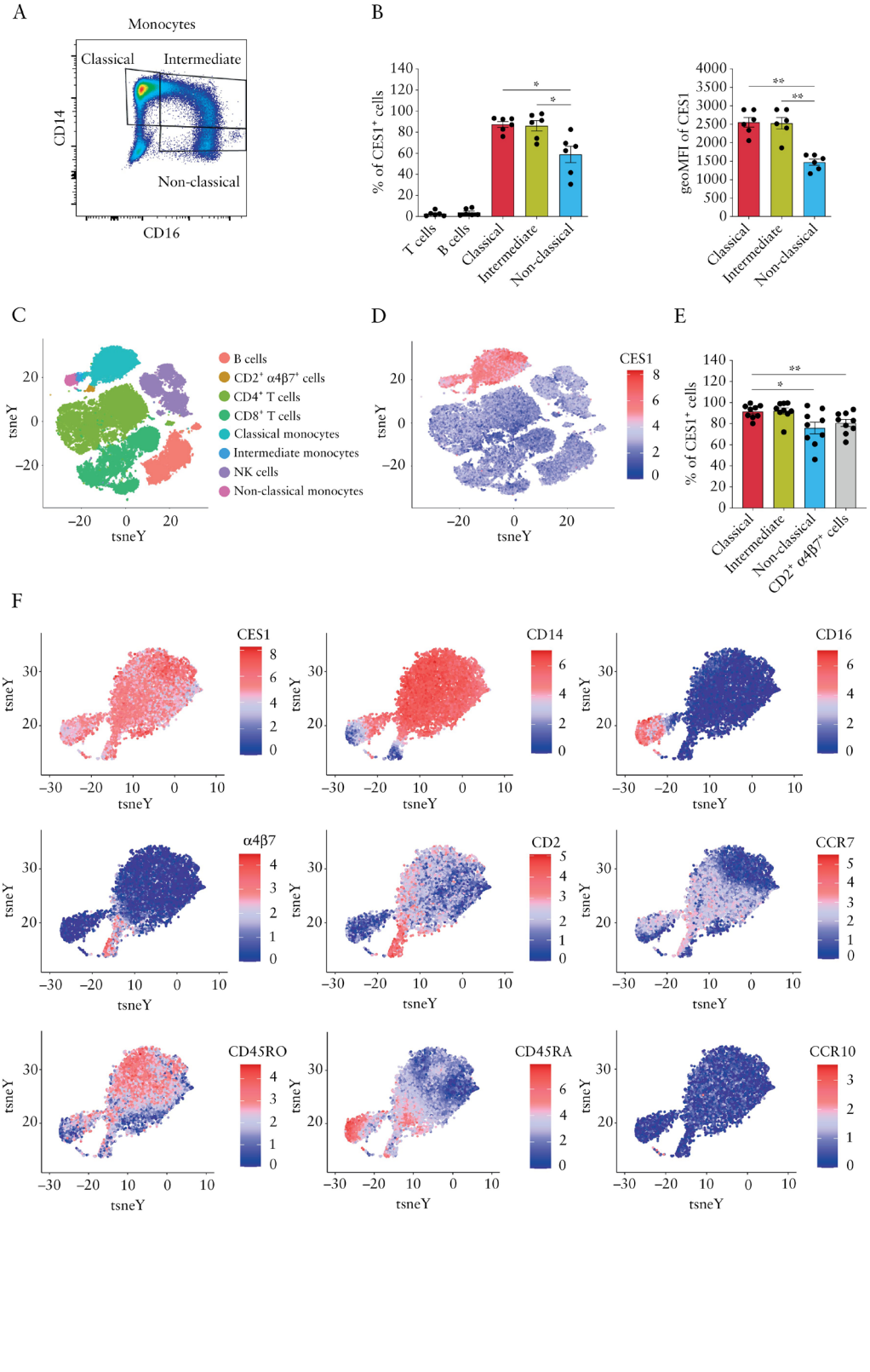
A
Monocytes
Classical
Intermediate
Non-classical
CD14
CD16
B
% of CES1+ cells
T cells
B cells
Classical
Intermediate
Non-classical
geoMFI of CES1
C
B cells
CD2+ α4β7+ cells
CD4+ T cells
CD8+ T cells
Classical monocytes
Intermediate monocytes
NK cells
Non-classical monocytes
tsneY
D
CES1
E
% of CES1+ cells
CD2+ α4β7+ cells
F
CES1
CD14
CD16
α4β7
CD2
CCR7
CD45RO
CD45RA
CCR10

**< Figure 2. CES1 expression profiling in peripheral blood monocyte populations reveals predominant expression in classical and intermediate monocytes.**

(**A**) Flow cytometry analysis of healthy donors PBMCs (n = 6) for CES1 expression within monocyte subsets, plots shown are gated on monocytes, identified by high FSC-A/ SSC-A; monocyte subsets are further distinguished by CD14/CD16 expression into; classical monocytes ($CD14^{++}CD16^{-}$), intermediate monocytes ($CD14^{++}CD16^{+}$), and non-classical monocytes ($CD14^{+}$ $CD16^{++}$). (**B**) Frequency of $CES1^{+}$ cells among $CD3^{+}$ T cells, $CD19^{+}$ B cells and monocyte subsets are shown, geoMFI of CES1 among monocytes subsets are plotted. (**C**) tSNE plots show immune cell subsets in healthy donor PBMCs (n = 9). (**D**) CES1 expression among clustered populations as analysed by mass cytometry. (**E**) Frequencies of $CES1^{+}$ cells among identified CES1-expressing immune cell subsets are shown. (**F**) Monocyte diversity tSNE plots are generated to demonstrate expression levels of monocyte-related markers (CD14 – CD16 – CD2 – α4β7 – CD45RO – CD45RA – CCR7 – CCR10) and CES1 among monocyte populations. The events identified as classical monocytes, intermediate monocytes, non-classical monocytes, and the $CD2^{+}a4b7^{+}$ myeloid cells were shown in the annotation of FlowSOM clusters. Data are represented as mean with SEM of six to nine patients, one technical replicate each. Statistical testing was performed using one-way ANOVA test or Student's t test; *p ≤0.05, **p ≤0.01. SEM, standard error of the mean; PBMC, peripheral blood mononuclear cells.

The frequency of colon mucosal macrophages, as defined by CD68 expression, which express CES1 was higher in inflamed mucosa compared with non-inflamed mucosa (**Figure. 3B**). In line with earlier reports, CES1 was mainly expressed in $CD68^{+}$ macrophages as quantified by percentage of $CD68^{+}$ macrophages among $CES1^{+}$ cells, confirming restricted CES1 expression among mucosal $CD68^{+}$ mononuclear myeloid cells (**Figure. 3B**).

Furthermore, RNAseq data retrieved from Bujko *et al.* 2018 [33] were re-examined for *CES1* mRNA expression, along with other myeloid cell-related genes, in peripheral blood monocytes (PBMo) and flow cytometry-sorted macrophages and dendritic cell subsets from small intestinal mucosa of patients undergoing a Whipple surgical procedure. *CES1* showed higher expression in blood monocytes (PBMo) and intestinal immature macrophages (MF1: $CD14^{+}CD11c^{+}HLA\text{-}DR^{int}$) queued, whereas more mature intestinal macrophage subsets (MF2: $CD14^{+}CD11c^{+}HLA\text{-}DR^{hi}$), (MF3: $CD14^{+}CD11c^{-}CD11b^{-}$),and (MF4: $CD14^{hi}CD11c^{-}CD11b^{+}$), as well as DC subsets (SP-DCs: $CD103^{+}SIRP\alpha^{-}$), (DP-DCs: $CD103^{+}SIRP\alpha^{+}$), and ($CD103^{-}$ DCs: $CD103^{-}SIRP\alpha^{+}$), showed less *CES1* expression (**Figure. 3C**). This observation was consistent with *CES1* mRNA expression dynamics during *in vitro* monocyte differentiation (**Figure. 1C**). Interestingly we could observe *ITGAX (CD11c), S100A8, S100A9*, and *S100A12* genes to be enriched in high *CES1*-expressing intestinal macrophages (MF1).

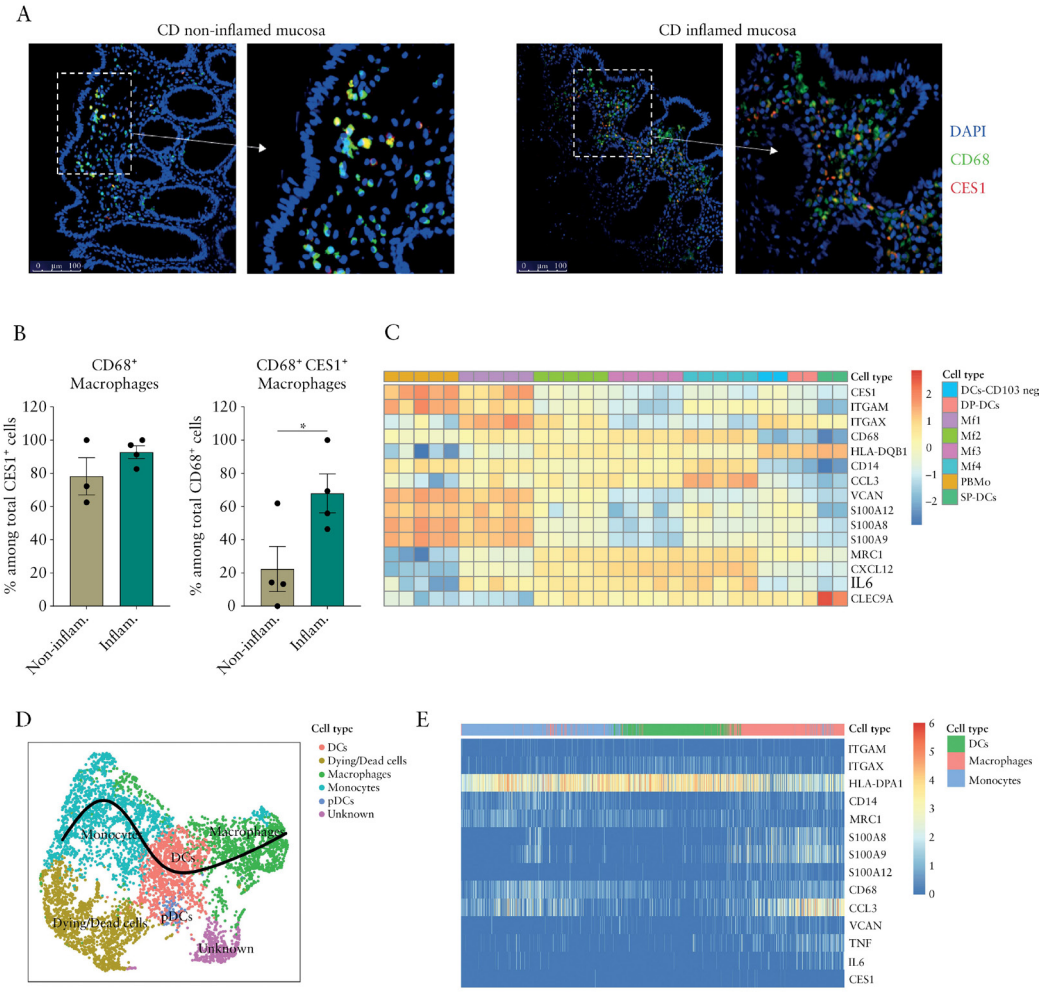


**Figure 3. Profiling CES1 expression in non-inflamed and inflamed intestinal mucosa.**
(**A**) Immunofluorescence staining for CES1, CD68, and DAPI is shown within paraffin-embedded sections from surgically resected colons of CD patients (n = 4). (**B**) Quantification of $CD68^+$ macrophages among $CES1^+$ cells and $CES1^+$ $CD68^+$ macrophages among total $CD68^+$ macrophages is shown. (**C**) Heat map of CES1 gene expression along with some other differentially expressed myeloid cell-related genes expression is shown among peripheral blood monocytes (PBMo) and small intestinal macrophage and DCs subsets; data are retrieved from Bujko et al. 2018. RNAseq data, cells are flow cytometry sorted from small intestine of patients undergoing the Whipple procedure (n = 2-5). (**D**) Developmental trajectory analysis of intestinal mononuclear phagocytes (MNPs) is conducted on (Martin et al. 2019) a scRNAseq dataset of CD patient intestinal biopsies (n = 11). (**E**) Gene expression of CES1 and myeloid cell-related genes along the MNPs trajectory are demonstrated. Data are represented as mean with SEM of four patients, one technical replicate each. RNAseq expression values (log2) were median-centred by transcript. Statistical testing was performed using Student's t test; *p ≤0.05. SEM, standard error of the mean; CD, Crohn's disease.

To examine CES1 expression development in intestinal mononuclear phagocytes (MNPs) of CD patients, a developmental trajectory analysis was conducted on scRNAseq data retrieved from Martin *et al*. 2019 [26] (**Figure. 3D**). There was lower *CES1* mRNA transcript expression in MNPs retrieved from this dataset as com- pared with Bujko *et al.*'s 2018 [33] dataset or protein expression as analysed by mass cytometry in PBMCs (**Figure. 2D**). Irrespectively, by analysing a developmental trajectory analysis for CD intestinal MNPs, *CES1* was relatively enriched in differentiated macrophages along with *S100A8*, *S100A9*, and *S100A12* genes that all follow the same pattern (**Figure. 3E**).

## ESM-HDAC528 attenuates colon monocytes to macrophage differentiation and peritoneal macrophage reactivity in DSS-induced colitis

We next aimed to evaluate the therapeutic potential of ESM-HDAC528 in a mouse model. To achieve CES1 expression in mice, we made use of *CES1/Es1e$^{lo}$* transgenic mice that express human CES1 (hCES1) predominantly in a monocyte-macrophage lineage-selective manner, driven by a human *CD68* promoter known from its expression pattern to reflect macrophage populations in the intestinal mucosa [34]. The ability of ESM-HDAC528 to accumulate in *CES1/Es1e$^{lo}$* mouse mononuclear myeloid cells was demonstrated both *in vitro* (**Figure. S2A** and **B**) and *in vivo* (**Figure. S2E**) by means of flow cytometry analysis of acetylated lysine expression as indirect measure of ESM-HDAC528 accumulation. Gene expression levels of *hCES1* were shown to be similar across differently polarised *CES1/Es1e$^{lo}$* mononuclear myeloid cells (**Figure. S2C).** However, enhanced acetylated lysine expression upon ESM-HDAC528 (50Nm) treatment of these cells showed higher activity in bone marrow-derived dendritic cells (BMDCs) compared with bone marrow-derived macrophages (BMDM) (**Figure. S2D**).

To evaluate the clinical relevance of the mononuclear myeloid cell-targeting approach by ESM-HDAC528, DSS colitis was induced in *CES1/Es1e$^{lo}$* mice using 2% DSS in drinking water. At the same time mice started to receive daily intraperitoneal injections of 1 or 3 mg/kg ESM-HDAC528 or vehicle (**Figure. 4A**). Both doses showed efficient targeting of ESM-HDAC528 to blood monocytes compared with other immune cells. The global acetylated lysine expression was particularly enhanced in blood monocytes (**Figure. 4B**), and a reduced frequency of monocytes was observed (**Figure. 4C**) when assessed 3 h after last injection at both tested doses. Despite efficient monocyte targeting of ESM-HDAC528, clinical improvement of colitis was limited to a number of clinical and biochemical parameters. Weight loss was significantly improved in a dose-dependent manner (**Figure. 4D**), although no significant effect was observed in dis- ease clinical activity index or colon

density (weight/length ratio) (**Figure. 4E**). Colon inflammation score was improved in mice dosed at 3 mg/kg, reflecting reduced mucosal ulceration and crypt loss (**Figure. 4F**). Colon inflammatory biomarkers (*TNF-α*, *IL1β*, *CCL2*, *TLR4*, *S100A8*, *CXCL1*, *CXCL2*, *CXCR2*) mRNA expression were measured. *S100A8*, *CXCL1*, *CXCL2*, and *CXCR2* mRNA levels tended to be reduced at both doses, whereas *CCL2* and *TLR4* were upregulated in ESM-HDAC528-treated mice only at the 3 mg/kg dose; but those trends did not meet significance in the groups tested. No change was detected in *TNF-α* or *IL1β* (**Figure. 4G**). However, serum levels of TNF-α, IL-10 and CCL2 were not significantly changed (**Figure. 4H**). In ESM-HDAC528-treated mice, peritoneal resident macrophages isolated at the end of the study showed a significantly reduced response to LPS (as assessed by IL-6 and TNF-α secretion) when cultured *ex vivo* (**Figure. 4I**).

Next, in a repeat experiment, mice were dosed at 3 and 10 mg/kg ESM-HDAC528 or vehicle, following analyses of colon cell dynamics through flow cytometry. $CD45^+$ live immune cells were identified and further analysed to define $CD3^+$ T cells and $Ly6G^+$ neutrophils. Monocytes and macrophages were defined as $CD64^+CD11b^+CD11c^-$ within $CD3^-Ly6G^-$ gating and were differentiated by pattern of Ly6C and MHCII expression, with monocytes being $Ly6C^{high}/MHCII^{low}$ and macrophages $Ly6C^{low}/MHCII^{high}$. DCs were defined as $CD11c^+$ $MHCII^+$ among $CD3^-Ly6G^-CD64^-CD11b^-$ gating, and two subsets of DCs were further identified as $CD11b^+$ and $CD11b^-$ DCs (**Figure. S3A**). ESM- HDAC528 treatment did not interfere with recruitment of total immune cells to the colon during inflammation (**Figure. S3B**), or with monocyte-macrophage population ($CD64^+CD11b^+$) recruitment in particular (data not shown).

**> Figure 4. ESM-HDAC528 improves clinical parameters in DSS-induced colitis and reduces peritoneal macrophage response to inflammatory stimulus.**

**(A)** A scheme of the acute DSS colitis model experimental design. (**B**) Flow cytometry analysis of acetylated lysine expression within blood immune cells, 3 h after IP dosing, along with (**C**) frequency of blood monocytes across all groups. (**D**) Weight changes are indicated as percentage of initial body weight. (**E**) Colon density (weight/length ratio) and average disease activity index (DAI) were measured at sacrifice. DAI consisted of average scores of oedema (0–3), diarrhoea (0–3), and the presence of blood in the stool (0–3), with a maximal DAI of 3 points. (**F**) Colon histopathology scores were graded from 0 to 4 points as indicated in Table S1. Crypt loss and mucosal ulceration scores are highlighted.(**G**) Colon mRNA expression of inflammation biomarkers are shown. (**H**) Serum CCL2, TNF-α, and IL-10 are demonstrated. (**I**) Ex vivo retrieved peritoneal macrophages after mouse sacrifice were stimulated with LPS. TNF-α, IL-6, and IL-10 were quantified. Data are represented as mean with SEM, DSS groups (n = 10) and no DSS groups (n = 5), one technical replicate each. The DSS vehicle group is compared with the DSS compound-treated groups. In (**E** and **F**), the no-DSS vehicle group is compared with the DSS-vehicle group as well. Statistical testing was performed using two-way ANOVA test (**B, D**) or otherwise one-way ANOVA test; *p ≤0.05, **p ≤0.01, *** p ≤0.001, **** p≤0.0001. SEM, standard error of the mean; DSS, dextran sulphate sodium.

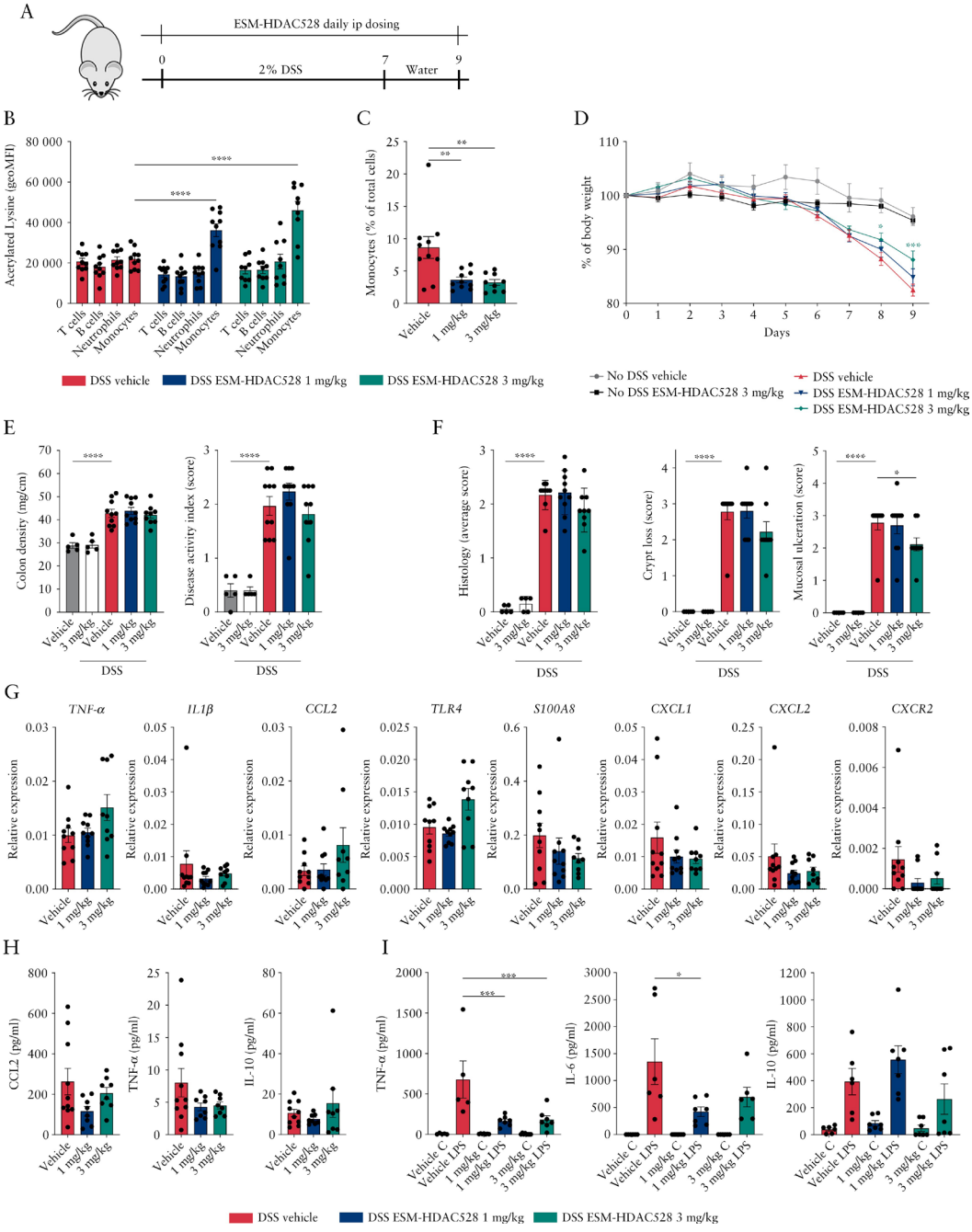
A
ESM-HDAC528 daily ip dosing
0
2% DSS
7
Water
9
B
Acetylated Lysine (geoMFI)
T cells
B cells
Neutrophils
Monocytes
C
Monocytes (% of total cells)
Vehicle
1 mg/kg
3 mg/kg
D
% of body weight
Days
DSS vehicle
DSS ESM-HDAC528 1 mg/kg
DSS ESM-HDAC528 3 mg/kg
No DSS vehicle
No DSS ESM-HDAC528 3 mg/kg
E
Colon density (mg/cm)
Disease activity index (score)
DSS
F
Histology (average score)
Crypt loss (score)
Mucosal ulceration (score)
G
TNF-α
IL1β
CCL2
TLR4
S100A8
CXCL1
CXCL2
CXCR2
Relative expression
H
CCL2 (pg/ml)
TNF-α (pg/ml)
IL-10 (pg/ml)
I
TNF-α (pg/ml)
IL-6 (pg/ml)
IL-10 (pg/ml)
Vehicle C
Vehicle LPS
1 mg/kg C
1 mg/kg LPS
3 mg/kg C
3 mg/kg LPS

However, ESM-HDAC528 attenuated colon monocyte to macrophage tissue differentiation in a dose-dependent manner (**Figure. 5A** and **B**). Monocytes found in the colon (Ly6C$^{high}$ MHCII$^{low}$) exhibited a less mature phenotype, with higher Ly6C expression and lower CD64 protein expression in ESM-HDAC528-treated groups (**Figure. 5C**). Colon macrophages (Ly6C$^{low}$ MHCII$^{high}$) exhibited reduced CD64 but no impact on MHCII expression (**Figure. 5D**). Total DC frequency was not affected, but the DCs subset distribution was modulated, with enrichment of the CD11b$^{+}$ subset compared with the CD11b$^{-}$ subset in a dose-dependent manner, but with no impact on MHCII expression in DCs (**Figure. 5E** and **F**). With regard to clinical outcome of the colitis, the 10 mg/kg dose did not lead to any additional improvement in disease activity or inflammation score compared with the 1 and 3 mg doses (data not shown).

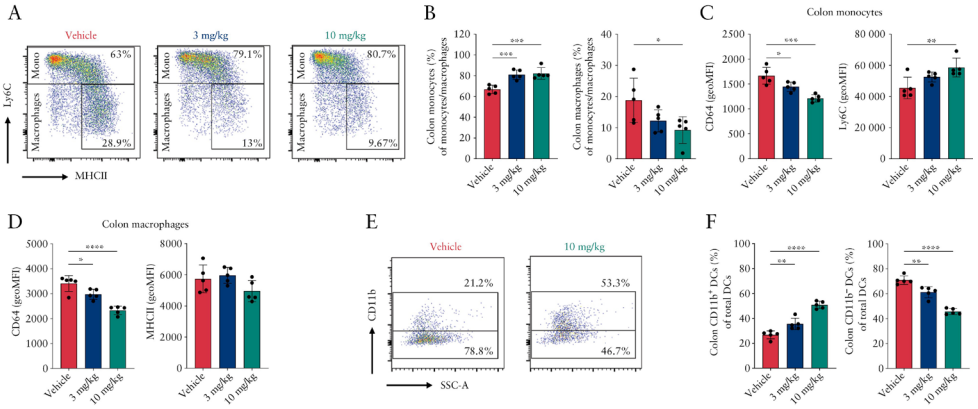


**Figure 5. ESM-HDAC528 modulates colon mononuclear myeloid cell populations during DSS-induced colitis.**

Acute DSS colitis was induced as described earlier; mice were simultaneously treated with vehicle or ESM-HDAC528 (3 or10 mg/kg) and colon mononuclear myeloid cells were analysed by flow cytometry. (**A**) Representative expression of MHCII and Ly6C among colon monocyte and macrophage populations w ere compared across treatment groups. (**B**) Frequencies of colon monocytes and macrophages among parent population (CD11b$^{+}$CD64$^{+}$CD11c$^{-}$) are shown. (**C**) GeoMFI of CD64 and Ly6C in colon monocytes are quantified. (**D**) GeoMFI of CD64 and MHCII in colon macrophages are quantified. (**E**) CD11b$^{+}$ and CD11b$^{-}$ dendritic cell (DCs) subsets are identified among colon DCs and shown across treatment groups. (**F**) Frequencies of colon DC subsets among total colon DCs population are compared across vehicle and 10 mg/kg groups. Data are represented as mean with SEM, DSS groups (n = 10) and no DSS groups (n = 5), two or three mouse colon were combined per sample. The DSS vehicle group is compared with DSS compound-treated groups. Statistical testing was performed using one-way ANOVA test; *p ≤0.05, **p ≤0.01, *** p ≤0.001, **** p ≤0.0001. SEM, standard error of the mean; DSS, dextran sulphate sodium.

### ESM-HDAC528 significantly improves colon inflammation in a T cell transfer colitis model

Next, we tested the potential of 3 mg/kg ESM-HDAC528 to reduce colitis in a T cell transfer colitis model. To this end, we generated transgenic *CES1/Es1e*$^{lo}$/Rag$^{-/-}$ mice to transfer CD45Rb$^{high}$ T cells into a RAG-/- host overexpressing the *hCES1* gene. Three weeks following transfer of CD4$^{+}$45Rb$^{high}$ T cells, mice started to receive daily intraperitoneal injections of 3 mg/kg ESM-HDAC528 or vehicle (**Figure. 6A**). Efficient targeting of blood monocytes was observed, as assessed by enhanced global acetylated lysine expression in blood monocytes compared with other blood immune cells (**Figure. 6B**) along with reduced frequency of blood monocytes (**Figure. 6C**) when assessed 3 h after IP injection. Clinical improvement of colitis was apparent in ESM-HDAC528-treated mice: weight loss was reduced in the ESM-HDAC528-treated group (**Figure. 6D**), and colon density and spleen weight were significantly improved compared with the vehicle-treated group. Additionally, the disease activity index (DAI) showed a trend towards improvement in ESM-HDAC528-treated mice (**Figure. 6E**) and a reduced colon inflammation histological score was noted after ESM-HDAC528 as compared with controls (**Figure. 6F**). As shown in representative images of haematoxylin-eosin stained colon histology sections, ESM-HDAC528-treated mice exhibited preserved crypt architecture along with reduced mucosal immune cell infiltration compared with colitis controls (**Figure. 6G**). A reduction in colon homogenate CCL2 protein expression was observed in ESM-HDAC528-treated mice (**Figure. 6H**). Finally, serum levels of IFN-γ, TNF-α, and CCL2 were reduced in ESM-HDAC528-treated mice, but only the reduction of TNF-α reached significance (**Figure. 6I**).

## Discussion

As the ESM drug delivery technology is based on the ability of CES1 to hydrolyse and retain the tagged compound in the targeted cells, we aimed to demonstrate that the ESM-HDAC528 is superior over non-ESM tagged HDAC800 to target mononuclear myeloid cells. Monocytes – as CES1 high expressing cells – showed efficient ability to hydrolyse and retain ESM-HDAC528. In comparison, non-hydrolysable HDAC800 control was minimally retained intracellularly. This was reflected in enhanced anti-inflammatory effect of ESM-HDAC528 in monocytes and to lesser extent, in macrophages. ESM-HDAC528 potently inhibited IL-6 and TNF-α at doses 1000 times lower than non-hydrolysable HDAC800 control. Notably, only at higher dose ranges, ESM-HDAC528 also reduced intracellular ATP levels in both monocytes and macrophages. In this context, intracellular ATP levels were reported to positively correlate with cell proliferation and were

widely used as a method to assess cell proliferation and cytotoxicity [35] . The anti-inflammatory and anti-proliferative effects of ESM-HDAC528 were all absent with HDAC800 treatment at similar doses, despite having the same chemical potency, as a consequence of the CES1-mediated accumulation of ESM-HDAC528 in monocytes and macrophages. Therefore administering low doses of ESM-HDAC528 is expected to affect the CES1-expressing myeloid cells only. This feature will improve the tolerability and safety of HDACi therapeutic application through selectively targeting CES1-expressing inflammatory myeloid cells.

In the *ex-vivo* setting, differential CES1 expression was observed in both peripheral blood and intestinal mucosa of the healthy and the IBD environments. We defined populations of $CD14^{+}$ and $CD16^{+}$ monocytes in healthy donor peripheral blood expressing CES1 at single cell resolution using mass cytometry, and observed that $CD14^{++}CD16^{-}$ classical monocytes showed higher CES1 expression compared with $CD14^{+}CD16^{++}$ non-classical monocytes. CES1 expression is also detected in $CD2^{+}\alpha4\beta7^{+}$ DCs precursors at lower levels compared with $CD14^{++}CD16^{-}$ classical monocytes, indicating that CES1 is expressed in mononuclear myeloid cells largely but not per se restricted to monocytes only.

In CD colonic mucosa, CES1 expression is largely seen in $CD68^{+}$ tissue macrophages. This confirms earlier observations that show CES1 expression confined to the monocyte-macrophage population but not infiltrating DCs [36]. The CES1-expressing macrophages were more abundant in inflamed mucosa compared with non-inflamed mucosa. This may be explained by upregulation of CES1 expression in macrophages in response to local inflammatory cues, as CES1 is shown to be regulated by inflammatory NF-κB signalling [37].

**> Figure 6. ESM-HDAC528 improves colon inflammation in aT cell transfer colitis model.**
(**A**) A schematic of the T cell transfer colitis model experimental design. (**B**) Flow cytometry analysis of acetylated lysine expression within blood immune cells, 3 h after ip dosing, along with (**C**) frequency of blood monocytes across indicated groups. (**D**) Weight changes are indicated as percentage of body weight on the first day of treatment. (**E**) Colon density (weight/length ratio), spleen weight (mg), and total Disease Activity Index (DAI) were measured at sacrifice. DAI; consisted of total scores of oedema (0–3), diarrhoea 90–3), and the presence of blood in the stool (0–3), with a maximal DAI of 9 points. (**F**) Colon histopathology scores were graded from 0 to 4 points, as indicated in Table. S2. Total scores are calculated according to this formula (total score = goblet cell loss score + 2 x crypt loss score + 2 x crypt hyperplasia score + 3 x submucosal inflammation score). (**G**) Representative images of colon haematoxylin and eosin staining are shown. (**H**) Colon CCL2 and (**I**) serum IFN-γ, TNF-α, and CCL2 protein expression are shown. Data are represented as mean with SEM, transfer groups (n = 5) and no transfer group (n = 2): the transfer vehicle group is compared with transfer compound-treated groups. Statistical testing was performed using two-way ANOVA test (**B, D**) or otherwise Student's t test; *p ≤0.05, **p ≤0.01, *** p ≤0.001. SEM, standard error of the mean.

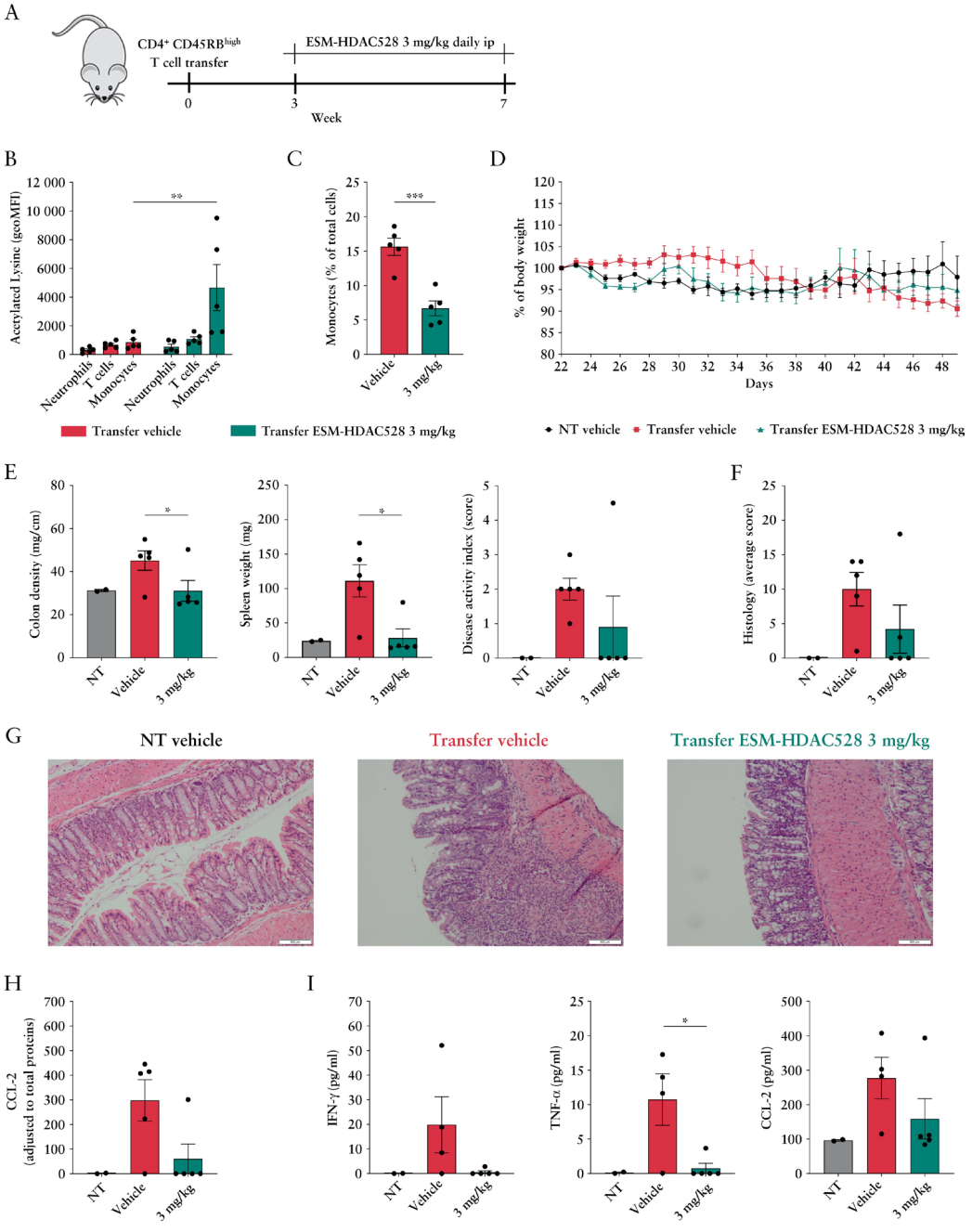
A
CD4+ CD45RBhigh
T cell transfer
ESM-HDAC528 3 mg/kg daily ip
0
3
7
Week
B
Acetylated Lysine (geoMFI)
Neutrophils
T cells
Monocytes
Transfer vehicle
Transfer ESM-HDAC528 3 mg/kg
C
Monocytes (% of total cells)
Vehicle
3 mg/kg
D
% of body weight
Days
NT vehicle
Transfer vehicle
Transfer ESM-HDAC528 3 mg/kg
E
Colon density (mg/cm)
Spleen weight (mg)
Disease activity index (score)
NT
Vehicle
3 mg/kg
F
Histology (average score)
G
NT vehicle
Transfer vehicle
Transfer ESM-HDAC528 3 mg/kg
H
CCL-2
(adjusted to total proteins)
I
IFN-γ (pg/ml)
TNF-α (pg/ml)
CCL-2 (pg/ml)

Another explanation could be the abundance of recently recruited CES1$^{high}$ classical monocytes to the inflamed colon and expansion of CES1$^{high}$ immature pro-inflammatory macrophages within inflamed colon. In line with that, *CES1* mRNA expression in the non-inflamed intestinal environment is highest in the CD14$^{+}$CD11c$^{+}$HLA-DR$^{int}$ immature macrophage population (MF1), a population that corresponds to the recently recruited monocytes in early stages of macrophage differentiation, in contrast to mature macrophages that show much reduced *CES1* expression [33]. Interestingly the *CES1*$^{high}$ MF1 population highly co-expressed *S100A12*, a previously reported reliable IBD biomarker that highly correlates with inflammation severity [38]. S100A12 is also enriched in inflammatory macrophages and neutrophils within intestinal mucosa and upon TLR2/1 ligand polarisation [39,40] .Concurrently, a developmental trajectory analysis of inflamed intestinal MNPs reveals relative enrichment of *CES1* mRNA expression in intestinal macrophages, along with *S100A12*. Next to S100A8 and S100A9 (also known as calprotectin), S100A12 is specifically found in human inflammatory IBD tissue macrophages and neutrophils [41] and is known to correspond to disease severity [42]. Such S100A proteins can endogenously activate TLR4 and subsequently induce the NF-κB signaling pathway [43,44], which in turn upregulates CES1 expression in response to inflammatory stimuli [37]. This can explain the correlation between CES1 and S100A protein expression in mononuclear myeloid cells.

Mononuclear myeloid cells play a major role in murine colitis models, driving both colon inflammation and healing [45]. In DSS-induced colitis, an innate immune cell driven model, inflammation is largely driven by recruitment of Ly6C$^{high}$ blood monocytes to colon and enrichment of pro-inflammatory signals (IL1β) in colon macrophages and DCs. Alternatively, CX3CR1$^{high}$ resident macrophages are essential to maintain colon homeostasis and tolerance [45]. In T cell transfer colitis, a T cell-driven colitis model, mononuclear phagocytes are essential to process antigens and induce T cell activation and expansion in the colon [46]. Whereas the CD103$^{-}$ DCs subset promotes IFN-γ producing T cell differentiation, the CD103$^{+}$ DCs subset is essential for Treg-mediated protective effect [47].

In both murine colitis models, ESM-HDAC528 demonstrated specific blood monocyte targeting at tested doses, as indicated by preferential enhanced lysine acetylation in monocytes This specific targeting reflects the restricted pattern of human CES1 expression in our transgenic *CD68* promoter-driven human *CES1* mice, used in our *in vivo* studies, which results in expression of human CES1 in mononuclear myeloid cells and subsequent ESM-HDAC528 accumulation [23]. In this setting, a reduction in blood monocytes was observed. This is consistent with earlier reports showing loss of

PU.1 expression in murine macrophages and subsequently myeloid cell markers like CD11b and CD115 (c-fsm) following HDAC inhibition [48]. Given that PU.1 is a critical transcription factor to maintain monocyte-macrophage cell lineages [49], this effect may well explain the notable loss of circulating blood monocytes following ESM-HDAC528 treatment.

When applied *in vivo*, ESM-HDAC528 partially reduced some endpoints of DSS-induced colitis and concurrently affected mononuclear myeloid cell differentiation in the colon. In conjunction, peritoneal macrophages showed less LPS-induced cytokine responses. Similar effects were reported with the same compound in a peritonitis model [27]. Some colon inflammation biomarkers of mRNA expression were improved; this included CXCL1 and CXCL2, known targets of HDAC inhibition [50]. The increased CCL2 and TL4 expression in the colon might be a compensatory mechanism for impaired monocyte-macrophage responses due to the specific compound targeting. However, the clinical outcome of colitis was unexpectedly moderate, with alleviation of weight loss, colonic mucosal ulceration, and crypt loss. The observed effect of ESM-HDAC528 is likely mediated through a combination of reduced chemokine secretion as well as reduced tissue monocyte differentiation and macrophage reactivity, as, in earlier studies in DSS-induced colitis, blocking monocyte recruitment to the colon ameliorated colitis [51,52]. ESM-HDAC528 targeted monocytes likely attain a reduced ability to induce gene expression allowing macrophages differentiation. Additionally, ESM-HDAC528 significantly improved multiple key clinical outcomes of T cell transfer colitis; attenuating colon inflammation and reducing serum IFN-γ, TNF-α, and CCL2. A reduced colon CCL2 level was observed, a key inflammatory biomarker in this model [53] indicative of less severe colonic inflammation. HDAC inhibitors are reported to modulate DC functions, compromising T cell stimulatory capacity [54] and secretion of IL-12 [54,55], a key Th1 polarising cytokine. HDAC inhibitor-treated DCs are less able to support Th1 cell skewing, resulting in less T cell IFN-γ secretion [56], while supporting type 1 T regulatory cell polarisation [57] in agreement with our observations. The observed discrepancy between the outcomes of the two colitis models, may be attributed to their different predominant mechanisms driving inflammation [58]. Earlier studies show that macrophage-DC depletion strategies to aggravate DSS induced colitis largely, mediated by increased colon *CXCL1* expression and neutrophils infiltration [59,60]. Several studies have addressed targeting DCs and macrophages in multiple murine colitis models, with conflicting outcomes [52,61,62]. This is largely attributed to the dual protective and inflammatory roles that these cell populations play in pathogenesis of colitis, depending on their phenotype or predominant subset.

Our data suggest that CES1 expression is more enriched in inflammatory subsets of mononuclear myeloid cells in the human setting. In contrast to that, transgenic *CD68* promoter-driven human *CES1* expression in the murine system (*CES1/ES1$^{lo}$* mice) shows similar CES1 expression and activity among different mononuclear myeloid cell subsets. Therefore, due to discrepancy between CES1 regulation in human vs transgenic murine systems, translating *in vivo* finding from murine studies to human should be done with care. A potential explanation of less efficacy in DSS-induced colitis model could be the universal targeting of all macrophages and DC subsets including anti-inflammatory subsets that play a role to limit colon inflammation in the DSS model; therefore any beneficial effect from targeting monocyte and pro-inflammatory macrophage subsets can be mitigated by dampening anti-inflammatory subsets activity. Unlike in humans where CES1 seems to be more expressed in inflamed setting, a beneficial therapeutic effect can be potentially achieved by refining treatment dosing.

Together, we addressed CES1 expression in a variety of IBD intestinal tissue and established high CES1 expression in pro-inflammatory cells. Given their high sensitivity to HDACi, and strong potential to drive excess inflammatory pathology and tissue damage, our findings warrant further application of ESM-based small molecule delivery to specific target cells in IBD.

## Funding

This project is funded by the European Union's Horizon 2020 research and innovation programme under Grant Agreement No. ITN-2014-EID-641665. PH, OW, IA, SR SH, and WJ are funded by a grant from Dutch Economic Affairs Top Sector Life Sciences & Health (LSH) - Top Consortia for Knowledge and Innovation's (TKI), grants no. TKI-LSH T2017, and European Crohn's and Colitis Organization (ECCO) Pioneer Grant, 2018.

## Conflict of Interest

The authors declare that the research was conducted in the absence of any commercial or financial relationships that could be construed as a potential conflict of interest. LT, RG, IR, RP, RF, HL, PM, and MB were employed by GSK at the time of conducting this study. AE, MG, MK, IH, PH, OW, IA, SR, SH, JV, JG, and WJ were employed by Amsterdam University Medical Centers at the time of conducting this study.

## Author Contributions

Conduct of the study, laboratory work, and writing of the manuscript: AE; study design: AE, WJ, MB and SH; mass cytometry analyses: JV and JJG; bioinformatics analysis: AY; mass spectrometry analyses: LT and RG; patient sample collection: MK and IH; supervision: WJ, MB, and SH; reviewing and editing: WJ, MG, MB, RF, HL, PM, IR, and RB; *in vivo* studies and technical support: AE, OW, PH, IA, SR, MG, and SH. All authors have read and agreed to the published version of the manuscript.

# References


1. Gregoretti I V., Lee YM, Goodson H V. Molecular evolution of the histone deacetylase family: Functional implications of phylogenetic analysis. J Mol Biol. 2004;338(1):17–31.
2. Sweet MJ, Shakespear MR, Kamal NA, Fairlie DP. HDAC inhibitors: Modulating leukocyte differentiation, survival, proliferation and inflammation. Immunol Cell Biol. 2012;90(1):14– 22.
3. Singh AK, Bishayee A, Pandey AK. Targeting histone deacetylases with natural and synthetic agents: An emerging anticancer strategy. Nutrients. 2018;10(6):731.
4. Li Y, Wang F, Chen X, Wang J, Zhao Y, He* YL and Bin. Zinc-dependent Deacetylase (HDAC) Inhibitors with Different Zinc Binding Groups. Vol. 19, Current Topics in Medicinal Chemistry. 2019;19(3):223–41.
5. Subramanian S, Bates SE, Wright JJ, Espinoza-Delgado I, Piekarz RL. Clinical toxicities of histone deacetylase inhibitors. Pharmaceuticals. 2010;3(9):2751–67.
6. Van Veggel M, Westerman E, Hamberg P. Clinical Pharmacokinetics and Pharmacodynamics of Panobinostat. Clin Pharmacokinet. 2018;57(1):21–9.
7. Das Gupta K, Shakespear MR, Iyer A, Fairlie DP, Sweet MJ. Histone deacetylases in monocyte/macrophage development, activation and metabolism: refining HDAC targets for inflammatory and infectious diseases. Clin Transl Immunol. 2016;5(1):e62-10.
8. Nijhuis L, Peeters JGC, Vastert SJ, Van Loosdregt J. Restoring T cell tolerance, exploring the potential of histone deacetylase inhibitors for the treatment of juvenile idiopathic arthritis. Front Immunol. 2019;10(FEB):1–14.
9. Kjær ASHK, Brinkmann CR, Dinarello CA, Olesen R, Ostergaard L, Søgaard OS, et al. The histone deacetylase inhibitor panobinostat lowers biomarkers of cardiovascular risk and inflammation in HIV patients. Aids. 2015;29(10):1195–200.
10. Brinkmann CR, Højen JF, Rasmussen TA, Kjær AS, Olesen R, Denton PW, et al. Treatment of HIV-Infected Individuals with the Histone Deacetylase Inhibitor Panobinostat Results in Increased Numbers of Regulatory T Cells and Limits Ex Vivo Lipopolysaccharide-Induced Inflammatory Responses. mSphere. 2018;3(1):1–14.
11. Choi SW, Gatza E, Hou G, Sun Y, Whitfield J, Song Y, et al. Histone deacetylase inhibition regulates inflammation and enhances Tregs after allogeneic hematopoietic cell transplantation in humans. Blood. 2015;125(5):815–9.
12. Glauben R, Batra A, Fedke I, Zeitz M, Lehr HA, Leoni F, et al. Histone Hyperacetylation Is Associated with Amelioration of Experimental Colitis in Mice. J Immunol. 2006 Apr;176(8):5015–22.
13. Glauben R, Siegmund B. Molecular basis of histone deacetylase inhibitors as new drugs for the treatment of inflammatory diseases and cancer. Methods Mol Biol. 2009;512:365–76.
14. Joosten LA, Leoni F, Meghji S, Mascagni P. Inhibition of hdac activity by itf2357 ameliorates joint inflammation and prevents cartilage and bone destruction in experimental arthritis. Mol Med. 2011;17(5–6):391–6.
15. Bombardo M, Saponara E, Malagola E, Chen R, Seleznik GM, Haumaitre C, et al. Class I histone deacetylase inhibition improves pancreatitis outcome by limiting leukocyte recruitment and acinar-to-ductal metaplasia. Br J Pharmacol. 2017 Nov 1;174(21):3865– 80.
16. Friedrich M, Gerbeth L, Gerling M, Rosenthal R, Steiger K, Weidinger C, et al. HDAC inhibitors promote intestinal epithelial regeneration via autocrine TGFβ1 signalling in inflammation. Mucosal Immunol. 2019;12(3):656–67.
17. Cui SN, Chen ZY, Yang XB, Chen L, Yang YY, Pan SW, et al. Trichostatin A modulates the macrophage phenotype by enhancing autophagy to reduce inflammation during polymicrobial sepsis. Int Immunopharmacol. 2019;77(1277):105973.

18. Ali MN, Choijookhuu N, Takagi H, Srisowanna N, Huynh MNN, Yamaguchi Y, et al. The HDAC inhibitor, SAHA, prevents colonic inflammation by suppressing proinflammatory cytokines and chemokines in DSS-induced colitis. Acta Histochem Cytochem. 2018;51(1):33–40.
19. Rius M, Lyko F. Epigenetic cancer therapy: Rationales, targets and drugs. Oncogene. 2012;31(39):4257–65.
20. Hadley M, Noonepalle S, Banik D, Villagra A. Functional Analysis of HDACs in Tumorigenesis. In: Brosh Jr. RM, editor. Protein Acetylation: Methods and Protocols. New York, NY: Springer New York; 2019. p. 279–307.
21. Suraweera A, O'Byrne KJ, Richard DJ. Combination therapy with histone deacetylase inhibitors (HDACi) for the treatment of cancer: Achieving the full therapeutic potential of HDACi. Front Oncol. 2018;8(MAR):1–15.
22. S h a h RR. Safety and Tolerability of Histone Deacetylase (HDAC) Inhibitors in Oncology [Internet]. Vol. 42, Drug Safety. Springer International Publishing; 2019. p. 235–45.
23. Needham LA, Davidson AH, Bawden LJ, Belfield A, Bone EA, Brotherton DH, et al. Drug targeting to monocytes and macrophages using esterase-sensitive chemical motifs. J Pharmacol Exp Ther. 2011;339(1):132–42.
24. Jones GR, Bain CC, Fenton TM, Kelly A, Brown SL, Ivens AC, et al. Dynamics of colon monocyte and macrophage activation during colitis. Front Immunol. 2018;9:2764.
25. Kamada N, Hisamatsu T, Okamoto S, Chinen H, Kobayashi T, Sato T, et al. Unique CD14+ intestinal macrophages contribute to the pathogenesis of Crohn disease via IL-23/IFN-γ axis. J Clin Invest. 2008 Jun 2;118(6):2269–80.
26. Martin JC, Chang C, Boschetti G, Ungaro R, Giri M, Grout JA, et al. Single-Cell Analysis of Crohn's Disease Lesions Identifies a Pathogenic Cellular Module Associated with Resistance to Anti-TNF Therapy. Cell. 2019;178(6):1493-1508.e20.
27. Luque-Martin R, Van Den Bossche J, Furze RC, Neele AE, Van Der Velden S, Gijbels MJJ, et al. Targeting histone deacetylases in myeloid cells inhibits their maturation and inflammatory function with limited effects on atherosclerosis. Front Pharmacol. 2019;10(OCT):1–14.
28. Finck R, Simonds EF, Jager A, Krishnaswamy S, Sachs K, Fantl W, et al. Normalization of mass cytometry data with bead standards. Cytom Part A. 2013 May;83 A(5):483–94.
29. Zunder ER, Finck R, Behbehani GK, Amir EAD, Krishnaswamy S, Gonzalez VD, et al. Palladium-based mass tag cell barcoding with a doublet-filtering scheme and single-cell deconvolution algorithm. Nat Protoc. 2015 Jan 1;10(2):316–33.
30. Van Gassen S, Callebaut B, Van Helden MJ, Lambrecht BN, Demeester P, Dhaene T, et al. FlowSOM: Using self-organizing maps for visualization and interpretation of cytometry data. Cytom Part A. 2015 Jul 1;87(7):636–45.
31. Crawford K, Gabuzda D, Pantazopoulos V, Xu J, Clement C, Reinherz E, et al. Circulating CD2+ monocytes are dendritic cells. J Immunol. 1999 Dec;163(11):5920–8.
32. Di Pucchio T, Lapenta C, Santini SM, Logozzi M, Parlato S, Belardelli F. CD2+/ CD14+ monocytes rapidly differentiate into CD83+ dendritic cells. Eur J Immunol. 2003 Feb;33(2):358–67.
33. Bujko A, Atlasy N, Landsverk OJB, Richter L, Yaqub S, Horneland R, et al. Transcriptional and functional profiling defines human small intestinal macrophage subsets. J Exp Med. 2018 Feb 1;215(2):441–58.

34. Gough PJ, Gordon S, Greaves DR. The use of human CD68 transcriptional regulatory sequences to direct high-level expression of class A scavenger receptor in macrophages in vitro and in vivo. Immunology. 2001;103(3):351–61.
35. Crouch SP, Kozlowski R, Slater KJ, Fletcher J. The use of ATP bioluminescence as a measure of cell proliferation and cytotoxicity. J Immunol Methods. 1993;160(1):81–8.
36. Satoh T, Hemmerlein B, Zschunke F, Radzun HJ. In situ detection of human monocyte/macrophage serine esterase-1 mRNA expression in human tissues. Pathobiology. 1999;67(3):158–62.
37. Capece D, D'Andrea D, Begalli F, et al. Enhanced triacylglycerol catabolism by carboxylesterase 1 promotes aggressive colorectal carcinoma. J Clin Invest. 2021 Jun 1;131(11) :e137845.
38. Sidler MA, Leach ST, Day AS. Fecal S100A12 and fecal calprotectin as noninvasive markers for inflammatory bowel disease in children. Inflamm Bowel Dis. 2008 Mar;14(3):359–66.
39. Realegeno S, Kelly-Scumpia KM, Dang AT, Lu J, Teles R, Liu PT, et al. S100A12 Is Part of the Antimicrobial Network against Mycobacterium leprae in Human Macrophages. PLoS Pathog. 2016 Jun 1;12(6):e1005705.
40. Heilmann RM, Nestler J, Schwarz J, Grützner N, Ambrus A, Seeger J, et al. Mucosal expression of S100A12 (calgranulin C) and S100A8/A9 (calprotectin) and correlation with serum and fecal concentrations in dogs with chronic inflammatory enteropathy. Vet Immunol Immunopathol. 2019 May 1;211:64–74.
41. Däbritz J, Musci J, Foell D. Diagnostic utility of faecal biomarkers in patients with irritable bowel syndrome. World J Gastroenterol. 2014;20(2):363.
42. Planell N, Masamunt MC, Leal RF, et al. Usefulness of Transcriptional Blood Biomarkers as a Non-invasive Surrogate Marker of Mucosal Healing and Endoscopic Response in Ulcerative Colitis. J Crohns Colitis. 2017 Nov 1;11(11):1335–46.
43. Foell D, Wittkowski H, Kessel C, Lüken A, Weinhage T, Varga G, et al. Proinflammatory S100A12 Can Activate Human Monocytes via Toll-like Receptor 4. 2013 Jun 14;187(12):1324–34.
44. Loes AN, Bridgham JT, Harms MJ. Coevolution of the Toll-Like Receptor 4 Complex with Calgranulins and Lipopolysaccharide. Front Immunol. 2018 Feb 21;9(FEB).
45. Grainger JR, Konkel JE, Zangerle-Murray T, Shaw TN. Macrophages in gastrointestinal homeostasis and inflammation. Pflügers Arch - Eur J Physiol 2017 4693. 2017 Mar 10;469(3):527–39.
46. Rossini V, Zhurina D, Radulovic K, Manta C, Walther P, Riedel CU, et al. CX3 CR1+ cells facilitate the activation of CD4 T cells in the colonic lamina propria during antigen-driven colitis. Mucosal Immunol 2014 73. 2013 Oct 16;7(3):533–48.
47. Toribio-Fernández R, Herrero-Fernandez B, Zorita V, López JA, Vázquez J, Criado G, et al. Lamin A/C deficiency in CD4+ T-cells enhances regulatory T-cells and prevents inflammatory bowel disease. J Pathol. 2019 Dec 1;249(4):509–22.
48. Laribee RN, Klemsz MJ. Loss of PU.1 Expression Following Inhibition of Histone Deacetylases. J Immunol. 2001 Nov 1;167(9):5160–6.
49. Rosa A, Ballarino M, Sorrentino A, Sthandier O, De Angelis FG, Marchioni M, et al. The interplay between the master transcription factor PU.1 and miR-424 regulates human monocyte/macrophage differentiation. Proc Natl Acad Sci U S A. 2007 Dec 11;104(50):19849–54.
50. Gatla HR, Muniraj N, Thevkar P, Yavvari S, Sukhavasi S, Makena MR. Regulation of chemokines and cytokines by histone deacetylases and an update on histone decetylase inhibitors in human diseases. Vol. 20, International Journal of Molecular Sciences. MDPI AG; 2019;20(5):1110.
51. Zigmond E, Varol C, Farache J, Elmaliah E, Satpathy AT, Friedlander G, et al. Ly6Chi Monocytes in the Inflamed Colon Give Rise to Proinflammatory Effector Cells and Migratory Antigen-Presenting Cells. Immunity. 2012;37(6):1076–90.

52. Becker F, Kurmaeva E, Gavins FNE, Stevenson E V., Navratil AR, Jin L, et al. A criti- cal role for monocytes/macrophages during intestinal inflammation-associated lymphangiogenesis. Vol. 22, Inflammatory Bowel Diseases. 2016. 1326–1345 p.

53. Scheerens H, Hessel E, De Waal-Malefyt R, Leach MW, Rennick D. Characterization of chemokines and chemokine receptors in two murine models of inflammatory bowel disease: IL-10-/- mice and Rag-2-/- mice reconstituted with CD4+CD45RBhigh T cells. Eur J Immunol. 2001 May 1;31(5):1465–74.

54. Misaki K, Morinobu A, Saegusa J, Kasagi S, Fujita M, Miyamoto Y, et al. Histone deacetylase inhibition alters dendritic cells to assume a tolerogenic phenotype and ameliorates arthritis in SKG mice. Arthritis Res Ther. 2011;13(3):R77.

55. Jiang H, Zhang S, Song T, Guan X, Zhang R, Chen X. Trichostatin a protects dendritic cells against oxygen-glucose deprivation via the SRSF3/PKM2/glycolytic pathway. Front Pharmacol. 2018;9:612.

56. Brogdon JL, Xu Y, Szabo SJ, An S, Buxton F, Cohen D, et al. Histone deacetylase activities are required for innate immune cell control of Th1 but not Th2 effector cell function. Blood. 2007;109(3):1123-1130.

57. Kaisar MMM, Pelgrom LR, van der Ham AJ, Yazdanbakhsh M, Everts B. Butyrate conditions human dendritic cells to prime type 1 regulatory T cells via both histone deacetylase inhibition and G protein-coupled receptor 109A signaling. Front Immunol. 2017;8:1429.

58. Kiesler P, Fuss IJ, Strober W. Experimental models of inflammatory bowel diseases [Internet]. Vol. 59, Medecine et Hygiene. Cell Mol Gastroenterol Hepatol; 2001. p. 241–8.

59. Qualls JE, Tuna H, Kaplan AM, Cohen DA. Suppression of experimental colitis in mice by CD11c+ dendritic cells. Inflamm Bowel Dis. 2009;15(2):236–47.

60. Qualls JE, Kaplan AM, Van Rooijen N, Cohen DA. Suppression of experimental colitis by intestinal mononuclear phagocytes. J Leukoc Biol. 2006 Oct;80(4):802– 15.

61. Muzaki ARBM, Tetlak P, Sheng J, Loh SC, Setiagani YA, Poidinger M, et al. Intestinal CD103+ CD11b- dendritic cells restrain colitis via IFN-γ-induced anti-inflammatory response in epithelial cells. Mucosal Immunol. 2016 Mar 1;9(2):336–51.

62. Steinbach EC, Plevy SE. The role of macrophages and dendritic cells in the initiation of inflammation in IBD. Vol. 20, Inflammatory Bowel Diseases. Lippincott Williams and Wilkins; 2014 p. 166–75.

# Supplementary materials and methods

## Compounds

ESM-HDAC528 (also known as CHR-4487) and its non-hydrolysable HDAC800 control were provided by GlaxoSmithKline (Stevenage, United Kingdom). For *in vivo* studies, ESM-HDAC528 was dissolved in 0.9% NaCl saline containing 10% (2-Hydroxypropyl)-ß-cyclodextrin (Sigma/Aldrich), 2% dimethyl sulfoxide (DMSO; Sigma/Aldrich) and dosed intra-peritoneally at 1, 3 and 10 mg/kg as indicated. For *in vitro* studies both compounds were dissolved in 100% DMSO and used at concentrations ranging from 0.61 nM to 10 mM (0.245ug/L to 4.025mg/L).

## Reagents and cytokines

The following reagents were used in *in vitro* studies; HEPES (Thermofisher Scientific), L-glutamine (Thermofisher Scientific), penicillin/streptomycin (Lonza), foetal bovine serum (FBS; Serana), β-mercaptoethanol (Sigma), phosphate buffered saline (PBS; Thermofisher Scientific), calcium/magnesium-free Hank's balanced salt solution (HBSS; Thermofisher Scientific), lipopolysaccharide (LPS *Escherichia . coli 0111:B4* or *Salmonella Typh*; Sigma), mouse interferon gamma (IFNγ; Peprotech) mouse interleukin 4 (IL-4; Peprotech), mouse granulocyte-macrophage colony-stimulating factor (GM-CSF; Peprotech), human granulocyte-macrophage colony-stimulating factor (GM-CSF; R&D Systems), human macrophage colony-stimulating factor (M-CSF; R&D Systems), human interleukin 4 (IL-4; R&D Systems).

## Animals

The human CES1 transgenic mouse (*CES1/Es1e$^{lo}$*) was generated as described earlier (1,2), by cross- breeding CES1 transgenic mice with naturally low plasma esterase (Ces1c$^{e}$) *Es1e$^{lo}$* mice. This mouse strain expresses human CES1 predominantly in a monocyte-macrophage lineage-selective way, driven by a human CD68 promoter (3)and therefore represents an attractive candidate gene for the generation of a Mφ-specific gene-targeting vector. A transgene expression cassette that combines 2·9 kb of CD68 5' flanking sequence with the 83-bp first intron (IVS-1 and has low plasma esterase activity. The mice were brought from Genoway (Lyon, France) and further bred in the animal facility of the Amsterdam University Medical Center, Amsterdam. The transgenic mouse (*CES1/Es1e$^{lo}$*/Rag$^{-/-}$) was generated by cross-breeding human CES1 transgenic mouse (*CES1/Es1e$^{lo}$*) with the immunodeficient RAG$^{-/-}$ mice. All mice were genotyped using primers provided in **Table 3**. All animal studies were ethically reviewed and carried out in accordance with European Directive 2010/63/EEC, the guidelines of the Ethical Animal Research Committee of the University of Amsterdam and the GSK Policy on the Care, Welfare and Treatment of Animals.

## DSS colitis model

Ten- fourteen week old female *CES1/Es1e*$^{lo}$ mice were given 2% Dextran sulfate sodium (DSS; TdB Consultancy) in their drinking water for 7 days, followed by 2 days of normal drinking water. Simultaneously, mice received daily intra peritoneal (IP) injections of 1 or 3 mg/kg (and 3 or 10 mg/kg in a repeat experiment) of ESM-HDAC528 or vehicle until sacrifice. This regimen was based on earlier pharmacokinetic and pharmacodynamics data originating from the murine collagen-induced model of rheumatoid arthritis (2) as well as data generated from a pharmacokinetic studies performed by GSK (data not shown). During the study, body weight and behavior were monitored daily. After 9 days, the animals were sacrificed and the colon, blood, and spleen were collected, peritoneum lavage was conducted as described below for *ex vivo* peritoneal macrophage culture, and wet weight of colon was recorded together with the total length of the colon. The disease activity index (DAI) score – consisting of average scores of weight loss, diarrhea, and the presence of blood in the stool - was used to determine the clinical outcome of DSS-induced colitis on the day of sacrifice. The colon was washed and cut longitudinally in half, and one part was processed for histology, the other part was snap frozen for later cytokine mRNA expression analysis or processed for flow cytometry analysis.

## T cell transfer colitis model

We applied the T cell transfer model as follows; $CD4^{+}CD45Rb^{high}$ cells were isolated from spleens of C57BL/6 WT mice by magnetic bead depletion using dynabeads™ sheep anti-rat IgG (ThermoFisher), anti-CD11b (Biolegend), anti-CD45R (Sony) and anti-CD8a (Biolegend) followed by fluorescence-activated cell sorting using anti-CD45RB-FITC and anti-CD4-PE/Cy5 (BD Bioscience). Ten to fourteen weeks old female *CES1/Es1e*$^{lo}$/$Rag^{-/-}$ mice received intraperitoneally $4.75 \times 10^5$ $CD4^{+}CD45Rb^{high}$ cells; mice that did not receive T cells transfer served as control groups. Three weeks following transfer; mice received daily intra peritoneal (IP) injections of 3 mg/kg of ESM-HDAC528 or vehicle for another 4 weeks until sacrifice. Body weight was assessed three times a week then daily after start of compound treatment until sacrifice. Animals losing > 20% from their highest weight or showing sickness behavior were euthanized before 7 weeks and were excluded from the analysis. After 7 weeks, the animals were euthanized and the colon, blood, and spleen were collected. Spleen weight, wet weight of colon and colon total length were recorded. Colon density (weight / length ratio), an indicator of colon edema, was assessed. The disease activity index (DAI) score – consisting of total scores of colon thickness (0-3), diarrhea (0-3), and the presence of blood in the stool (0-3) – was used to determine the clinical outcome of the colitis on the day of sacrifice. Each colon was washed and cut longitudinally in half, and one part was processed for histology, the other part was snap frozen for subsequent cytokine protein expression analysis.

## Histopathology

Murine colon tissue was fixed in 10 % formalin and embedded in paraffin for routine histology. A blinded and experienced researcher evaluated formalin-fixed hematoxylin-eosin-stained tissue sections microscopically and scored the sections. For DSS model; scoring was evaluated based on the extent of the area involved, the number of follicle aggregates, edema, fibrosis, hyperplasia, erosion/ulceration, crypt loss, and infiltration of granulocytes and mononuclear cells as indicated in the **Table S1**. The total inflammation score was calculated as the average score of the above. For the T cell transfer model; scoring was evaluated as described earlier [4], based on goblet cell loss, crypt loss, crypt hyperplasia and submucosal inflammation as indicated in the **Table S2**. The total scores are calculated according to the formula (total score = goblet cell loss score + 2 x crypt loss score + 2 x crypt hyperplasia score + 3 x submucosal inflammation score).

## Mice colon and serum cytokines measurement

Frozen colon tissue was homogenized on ice in lysis buffer (150 mM NaCl, 15 mM Tris, 1 mM $MgCl{\cdot}6H_2O$, 1 mM $CaCl_2$, 1% Triton) with added protease inhibitor cocktail (Roche Applied Science), pH 7.4, diluted 1:1 with PBS. Blood was collected via cardiac puncture following mice sacrifice, allowed to clot at room temperature, then centrifuged and serum was collected. In colon tissue lysates or serum, protein concentrations of IL-6, IL-10, TNF-α, IFN-γ, IL-12 and CCL2 were measured with a mouse inflammation kit by BD cytometric bead assay (BD Bioscience) according to the manufacturer's protocol. Some cytokines were below detection limits of the kit, therefore only cytokines that were high enough to be reliably detected were shown. Colon protein expression was normalized to total protein per sample as measured by BCA Protein Assay Kit (Pierce).

## *Ex vivo* peritoneal macrophage assay

Upon sacrifice, the peritoneum was flushed with 10 mL ice cold PBS and the flush was collected. Flushed cells were cultured at a density of 1x10^6 cells/ mL in 24-well tissue culture plates in RPMI-1640 medium containing 25 mM HEPES, 2 mM L-glutamine, 100 U/mL penicillin/streptomycin, and 10% FBS. After 24 hours, non-adherent cells were washed away, and the adherent cells (macrophages) were left without stimulation or stimulated for another 24 hours with 10 ng/mL LPS. Supernatants were collected for IL-6, TNF-α and IL-10 protein quantification.

## Bone marrow derived macrophage and dendritic cell culture

Bone marrow was harvested from the femurs of *CES1/Es1e*$^{lo}$ or WT mice by flushing. For bone marrow derived macrophages (BMDM), cells were cultured in triple-

vented, 145mm, sterile Petri dish (Sigma/Aldrich), in 25mL L929-conditioned culture medium (ATCC, Manassas, VA, USA) for 6 days, 10 mL. Fresh medium was added on day 3. On day 6, BMDM were harvested with cold PBS, plated out at $2x10^6$ cells/mL in 6-well culture plate in BMDM medium (RPMI-1640 containing 25mM HEPES, 2mM L-glutamine, 100 U/mL penicillin/streptomycin, and 10% FBS) and polarized for further 2 days with 50 ng/mL IFNγ (for $M_{IFNg}$) or 40 ng/mL IL-4 (for $M_{IL-4}$) or BMDM medium (for M0). For Bone marrow derived dendritic cells (BMDCs), cells were cultured in the presence of 20 ng/mL GM-CSF for 6 days in BMDCs medium (RPMI-1640 containing 25mM HEPES, 2mM L-glutamine, 100 U/mL penicillin/streptomycin, 10% FCS and $4x10^{\wedge-6}$ % β-mercaptoethanol). Media was refreshed at days 3 and 6. On day 7, BMDCs were harvested and plated out in $1x10^6$ cells/mL in 24-well culture plate with or without 10 ng/mL LPS for 1 day to generate mature dendritic cells (mDCs). At the end of culture, cells were harvested for RNA isolation or further incubated for 4 hours with 50 nM ESM-HDAC528 or DMSO (0.00025 %) for subsequent flow cytometry analysis of acetylated lysine levels.

## Flow cytometry analysis of murine blood and colon tissue

For *ex vivo* mouse blood flow cytometry analysis, 100 µL of blood was collected from mice 3 h after i.p. injection of ESM-HDAC528 or vehicle. The blood was stained for immune cells surface markers and intracellular acetylated lysine as described previously [1], using anti-CD3-AlexaFlour700 (clone 500A2, Biolegend), anti-B220-Pacific Blue (clone RA3-6B2, Biolegend), anti-Ly6G-FITC (clone 1A8, Biolegend), anti-Ly6C-BV510 (clone HK1.4, Biolegend), anti-CD11b-Percp (clone M1/70, Biolegend), anti-CD115-PECy7 (clone AFS98, Biolegend) and anti-PanAck-AlexaFlour647 (clone 15G10, Biolegend) antibodies.

For analysis of murine colonic tissue, colons were removed and cut in half longitudinally; one part was used for flow cytometry analysis, the other for histological assessment. Two colons were pooled, cut into pieces and washed with PBS. Subsequently, colon pieces were incubated in HBSS supplemented with 5 mM EDTA and 2% FBS for 20 minutes while shaking. Cells and remaining tissue were pelleted, minced very finely, and incubated for 40 min while stirring at 37°C with HBSS supplemented with 2% FCS, 62.5 µg/mL Liberase TL, and 200 µg/mL DNase I (both enzymes from Roche Applied Bioscience). Suspensions were then passed through a cell strainer, pelleted and stained. Cells were washed with FACS buffer (0.5% BSA, 0.01% NaN3 in PBS), and stained for CD45-APC/CY7 (clone F11 , Biolegend), CD3-AF700 (clone 500A2, Biolegend), Ly6G-FITC (clone 1A8, Biolegend), CD11b-Percp (clone M1/70, Biolegend), CD11c (clone HL3, Biolegend), CD64-PE (clone X54-5/7.1, Biolegend), Ly6C-BV510 (clone HK1.4, Biolegend) and MHCII-PE7 (clone AF6-120.1, Biolegend). Cells were then stained with DAPI to discriminate live cells.

## Flow cytometry analysis of human PBMC

Peripheral blood mononuclear cells (PBMC) were isolated from whole blood using Ficoll density centrifugation, washed in FACS Buffer and stained for CD3-PE (clone HIT3a, Biolegend), CD19-PerCP/Cy5.5 (clone HIB19, Biolegend), CD14-FITC (clone M5E2, Biolegend) and CD16-BV421 (clone 3G8, BD). Cells were then fixed and permeabilized using FIX & PERM Cell Permeabilization kit (ThermoFisher), stained with CES1 antibody (polyclonal, Thermo Scientific) then goat anti-rabbit secondary antibody, AF647 (Invitrogen). All samples were acquired using a FACS Fortessa (BD Biosciences) and analyzed using FlowJo software (Treestar Inc., Ashland, OR). All clinical samples were collected with patient consent; the accredited Medical Ethics Committee at the Amsterdam UMC, University of Amsterdam approved the protocol.

## Mass cytometry of human PBMC

*Antibodies*; the details of the antibody mass cytometry panel (including clone, metal tag, and supplier) are listed in **Table S4**. The antibodies that were not purchased from Fluidigm were conjugated using the MAXPAR X8 Metal Labeling Kit (Fluidigm), following manufacturer's instructions. After conjugation, antibody recovery was determined on a spectrophotometer (Nanodrop, ThermoFisher) at 280 nm and validated in a test staining with a positive control.

## Staining and barcoding

Cryopreserved PBMCs, previously collected from healthy donors (n=9) were thawed, washed with Cell Staining Buffer (CSB, Fluidigm), and incubated with Human TruStain FcX™ Fc Receptor Blocking Solution (Biolegend). Cells were stained with a cocktail of metal-conjugated antibodies against cell surface markers (CCR4, CCR5, CXCR3, α4β7, CCR9, CCR10), washed and fixed with 1.6% paraformaldehyde (PFA). Cells were permeabilized by Maxpar Barcode Perm Buffer (Fluidigm), incubated with mass tag barcodes in permeabilization buffer, and then stained with antibodies against surface targets. For intracellular staining, cells were washed and incubated with antibodies for intracellular markers (CES1 and CTLA-4), washed and then stained with goat anti-rabbit antibody, AF647 (Invitrogen) as a secondary staining for CES1. After washing with CSB, antibodies were fixed with 1.6% PFA, washed and incubated overnight with $^{191/193}$Ir DNA intercalator (1:4000) diluted in Fix-and-Perm Buffer (Fluidigm). The next day cells were washed before acquisition on the CyTOF3-Helios.

## Mass cytometry data acquisition

0.1X EQ Four Element Calibration Beads was prepared using Maxpar cell acquisition solution (CAS) and used as a carrier fluid for the cell samples. Samples were acquired on a CyTOF Helios mass cytometer at a rate of 200-250 events/second. Data were

normalized using bead normalization [5]. Deconvolution of pooled samples was performed by processing FCS files with the standard single-cell debarcoding algorithm for CyTOF data [6].

## Mass cytometry data analysis

FCS files were uploaded into Cytobank [7] for analysis and quality control. Signal intensities and sample acquisition rates were reviewed for stability over time and events gated based on the condition that flow was stable, excluding calibration beads, and within the 90 % percentile of all Gaussian parameters. Afterwards, $CD45^+$ live cells were selected through sequential gating as described before [8]. $CD45^+$ live cells were further analyzed using R Studio. Clusters of phenotypically similar cells were identified using the FlowSOM-package [9]. Initial SOM-clustering was set to 225 clusters, using markers listed in Table 4. The 225 formed clusters were manually metaclustered according to their phenotype lineages. For visualization and cluster interpretation we performed a tSNE dimensionality reduction in R using the same markers as the FlowSOM clustering as input, except CCR9 and CCR10. 10,000 events from each sample were randomly sampled to prevent overcrowding of the tSNE space. Perplexity was set at 30, theta at 0.5 and the number of iterations at 1500. A subsequent tSNE projection was performed only on events metaclustered and identified as monocytes, using all antibody marker parameters.

## Quantitative real time PCR

RNA was isolated using RNeasy mini kit (Qiagen) following the manufacturer's protocol. For human samples; cDNA was synthesized using cDNA synthesis kit (Qiagen) following the manufacturer's protocol. Quantitative PCR was performed using SensiFAST SYBR No-ROX (GC Biotech) on a QuantStudio Flex 7 (Applied Biosystems) to analyze expression levels of human *CES1* using QuantStudio real time PCR software. For murine samples, cDNA was synthesized using deoxynucleotide triphosphates (Thermo Fisher Scientific), Random primers (Promega), Oligo dT primers (Invitrogen), Revertaid, and Ribolock (both Fermentas). Murine samples were run on a LightCycler 480 II (Roche Applied Science) to analyze expression levels of human *CES1,* murine *TNFα, IL1β, CCL2, TLR4, S100A8, CXCL1, CXCL2* and *CXCR2* using LinRegPCR software. For normalization, human UBB or mouse NONO and TBP were used as reference genes. Primers are listed in **Table 3**.

## Immunofluorescence

Paraffin sections prepared from surgically resected colons of CD patients undergoing colectomy at Amsterdam University Medical Center were used, clinical characteristics of patients are provided in **Table S5**. Sections from macroscopically inflamed and

non-inflamed areas of the colon were deparaffinized, then slides were treated at 96°C for 5 minutes in 10 mM sodium citrate buffer pH 6.0 for antigen retrieval and cooled afterwards. PBT (PBS, 0.1% Triton X-100, 1% BSA) were used for blocking then slides were incubated for 2 hours at room temperature (RT) with PBT containing anti-CD68 (clone PG-M1, Dako) and anti-CES1 (polyclonal, Novus Biologicals). Slides were washed in TBS buffer ($ddH_2O$ containing 50nM Tris, 160 mM NaCl) and stained at RT with secondary antibodies labeled with a fluorescent dye (AlexaFluor 546 or AlexaFluor 488, polyclonal, Invitrogen). Slides were washed in TBS buffer and mounted with ProLong Gold Antifade reagent along with DAPI (Thermo Fisher Scientific). Images were taken with Leica DM6000 microscope using LAS AF software (Leica, Wetzlar, Germany). Counting cells positive for CD68 and CES1 was performed manually by a blinded researcher. Objective: X 20. All clinical samples were collected with patient consent, the accredited Medical Ethics Committee at the Amsterdam UMC, University of Amsterdam approved the protocol.

### *In vitro* human monocyte and macrophage assays

Peripheral blood mononuclear cells (PBMC) were isolated from whole blood using Ficoll density centrifugation. $CD14^+$ monocytes were isolated from the PBMC with a positive selection kit (Miltenyi Biotech). For macrophage generation, $CD14^+$ monocytes were incubated with 5 ng/mL GM-CSF for 5 days to generate macrophages. Freshly isolated $CD14^+$ monocytes or GM-CSF differentiated macrophages were then pre-incubated for 1 hour with ESM-HDAC528 or HDAC800 serially diluted (10 µM-0.61 nM final concentrations), then stimulated with 1 ng/mL LPS for 24 hours. Supernatants were then collected for cytokine analysis and cells were used for ATP bioluminescence assay. For CES1 expression analysis and mass spectrometry assays, immature DCs (imDCs) were generated after 5 days of $CD14^+$ monocyte incubation with 30 ng/mL GM-CSF and 20 ng/mL IL-4, then further matured for 1 day with 1 ng/mL LPS to generate mDCs. For mass spectrometry assay, the cells were further incubated with ESM-HDAC528 (1 µM) for 4 hours, supernatants were harvested at 0, 0.5, 1, 2 and 4 hours. The cells were lysed after 4 hours with M-PER (Mammalian Protein Extraction Reagent) buffer and used for both mass spectrometry analysis of parent and hydrolyzed forms of ESM-HDAC528 and HDAC800. The culture media used for incubation was RPMI 1640 medium supplemented with 10% FBS, 2 mM l-glutamine, and 100 U/mL penicillin/streptomycin. The human biological samples were sourced ethically and their research use was in accord with the terms of the informed consents under an IRB/EC approved protocol.

### Mass spectrometry assay

The analytical internal standard used in the HPLC-MS/MS quantification of samples was Labetalol with all concentrations and supporting data expressed in terms of free base. Cell lysate samples were matrix matched with MPER buffer (Thermo Fisher Scientific). Samples were extracted using protein precipitation with acetonitrile containing the internal standard Labetalol at 62.5 ng/mL. Samples were capped, mechanically shaken then centrifuged. The protein precipitated samples then were directly injected onto the HPLC-MS/MS system for analysis, or (in one experiment) first evaporated to dryness under a stream of nitrogen, then reconstituted in acetonitrile (1:10 diluted in water) before analysis. Analysis was conducted by reverse phase HPLC-MS/MS using a heat assisted electrospray interface in positive ion mode. Nominal MRM transitions for HDAC800, hydrolysed ESM-HDAC528 and parent ESM-HDAC528 were 391 to 178, 335 to 178 and 403 to 178, respectively. Samples were assayed against calibration standards prepared using a Tecan D300e digital dispenser. Stock solutions (0.01 & 0.2 mg/mL) were added for dispensing standard concentrations into control matrix over the range 0.1 to 8000 ng/mL. The lower limit of quantification was 0.4 ng/mL for HDAC800 and parent ESM-HDAC528 and 0.2 ng/mL (or 0.8 ng/mL in another experiment) for hydrolysed ESM-HDAC528.

### Human cytokine measurement

Cytokines were measured in supernatants using either Meso Scale Discovery (MSD) plates or enzyme-linked immunosorbent assay (ELISA) kits (R&D systems) according to the manufacturer's protocol. For MSD assay; plates were read on an MSD Sector Imager S 600 Reader and data were analyzed using Discovery Workbench 4.0.12.1 software.

### ATP luminescence assay

The CellTiter-Glo® Luminescent Cell Viability Assay was performed according to the manufacturer's protocol (Promega, UK). This assay quantifies ATP, an indicator of metabolically active cells. In brief, CellTiter-Glo Substrate and CellTiter-Glo Buffer were combined then added to cells (1:1) ratio, incubated for 5 minutes with shaking. Viability was assessed by measuring luminescence immediately using Envision. Data were normalized to the DMSO control.

### Bioinformatics analysis of publically available RNAseq data

The analysis performed was identical to what was published before [10]mainly expressed in immune cells, which contains multiple domains suggestive of an epigenetic reader function; namely a bromodomain, a PHD domain and a SAND domain. Single nucleotide polymorphisms and epigenetic modifications in the SP140 locus have been linked to autoimmune and inflammatory diseases including

Crohn's disease (CD. In brief, single-cell RNA-sequencing data from 11 involved and 11 paired uninvolved ileal biopsies was downloaded from the sequence read archive (SRP21627323) [11]. Cellranger (v3.1.0) was used to map the raw reads against GRCh38 and generate the unique molecular identifier (UMI) count matrices. The resulting UMI count matrices were then imported into the R statistical environment (v4.0.2) whereupon the samples were analyzed in an integrative fashion using Seurat (v4.0) [12]. The mononuclear phagocyte cells were identified based on the expression of monocyte markers (CD14 and FCGR3A), macrophage markers (CD163 and CD68), and dendritic cell markers (CLEC4A and CD1C). The MNP cells were then subsetted and subjected to trajectory inference using slingshot (v1.8) [13] on the 2000 most variable genes.

## Statistical analysis

Statistical analysis was performed using GraphPad Prism 7.0 (GraphPad Software). For analysis between two groups, non-parametric data were subjected to a Mann-Whitney U test and parametric data were subjected to a T-test. For multi-group analysis, non-parametric data were subjected to one-way ANOVA (Kruskall Wallis) followed by Dunn's post hoc analysis or two-way ANOVA test. P-value (p) $< 0.05$ was considered significant and was illustrated at $p \leq 0.05$ (*), 0.01 (**), 0.001 (***) or 0.0001 (****).

# References


1. Luque-Martin R, Van Den Bossche J, Furze RC, Neele AE, Van Der Velden S, Gijbels MJJ, et al. Targeting histone deacetylases in myeloid cells inhibits their maturation and inflammatory function with limited effects on atherosclerosis. Front Pharmacol. 2019;10(OCT):1–14.
2. Needham LA, Davidson AH, Bawden LJ, Belfield A, Bone EA, Brotherton DH, et al. Drug targeting to monocytes and macrophages using esterase-sensitive chemical motifs. J Pharmacol Exp Ther. 2011;339(1):132–42.
3. Gough PJ, Gordon S, Greaves DR. The use of human CD68 transcriptional regulatory sequences to direct high-level expression of class A scavenger receptor in macrophages in vitro and in vivo. Immunology. 2001;103(3):351–61.
4. Scheerens H, Hessel E, De Waal-Malefyt R, Leach MW, Rennick D. Characterization of chemokines and chemokine receptors in two murine models of inflammatory bowel disease: IL-10-/- mice and Rag-2-/- mice reconstituted with CD4+CD45RBhigh T cells. Eur J Immunol. 2001 May 1;31(5):1465–74.
5. Finck R, Simonds EF, Jager A, Krishnaswamy S, Sachs K, Fantl W, et al. Normalization of mass cytometry data with bead standards. Cytom Part A. 2013 May;83 A(5):483–94.
6. Zunder ER, Finck R, Behbehani GK, Amir EAD, Krishnaswamy S, Gonzalez VD, et al. Palladium-based mass tag cell barcoding with a doublet-filtering scheme and single-cell deconvolution algorithm. Nat Protoc. 2015 Jan 1;10(2):316–33.
7. Kotecha N, Krutzik PO, Irish JM. Web-based analysis and publication of flow cytometry experiments. Vol. 0 10, Current Protocols in Cytometry. NIH Public Access; 2010. p. Unit10.17.
8. Approach to Bivariate Analysis of Data Acquired Using the Maxpar Human Immune Monitoring Panel Kit Technical Note Approach to Bivariate Analysis of Data Acquired Using the Maxpar Human Immune Monitoring Panel Kit.
9. Van Gassen S, Callebaut B, Van Helden MJ, Lambrecht BN, Demeester P, Dhaene T, et al. FlowSOM: Using self-organizing maps for visualization and interpretation of cytometry data. Cytom Part A. 2015 Jul 1;87(7):636–45.
10. Ghiboub M, Koster J, Craggs PD, Li Yim AYF, Shillings A, Hutchinson S, et al. Modulation of macrophage inflammatory function through selective inhibition of the epigenetic reader protein SP140. bioRxiv. bioRxiv; 2020. p. 2020.08.10.239475.
11. Martin JC, Chang C, Boschetti G, Ungaro R, Giri M, Grout JA, et al. Single-Cell Analysis of Crohn's Disease Lesions Identifies a Pathogenic Cellular Module Associated with Resistance to Anti-TNF Therapy. Cell. 2019 Sep 5;178(6):1493- 1508.e20.
12. Hao Y, Hao S, Andersen-Nissen E, Mauck WM, Zheng S, Butler A, et al. Integrated analysis of multimodal single-cell data]. bioRxiv. bioRxiv; 2020. p. 2020.10.12.335331.
13. Street K, Risso D, Fletcher RB, Das D, Ngai J, Yosef N, et al. Slingshot: Cell lineage and pseudotime inference for single-cell transcriptomics. BMC Genomics. 2018 Jun 19;19(1):477.

# Supplementary figures

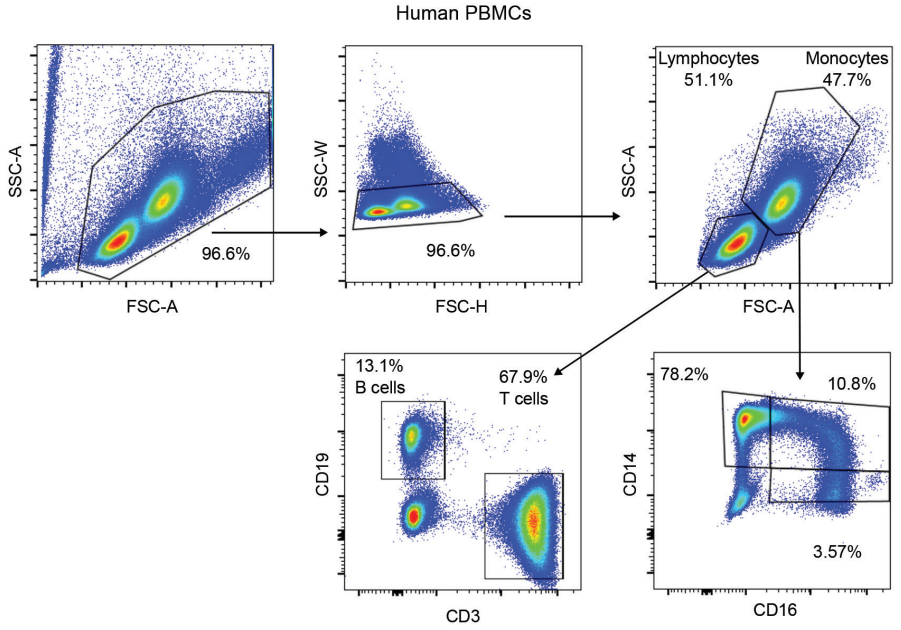


**Figure S1. Flow cytometry analysis of human PBMCs from healthy donors.**
Gating strategy for flow cytometry analysis of CES1 expression among T cells, B cells and monocytes subsets

> **Figure S2. ESM-HDAC528 specifically targets murine mononuclear myeloid cells both *in vivo* and *in vitro* in CES1\ES1$^{lo}$ mice.**
**(A)** Flow cytometry plots of bone marrow derived macrophage (BMDM) from both WT and CES1/Es1$^{lo}$ mice, treated with ESM-HDAC528 or DMSO and stained for acetylated lysine. **(B)** geoMFI of acetylated lysine expression were quantified, WT and CES1/Es1$^{lo}$ BMDM were compared **(C)** Human CES1 mRNA expression is shown among in vitro polarized BMDM and bone marrow derived dendritic cell (BMDC) subsets, generated from CES1\Es1$^{lo}$ mice. **(D)** In vitro generated BMDM and BMDC subsets were incubated with ESM-HDAC528 (50nM) or DMSO, acetylated lysine expression was assessed by flow cytometry and geoMFI was quantified, values are presented as fold change to DMSO control of each cell subset. **(E)** CES1/Es1$^{lo}$ mice received 3mg/kg ESM-HDAC528 or vehicle, 3 hours later acetylated lysine expression was analyzed by flow cytometry among blood immune cells, geoMFI of acetylated lysine expression was quantified within each cell types and compared across the groups. Data are represented as mean with SEM, n=2-3 for in vitro studies and n=5 for in vivo studies. Statistical testing was performed using two-way ANOVA test **(B, E)** or otherwise one-way ANOVA test, *P ≤ 0.05, **P ≤ 0.01, **** P ≤ 0.0001

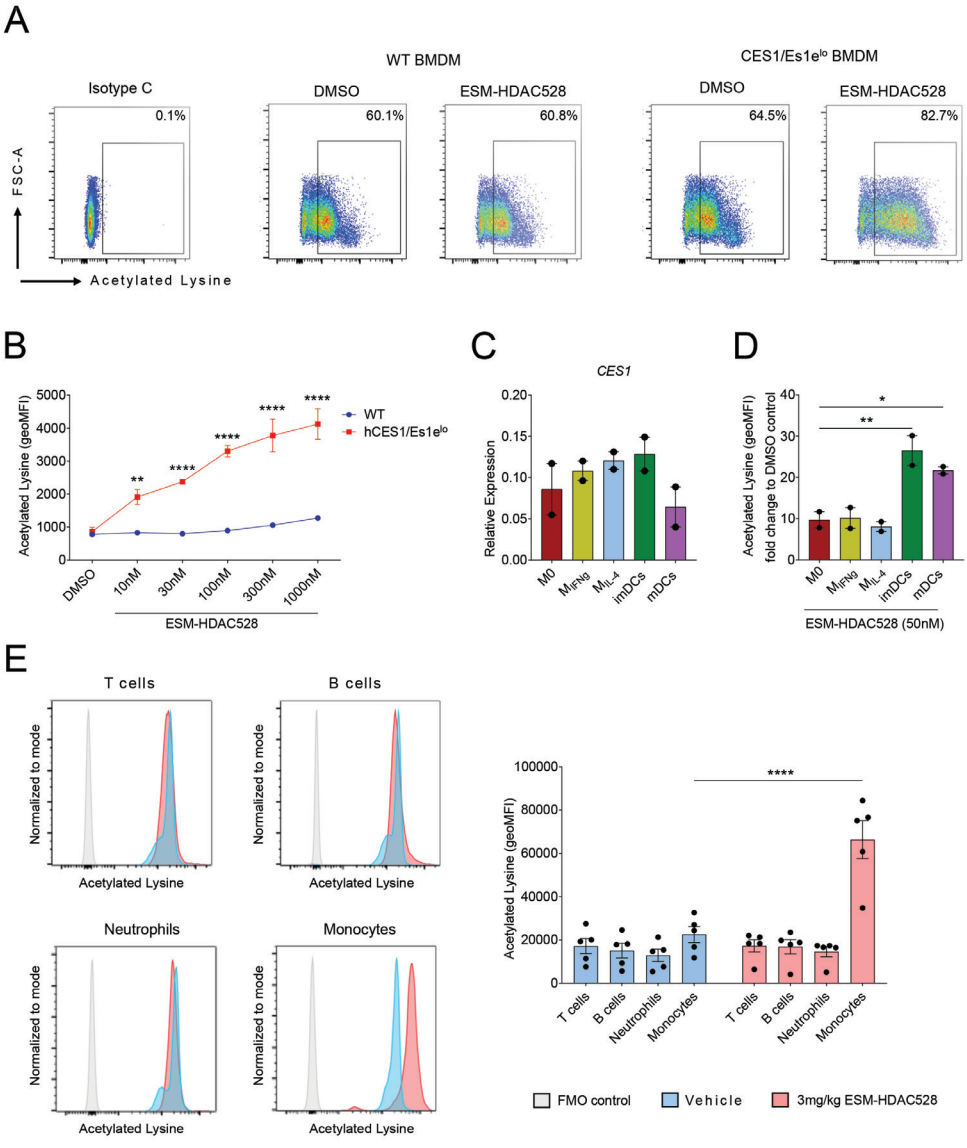
A
WT BMDM
CES1/Es1e^lo BMDM
Isotype C
DMSO
ESM-HDAC528
DMSO
ESM-HDAC528
0.1%
60.1%
60.8%
64.5%
82.7%
FSC-A
Acetylated Lysine
B
Acetylated Lysine (geoMFI)
WT
hCES1/Es1e^lo
DMSO
10nM
30nM
100nM
300nM
1000nM
ESM-HDAC528
C
CES1
Relative Expression
M0
M_IFNg
M_IL-4
imDCs
mDCs
D
Acetylated Lysine (geoMFI) fold change to DMSO control
ESM-HDAC528 (50nM)
E
T cells
B cells
Neutrophils
Monocytes
Normalized to mode
Acetylated Lysine
Acetylated Lysine (geoMFI)
FMO control
Vehicle
3mg/kg ESM-HDAC528

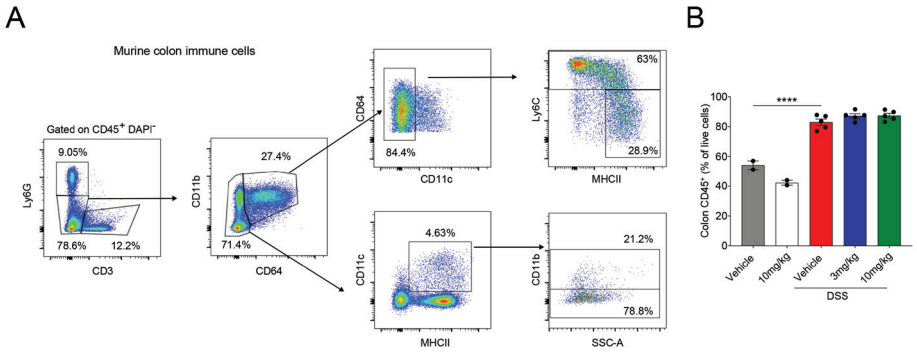


**Figure S3. Flow cytometry analysis for murine colon immune cells.**
(**A)** Flow cytometry analysis of murine colon mononuclear myeloid cells in DSS induced colitis model. **(B)** Frequency of total colon CD45$^+$ live cells are shown across all mice groups. Data are represented as mean with SEM, DSS groups (n=10) and no DSS groups (n=5), 2-3 mice colon were combined per sample. No DSS vehicle group is compared to DSS vehicle group. Statistical testing was performed using one-way ANOVA test, **** $P \leq 0.0001$.

# Supplementary Tables

**Table S1: inflammation score (DSS colitis model).**

| Score | 0 | 1 | 2 | 3 | 4 |
|---|---|---|---|---|---|
| **Area involved** | 0% | 1-10% | 10-25% | 25-50% | > 50% |
| **Follicles** | Normal (0-1) | Minimal (2-3) | Mild (4-5) | Moderate (6-7) | Severe (>7) |
| **Edema** | Absent | Minimal | Mild | Moderate | Severe |
| **Fibrosis** | Absent | Minimal | Mild | Moderate | Severe |
| **Erosion/ ulceration** | 0% | 1-10% | 10-25% | 25-50% | >50% |
| **Crypt loss** | 0% | 1-10% | 10-25% | 25-50% | > 50% |
| **Granulocytes** | Normal | Minimal increase | Mild increase | Moderate increase | Severe increase |
| **Mononuclear cells** | Normal | Minimal increase | Mild increase | Moderate increase | Severe increase |

**Table S2: inflammation score (T cell transfer colitis model).**

| Score | 0 | 1 | 2 | 3 |
|---|---|---|---|---|
| **Goblet cell loss** | 0% | <10% | 10-50% | > 50% |
| **Crypt density** | Normal | <10% decrease in density | >10% decrease in density | --- |
| **Hyperplasia** | None | slightly increased crypt length | 2 to 3 times increase in crypt length | >3 times increase in crypt length |
| **Submucosal infiltrate** | None | individual infiltrating cells | infiltrates | large infiltrates |

**Table S3: primers**

| Gene | Forward sequence | Backward sequence |
|---|---|---|
| **m-TNFα** | TGGAACTGGCAGAAGAGGCACT | CCATAGAACTGATGGAGGGAGGC |
| **m-IL1β** | GCCCATCCTCTGTGACTCAT | AGGCCACAGGTATTTTGTCG |
| **m-CCL2** | AGGTCCCTGTCATGCTTCTG | TCTCCAGCCTACTCATTGGG |
| **m-TLR4** | TGTCATCAGGGACTTTGCTG | TGTTCTTCTCCTGCCTGACA |
| **m-S100A8** | ACTTCGAGGAGTTCCTTGCG | TGCTACTCCTTGTGGCTGTC |
| **m-CXCL1** | CCACACTCAAGAATGGTCGC | TCTCCGTTACTTGGGGACAC |
| **m-CXCL2** | CCCAGACAGAAGTCATAGCCAC | TGGTTCTTCCGTTGAGGGAC |
| **m-CXCR2** | GCTCACAAACAGCGTCGTAGA | AGAATAGAGGGCATGCCAGA |
| **Es1e (for genotyping)** | TTGCCCACTTCTCAGCAC | CTACGTCCCTAACCTCACATACTC |
| **h-CES1 (for genotyping)** | GAAGGTCAACTGCATAGTGAG-TTTTAGGTTATGGCGACCCGCAG | CCTGAATTTTAGGCCAGCAAG |
| **m-TBP** | ACCGTGAATCTTGGCTGTAAAC | GCAGCAAATCGCTTGGGATTA |
| **m-NONO** | AAAGCAGGCGAAGTTTTCATTC | ATTTCCGCTAGGGTTCGTGTT |
| **h-UBB** | CGGCAAGACCATCACTCTGG | AAAGAGTGCGGCCATCTTCC |
| **h-CES1 (for mice samples)** | GGAACAGACGACACTGTCAAA | GCTCCAGCATCTCTGTGGTT |
| **h-CES1 (for human samples)** | CAAAGACTGGGGTCTTTTGC | AGCCATGGTAAGATGCCTTC |

**Table S4: Mass cytometry antibodies.**

| Target protein | Clone | Metal | Source | Used in high dimensional clustering and initial tSNE projection |
|---|---|---|---|---|
| **Cell identification** | | | | |
| **Barcodes** | | 103-110Pd | Fluidigm | |
| **Iridium** | | 191-193Ir | Fluidigm | |
| **Cisplatin** | | 194-195Pt | Fluidigm | |
| **Antibody markers** | | | | |
| **CD45** | HI30 | 89Y | Fluidigm | Yes |
| **CD49d** | 9F10 | 141Pr | Fluidigm | Yes |
| **CD11a** | HI111 | 142Nd | Fluidigm | Yes |
| **CD5** | UCHT2 | 143Nd | Fluidigm | Yes |
| **CD195 (CCR5)** | NP-6G4 | 144Nd | Fluidigm | Yes |
| **CD4** | RPA-T4 | 145Nd | Fluidigm | Yes |
| **CD8a** | RPA-T8 | 146Nd | Fluidigm | Yes |
| **CD7** | CD7-6B7 | 147Sm | Fluidigm | Yes |
| **CD25 (IL-2R)** | 2A3 | 149Sm | Fluidigm | Yes |
| **CD2** | TS1/8 | 151Eu | Fluidigm | Yes |
| **CD14** | 61D3 | 154Sm | eBioscience | Yes |
| **CD183 (CXCR3)** | G025H7 | 156Gd | Fluidigm | Yes |
| **CD194 (CCR4)** | L291H4 | 158Gd | Fluidigm | Yes |
| **CD197 (CCR7)** | G043H7 | 159Tb | Fluidigm | Yes |
| **CD28** | CD28.2 | 160Gd | Fluidigm | Yes |
| **CD69** | FN50 | 162Dy | Fluidigm | No |
| **CD161** | HP3G10 | 164Dy | Fluidigm | Yes |
| **CD45RO** | UCHL1 | 165Ho | Fluidigm | Yes |
| **CD44** | BJ18 | 166Er | Fluidigm | Yes |
| **CD27** | 323 | 167Er | Fluidigm | Yes |
| **CD45RA** | HI100 | 169Tm | Fluidigm | Yes |
| **CD3** | UCHT1 | 170Er | Fluidigm | Yes |
| **CD57** | HCD57 | 172Yb | Fluidigm | Yes |
| **HLA-DR** | L243 | 174Yb | Fluidigm | Yes |
| **CD127 (IL-7Ra)** | A019D5 | 176Yb | Fluidigm | Yes |
| **CD16** | 3G8 | 209Bi | Fluidigm | Yes |
| **CCR10** | 314305 | 148Nd | R&D Systems | No |

**Table S4: Continued**

| Target protein | Clone | Metal | Source | Used in high dimensional clustering and initial tSNE projection |
|---|---|---|---|---|
| **CD134 (OX40)** | ACT35 | 150Nd | Fluidigm | No |
| **CD95 (Fas)** | DX2 | 152Sm | Fluidigm | No |
| **CD366 (TIM-3)** | F382E2 | 153Eu | Fluidigm | No |
| **CD279 (PD-1)** | EH12.2H7 | 155Gd | Fluidigm | No |
| **CD152 (CTLA-4)** | 14D3 | 161Dy | Fluidigm | No |
| **CCR9** | L053E8 | 168Er | Fluidigm | No |
| **α4β7 (Vedolizumab)** | | 171Yb | Takeda | Yes |
| **CES-1** | Polyclonal | 175Lu | Fluidigm | No |

**Table S5: Colon immunofluorescence staining patients' characteristics (Figure. 3A-B)**

| Patient | Gender | Year of birth | Smoking | Diagnosis | Surgery | Medications | Colon IF staining |
|---|---|---|---|---|---|---|---|
| IRB045 | F | 1974 | No | CD | Colectomy | Systemic steroids | inflamed / non-inflamed portions |
| IRB058 | M | 1967 | Yes | CD | Ileocecal resection | Systemic steroids | inflamed portion |
| IRB059 | F | 1956 | Unknown | CD | Completion proctectomy | None | non-inflamed portion |
| IRB070 | F | 1990 | No | CD | Ileocecal resection | Topical steroids | inflamed portion |
| IRB071 | M | 1958 | No | CD | Proctectomy | Thiopurines | non-inflamed portion |
| IRB103 | F | 1989 | No | CD | Colectomy | VitD | non-inflamed portion |

# 3

# Chapter 3

## A BET Protein Inhibitor Targeting Mononuclear Myeloid Cells Affects Specific Inflammatory Mediators and Pathways in Crohn's Disease

**Ahmed M. I. Elfiky**†, Ishtu L. Hageman†, Marte A. J. Becker, Jan Verhoeff, Andrew Y. F. Li Yim, Vincent W. Joustra, Lieven Mulders, Ivan Fung, Inmaculada Rioja, Rab K. Prinjha, Nicholas N. Smithers, Rebecca C. Furze, Palwinder K. Mander, Matthew J. Bell, Christianne J. Buskens, Geert R. D'Haens, Manon E. Wildenberg and Wouter J. de Jonge

† Equally Contributing First authors

Cells, 2022.

# Abstract

## Background

Myeloid cells are critical determinants of the sustained inflammation in Crohn's Disease (CD). Targeting such cells may be an effective therapeutic approach for refractory CD patients. Bromodomain and extra-terminal domain protein inhibitors (iBET) are potent anti-inflammatory agents; however, they also possess wide-ranging toxicities. In the current study, we make use of a BET inhibitor containing an esterase sensitive motif (ESM-iBET), which is cleaved by carboxylesterase-1 (CES1), a highly expressed esterase in mononuclear myeloid cells.

## Methods

We profiled CES1 protein expression in the intestinal biopsies, peripheral blood, and CD fistula tract (fCD) cells of CD patients using mass cytometry. The anti-inflammatory effect of ESM-iBET or its control (iBET) were evaluated in healthy donor $CD14^+$ monocytes and fCD cells, using cytometric beads assay or RNA-sequencing.

## Results

CES1 was specifically expressed in monocyte, macrophage, and dendritic cell populations in the intestinal tissue, peripheral blood, and fCD cells of CD patients. ESM-iBET inhibited IL1β, IL6, and TNFα secretion from healthy donor $CD14^+$ monocytes and fCD immune cells, with 10- to 26-fold more potency over iBET in isolated $CD14^+$ monocytes. Transcriptomic analysis revealed that ESM-iBET inhibited multiple inflammatory pathways, including TNF, JAK-STAT, NF-kB, NOD2, and AKT signaling, with superior potency over iBET.

## Conclusions

We demonstrate specific CES1 expression in mononuclear myeloid cell subsets in peripheral blood and inflamed tissues of CD patients. We report that low dose ESM-iBET accumulates in CES1-expressing cells and exerts robust anti-inflammatory effects, which could be beneficial in refractory CD patients.



## Keywords

BET inhibitor; CES1; IBD.

# Introduction

Crohn's disease (CD) is a complex immune-mediated disease presenting as chronic inflammation of the gastrointestinal tract [1]. Immunomodulatory therapies are the mainstay of treatment, which include steroids, thiopurines, and biological agents, such as anti-TNF (infliximab, adalimumab), anti-α4β7 integrin (vedolizumab), and anti-IL12p40 (ustekinumab) [2, 3]. Current therapeutic strategies have a response rate of approximately 30% [4], making non-responsiveness to therapy, along with disease progression to a severe clinical phenotype, such as fistulizing CD (fCD) [3, 5, 6], a clinical challenge. Unfortunately, surgical removal of affected intestinal tissue is required in approximately 70% of CD patients [7], highlighting the unmet need to introduce new treatments that are better tolerated and demonstrate superior clinical efficacy.



Bromodomain and extra terminal (BET) domain-containing proteins are a family of epigenetic readers (BRD2, BRD3, BRD4, and BRDT) that bind acetylated lysine residues of histone proteins to allow for transcriptional complex formation and gene expression [8]. Regarding regulation of the immune response, the BET proteins are essential for the transcription of several inflammation-related genes and have therefore been targets of interest in drug development for inflammatory diseases and cancer [8, 9]. Small molecule inhibitors for BET proteins (iBET) show demonstrable therapeutic benefits in multiple pre-clinical models of inflammatory diseases [10, 11]. However, in relation to murine models of IBD, the outcome was uncertain. In T-cell mediated colitis, iBET improved colon inflammation [12], while in a dextran sulfate sodium (DSS)-induced colitis mouse-model (with chemically driven epithelia damage), colon inflammation was aggravated [13]. This unexpected outcome in the DSS-induced colitis model is largely explained by iBET toxicity to colon epithelium [14], which may limit the beneficial immunosuppressive effect. Several iBET compounds have been investigated in randomized clinical trials in cancer patients; overall, the clinical efficacy was limited, despite promising outcomes in pre-clinical cancer models [15]. Multiple adverse events (AE) were reported [16-18], including thrombocytopenia, anemia, neutropenia, diarrhea, and pneumonia, which limit further clinical development of these iBET compounds. Redirecting iBET to specific cell types may limit the wide-range toxicity and allow efficacy at a very low dose.

Esterase sensitive motif (ESM) technology has previously been described to achieve cell specific accumulation of the active drug, targeting mononuclear myeloid cells based on the presence of carboxylesterase-1 (CES1) [19]. This approach has demonstrated therapeutic benefits in pre-clinical models of arthritis [19], colitis [20],

peritonitis, and atherosclerosis [21], using an ESM-conjugated histone deacetylase enzyme (HDAC) inhibitor. We hypothesize that an ESM-conjugated iBET could improve tolerability by specifically targeting iBET to CES1 expressing cells within CD. This approach might be of great interest in the treatment of CD, as myeloid cells are key players in sustained inflammation [1]. In the current study, we are the first to investigate the efficacy of an iBET with an esterase sensitive motif (GSK3361191 or ESM-iBET) application in CD. We first profile CES1 expression in multiple CD or inflammatory bowel related clinical samples, such as intestinal biopsies, PBMCs from CD patients, and curettage material from fistula tracts of CD patients. Next, we provide comprehensive analysis of proteins and genes modulated by iBET in monocytes and compare the effect of ESM-iBET (GSK3361191) with the non-hydrolysable iBET control (GSK3235220)

## Materials and Methods

Detailed information on the materials, methods, and associated references can be found in the Supplementary Materials (SM).

### Compounds

GSK3361191 (ESM-iBET) and its non-hydrolysable control GSK3235220 (iBET) were provided by GlaxoSmithKline (Stevenage, UK). GSK3361191 (ESM-iBET) is a BET inhibitor with an esterase sensitive motif (ESM), and GSK3235220 (iBET) is a pan BET-inhibitor. GSK3361191 (ESM-iBET) is similar in its mechanism of action compared to an earlier published compound, GSK3358699 [22], and is cleaved by carboxylesterase 1 (CES1), which allows selective hydrolyzation within CES1 positive cells to a charged, intracellularly retained drug [19]. For in vitro studies, both compounds were dissolved in 100% DMSO and used at concentration ranges of 0.002 μM to 10 μM.

### Human Clinical Samples

The following clinical samples were analyzed: intestinal biopsies of inflammatory bowel disease (IBD) patients (CD patients and ulcerative colitis patients), PBMCs of CD patients, and fistula tract tissue of fCD patients. Samples were obtained from the department of gastroenterology and/or surgery at the Amsterdam UMC, University of Amsterdam, under the approval of the accredited Medical Ethics Committee (METC #NL53989.018.15, #NL75341.018.20) or the biobank committee of the Amsterdam UMC (178 #A201470). Intestinal biopsies, PBMCs, and fistula samples were cryopreserved and handled according to the methodology published by Konnikova *et al* [23]. Detailed information about the clinical sampling and experimental details

are found in the SM, "Additional information on clinical sampling and experimental work-up." The patient characteristics can be found in **Supplementary Tables S1–S3**.

## Mass Cytometry

Human clinical samples (see description above) were immunophenotyped using a CyTOF Helios mass cytometer. Staining, barcoding, data acquisition, and mass cytometry analysis are described in the supplementary methods. We made use of three different antibody panels: a biopsy panel, a PBMC panel, and a fistula panel (found in Supplementary Table S4). Acquisition was performed on the Cytometry by time of flight (CyTOF) 3-Helios. The sample was diluted in H2O and supplemented with 10% v/v of EQ Four Element Calibration beads (Fluidigm, San Francisco, U.S.). After acquisition, the data were normalized, and individual files were deconvoluted using the CyTOF software v6.7 functions. Different lineages (B cells, CD4 T cells, CD8 T cells, myeloid cells, and NK cells) were clustered using FlowSOM and subsequent manual annotation [24]. Data is visualized using tSNE, a dimensionality reduction tool for high-dimensional single-cell data in R [25, 26].



## Human PBMCs and Monocyte In Vitro Culture

We obtained buffy coats (healthy donors) from Sanquin Blood Bank, Amsterdam, and isolated the peripheral blood mononuclear cells (PBMCs) according to standard Ficoll (GE Healthcare Bio-Sciences AB, Danderyd, Sweden) density gradient centrifugation protocol [27]. We further isolated CD14+ monocytes using a human CD14 positive selection kit (Miltenyi Biotech, Germany).

For the in vitro culture for cytokine analysis, the CD14+ monocytes or PBMCs were pre-treated for 1 h with a concentration range of 0.002, 0.01, 0.04, 0.156, 0.625, 2.5, and 10 μM of either GSK3361191 (ESM-iBET), non-hydrolysable control GSK3235220 (iBET), or DMSO. After 1 h, cells were washed to remove the extracellular compound, stimulated with 10 ng/mL LPS dissolved in RPMI medium (Thermofisher Scientific, Waltham, MA U.S.), and incubated overnight. Supernatant was collected, and cytokine (TNFα, IL1β, and IL6) analysis was performed using Cytometric Bead Array (CBA) (BD Biosciences, Australia). Intracellular TNFα protein expression was detected by flow cytometry analysis (FACS Fortessa, BD Biosciences, New Jersey, U.S.) and analyzed using FlowJo software (Treestar Inc., Ashland, OR, USA). Cytokine data is visualized by normalizing the actual measured values to the DMSO control to correct for the biological variation in every individual donor.

For in vitro culture for RNA transcriptomics analysis, CD14+ monocytes were pre-treated for 1 h with 40 nM of either GSK3361191 (ESM-iBET), non-hydrolysable control GSK3235220 (iBET), or DMSO. After 1 h, cells were washed and stimulated with 10 ng/mL LPS dissolved in RPMI medium (Thermofisher Scientific, Waltham, MA, U.S.) and incubated for 4 h.

### *Ex vivo* Derived CD Fistula Tract Cells Culture

CD fistula samples were obtained from fistulizing CD patients undergoing surgery (Seton placement/removal, or inspection) at the Amsterdam UMC, location AMC. Fistula scrapings were mechanically digested by mashing and flushing through a 100 µm cell strainer (BD Falcon, Franklin Lakes, New Jersey, U.S.) placed on a 50 mL tube (Sarstedt, Germany), and immune cells were isolated using Ficoll isolation [26]. Immune cells were incubated for 16 h with a concentration range of 0.0025, 0.01, 0.04, 0.625, 2.5, and 10 µM of either GSK3361191 (ESM-iBET), non-hydrolysable control GSK3235220 (iBET), or DMSO resolved in RPMI medium (Thermofisher Scientific, Waltham, MA, U.S.). After incubation, the cells were either collected for cytokine analysis by CBA or flow cytometric analysis of intracellular TNFα. Cytokine data is visualized by normalizing the actual measured values to the DMSO control to correct for the biological variation in every individual patient.

### RNAseq Transcriptome Analysis

Transcriptomic analyses were performed through RNA sequencing. Briefly, mRNA was isolated using the Isolate RNA mini kit (Bioline, UK) and converted into cDNA. Subsequently, cDNA was sequenced in a 150 bp paired-ended fashion on the Illumina NovaSeq6000 to a depth of 40 million reads at the Amsterdam UMC Genomics Core Facility. The quality control of the reads was performed with FastQC (v0.11.8) and summarization through MultiQC (v1.0) [28]. The raw reads were aligned to the human genome (GRCh38) using STAR (v2.7.0) [29] and annotated using the Ensembl v95 annotation. Post-alignment processing was performed through SAMtools (v1.9), after which the reads were counted using the featureCounts function found in the Subread package (v1.6.3) [30]. Differential expression (DE) analysis was performed using the Bioconductor (v3.14) [31] package DESeq2 (v1.22.2) [32] in the R statistical environment (v3.46.0) [33], where we compared both BET-inhibitors (GSK3361191/ESM-iBET and control GSK3235220/iBET) with DMSO or GSK3361191/ESM-iBET with DMSO. Differentially expressed genes (DEGs) were defined as genes whose difference presented a Benjamini–Hochberg-adjusted p-value $< 0.05$. Gene set enrichment analysis was conducted with the fgsea package (v1.20) [34] using the Kyoto Encyclopedia of Genes and Genomes (KEGG) database as a reference [35]. Visualizations were created in ggplot2 (v3.3.5) [36].

### Statistical Analysis

Statistical analysis was performed using GraphPad Prism 7.0 (GraphPad Software, La Jolla, CA). Statistical testing was performed using a two-way ANOVA test; * $p \leq 0.05$, ** $p \leq 0.01$, *** $p \leq 0.001$, **** $p \leq 0.0001$; SEM is the standard error of the mean.

## Results



### Immuno-Phenotyping of IBD Intestinal Biopsies Reveals Specific CES1 Expression in CD14+ Myeloid Cell Population

In order to explore the potential application of ESM-conjugated molecules in the treatment of IBD, we examined CES1 expression in IBD clinical samples using mass cytometry analysis, with particular emphasis on the inflamed local tissue environment. First, we investigated the immune cell composition in intestinal biopsies collected from IBD patients during endoscopy. Biopsies were taken from six IBD patients and collected from inflamed areas (n = 6) or non-inflamed areas (n = 2). We were able to identify CD27− (naïve) and CD27+ (memory) B cells (CD45+CD45RA+HLA-DR+CD69+CD44+), CD4 T cells (CD45+CD3+CD69+ CD2+CD4+CD5+CD28+), CD8 T cells (CD45+CD3+CD8a+CD5+), mononuclear myeloid cells (CD45+CD14+CES1+HLA-DR+CD11a+CD44+CD11b+), epithelial cells (CD45−EpCAM+CD95+), and NK cells (CD45+CD45RA+CD161+CD2+CD7+) (**Figure 1A,C**). Furthermore, we identified a CD4−CD8− T cell population (CD45+CD3+CD69+CD44+), which is the double negative T cell fraction [37]. The mononuclear myeloid cells demonstrated a high expression of CD14 and a low expression of CD16. Among the defined CD intestinal biopsy-derived cells, we demonstrated that CES1 expression was restricted to the mononuclear myeloid population (**Figure 1B, C**), with a median of 80% CES1 expressing cells within this population (**Figure 1D**). Interestingly, we also demonstrated some CES1+ cells within the EpCAM+ fraction (epithelial cells), compared to the B cell, T cell, or NK cell fraction, however, with much less in frequency compared to CD14+ myeloid cells.

### CES1 Is Expressed in Peripheral Blood Mononuclear Myeloid Cells of CD Patients

Next, we aimed to define CES1-expressing immune cell populations in the peripheral blood of CD patients, determining whether CES1 expression, among identified populations, differs between biological therapy-responsive and non-responsive patients. Therefore, we isolated PBMCs from CD patients treated with the biological agent vedolizumab and analyzed them using CyTOF to define CES1 expression among identified immune cell populations.

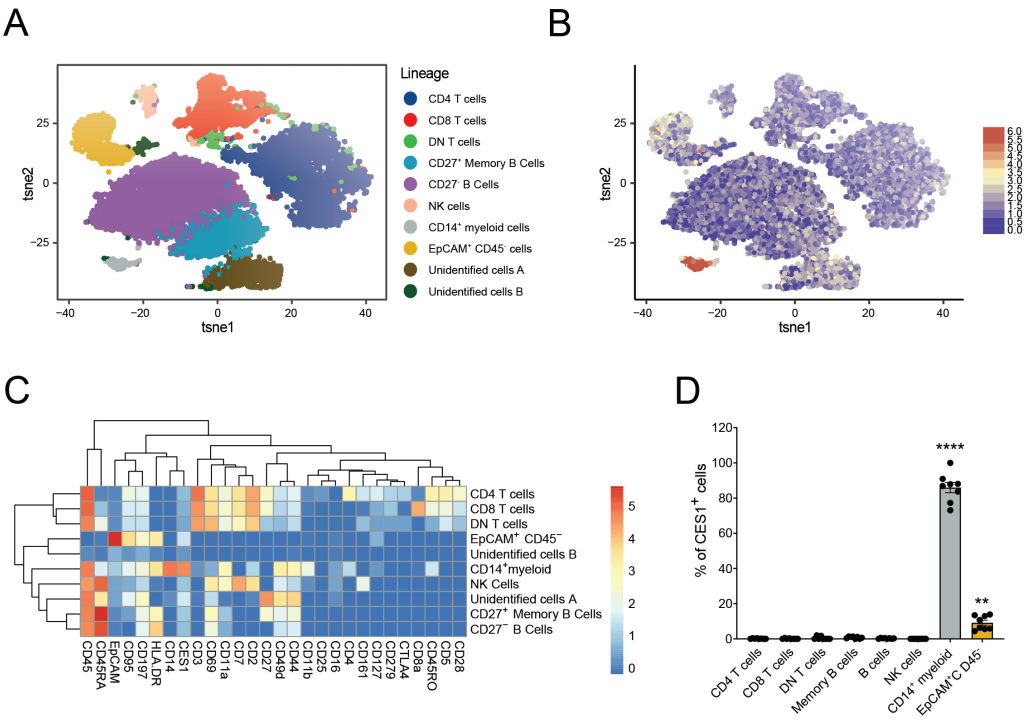


**Figure 1. Immunophenotyping of IBD intestinal biopsies reveals specific CES1 expression in CD14⁺ myeloid cells population.** (**A**) Intestinal biopsies were collected from 6 IBD patients. In total, 8 biopsies were collected (non-inflamed biopsies, n = 2, inflamed biopsies, n = 6, two pairs of non-inflamed and inflamed biopsies from the same patients, n = 2). Cells from intestinal biopsies of 6 IBD patients were barcoded, stained, and pooled for CyTOF and visualized in a tSNE plot after mass cytometry analysis. B cells, CD4 T cells, CD8 T cells, DN T cells, CD14⁺ myeloid cells, EpCAM⁺ cells, and NK cells were identified. (**B**) CES1 expression intensity was demonstrated among identified cell clusters in (**A**). (**C**) A heat map shows expression intensity of different (lineage) markers in relation to the identified cell clusters in (**A**). (**D**) Percentages of CES1⁺ cells among identified cell subsets are shown. Data are represented as mean with SEM of 8 samples; CD14⁺ myeloid cells, and EpCAM⁺ CD45⁻ cells were compared to the rest, Statistical testing was performed using a one-way ANOVA test; ** $p \leq 0.01$, **** $p \leq 0.0001$; SEM, standard error of the mean.

We identified CD4+ T cells, CD8+ T cells, NK cells, and B cells and extended the analysis of myeloid subsets to include classical monocytes (CD14+++CD16–), intermediate monocytes (CD14++CD16+), non-classical monocytes (CD14+CD16++), cDCs (CD16–CD14–HLADR++CD11a+ CD2+), and pDCs (CD16–CD14–HLADR+++CD45RA+ CD2++) (**Figure 2A,C**), although in the latter, we are missing the typical CD123 marker for classifying pDCs [38]. We demonstrated a high CES1 expression in the above-mentioned mononuclear myeloid populations (**Figure 2B, C**), with the highest expression in the intermediate monocytes and the non-classical monocytes (**Figure 2D**). PBMCs collected from vedolizumab non-responsive patients (n = 6) did not statistically differ

from responsive patients in the percentage of CES1+ cells in these myeloid subsets (**Figure 2D**).

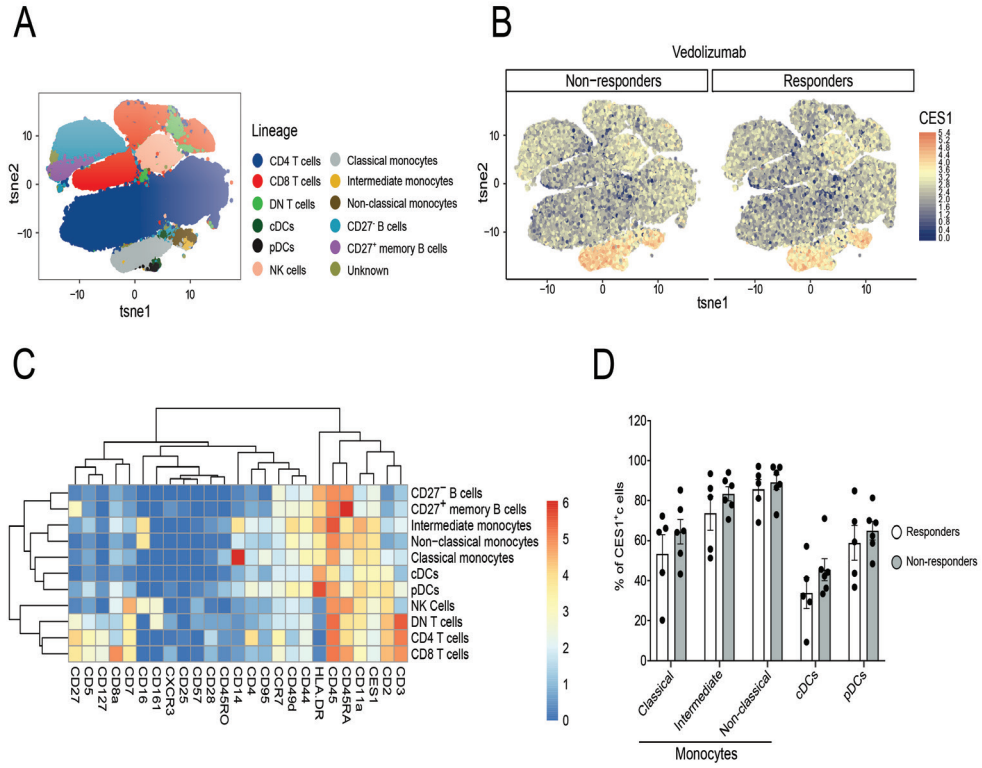


**Figure 2. CES1 is expressed in the mononuclear myeloid cells of peripheral blood from CD patients independent of therapy response.** (**A**) PBMCs from 11 CD patients (vedolizumab responders; n = 5, and vedolizumab non-responders; n = 6) were barcoded, stained, and pooled for CyTOF and visualized in a tSNE plot after mass cytometry analysis. B cells, CD4 T cells, CD8 T cells, DN T cells, NK cells, classical monocytes, intermediate monocytes, non-classical monocytes, cDCs, and pDCs were identified. (**B**) CES1 expression intensity in PBMCs was demonstrated among identified cell clusters in (**A**); responders (non-inflamed) and non-responders (inflamed) are displayed separately. (**C**) A heat map showing expression intensity of different (lineage) markers in relation to the identified cell clusters in (**A**). (**D**) Percentages of CES1$^{+}$ cells are shown among identified mononuclear myeloid cells subsets (pDCs, classical monocytes, cDCs, intermediate monocytes, and non-classical monocytes); responders (non-inflamed) and non-responders (inflamed) are compared.

## CES1 Is Expressed within Macrophages and Dendritic Cells Retrieved from Inflamed Fistula Tracts of CD Patients

Next, we explored the immune cell composition within the highly inflamed tissue environment of the fistula tracts of CD patients, using a penetrating phenotype that underwent surgical intervention (n = 13). We analyzed cells retrieved from CD

fistula tract curettage material using CyTOF and established the presence of different immune cell subsets, including basophils, B cells, CD4+ T cells, CD8+ T cells, NK cells, and mononuclear myeloid cell subsets (**Figure 3A, C**).

CES1 was highly expressed in the mononuclear myeloid cell compartment that includes macrophages (CD68+CD14+HLA-DR+CD44+CD11b++), CD163+ macrophages (CD68+CD14+HLA-DR++CD44++CD11b+CD163+), DCs (CD11c+HLA-DR+++CD14−CD141−CD123−), CD141+DCs type 1 (CD11c+HLA-DR+++CD14−CD141+CD123−), and pDCs (CD11c−HLA-DR++CD14−CD141−CD123+) (**Figure 3B, C**). We observed that the percentage of CES1 positive cells was higher in the macrophage populations compared to the DCs populations, with the lowset CES-1 expression noted in pDCs (**Figure 3D**). Other identified immune cell types showed minimal to no CES1 expression (**Figure 3C, D**).

## ESM-iBET Demonstrated an Increased Anti-Inflammatory Effect Compared to Its Non-Hydrolysable Control iBET in Healthy Donors Monocytes

Next, we evaluated the anti-inflammatory efficacy of an ESM-iBET (GSK33611910) and compared this to its non-hydrolysable iBET control (GSK3235220) in LPS stimulated monocytes and PBMCs from healthy donors. Since ESM-iBET specifically accumulates in CES1-positive myeloid cells, we hypothesized a more potent immunosuppressive effect in the monocytes. PBMCs from healthy donors (n = 3) were treated with a concentration range (0.002–10 μM) of ESM-iBET or iBET, and TNFα expression from CD14-expressing cells was determined using flow cytometry (**Figure 4A**). The frequency of TNFα-expressing CD14+ monocytes was significantly reduced in ESM-iBET treated cells (23.9%) compared to iBET 50.3%) or DMSO treated cells (49.0%) at 156 nM (**Figure 4B**).

Next, CD14+ monocytes from healthy donors (n = 3) were treated with a concentration range (0.002–10 μM) of ESM-iBET or iBET, and secreted inflammatory cytokines (IL1β, IL6, TNFα) were quantified with cytometric bead array (CBA). ESM-iBET demonstrated significantly increased potency to inhibit IL1β, IL6, and TNFα secretion when compared to the control iBET, with calculated IC50 of 9.6 nM vs. 257.4 nM (IL1β), 19.1 nM vs. 269.4 nM (IL6), and 14.8 nM vs. 145.6 nM (TNFα) for ESM-iBET or iBET, respectively (**Figure 4C**).

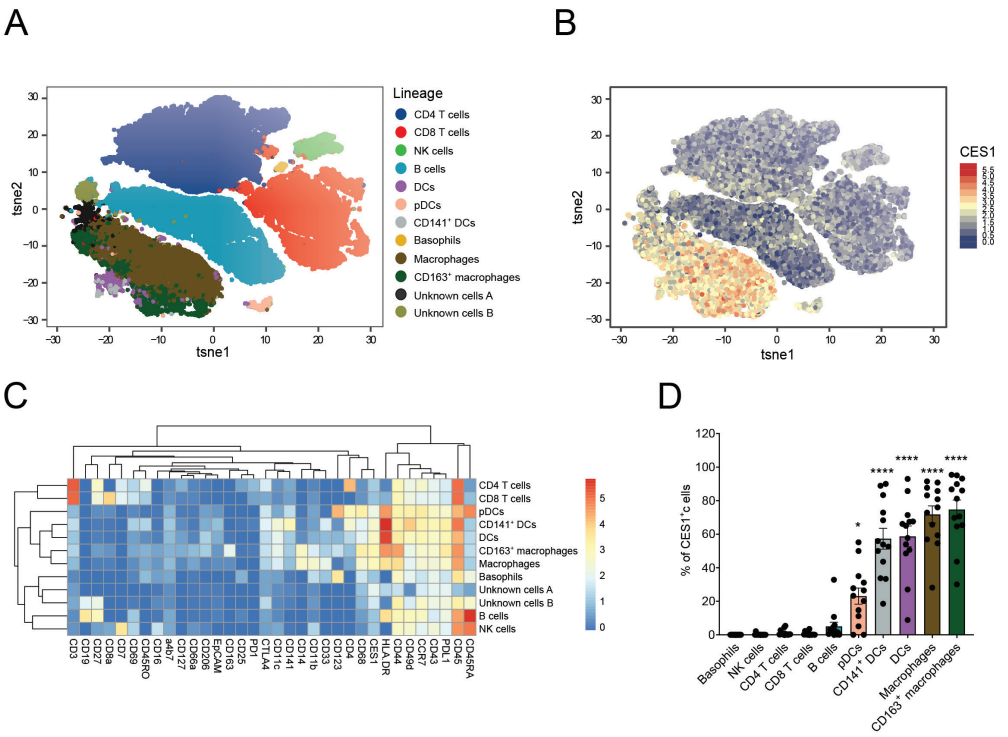


**Figure 3. CES1 is expressed within macrophages and dendritic cells retrieved from inflamed fistula tracts of CD patients.** (**A**) Fistula cells from CD patients (n = 13) fistula tract scrapings were barcoded, stained, and pooled for CyTOF and then visualized in a tSNE plot after mass cytometry analysis. Basophils, B cells, CD141$^+$ DC type1, CD4 T cells, CD8 T cells, NK cells, macrophages, CD163$^+$ resident macrophages, pDCs, and DCs were identified. (**B**) CES1 expression was demonstrated among identified cell clusters in (**A**). (**C**) A heat map showing expression intensity of different (lineage) markers in relation with the identified cell clusters in (**A**). (**D**) Percentages of CES1$^+$ cells are shown among identified cell clusters in (**A**). Data are represented as mean with SEM of 13 patients; pDCs, CD141$^+$ DCs, DCs, macrophages, and CD163$^+$ macrophages were compared to the other cells. Statistical testing was performed using a one-way ANOVA test; * $p \leq 0.05$, **** $p \leq 0.0001$. SEM; standard error of the mean.

## ESM-iBET and iBET Similarly Inhibited Inflammatory Cytokine Secretion from CD Fistula Tract-Derived Immune Cells in a Dose-Dependent Fashion

Subsequently, we extended these observations to evaluate ESM-iBET (GSK33611910) or iBET (GSK3235220) anti-inflammatory activity in immune cells retrieved from inflamed fistula tract of CD patients. *Ex vivo* isolated immune cells were treated with a concentration range (0.002–10 μM) of ESM-iBET or iBET, and inflammatory cytokines (IL1β, IL6, TNFα), secreted overnight, were quantified.

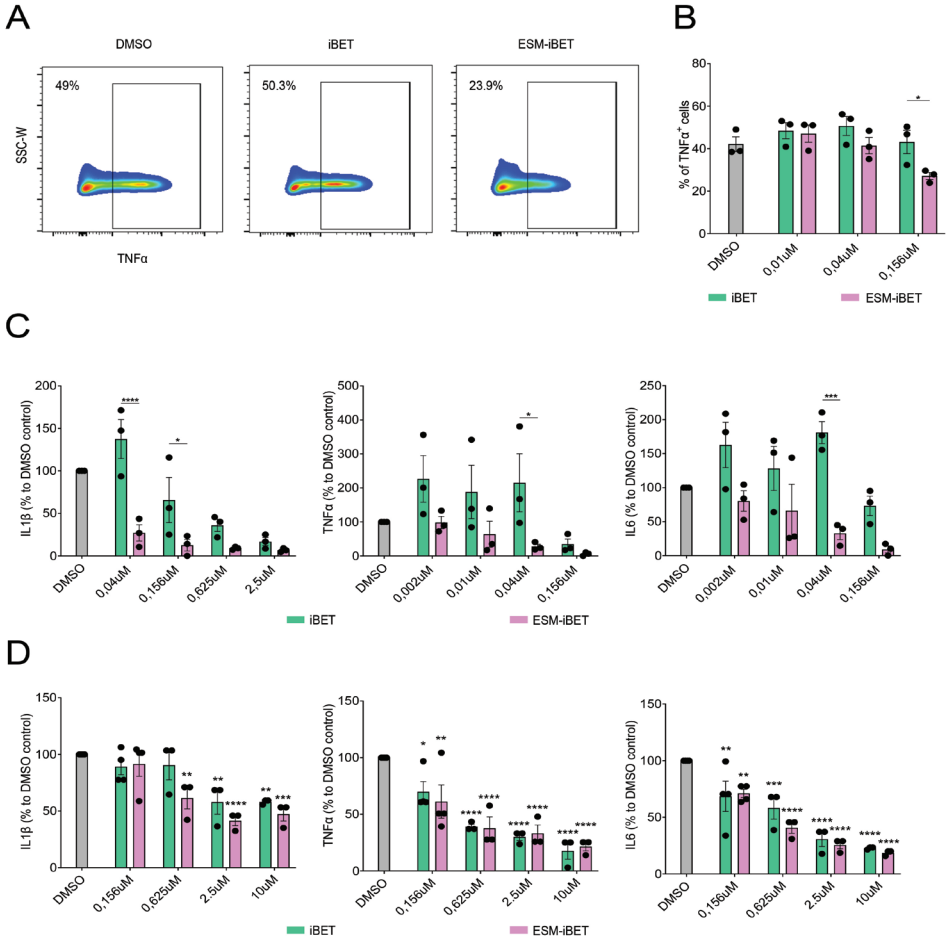


**Figure 4. The capacity of ESM-iBET and its non-hydrolysable control iBET to inhibit cytokines production in healthy donor CD14⁺ monocytes and CD fistula tract-derived immune cells.** All cell cultures were performed in a concentration range of 0.002–10 μM, and we visualized the concentrations, which demonstrated a clear difference between the iBET and the ESM-iBET (**A**) Representative flow cytometry plots showing TNF expression among CD14⁺ monocytes in PBMCs pre-treated with DMSO, iBET GSK33611910, or ESM-iBET GSK3235220 for 1 h, followed by LPS 40 ng/mL stimulation overnight. Representative plots are shown and are pre-gated on CD14⁺ cells after the exclusion of dead cells, CD3⁺, and CD19⁺ cells. (**B**) The percentage of TNF⁺ cells among total CD14⁺ monocytes in PBMCs is shown (n = 3). (**C**) IL1β, IL6 and TNFα protein secretion are measured with CBA in the supernatant of CD14⁺ isolated monocytes from healthy donors (n = 3), pre-treated with DMSO, iBET GSK33611910, or ESM-iBET GSK3235220, followed by LPS 10 ng/mL stimulation overnight. (**D**) IL1β, IL6, and TNFα protein secretion are measured with CBA in the supernatant of *ex vivo* CD fistula tract-derived immune cells, pretreated with DMSO, iBET GSK33611910, or ESM-iBET GSK3235220 (n = 3–4). Data are represented as mean with SEM of three to four donors/patients. In **(B)** and **(C)**, similar doses of iBET GSK33611910 or ESM-iBET GSK3235220 treatment are compared. In (**C**) and **(D)**, iBET GSK33611910 or ESM-iBET GSK3235220 are compared to the DMSO control. Statistical testing was performed using a two-way ANOVA test; * $p \leq 0.05$, ** $p \leq 0.01$, *** $p \leq 0.001$, **** $p \leq 0.0001$. SEM; standard error of the mean.

Both inhibitors efficiently reduced secreted inflammatory cytokines at relatively higher concentrations when compared to PBMC and monocyte cultures, with calculated IC50 of 441.3 nM vs. 1185 nM (IL1β), 280.3 nM vs. 358.3 nM (IL6), and 150.4 nM vs. 255.2 nM (TNFα) for ESM-iBET and iBET, respectively. There was no significant difference between the concentration of ESM-iBET and iBET required to inhibit inflammatory cytokine secretions from fCD *ex vivo* isolated immune cells (**Figure 4D**).



## ESM-iBET Influences the Transcription of Inflammatory Related Genes and Pathways with Increased Potency over iBET in Blood $CD14^+$ Monocytes

In order to gain more insight into the transcriptome changes mediated by BET inhibition, we compared monocytes pre-treated with ESM-iBET or iBET to the DMSO control treatment. In line with earlier functional assays (**Figure 4**), we expected the immunosuppression of different inflammatory pathways and aimed to assess the differences between ESM-iBET and iBET. In addition to this, CD14+, monocytes were isolated from healthy donor PBMCs (n = 5), pre-treated with 40 nM of either ESM-iBET (GSK33611910), iBET (GSK3235220), or DMSO, then stimulated with LPS for 4 h. Through principal component (PC) analysis, we observed a separation between DMSO+LPS, ESM-iBET+LPS, and iBET+LPS from non-LPS DSMO in PC2 (**Figure 5A**), suggesting an association within PC2 with LPS stimulation. By contrast, PC1 presented a separation between ESM-iBET pre-treated samples and the other sampels, which was not immediately visible for iBET, indicating that ESM-iBET pre-treatment affects monocytes more profoundly than iBET.

We identified 253 significantly differentially expressed genes (DEGs), of which 163 were upregulated and 90 were downregulated. Interestingly, visualizing the top 20 upregulated or downregulated DEGs in response to BET inhibition suggested that while both BET inhibitors functioned concordantly, ESM-iBET conferred a stronger effect, as opposed to iBET, at equimolar level concentrations (**Figure 5B**), in line with earlier cytokine inhibition data on monocytes (**Figure 4A–C**). Moreover, we compared the effect sizes of the top 10 upregulated or downregulated inflammation-related genes using the Wald statistic when comparing ESM-iBET to DMSO on the x-axis, and iBET compared to DMSO on the y-axis (**Figure 5C**). While most of the genes were affected in same direction by both BET inhibitors, the strongest effect was observed for ESM-iBET (**Figure 5C**). Focusing on the inflammation-related genes, we identified chemokines (CCL14—CCL25), cytokines (IL12B—IL36B—CSF2), and members of the MAPK signaling pathway (MAP3K4—MAP3K20) to be the most significantly downregulated after pretreatment with ESM-iBET relative to DMSO.

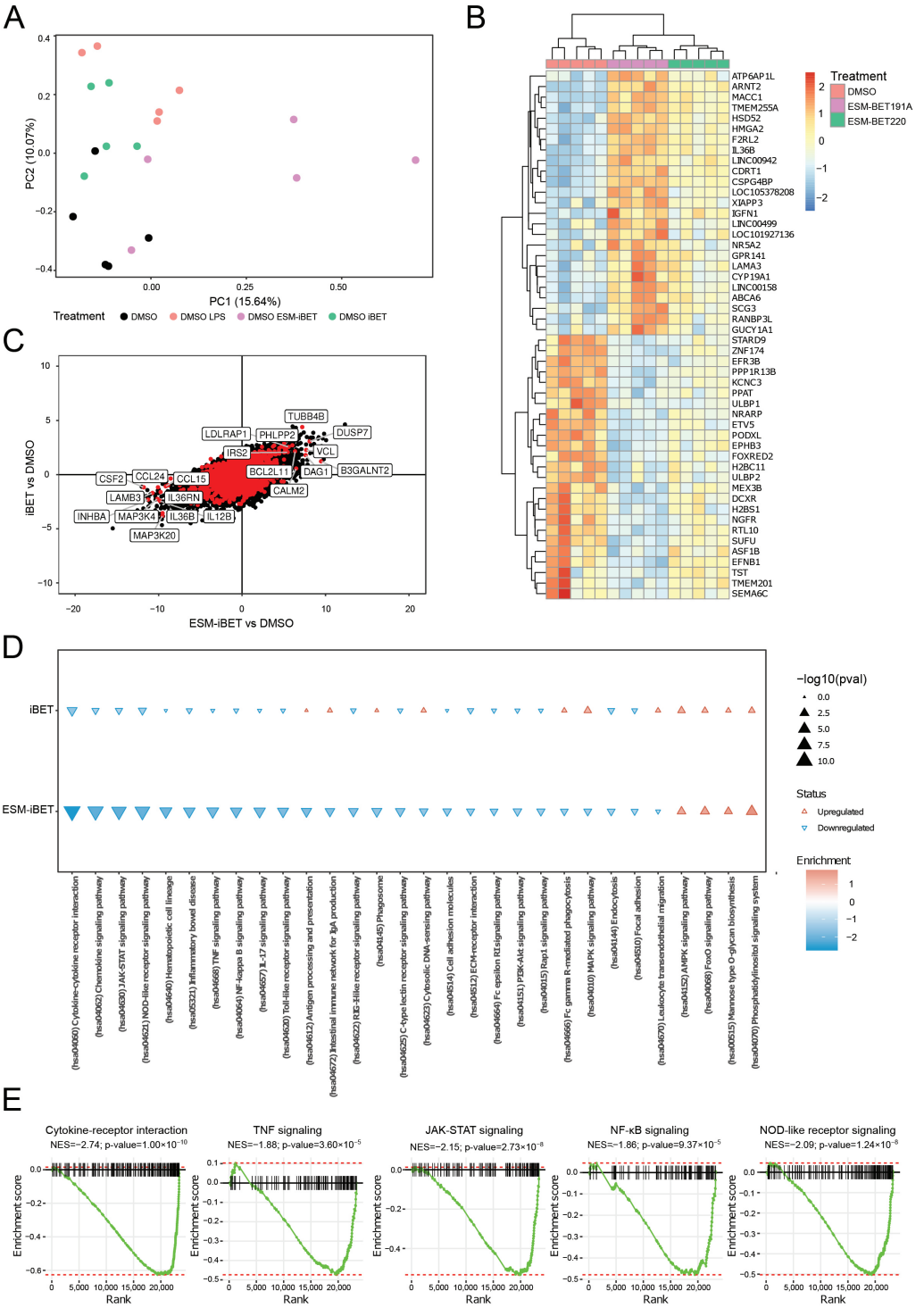
A
PC2 (10.07%)
PC1 (15.64%)
Treatment DMSO DMSO LPS DMSO ESM-iBET DMSO iBET
B
Treatment
DMSO
ESM-BET191A
ESM-BET220
ATP6AP1L
ARNT2
MACC1
TMEM255A
HSD52
HMGA2
F2RL2
IL36B
LINC00942
CDRT1
CSPG4BP
LOC105378208
XIAPP3
IGFN1
LINC00499
LOC101927136
NR5A2
GPR141
LAMA3
CYP19A1
LINC00158
ABCA6
SCG3
RANBP3L
GUCY1A1
STARD9
ZNF174
EFR3B
PPP1R13B
KCNC3
PPAT
ULBP1
NRARP
ETV5
PODXL
EPHB3
FOXRED2
H2BC11
ULBP2
MEX3B
DCXR
H2BS1
NGFR
RTL10
SUFU
ASF1B
EFNB1
TST
TMEM201
SEMA6C
C
iBET vs DMSO
ESM-iBET vs DMSO
TUBB4B
LDLRAP1
PHLPP2
DUSP7
IRS2
VCL
CSF2
CCL24
CCL15
BCL2L11
DAG1
B3GALNT2
CALM2
LAMB3
IL36RN
INHBA
MAP3K4
IL36B
IL12B
MAP3K20
D
iBET
ESM-iBET
−log10(pval)
0.0
2.5
5.0
7.5
10.0
Status
Upregulated
Downregulated
Enrichment
(hsa04060) Cytokine-cytokine receptor interaction
(hsa04062) Chemokine signaling pathway
(hsa04630) JAK-STAT signaling pathway
(hsa04621) NOD-like receptor signaling pathway
(hsa04640) Hematopoietic cell lineage
(hsa05321) Inflammatory bowel disease
(hsa04668) TNF signaling pathway
(hsa04064) NF-kappa B signaling pathway
(hsa04657) IL-17 signaling pathway
(hsa04620) Toll-like receptor signaling pathway
(hsa04612) Antigen processing and presentation
(hsa04672) Intestinal immune network for IgA production
(hsa04622) RIG-I-like receptor signaling pathway
(hsa04145) Phagosome
(hsa04625) C-type lectin receptor signaling pathway
(hsa04623) Cytosolic DNA-sensing pathway
(hsa04514) Cell adhesion molecules
(hsa04512) ECM-receptor interaction
(hsa04664) Fc epsilon RI signaling pathway
(hsa04151) PI3K-Akt signaling pathway
(hsa04015) Rap1 signaling pathway
(hsa04666) Fc gamma R-mediated phagocytosis
(hsa04010) MAPK signaling pathway
(hsa04144) Endocytosis
(hsa04510) Focal adhesion
(hsa04670) Leukocyte transendothelial migration
(hsa04152) AMPK signaling pathway
(hsa04068) FoxO signaling pathway
(hsa00515) Mannose type O-glycan biosynthesis
(hsa00770) Pantothenate and CoA biosynthesis
(hsa04070) Phosphatidylinositol signaling system
E
Cytokine-receptor interaction
NES=−2.74; p-value=1.00×10−10
TNF signaling
NES=−1.88; p-value=3.60×10−5
JAK-STAT signaling
NES=−2.15; p-value=2.73×10−8
NF-κB signaling
NES=−1.86; p-value=9.37×10−5
NOD-like receptor signaling
NES=−2.09; p-value=1.24×10−8
Enrichment score
Rank

**< Figure 5. ESM-iBET influences the transcription of inflammatory related genes and pathways with increased potency over iBET in blood CD14+ monocytes.** (**A**) RNA sequencing data of peripheral CD14+ monocytes (n= 5 healthy donors) pre-treated for 1 h with DMSO, 40 nM ESM-iBET (GSK33611910), or 40 nM iBET (GSK3235220), then stimulated with LPS (4 h). Principle component analysis is shown. (**B**) A heat map depicting the top 20 up- and downregulated genes when comparing BET inhibitors vs. DMSO. Colors represent the scaled log2 (counts). (**C**) Comparison of the Wald statistic obtained from DESeq2 when comparing ESM-iBET with DMSO, and iBET with DMSO on the x- and y-axes, respectively. In red are genes that encode proteins involved in the inflammation-related pathways; highlighted genes are the top 10 up- and downregulated genes (DEGs), comparing ESM-iBET (n = 5) vs. DMSO (n = 5) pre-treated, LPS-stimulated monocytes. **(D**) Gene set enrichment analysis (GSEA) of inflammation-related pathways with functional annotation using Kyoto Encyclopedia of Genes and Genomes (KEGG) pathways, the direction of the arrow indicates either up- or downregulation, while the size and shading of the arrow represent the –log10 (*p*-value) and normalized enrichment score, respectively. (**E**) Enrichment scores of the cytokine–cytokine receptor interaction, TNF signaling, JAK-STAT signaling, NF-kB signaling, and NOD-like receptor signaling pathways in the $CD14^+$ monocytes (n = 5 healthy donors), pre-treated for 1 h with DMSO, ESM-iBET (GSK33611910), or iBET (GSK3235220), then stimulated with LPS (4 h).



Among the top upregulated ESM-iBET targets, we identified pro-apoptotic genes (BCL2L11), phosphatases such as PHLPP2 and DUSP7, which are known to dephosphorylate effective mediators of the AKT [39] and MAPK [40, 41] signaling pathways, respectively, and therefore, act as negative regulators.

Furthermore, we performed gene set enrichment analysis (GSEA) with functional annotation using the Kyoto Encyclopedia of Genes and Genomes (KEGG) pathways. Multiple inflammation-related pathways were among the top significantly negatively enriched pathways in response to ESM-iBET pre-treatment (**Figure 5D**). We could identify pathways of therapeutic and pathogenic relevance to CD, including cytokine–cytokine receptor interaction, TNFα signaling, JAK-STAT signaling, NF-kappa B signaling, MAPK signaling, NOD-like receptor signaling, and PI3K-Akt signaling pathways [42-46] (**Figure 5D,E**).

## ESM-iBET Potently Modulates Cytokines/Chemokines Transcription in Monocytes

Next, we aimed to explore the inflammation related cytokines and chemokines ligands and their receptors that are targeted by BET inhibition in the monocytes. The gene set enrichment analysis (GSEA) of the cytokine–cytokine receptor interaction pathway was negatively enriched in response to ESM-iBET treatment when compared to the DMSO-treated monocytes (**Figure 5E**). Multiple chemokines were significantly inhibited, including CCL1, CCL4, and CXCL5. Notably, CXCL14 expression was found to be enhanced (**Supplementary Figure S1**). In regards to the effect on cytokines following ESM-iBET treatment, we identified the inhibition of multiple genes related

to the IL6, IL1, IL10, TNFα, TGF-β, and interferon families. Alternatively, the expression of selected cytokine receptors was attenuated, including IL1R1, IL17RA, and IFNGR2 (**Supplementary Figure S1**).

### ESM-iBET Affects Transcription of Key Pathways in CD Pathogenesis, Such as TNFα, JAK-STAT, NF-kB, and NOD2 Signaling

Next, we explored whether ESM-iBET affects the transcription of inflammatory pathways and target genes of therapeutic interest in CD. TNFα and JAK-STAT signaling pathways are key players in CD pathogenesis and therefore, are of important therapeutic relevance [44]. GSEA showed a strong negative enrichment of both the TNFα (**Figure 5E, Supplementary Figures S3A** and **S4A**) and JAK-STAT signaling pathways (Figure 5E, Supplementary Figures S3B and S4B) in ESM-iBET-treated monocytes compared to the DMSO-treated monocytes. We further explored effector genes and downstream signaling pathways to identify ESM-iBET targets. We showed that TNFα itself was strongly downregulated by ESM-iBET treatment, while both TNFα receptors (TNFR1 and TNFR2) remained unaffected. Additionally, ESM-iBET targeted the inflammatory signaling pathways that are activated farther downstream of TNFα signaling, such as the MAPK, NF-kB, and PI3K-Akt pathways (**Figure 5D, Supplementary Figures S3C, S5,** and **S6**). Moreover, within the JAK-STAT downstream signaling mediators, we identified STAT5A to be strongly downregulated by ESM-iBET treatment, while SOCS6 and PIAS3, known negative regulators of JAK-STAT signaling [47], were strongly upregulated (**Supplementary Figures S2, S3B,** and **S4B**). Moreover, the NF-κB signaling pathway was found to be negatively enriched in response to ESM-iBET treatment compared to DMSO treatment (**Figure 5E**), as is illustrated by a downregulation of RELA (P65), a key functional subunit in the NF-κB canonical pathway (**Supplementary Figures S2, S3C,** and **S5**). Furthermore, GSEA of the NOD2 signaling pathway was negatively enriched by ESM-iBET treatment (**Figure 5E**), with key effector caspase genes (CASP1, CASP4, and CASP5) being efficiently downregulated (**Supplementary Figures S2** and **S3D**).

## Discussion

Dysregulated innate immunity plays a fundamental role in the sustained and recurring inflammation in CD. Through epigenetic mechanisms, BET proteins are essential for inflammatory gene expression [8]. In the current study, we investigated the potential benefits of BET inhibition, specifically in the mononuclear myeloid cell compartment in the context of CD, and highlighted potential mechanisms of the iBET-mediated anti-inflammatory response in monocytes. We introduced a

mononuclear myeloid cell-targeted iBET (ESM-iBET GSK3361191) as a small molecule BET inhibitor that is effective in reducing inflammatory cytokine production from mononuclear myeloid cells due to its accumulation in CES1 expressing cells [19]. ESM-iBET is expected to be specifically retained in CES1-expressing cells, while demonstrating a reduced effect in non-CES1 expressing cells [19, 22]. In order to understand the exact profile of CES1 expression in inflamed and non-inflamed CD tissue, we performed CyTOF-based profiling of CES1 protein expression in CD patient cells, which revealed a specific pattern of expression, confined within mononuclear myeloid cell populations, across peripheral blood cells, in inflamed intestinal tissue, and in fistula tract-derived cells.



In intestinal biopsies, CES1 was mainly restricted to the CD14-expressing myeloid cells. An earlier study demonstrated a toxic effect of non-selective BET-inhibitors on intestinal epithelial cells [14] and a worsening of DSS-induced colitis in a mouse model upon BET-inhibition [13], suggesting the toxicity of non-selective BET-inhibition on intestinal epithelial cells. In this context, we demonstrated that the majority of EpCAM+ epithelial cells did not express CES1, which is of particular interest here for the application of ESM-iBET in inflammatory intestinal diseases by sparing intestinal epithelial cells, while targeting inflammatory mononuclear myeloid cells. However, a small fraction of CES1-expressing epithelial cells (median of 8.5%) is noted, which may require further investigation to determine whether this reflects a specific epithelial cell subset and whether it may have a detrimental effect on CES1-assisted drug delivery applications in IBD.

In CD peripheral blood PBMCs, CES1 expression is confined to the myeloid compartment, including classical monocytes (CD14+++CD16–), intermediate monocytes (CD14++CD16+), non-classical monocytes (CD14+CD16++), cDCs (CD16–CD14–HLADR++CD11a+CD2+), and pDCs (CD16–CD14–HLADR+++CD45RA+CD2++), similar to the expression pattern demonstrated earlier in healthy donor blood [20]. Interestingly, we observe the highest CES1 expression among circulating non-classical (CD14+CD16++) monocytes from CD patients, in contrast to healthy donors, where CES1 expression was the highest among classical monocytes (CD14+++CD16–) [20]. This may potentially be reflective of a preferential trafficking of CES1-expressing classical monocytes to the locally inflamed colon in CD patients, as classical monocytes are recruited to fuel the inflammatory process [48, 49]. The CES1 expression within mononuclear myeloid cells is also shown within *ex vivo* cells retrieved from CD fistula tracts, supporting the possibility that these cells can be potentially targeted by ESM-iBET to achieve a therapeutic response in these patients. A high CES1 expression is found across the macrophage subsets within

these fistula samples. Moreover, our earlier findings show that CES1-expressing macrophages are enriched in inflamed CD intestinal mucosa [20]; altogether, this suggests that these macrophage populations in the CD inflamed environment would be the most targeted cells of ESM-iBET. Notably, no significant difference in CES1 expression is observed between identified macrophage and DCs subsets, except for pDCs, which show relatively lower CES1 expression, possibly reflecting an equally pronounced effect of ESM-iBET on those tissue CES1+ myeloid subsets.

Using a non-hydrolysable iBET control (GSK3235220), we demonstrated a higher potency of ESM-iBET (GSK3361191) to inhibit inflammatory cytokines in CES1-expressing monocytes in both PBMCs and purified CD14+ monocyte culture compared to equimolar concentrations of iBET (GSK3235220). This validates the specific CES1 assisted delivery of ESM-iBET and the augmented anti-inflammatory effect. However, despite the inhibition of inflammatory cytokine secretion from *ex vivo* immune cells retrieved from CD fistula tracts by ESM-iBET, no differential efficacy over similar concentrations of iBET was observed. This can be explained by the presence of other immune cells, such as T cells and B cells mixed with a low yield of CES1-expressing myeloid cells, within these cell preparations compared to PBMCs and purified monocytes; therefore, the contribution of ESM-iBET targeted CES1-expressing cells to overall secreted cytokines is minimal to demonstrate an observed difference.

The transcriptomic analysis of ESM-iBET (GSK3361191)-treated monocytes demonstrates a potent inhibitory effect on multiple inflammation related genes and pathways. This is in line with earlier reports using other iBET in human primary monocytes [50], human and murine microglial cell lines [51, 52], and murine bone marrow derived macrophages [53]. Additionally, we demonstrated a higher potency of ESM-iBET (GSK3361191) compared to iBET (GSK3235220) control at a low dose of 40 nM. Among the downregulated inflammatory genes, we could identify multiple targets of therapeutic relevance to CD, such as IL12B and TNFα, known therapeutic targets of biological agents such as ustekinumab, infliximab, or adalimumab [2]. Additionally, ESM-iBET efficiently downregulated oncostatin M (OSM), IL1α, and IL1R,1 which were previously reported to be involved in anti-TNF therapy non-responsiveness [54-56] in IBD. Interestingly, among the key anti-inflammatory mediators, ESM-iBET upregulated the TGFβ receptor. In this context, TGFβ signaling by intestinal DCs [57] and circulating monocytes [58] exerts an anti-inflammatory effect, and therapeutically augmenting this pathway shows therapeutic benefits in CD patient clinical trials [59].

The monocyte transcriptional analysis detailed herein demonstrates that ESM-iBET can efficiently target key components of multiple inflammatory pathways involved

in the pathophysiology of CD. Within the JAK-STAT signaling pathway, ESM-iBET specifically downregulated STAT5A gene expression, in line with earlier reports [60, 61], while upregulating SOCS6 and PIAS3, both of which are negative regulators of phosphorylated JAKs that act to dampen JAK-STAT signaling [47]. Additionally, we demonstrate a downregulation of RELA, CASP1, CASP4, and CASP5 gene expression by ESM-iBET treatment, which are key functional effectors downstream of the canonical NF-kB and NOD2 signaling pathways, respectively.



Overall, the monocyte transcriptomic analysis demonstrates a potent effect on multiple pathways of potential therapeutic relevance to CD by ESM-iBET. Current biologic therapies are aimed at targeting specific cytokines or pathway components, which can only be beneficial to patients in which this particular pathway is predominantly driving inflammation. The advantage of a CES1-targeted iBET (ESM-iBET) is that it can interfere with multiple CD-relevant inflammatory pathways simultaneously in monocyte/myeloid cells expressing CES1, while minimizing broad iBET effects in non-CES1 expressing cells. Whether specific targeting of mononuclear myeloid cells would demonstrate clinical benefits remains uncertain. In a complex in vivo environment, other cell types, such as intestinal B cells, T cells, epithelial, and stromal cells, all contribute to intestinal inflammation.

## Conclusions

We demonstrated a specific pattern of CES1 expression in CD patients, which is confined to monocytes, macrophages, and DC populations, across blood and local inflamed tissues of CD patients. We demonstrated the increased potency of ESM-iBET (GSK3361191) in CES1-expressing monocytes compared to the non-targeted control, iBET (GSK3235220). We also defined ESM-iBET targets at the transcriptional level in the peripheral monocytes, which are therapeutically relevant in CD patients.

### Author Contributions

Management of the study, laboratory, and writing of the manuscript: A.M.I.E., I.L.H.; study design: A.M.I.E., I.L.H., W.J.d.J., R.C.F., M.E.W., and N.N.S.; mass cytometry analyses: J.V.; bioinformatics analysis: A.Y.F.L.Y.; patients sample collection: I.L.H., M.A.J.B., C.J.B., V.W.J., L.M., and I.F.; supervision: WJ; reviewing and editing: W.J.d.J., M.J.B., R.C.F., N.N.S., I.R., G.R.D., M.E.W., R.K.P. and P.K.M. All authors have read and agreed to the published version of the manuscript.

## Funding

This work was supported by the European Union's Horizon 2020 research and innovation program under grant agreement no. ITN-2014-EID-641665. WJ was funded by a grant from the Dutch Economic Affairs Top Sector Life Sciences and Health (LSH)—Top Consortia for Knowledge and Innovation's (TKI), grant no. TKI-LSH T2017, and the European Crohn's and Colitis Organization (ECCO) Pioneer Grant, 2018. Furthermore, this project was in collaboration with GlaxoSmithKline Research Collaboration Agreement No. COL300035595.

## Institutional Review Board Statement

Samples were obtained from the department of gastroenterology and/or surgery at the Amsterdam UMC, University of Amsterdam, under the approval of the accredited Medical Ethics Committee (METC #NL53989.018.15, #NL75341.018.20) or the biobank committee of the Amsterdam UMC (178 #A201470).

## Informed Consent Statement

Informed consent was obtained from all subjects involved in the study.

## Data Availability Statement

The datasets analyzed during the current study are available from the corresponding author on request.

## Acknowledgments

The authors would like to thank the participants in the different studies. Furthermore, the authors thank the Microscopy and Cytometry Core Facility at the VU Medical Center, Amsterdam, for use of the Helios and support in sample preparation and acquisition.

## Conflicts of Interest

The authors declare that the research was conducted in the absence of any commercial or financial relationships that could be construed as a potential conflict of interest. NS, IR, RP, RF, HL, PM, and MB were employed by GSK at the time this study was conducted. AE, MG, IH, JV, AY, MJB, MW, GD, CB, IF, LM, VJ, and WJ were employed by Amsterdam University Medical Centers at the time this study was conducted.

# References


1. Geremia A, Biancheri P, Allan P, Corazza GR, Di Sabatino A. Innate and adaptive immunity in inflammatory bowel disease. Autoimmun Rev. 2014;13(1):3-10.
2. Torres J, Bonovas S, Doherty G, Kucharzik T, Gisbert JP, Raine T. ECCO Guidelines on Therapeutics in Crohn's Disease: Medical Treatment. J Crohns Colitis. 2020;14(1):4-22.
3. Lichtenstein GR, Loftus EV, Isaacs KL, Regueiro MD, Gerson LB, Sands BE. ACG Clinical Guideline: Management of Crohn's Disease in Adults. Am J Gastroenterol. 2018;113(4):481-517.
4. Yeshi K, Ruscher R, Hunter L, Daly NL, Loukas A, Wangchuk P. Revisiting Inflammatory Bowel Disease: Pathology, Treatments, Challenges and Emerging Therapeutics Including Drug Leads from Natural Products. J Clin Med. 2020;9(5). 1273
5. Molendijk I, Peeters KC, Baeten CI, Veenendaal RA, van der Meulen-de Jong AE. Improving the outcome of fistulising Crohn's disease. Best Pract Res Clin Gastroenterol. 2014;28(3):505-18.
6. Zaboli P, Abdollahi M, Mozaffari S, Nikfar S. Tumor Necrosis Factor-alpha Antibodies in Fistulizing Crohn's Disease: An Updated Systematic Review and Meta-analysis. J Res Pharm Pract. 2017;6(3):135-44.
7. Shaffer VO, Wexner SD. Surgical management of Crohn's disease. Langenbecks Arch Surg. 2013;398(1):13-27.
8. Wang N, Wu R, Tang D, Kang R. The BET family in immunity and disease. Signal Transduct Target Ther. 2021;6(1):23.
9. Kulikowski E, Rakai BD, Wong NCW. Inhibitors of bromodomain and extra-terminal proteins for treating multiple human diseases. Med Res Rev. 2021;41(1):223-45.
10. Jahagirdar R, Attwell S, Marusic S, Bendele A, Shenoy N, McLure KG. RVX-297, a BET Bromodomain Inhibitor, Has Therapeutic Effects in Preclinical Models of Acute Inflammation and Autoimmune Disease. Mol Pharmacol. 2017;92(6):694-706.
11. Chen L, Zhong X, Cao W, Mao M, Li W, Yang H. JQ1 as a BRD4 Inhibitor Blocks Inflammatory Pyroptosis-Related Acute Colon Injury Induced by LPS. Front Immunol. 2021;12:609319.
12. Cheung K, Lu G, Sharma R, Vincek A, Zhang R, Plotnikov AN. BET N-terminal bromodomain inhibition selectively blocks Th17 cell differentiation and ameliorates colitis in mice. Proc Natl Acad Sci U S A. 2017;114(11):2952-7.
13. Wienerroither S, Rauch I, Rosebrock F, Jamieson AM, Bradner J, Muhar M. Regulation of NO synthesis, local inflammation, and innate immunity to pathogens by BET family proteins. Mol Cell Biol. 2014;34(3):415-27.
14. Bolden JE, Tasdemir N, Dow LE, van Es JH, Wilkinson JE, Zhao Z. Inducible in vivo silencing of Brd4 identifies potential toxicities of sustained BET protein inhibition. Cell Rep. 2014;8(6):1919-29.
15. Shorstova T, Foulkes WD, Witcher M. Achieving clinical success with BET inhibitors as anti-cancer agents. Br J Cancer. 2021;124(9):1478-90.
16. Sun Y, Han J, Wang Z, Li X, Sun Y, Hu Z. Safety and Efficacy of Bromodomain and Extra-Terminal Inhibitors for the Treatment of Hematological Malignancies and Solid Tumors: A Systematic Study of Clinical Trials. Front Pharmacol. 2020;11:621093.
17. Roboz GJ, Desai P, Lee S, Ritchie EK, Winer ES, DeMario M. A dose escalation study of RO6870810/TEN-10 in patients with acute myeloid leukemia and myelodysplastic syndrome. Leuk Lymphoma. 2021;62(7):1740-8.

18. Postel-Vinay S, Herbschleb K, Massard C, Woodcock V, Soria JC, Walter AO. First-in-human phase I study of the bromodomain and extraterminal motif inhibitor BAY 1238097: emerging pharmacokinetic/pharmacodynamic relationship and early termination due to unexpected toxicity. Eur J Cancer. 2019;109:103-10.

19. Needham LA, Davidson AH, Bawden LJ, Belfield A, Bone EA, Brotherton DH. Drug targeting to monocytes and macrophages using esterase-sensitive chemical motifs. J Pharmacol Exp Ther. 2011;339(1):132-42.

20. Elfiky AMI, Ghiboub M, Li Yim AYF, Hageman IL, Verhoeff J, de Krijger M. Carboxylesterase-1 assisted targeting of HDAC inhibitors to mononuclear myeloid cells in Inflammatory Bowel Disease. J Crohns Colitis. 2021. 16, 668–681

21. Luque-Martin R, Van den Bossche J, Furze RC, Neele AE, van der Velden S, Gijbels MJJ. Targeting Histone Deacetylases in Myeloid Cells Inhibits Their Maturation and Inflammatory Function With Limited Effects on Atherosclerosis. Front Pharmacol. 2019;10:1242.

22. Brown JA, Bal J, Simeoni M, Williams P, Mander PK, Soden PE. A randomized study of the safety and pharmacokinetics of GSK3358699, a mononuclear myeloid-targeted bromodomain and extra-terminal domain inhibitor. Br J Clin Pharmacol. 2022, 88, 2140–2155.

23. Konnikova L, Boschetti G, Rahman A, Mitsialis V, Lord J, Richmond C. High-dimensional immune phenotyping and transcriptional analyses reveal robust recovery of viable human immune and epithelial cells from frozen gastrointestinal tissue. Mucosal Immunol. 2018;11(6):1684-93.

24. Van Gassen S, Callebaut B, Van Helden MJ, Lambrecht BN, Demeester P, Dhaene T. FlowSOM: Using self-organizing maps for visualization and interpretation of cytometry data. Cytometry A. 2015;87(7):636-45.

25. Amir el AD, Davis KL, Tadmor MD, Simonds EF, Levine JH, Bendall SC. viSNE enables visualization of high dimensional single-cell data and reveals phenotypic heterogeneity of leukemia. Nat Biotechnol. 2013;31(6):545-52.

26. A language and environment for statistical computing. R Foundation for Statistical Computing. In: Team RC, editor. Vienna, Austria. URL http://www.R-project.org/2014. (accessed on 12th of March, 2021)

27. Jaatinen T, Laine J. Isolation of mononuclear cells from human cord blood by Ficoll-Paque density gradient. Curr Protoc Stem Cell Biol. 2007;Chapter 2:Unit 2A.1.

28. Ewels P, Magnusson M, Lundin S, Käller M. MultiQC: summarize analysis results for multiple tools and samples in a single report. Bioinformatics. 2016;32(19):3047-8.

29. Dobin A, Davis CA, Schlesinger F, Drenkow J, Zaleski C, Jha S. STAR: ultrafast universal RNA-seq aligner. Bioinformatics. 2013;29(1):15-21.

30. Liao Y, Smyth GK, Shi W. The Subread aligner: fast, accurate and scalable read mapping by seed-and-vote. Nucleic Acids Res. 2013;41(10):e108.

31. Gentleman RC, Carey VJ, Bates DM, Bolstad B, Dettling M, Dudoit S. Bioconductor: open software development for computational biology and bioinformatics. Genome Biol. 2004;5(10):R80.

32. Love MI, Huber W, Anders S. Moderated estimation of fold change and dispersion for RNA-seq data with DESeq2. Genome Biol. 2014;15(12):550.

33. Ihaka R, Gentleman R. R: A Language for Data Analysis and Graphics. Journal of Computational and Graphical Statistics. 1996;5(3):299-314.

34. Sergushichev AA. An algorithm for fast preranked gene set enrichment analysis using cumulative statistic calculation. bioRxiv. 2016:060012.

35. Kanehisa M, Sato Y, Kawashima M, Furumichi M, Tanabe M. KEGG as a reference resource for gene and protein annotation. Nucleic Acids Res. 2016;44(D1):D457-62.

36. Wickham H. ggplot2: elegant graphics for data analysis. Springer New York. 2009.
37. Li H, Tsokos GC. Double-negative T cells in autoimmune diseases. Curr Opin Rheumatol. 2021;33(2):163-72.
38. See P, Dutertre CA, Chen J, Günther P, McGovern N, Irac SE. Mapping the human DC lineage through the integration of high-dimensional techniques. Science. 2017;356(6342). eaag3009
39. Newton AC, Trotman LC. Turning off AKT: PHLPP as a drug target. Annu Rev Pharmacol Toxicol. 2014;54:537-58.
40. Ham JE, Oh EK, Kim DH, Choi SH. Differential expression profiles and roles of inducible DUSPs and ERK1/2-specific constitutive DUSP6 and DUSP7 in microglia. Biochem Biophys Res Commun. 2015;467(2):254-60.
41. Seternes OM, Kidger AM, Keyse SM. Dual-specificity MAP kinase phosphatases in health and disease. Biochim Biophys Acta Mol Cell Res. 2019;1866(1):124-43.
42. Caruso R, Warner N, Inohara N, Núñez G. NOD1 and NOD2: signaling, host defense, and inflammatory disease. Immunity. 2014;41(6):898-908.
43. Salas A, Hernandez-Rocha C, Duijvestein M, Faubion W, McGovern D, Vermeire S. JAK-STAT pathway targeting for the treatment of inflammatory bowel disease. Nat Rev Gastroenterol Hepatol. 2020;17(6):323-37.
44. Schreiner P, Neurath MF, Ng SC, El-Omar EM, Sharara AI, Kobayashi T. Mechanism-Based Treatment Strategies for IBD: Cytokines, Cell Adhesion Molecules, JAK Inhibitors, Gut Flora, and More. Inflamm Intest Dis. 2019;4(3):79-96.
45. Li R, Zhu S. NLRP6 inflammasome. Mol Aspects Med. 2020;76:100859.
46. Larabi A, Barnich N, Nguyen HTT. New insights into the interplay between autophagy, gut microbiota and inflammatory responses in IBD. Autophagy. 2020;16(1):38-51.
47. Hu X, li J, Fu M, Zhao X, Wang W. The JAK/STAT signaling pathway: from bench to clinic. Signal Transduction and Targeted Therapy. 2021;6(1):402.
48. Jones GR, Bain CC, Fenton TM, Kelly A, Brown SL, Ivens AC. Dynamics of Colon Monocyte and Macrophage Activation During Colitis. Front Immunol. 2018;9:2764.
49. Thiesen S, Janciauskiene S, Uronen-Hansson H, Agace W, Högerkorp CM, Spee P. CD14(hi)HLA-DR(dim) macrophages, with a resemblance to classical blood monocytes, dominate inflamed mucosa in Crohn's disease. J Leukoc Biol. 2014;95(3):531-41.
50. Wasiak S, Dzobo KE, Rakai BD, Kaiser Y, Versloot M, Bahjat M. BET protein inhibitor apabetalone (RVX-208) suppresses pro-inflammatory hyper-activation of monocytes from patients with cardiovascular disease and type 2 diabetes. Clin Epigenetics. 2020;12(1):166.
51. Jung KH, Das A, Chai JC, Kim SH, Morya N, Park KS. RNA sequencing reveals distinct mechanisms underlying BET inhibitor JQ1-mediated modulation of the LPS-induced activation of BV-2 microglial cells. J Neuroinflammation. 2015;12:36.
52. Baek M, Yoo E, Choi HI, An GY, Chai JC, Lee YS. The BET inhibitor attenuates the inflammatory response and cell migration in human microglial HMC3 cell line. Sci Rep. 2021;11(1):8828.
53. Das A, Chai JC, Yang CS, Lee YS, Das ND, Jung KH. Dual transcriptome sequencing reveals resistance of TLR4 ligand-activated bone marrow-derived macrophages to inflammation mediated by the BET inhibitor JQ1. Sci Rep. 2015;5:16932.
54. West NR, Hegazy AN, Owens BMJ, Bullers SJ, Linggi B, Buonocore S. Oncostatin M drives intestinal inflammation and predicts response to tumor necrosis factor-neutralizing therapy in patients with inflammatory bowel disease. Nat Med. 2017;23(5):579-89.
55. Li H, Feng C, Fan C, Yang Y, Yang X, Lu H. Intervention of oncostatin M-driven mucosal inflammation by berberine exerts therapeutic property in chronic ulcerative colitis. Cell Death Dis. 2020;11(4):271.

56. Bordon Y. Cytokines: Oncostatin M - a new target in IBD? Nat Rev Immunol. 2017;17(5):280.
57. Fenton TM, Kelly A, Shuttleworth EE, Smedley C, Atakilit A, Powrie F. Inflammatory cues enhance TGFβ activation by distinct subsets of human intestinal dendritic cells via integrin αvβ8. Mucosal Immunol. 2017;10(3):624-34.
58. Hilt ZT, Maurya P, Tesoro L, Pariser DN, Ture SK, Cleary SJ. β2M Signals Monocytes Through Non-Canonical TGFβ Receptor Signal Transduction. Circ Res. 2021;128(5):655-69.
59. Ihara S, Hirata Y, Koike K. TGF-β in inflammatory bowel disease: a key regulator of immune cells, epithelium, and the intestinal microbiota. J Gastroenterol. 2017;52(7):777-87.
60. Toniolo PA, Liu S, Yeh JE, Moraes-Vieira PM, Walker SR, Vafaizadeh V. Inhibiting STAT5 by the BET bromodomain inhibitor JQ1 disrupts human dendritic cell maturation. J Immunol. 2015;194(7):3180-90.
61. Pinz S, Unser S, Buob D, Fischer P, Jobst B, Rascle A. Deacetylase inhibitors repress STAT5-mediated transcription by interfering with bromodomain and extra-terminal (BET) protein function. Nucleic Acids Res. 2015;43(7):3524-45.
62. de Krijger M, Hageman IL, Li Yim AYF, Verhoeff J, Garcia Vallejo JJ, van Hamersveld PHP. Signatures Discriminate Patients With Primary Sclerosing Cholangitis and Ulcerative Colitis From Patients With Ulcerative Colitis. Front Immunol. 2022;13:840935.

# Supplementary information for the manuscript

## Materials and methods

***Additional information on clinical sampling and experimental work-up***

Intestinal biopsies: biopsies from IBD patients were collected during colonoscopy for assessment of disease activity and/or therapy response (see patient characteristics in Supplementary Table A1: Baseline characteristics IBD patients' biopsies). Fresh biopsies (1 or 2 pieces at the time, 2 mm maximum size) were slow frozen in 1 mL of freeze medium (10% dimethyl sulfoxide (DMSO) (Sigma-Aldrich, Burlington, MA, U.S.) and 90% fetal bovine serum (FBS)(Serana, Pessin, Germany), and placed in a Corning CoolCell Cell Freezing Vial Containers (Sigma-Aldrich, Burlington, MA, U.S.) to freeze at a 1°C per minute cooling rate in a -80°C freezer. Samples were stored at -80°C for at least 24 hours and transferred to liquid nitrogen for longterm storage [1]. After thawing, a single cell suspension was obtained by incubating the biopsies in digestion medium: collagenase IV C-5138 0.5 mg/ml (Sigma-Aldrich, Burlington, MA, U.S.), DNAse 50 ug/ml (Thermo Fisher Scientific, Waltham U.S.), FBS 2 % (Serana, Germany) in RPMI-1640 medium (Thermo Fisher Scientific, Waltham U.S.) for 45 minutes at 37°C. Biopsies were detached in cells on a 100 µm cell strainer (BD Falcon, Switzerland) placed on a 50-ml tube (Sarstedt, Germany), using the green rubber part of a 2-ml syringe, while rinsing a few times with RPMI-1640 medium (Thermofisher Scientific, Waltham U.S.). The supernatant was then spun at 500 g for 5 min to pellet the cells.

PBMCs of vedolizumab treated CD-patients: venous blood was collected during the course of the biological treatment and PBMCs were isolated and cryopreserved according to standard protocol [1, 2]. In accordance with the procedure of the intestinal biopsies, PBMCs were placed in a Corning CoolCell Cell Freezing Vial Containers (Sigma-Aldrich, Burlington, MA, U.S.) to freeze at a 1°C per minute cooling rate in a -80°C freezer. Samples were stored at -80°C for at least 24 hours and transferred to liquid nitrogen for longterm storage [1]. Patients were categorized as therapy responders or non-responders based a strict combination of endoscopic- (≥50% reduction in SES-CD score) and steroid-free clinical response (≥3 point drop in HBI and HBI ≤4 AND no systemic steroids) and/or biochemical response (≥50% reduction in C-reactive protein (CRP) and fecal calprotectin or a CRP ≤5 g/mL and fecal calprotectin ≤250 µg/g).

Fistula tract tissue of CD patients: CD patients with an active open fistula tract due to their penetrating clinical phenotype underwent surgical intervention (Seton placement or drainage of tract) at the Amsterdam UMC, location AMC, the Netherlands.

During the surgical intervention, tissue or flush from the tract was obtained. After mechanical digestion, as described in the Material and Methods section, immune cells were isolated according to Ficoll density gradient centrifugation protocol [2]. Immune cells obtained from fistulae samples were placed in a Corning CoolCell Cell Freezing Vial Containers (Sigma-Aldrich, Burlington, MA, U.S.) to freeze at a 1°C per minute cooling rate in a -80°C freezer. Samples were stored at -80°C for at least 24 hours and transferred to liquid nitrogen for longterm storage [1].

***Reagents***

The following reagents were used in in vitro studies; L-glutamine (Thermo Fisher Scientific, Waltham U.S.), penicillin/streptomycin (Lonza, Switzerland), foetal bovine serum (FBS; Serana, Pessin, Germany), phosphate buffered saline (PBS; Thermofisher Scientific, Waltham U.S.), lipopolysaccharide (LPS Escherichia coli 0111:B4 or Salmonella Typh; Sigma-Aldrich, Burlington, MA, U.S.) and RPMI-1640 medium (Thermofisher Scientific, Waltham U.S.). RPMI-1640 containing 2 mM L-glutamine, 100 U/mL penicillin/streptomycin, and 10% FBS was used for all in vitro cultures.

***Mass cytometry analysis***

Antibodies; the details of the antibody mass cytometry panel (including clone, metal tag, and supplier) are listed in **Supplementary Table A4**.

Staining and barcoding; single cell suspensions were thawed, washed with PBS and incubated with Cell-ID cisplatin to identify dead cells for 5 minutes at room temperature. Cisplatin signal is quenched by washing with Cell Staining Buffer (CSB, Fluidigm, San Francisco, CA, U.S.). Cells were permeabilized by Maxpar Barcode Perm Buffer (Fluidigm, San Francisco, CA, U.S.), incubated with mass tag barcodes in permeabilization buffer, then stained with antibodies against surface targets in the presence of Human TruStain FcX™ Fc Receptor Blocking Solution (Biolegend, San Diego, CA U.S.).

For intracellular staining, cells were washed and incubated with antibodies for intracellular markers (CES1 Polyclonal Antibody, Thermo Fisher Scientific, Waltham U.S.), washed and then stained with a secondary antibody goat-anti-rabbit (polyclonal)-175Lu (Fluidigm, San Francisco, CA, U.S.). CES1 staining in particular was performed with an antibody dilution of 1:800 and 1:200 for the goat-anti-rabbit-175Lu antibody. After washing with CSB, antibodies were fixed with 1.6% PFA, washed and incubated overnight with 191/193Ir DNA intercalator (1:4000) diluted in Fix-and-Perm Buffer (Fluidigm, San Francisco, CA, U.S.). The next day cells were washed before acquisition on the CyTOF3-Helios.

Mass cytometry data analysis; FCS files were uploaded to R for analysis and quality control. Signal intensities and sample acquisition rates were reviewed for stability over time and events gated based on the condition that flow was stable, excluding calibration beads, and within the 90 % percentile of all Gaussian parameters. Afterwards, $CD45^+$ live cells were selected through sequential gating as described before [3]. Clusters of phenotypically similar cells were identified using the FlowSOM-package. Initial SOM-clustering was set to 300 clusters, using markers listed in Supplementary Table A4, with the exception of CES1 itself. By excluding CES1 from the calculations, we can make comparisons of the CES1 levels between cell types. The 300 formed clusters were manually metaclustered according to their phenotype lineages. For visualization and cluster interpretation we performed a tSNE dimensionality reduction in R using the same markers as the FlowSOM clustering as input. 50,000 events from each sample were randomly sampled to prevent overcrowding of the tSNE space. Perplexity was set at 30, theta at 0.5 and the number of iterations at 1500. In the case of the PBMC and fistula analysis, a subsequent tSNE projection was performed only on events metaclustered and identified as myeloid cells, using all antibody marker parameters excluding CES1. Different cell types within the myeloid lineage were identified. Different CES1 levels were investigated through median expression levels and percentage of positive cells within the cell subset. Plots were generated using the ggplot2 package [4].

***Flow cytometry analysis***

Cells were washed in PBS and stained for a LiveDead cell viability marker (LifeScience, Amsterdam, The Netherlands). Then cells were stained for surface markers in FACS buffer (0.5% BSA, 0.01% NaN3 in PBS), fixed, permealized and stained for intracellular anti-TNF using Foxp3 / Transcription Factor Staining Buffer Set (eBioscience, San Diego, CA, U.S.). For PBMCs culture; we used the following antibodies; anti-CD3-PerCP (Becton Dickinson, US), anti-CD19-BV421 (Biolegend, US), anti-CD14-PE-Cy7 (Invitrogen), anti-MHCII-AlexaFluor700 (eBioscience, San Diego, CA, U.S.) and anti-TNF-FITC (Invitrogen, US). For *ex vivo* derived CD fistulae tract cells culture: we used the following antibodies; anti-CD45-PE (eBioscience, San Diego, CA, U.S.), anti-CD3-APC (Biolegend, San Diego, CA U.S.), anti-CD19-BV421(Biolegend, US), anti-CD66b-FITC (eBioscience, San Diego, CA, U.S.), anti-CD14-PE7 (Becton Dickinson, US), anti-MHCII-AF700 (eBioscience, San Diego, CA, U.S.).

# References


1. Konnikova L, Boschetti G, Rahman A, Mitsialis V, Lord J, Richmond C. High-dimensional immune phenotyping and transcriptional analyses reveal robust recovery of viable human immune and epithelial cells from frozen gastrointestinal tissue. Mucosal Immunol. 2018;11(6):1684-93.
2. Jaatinen T, Laine J. Isolation of mononuclear cells from human cord blood by Ficoll-Paque density gradient. Curr Protoc Stem Cell Biol. 2007;Chapter 2:Unit 2A.1.
3. Van Gassen S, Callebaut B, Van Helden MJ, Lambrecht BN, Demeester P, Dhaene T. FlowSOM: Using self-organizing maps for visualization and interpretation of cytometry data. Cytometry A. 2015;87(7):636-45.
4. Wickham H. ggplot2: elegant graphics for data analysis. Springer New York. 2009.


# Supplementary Figures

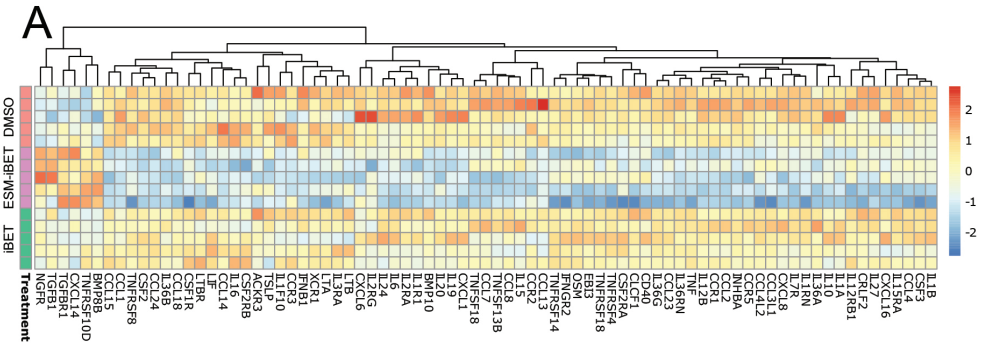


**Supplementary figure S1: ESM-iBET potently modulates multiple cytokines / chemokines transcription in monocytes.** (**A-B**) CD14+ monocytes (n=5 healthy donors) pre-treated (1hr) with DMSO, ESM-iBET (GSK33611910) or iBET (GSK3235220), then stimulated with LPS (4hrs). ESM-iBET (n=5) is compared to DMSO (n=5), iBET (n=5) is shown alongside. (**A**) Heatmap of top differentially expressed genes in the cytokine-cytokine receptor interaction pathway comparing ESM-iBET (n=5) vs. DMSO (n=5) pre-treated, LPS stimulated monocytes, iBET pre-treated monocytes (n=5) are shown alongside.

B

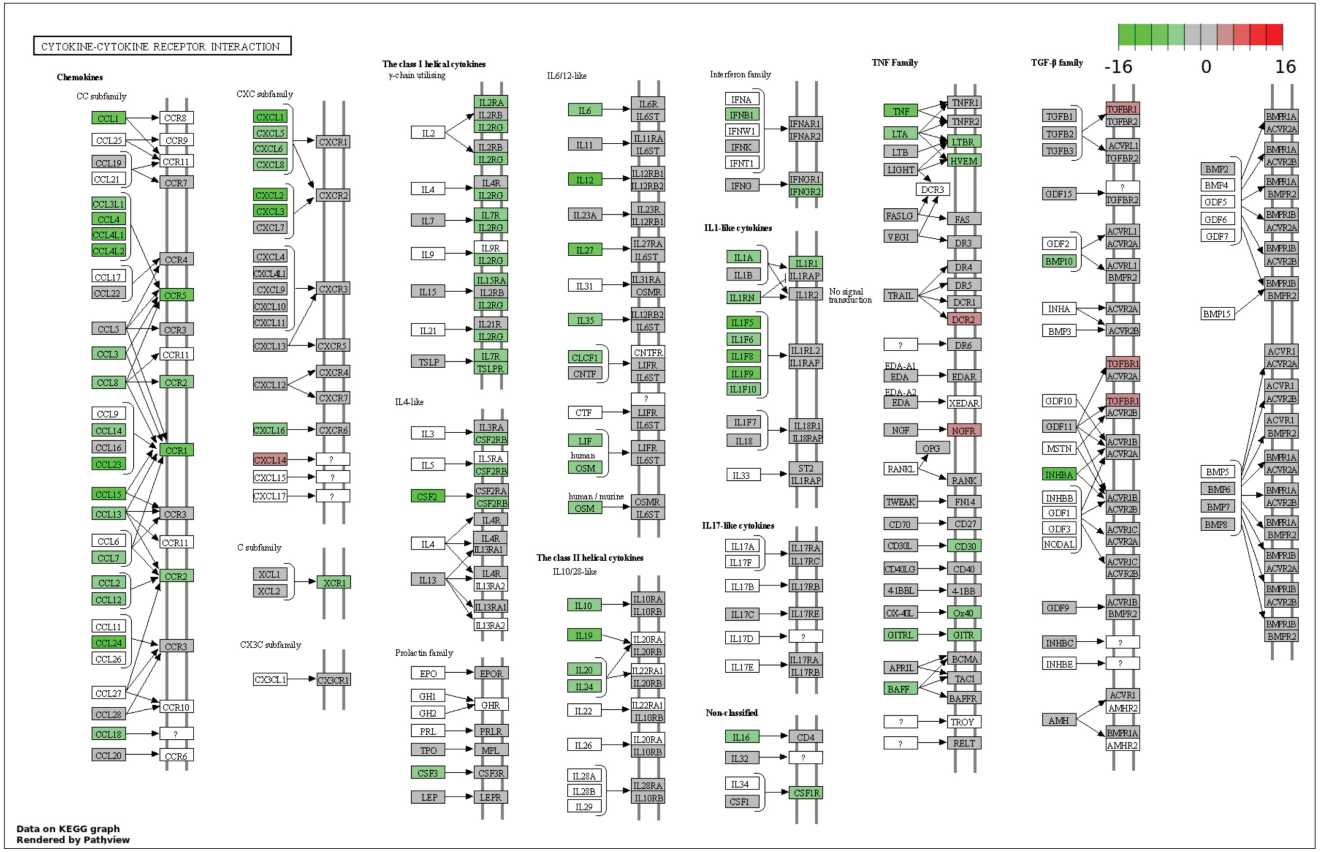


**Supplementary figure S1: ESM-iBET potently modulates multiple cytokines / chemokines transcription in monocytes.** (**A-B**) CD14+ monocytes (n=5 healthy donors) pre-treated (1hr) with DMSO, ESM-iBET (GSK33611910) or iBET (GSK3235220), then stimulated with LPS (4hrs). ESM-iBET (n=5) is compared to DMSO (n=5), iBET (n=5) is shown alongside. (**B**) The KEGG cyto-kine-cytokine receptor interaction pathway with colors representing the effect size obtained from interaction analysis. ESM-iBET (n=5) vs. DMSO (n=5) pre-treated, LPS stimulated monocytes are compared.

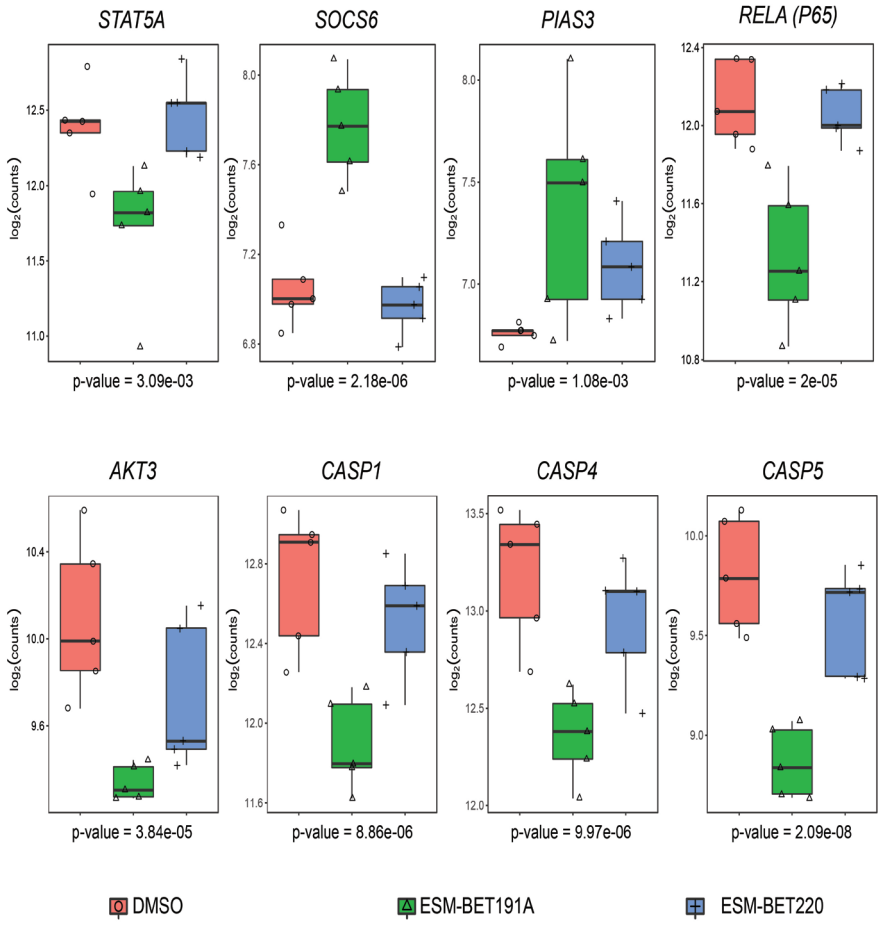


**Supplementary figure S2: ESM-iBET affects transcription of key effector genes in CD within the TNFα, JAK-STAT, NF-kB and NOD2 signaling pathways, with superior potency over iBET.** $CD14^{+}$ monocytes (n=5 healthy donors) pre-treated (1hr) with DMSO, ESM-iBET (GSK33611910) or iBET (GSK3235220), then stimulated with LPS (4hrs). ESM-iBET (n=5) is compared to DMSO (n=5), iBET (n=5) is shown alongside. Box plots show the expression of selected differentially expressed key effector genes among TNFα, JAK-STAT and NF-kB pathway, expression values are displayed as log2(counts) on the y-axis. In the NF-kB signaling pathway, expression of RELA (P65), a key functional subunit in NF-κB canonical pathway, was found to be downregulated. In PI3K-Akt signaling pathway, AKT3 expression was strongly downregulated. Key effector caspase genes family were targeted with CASP1, CASP4 and CASP5 being efficiently downregulated.

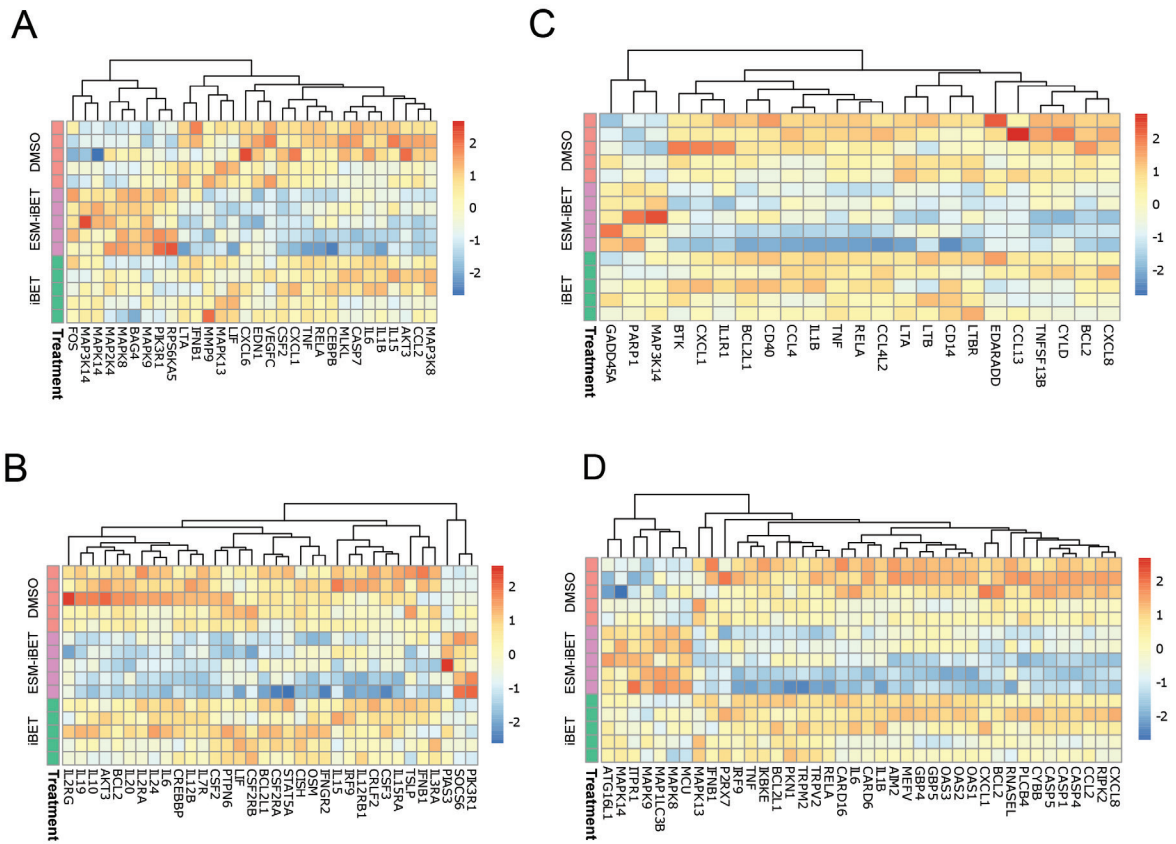


**Supplementary figure S3. ESM-iBET modulate multiple genes within TNFα, JAK-STAT, NF-kB and NOD-like receptor signaling pathways.** Heat maps of (**A**) significant 30 differentially expressed genes (DEG) in the TNFα signaling pathway (**B**) 34 DEGs in JAK-STAT signaling pathway (**C**) 23 DEGs in the NF-kB signaling pathway (**D**) and 40 DEGs in the NOD-like receptor signaling pathway, in $CD14^{+}$ monocytes (n=5 healthy donors) pre-treated (1hr) with DMSO, ESM-iBET (GSK33611910) or iBET (GSK3235220), then stimulated with LPS (4hrs). ESM-iBET (n=5) is compared to DMSO (n=5), iBET (n=5) is shown alongside.

A

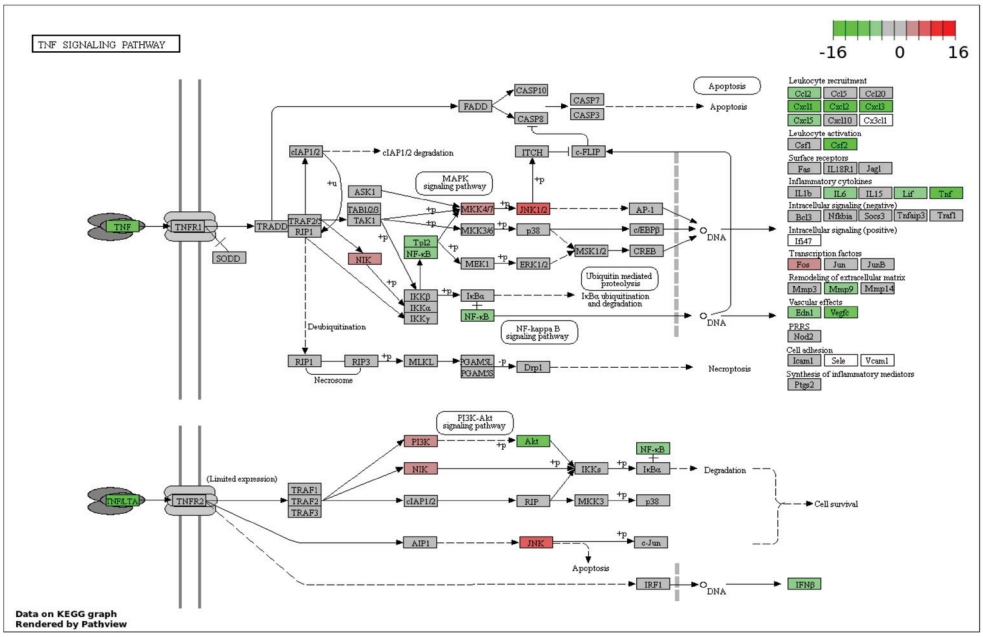


B

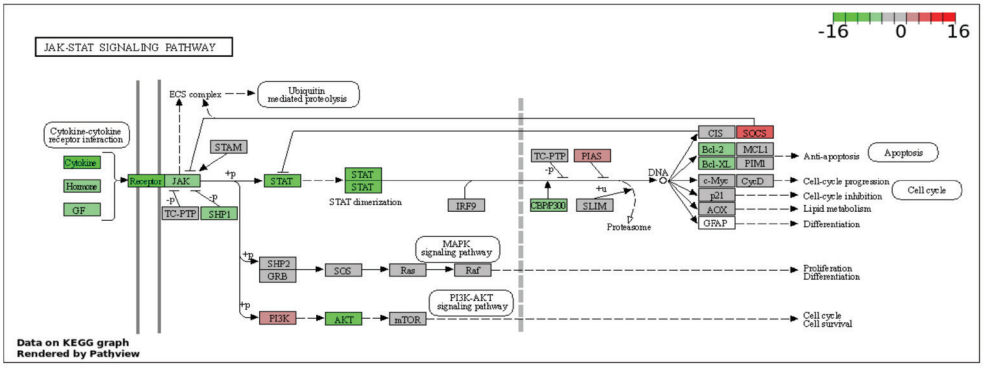


**Supplementary figure S4. The KEGG TNFα and JAK-STAT signaling pathway.** (**A**) The KEGG TNFα signaling pathway and (**B**) JAK-STAT receptor interaction pathway with colors representing the effect size obtained from interaction analysis. In CD14$^{+}$ monocytes (n=5 healthy donors) pre-treated (1hr) with DMSO, ESM-iBET (GSK33611910) or iBET (GSK3235220), then stimulated with LPS (4hrs). ESM-iBET (n=5) is compared to DMSO (n=5), iBET (n=5) is shown alongside.

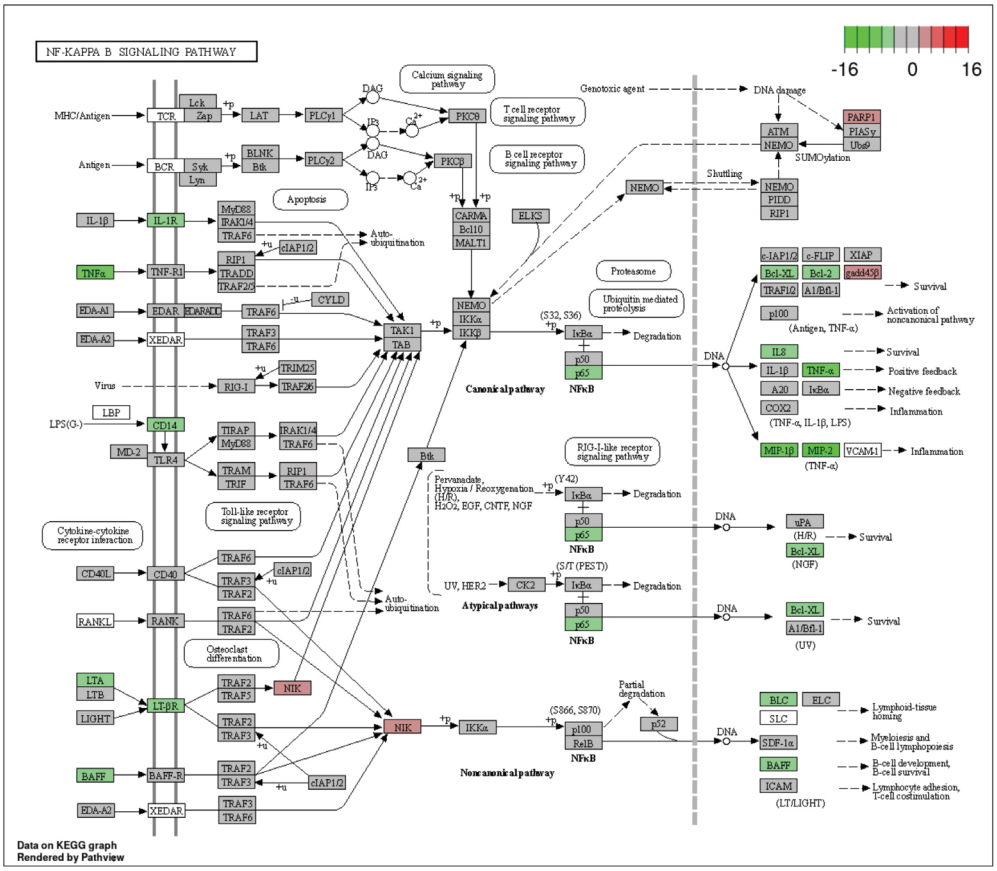


**Supplementary figure S5. The KEGG NF-kB signaling pathway.** The KEGG NF-kB signaling pathway with colors representing the effect size obtained from interaction analysis. In CD14+ monocytes (n=5 healthy donors) pre-treated (1hr) with DMSO, ESM-iBET (GSK33611910) or iBET (GSK3235220), then stimulated with LPS (4hrs). ESM-iBET (n=5) is compared to DMSO (n=5), iBET (n=5) is shown alongside.

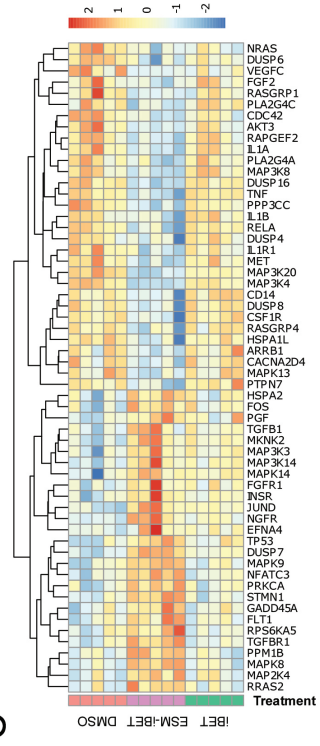
C
2
1
0
-1
-2
NRAS
DUSP6
VEGFC
FGF2
RASGRP1
PLA2G4C
CDC42
AKT3
RAPGEF2
IL1A
PLA2G4A
MAP3K8
DUSP16
TNF
PPP3CC
IL1B
RELA
DUSP4
IL1R1
MET
MAP3K20
MAP3K4
CD14
DUSP8
CSF1R
RASGRP4
HSPA1L
ARRB1
CACNA2D4
MAPK13
PTPN7
HSPA2
FOS
PGF
TGFB1
MKNK2
MAP3K3
MAP3K14
MAPK14
FGFR1
INSR
JUND
NGFR
EFNA4
TP53
DUSP7
MAPK9
NFATC3
PRKCA
STMN1
GADD45A
FLT1
RPS6KA5
TGFBR1
PPM1B
MAPK8
MAP2K4
RRAS2
Treatment
IBET
ESM-IBET
DMSO

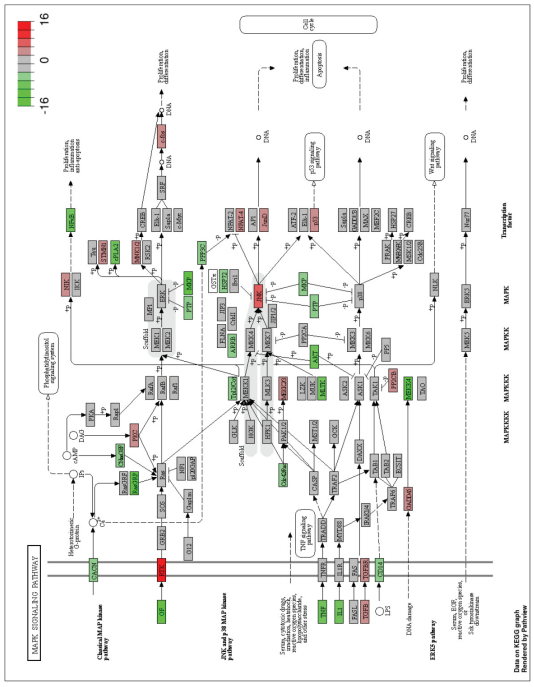
D
MAPK SIGNALING PATHWAY
16
0
-16

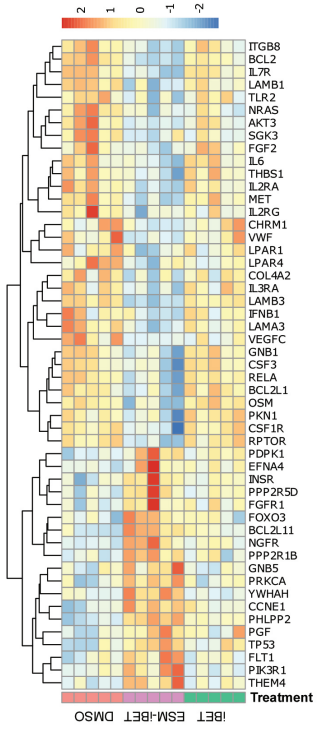
A
2
1
0
-1
-2
ITGB8
BCL2
IL7R
LAMB1
TLR2
NRAS
AKT3
SGK3
FGF2
IL6
THBS1
IL2RA
MET
IL2RG
CHRM1
VWF
LPAR1
LPAR4
COL4A2
IL3RA
LAMB3
IFNB1
LAMA3
VEGFC
GNB1
CSF3
RELA
BCL2L1
OSM
PKN1
CSF1R
RPTOR
PDPK1
EFNA4
INSR
PPP2R5D
FGFR1
FOXO3
BCL2L11
NGFR
PPP2R1B
GNB5
PRKCA
YWHAH
CCNE1
PHLPP2
PGF
TP53
FLT1
PIK3R1
THEM4
Treatment
IBET
ESM-IBET
DMSO

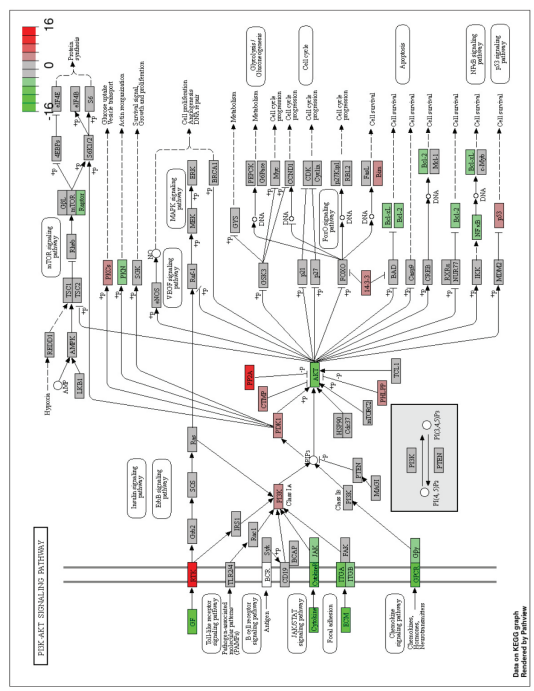
B
PI3K-AKT SIGNALING PATHWAY
16
0
-16

**< Supplementary figure S6: ESM-iBET interferes with PI3K-Akt and MAPK signaling pathways via modulating the expression of multiple key effector genes.** (A-D) $CD14^+$ monocytes (n=5 healthy donors) pre-treated (1hr) with DMSO, ESM-iBET (GSK33611910) or iBET (GSK3235220), then stimulated with LPS (4hrs). ESM-iBET (n=5) is compared to DMSO (n=5), iBET (n=5) is shown alongside. Heat map of (A) significant 51 differentially expressed genes in the PI3K-Akt signaling pathway together with (B) the KEGG PI3K-Akt signaling pathway. Heat map of (C) 58 differentially expressed genes in the MAPK signaling pathway together with (D) KEGG MAPK signaling pathway. Colors representing the effect size obtained from interaction analysis.

# Supplementary tables



**Table S1.** Baseline characteristics IBD patients' biopsies.

| Baseline characteristics | IBD patients biopsy retrieved n=6 |
|---|---|
| IBD, CD (%) | 3 (50) |
| Gender, n (%) | |
| - Female | 3 (50) |
| Age, years, median (IQR) | 44 (31.25-55.25) |
| Disease duration, years, median (IQR) | 4 (0.75 - 8) |
| Disease location in CD, n (%) | |
| - Ileal disease (L1) | 1 (17) |
| - Colonic disease (L2) | 0 (0) |
| - Ileocolonic disease (L3) | 2 (33.3) |
| - Upper GI involvement (L4) | 0 (0) |
| Disease behavior in CD, n (%) | |
| - Non structuring non-penetrating (B1) | 3 (50) |
| - Stricturing (B2) | 0 (0) |
| - Penetrating (B3) | 0 (0) |
| - Perianal disease (p) | 0 (0) |
| | |
| Disease extension UC (E3, %) | 3 (50) |
| Disease severity UC (S3, %) | 1 (17) |
| Previous IBD related surgery (resection, seton, stricturoplasty), n (%) | 3 (50) |
| Medication, n (%) | |
| - Immunomodulators | 3 (50) |
| - Prednisone taper scheme | 3 (50) |
| Biological agents, n (%) | 0 (0) |

**Table S2.** Baseline characteristics of Vedolizumab responders and non-responders.

| | **Responders (N = 5)** | **Non-responders (N = 6)** |
|---|---|---|
| Female, N (%) | 4 (80) | 5 (83) |
| Age, years, median (IQR) | 42 (38-44) | 58.5 (43-68) |
| Disease location, n (%) | | |
| - Ileal disease (L1) | 3 (60) | 3 (50) |
| - Colonic disease (L2) | 1 (20) | - |
| - Ileocolonic disease (L3) | 1 (20) | 3 (50) |
| | **Responders (N = 5)** | **Non-responders (N = 6)** |
| Disease behavior, N (%) | | |
| - Non structuring/penetrating (B1) | 2 (40) | 4 (66.6) |
| - Stricturing (B2) | 3 (60) | 2 (33.3) |
| - Penetrating (B3) | 0 (0) | 0 (0) |
| - Perianal disease (p) | 1 (20) | 1 (0.17) |
| Previous IB- related surgery, N (%) | 3 (60) | 3 (50) |
| Concomitant medication, N (%) | | |
| - Immunomodulators | - | - |
| - Prednisone | - | - |

**Table S3: Baseline characteristics Fistulizing CD patients**

| **Baseline characteristics Fistula CD patients Samples used for cyTOF and cell culture** | **(N=18)** |
|---|---|
| Gender, n (%) | |
| - Female | 10 (55.6) |
| Age, years, median (IQR) | 35 (32.25-39) |
| Disease duration, years, median (IQR) | 7.5(3.75-14) |
| Disease location, n (%) | |
| - Ileal disease (L1) | 4 (22) |
| - Colonic disease (L2) | 5 (28) |
| - Ileocolonic disease (L3) | 9 (50) |
| - Upper GI involvement (L4) | 0 (0) |
| Disease behavior, n (%) | |
| - Non structuring non-penetrating (B1) | 13 (72) |
| - Stricturing (B2) | 1 (6) |
| - Penetrating (B3) | 4 (22) |
| - Perianal disease (p) | 18 (18) |
| Previous IBD related surgery (resection, seton, stricturoplasty), n (%) | 15 (83) |

**Table S3.** Continued

| **Baseline characteristics Fistula CD patients Samples used for cyTOF and cell culture** | **(N=18)** |
|---|---|
| Medication, n (%) | |
| - Immunomodulators | 4 (22) |
| - Prednisone taper scheme | 0 (0) |
| Biological agents, n (%) | |
| - Infliximab | 6 (33) |
| - Adalimumab | 4 (22) |
| - Other (vedolizumab, ustekinumab) | 0 (0) |
| Smoking, n (%) | |
| - Never | 10 (56) |
| - Active | 2 (11) |
| - Former | 3 (17) |

**Table S4: Antibody Panel Mass Cytometry**

*Antibodies pre-fixation:*

| Target | Metal/Clone | Source | Panel | Purpose |
|---|---|---|---|---|
| CD194 (CCR4) | 158Gd/L291H4 | Fluidigm | PBMC | T and B lymphocytes, basophils, monocytes and NK cells |
| CD195 (CCR5) | 144Nd/NP6G4 | Fluidigm | PBMC | T lymphocytes and monocytes |
| CD183 (CXCR3) | 156Gd/G025H7 | Fluidigm | PBMC | Chemokine receptor, T lymphocytes |
| α4β7 | 171Yb/- | Takeda | PBMC, fistula tract | Intestinal homing T lymphocytes |
| CCR9 | 168Er/L053E8 | Fluidigm | PBMC | Intestinal homing T lymphocytes |
| CCR10 | 148Nd/314305 | R&D | PBMC | Intestinal homing T lymphocytes |
| Cisplatin | 194Pt/- | Fluidigm | Biopsy,PBMC,fistula tract | Live/dead discrimination |

*Antibodies nuclear staining:*

| Target | Metal/Clone | Source | Panel | Purpose |
|---|---|---|---|---|
| CD152 (CTLA-4) | 161Dy/14D3 | Fluidigm | Biopsy, PBMC, fistula tract | Co inhibitory molecule |
| αRabbit IgG | 175Lu/polyclonal | Fluidigm | Biopsy, PBMC, fistula tract | CES1 Rabbit IgG antibody |
| CES1 | -/polyclonal | Thermo Scientific | Biopsy, PBMC, fistula tract | Myeloid cells |

*Antibodies post-fixation:*

| Target | Metal/Clone | Source | Panel | Purpose |
|---|---|---|---|---|
| CD45 | 89Y/HI30 | Fluidigm | Biopsy, PBMC, fistula tract | All leukocytes |
| CD49d | 141Pr/9F10 | Fluidigm | Biopsy, PBMC, fistula tract | Integrin alpha subunit. |
| CD11a | 142Nd/HI111 | Fluidigm | Biopsy, PBMC | Integrin alpha L chain |

**Table S4: Continued**

*Antibodies post-fixation:*

| Target | Metal/Clone | Source | Panel | Purpose |
|---|---|---|---|---|
| CD19 | 142Nd/HIB19 | Fluidigm | Fistula tract | B lymphocytes |
| CD5 | 143Nd/UCHT2 | Fluidigm | Biopsy, PBMC | Activated lymphocytes |
| CD127 (IL7Ra) | 143Nd/A019D5 | Fluidigm | Fistula tract | Memory and effector T cells, immature B cell proliferation |
| CD4 | 145Nd/RPA-T4 | Fluidigm | Biopsy, PBMC | T helper lymphocytes |
| CD68 | 145Nd/Y182A | Biolegend | Fistula tract | Macrophages |
| CD8a | 146Nd/RPA-T8 | Fluidigm | Biopsy, PBMC, fistula tract | Cytoxic T lymphocytes |
| CD7 | 147Sm/CD76B7 | Fluidigm | Biopsy, PBMC, fistula tract | T lymphocytes |
| CD66a | 148Nd/B1.1/CD66 | BD | Fistula tract | Granulocytes |
| CD25 (IL2R) | 149Sm/2A3 | Fluidigm | Biopsy, PBMC, fistula tract | Activated T lymphocytes, regulatory T cells |
| CD134 (OX40) | 150Nd/ACT35 | Fluidigm | Biopsy, PBMC | Co-stimulatory molecule |
| CD11c | 150Nd/Bu15 | Biolegend | Fistula tract | Myeloid cells |
| CD2 | 151EuTS1/8/ | Fluidigm | Biopsy, PBMC | T lymphocytes, NK cells |
| CD123 | 151Eu/6H6 | Fluidigm | Fistula tract | Plasmacytoid dendritic cells, basophils |
| CD95/Fas | 152Sm/DX2 | Fluidigm | Biopsy, PBMC | Apoptosis |
| CD141 | 152Sm/ | Fluidigm | Fistula tract | Dendritic cells, myeloid cells |
| TIM-3 | 153Eu/F38-2E2 | Fluidigm | Biopsy, PBMC | Co inhibitory molecule |
| CD14 | 154Sm | Fluidigm | Biopsy, PBMC | Monocytes |
| CD3 | 154Sm/UCHT1 | Fluidigm | Fistula tract | T lymphocytes |
| CD279 (PD-1) | 155Gd/EH12.2H7 | Fluidigm | Biopsy, PBMC, fistula tract | Activated lymphocytes, immune checkpoint |
| CD163 | 156Gd/GHI/61 | Biolegend | Fistula tract | Macrophages |

**Table S4: Continued**

*Antibodies post-fixation:*

| Target | Metal/Clone | Source | Panel | Purpose |
|---|---|---|---|---|
| CD197 (CCR7) | 159Tb/GO43H7 | Fluidigm | Biopsy, PBMC, fistula tract | Activated lymphocytes, homing to secondary lymphoid organs |
| CD28 | 160Gd/CD28.2 | Fluidigm | Biopsy, PBMC | Co-stimulatory molecule, activated T lymphocytes |
| CD14 | 160Gd/M5E2 | Fluidigm | Fistula tract | Monocytes |
| CD69 | 162Dy/FN50 | Fluidigm | Biopsy, PBMC, fistula tract | Activated lymphocytes |
| CD206 | 163Dy/15-2 | Biolegend | Fistula tract | Macrophages, dendritic cells |
| CD161 | 164Dy/HP-3G10 | Fluidigm | Biopsy, PBMC | NK cells |
| CD43 | 164Dy/CD43-10G7 | Biolegend | Fistula tract | Cell adhesion, T cell costimulation |
| CD45RO | 165Ho/UCHL1 | Fluidigm | Biopsy, PBMC, fistula tract | All leukocytes |
| CD44 | 166Er/BJ18 | Fluidigm | Biopsy, PBMC, fistula tract | Activated lymphocytes |
| CD27 | 167Er/O323 | Fluidigm | Biopsy, PBMC, fistula tract | Activated lymphocytes |
| CD45RA | 169Tm/HI100 | Fluidigm | Biopsy, PBMC | All leukocytes |
| CD33 | 169Tm/WM53 | Fluidigm | Fistula tract | Myeloid cells |
| CD3 | 170Er/UCHT1 | Fluidigm | Biopsy, PBMC | T lymphocytes |
| CD45RA | 170Er/HI100 | Fluidigm | Fistula tract | All leukocytes |
| CD57 | 172Yb/HCD57 | Fluidigm | Biopsy, PBMC | NK cells |
| CD137/4-1BB | 173Yb/4B4-1 | Fluidigm | Biopsy, PBMC | Macrophages, activated B cells, and dendritic cells |
| EpCAM | 173Yb/ | Biolegend | Fistula tract | Epithelial cells |
| HLA-DR | 174Yb/L243 | Fluidigm | Biopsy, PBMC, fistula tract | Antigen presenting cells |
| CD127 (IL7Ra) | 176Yb/A019D5 | Fluidigm | Biopsy, PBMC | Memory and effector T cells, immature B cell proliferation |

**Table S4: Continued**

*Antibodies post-fixation:*

| Target | Metal/Clone | Source | Panel | Purpose |
|---|---|---|---|---|
| CD4 | 176Yb/RPA-T4 | Fluidigm | Fistula tract | T helper lymphocytes |
| CD16 | 209Bi/3G8 | Fluidigm | Biopsy, PBMC, fistula tract | Monocytes, NK cells, dendritic cells |
| Barcodes | 103–110Pd/- | Fluidigm | Biopsy, PBMC, fistula tract | Staining standardization and doublet discrimination |
| Iridium | 191–193Ir/- | Fluidigm | Biopsy, PBMC, fistula tract | Cell identification |

4

# Chapter 4

## Carboxylesterase 1 Mediates a Distinctive Metabolic Profile of Dendritic Cells to Attain an Inflammatory Phenotype

**Ahmed M. I. Elfiky**, Jessica Lopez, Mohammed Ghiboub, Andrew Y. F. Li Yim, Arthur J Verhoeven, Wouter J. de jonge.

Under revision in Journal of Leukocyte Biology

## Abstract

The metabolic profile of dendritic cells (DCs) shapes their phenotype and functions. Carboxylestrase 1 (CES1) enzyme is highly expressed in mononuclear myeloid cells however its exact role in DCs is elusive. We used a CES1 inhibitor (WWL113) and genetic overexpression to explore the role of CES1 in DCs differentiation in inflammatory models.

*CES1* expression was analyzed during $CD14^+$ monocytes differentiation to DCs (MoDCs) using quantitative PCR. CES1 Inhibitor (WWL113) was applied during MoDCs differentiation. Surface markers, secreted cytokines, lactic acid production, phagocytic and T cell polarization capacity were analyzed. Transcriptomic and metabolic profile were assessed with RNA-sequencing and mass spectrometry. Cellular respiration was assessed with seahorse respirometry. Transgenic mice were used to assess CES1 overexpression in DCs in inflammatory models.

*CES1* expression peaks early during MoDCs differentiation. Pharmacological inhibition of CES1 led to higher expression of CD209, CD86 and MHCII. WWL113 treated MoDCs secreted higher quantities of IL6, IL8, TNF and IL10 and demonstrated stronger phagocytic ability and higher capacity to polarize Th17 differentiation in autologous DCs-T cells co-culture model. Transcriptomic profiling revealed enrichment of multiple inflammatory and metabolic pathways. Functional metabolic analysis shows impaired maximal mitochondrial respiration capacity, increased lactate production and decreased intracellular amino acids and TCA intermediates. Transgenic human *CES1* overexpression in murine DCs generated less inflammatory phenotype and increased resistance to T cell mediated colitis.

In conclusion, CES1 inhibition directs DCs differentiation towards more inflammatory phenotype that shows stronger phagocytic capacity and supports Th17 skewing. This is associated with disrupted mitochondrial respiration and amino acids depletion.


**Keywords:** CES1, Dendritic cells, Inflammation,

## Introduction

Dendritic cells (DCs) are antigen presenting cells that play a pivotal role at the intersection between the innate and adaptive arms of immune system [1]. They are essential for mounting a regulated immune response. Therefore, disturbances in their functions are strongly associated with the pathogenesis of multiple inflammatory diseases [2, 3]. Immune metabolism studies demonstrate that DCs phenotypes and functions are closely associated with their metabolic profile, which is responsive to external and internal cues [4]. Inflammatory signals, like TLR agonists, enhance intracellular glycogenolysis [5] and induce shift towards glycolytic energy production in monocytes derived dendritic cells (MoDCs), while reducing oxidative phosphorylation, a metabolic hall mark of the MoDCs inflammatory phenotype [6, 7]. This is similarly observed in the naturally occurring blood $CD1c^+$ myeloid DCs [8]. Alternatively, DCs rely on fatty acid oxidation during early differentiation to fuel the tricarboxylic acid (TCA) cycle and produce energy by oxidative phosphorylation, which are essential for DCs tolerance [9-11]. Interfering with DCs metabolism can modulate their phenotype and function and can therefore be an interesting point of therapeutic intervention in inflammatory diseases [12].



CES1 enzyme is a serine hydrolase for xenobiotics and endogenous compounds containing esters, thioesters and amide-groups such as triacylglycerols and cholesterol esters [13]. CES1 is mainly expressed in hepatocytes, mononuclear myeloid cells and adipose tissue [14]. Among immune cells, CES1 is exclusively expressed in mononuclear myeloid cells [15] and increases significantly in response to inflammatory stimuli, downstream of NFκB signaling [16]. In vitro studies of CES1 in mononuclear myeloid cells have largely focused on THP-1 cell line and macrophages, however, very little is known about DCs. Genetic deletion or pharmacological inhibition of CES1 in THP-1 cell line promotes foamy macrophage phenotypes due to impaired cholesterol ester hydrolysis and free cholesterol efflux [17, 18]. On the other hand, in vivo studies have largely focused on role of ces1d, murine ortholog of human CES1, in atherosclerosis and obesity [14, 19]. However, recent reports point to a role of CES1 in modulating inflammation. CES1 pharmacological inhibition and ces1d knockout models have both shown augmented lung inflammation [20]. Moreover, Reduced CES1 expression has been observed in alveolar macrophages from tuberculosis patients [21] and livers of alcoholic steatohepatitis patients [22]. In vivo, ces1 genetic deletion augments alcohol induced liver inflammation [22]. While CES1 may play a role in inflammation, the underlying mechanisms remain unclear.

In the current study, we aim to explore the potential effect of CES1 pharmacological inhibition using WWL113, a potent and specific CES1 inhibitor [23], on DCs differentiation, phenotype and function. We further explore the transcriptomic and metabolic profile of the generated DCs as well as characteristic metabolomics changes. We hereby report that blocking CES1 promotes generation of MoDCs with enhanced inflammatory phenotype and stronger phagocytic capacity. These MoDCs have a distinct metabolic profile, characterized by impaired mitochondrial respiration and decreased intracellular amino acids. In contrary, overexpression of human CES1 in murine system shows less DCs inflammatory phenotype in both *in vitro* and *in vivo* inflammatory models.

## Methods

### Compounds and reagents

CES1 inhibitor; WWL113 (Sigma-Aldrich) was dissolved in 100% DMSO and used at concentrations of 0.15 μM, 0.62 μM, 2.5μM and 10μM. Detailed characterization of WWL113 was reported earlier [23]. Roswell Park Memorial Institute Medium (RPMI)-1640 (Gibco), Iscove's Modified Dulbecco's Medium (IMDM)(Gibco), penicillin/streptomycin (Lonza), L-Glutamine (Thermofisher Scientific), Foetal bovine serum (FBS) (Serana), HEPES (Thermo Fisher Scientific), phosphate buffered saline (PBS) (Thermofisher Scientific), ficoll (Invitrogen), MACS buffer (Miltenyi Biotec), MACS CD14 beads (Miltenyi Biotec), human interleukin-4 (IL4) (R&D Systems), human granulocyte macrophage colony-stimulating factor (hGM-CSF; R&D Systems), mouse granulocyte macrophage colony-stimulating factor (mGM-CSF; R&D Systems), LPS (E. coli 0111:B4; Sigma) and β-mercaptoethanol (Sigma-Aldrich), Zymosan particles (Sigma-Aldrich Chemie BV), Pam3Cys (Sigma-Aldrich).

### Human monocyte-derived dendritic cell (MoDCs) culture

Human buffy coats from healthy donors (Sanquin Institute, Amsterdam, The Netherlands) were obtained ethically and their utilization in research was in compliance with the informed consent agreements, under a protocol approved by the IRB/EC or with the approval of the Medical Ethics Committee at Amsterdam UMC, University of Amsterdam. Peripheral mononuclear cells (PBMCs) were isolated from buffy coats as described earlier [24], then monocytes were separated by positive selection using MACS $CD14^+$ microbeads (Miltenyi Biotec) according to the manufacturer's instructions. $CD14^+$ monocytes were cultured for five days in RPMI-1640 medium supplemented with 10% FBS, 100 U/mL penicillin/streptomycin and 2mM L-Glutamine and in the presence of GM-CSF (30 ng/mL) and IL4 (20 ng/mL) to

generate monocytes derived immature DCs (imMoDCs), then was stimulated with LPS (10 ng/mL) for extra 24 hours to generate mature DCs (mMoDCs). Monocytes were cultured at a concentration of $1x10^6$/mL in 6-well plates during differentiation, then collected and re-plated in 24-well plates for LPS maturation. Monocytes were pre-treated with DMSO or WWL113 at indicated concentrations for 1 hour prior to incubation with GM-CSF and IL4, then compound was washed prior to LPS maturation. The supernatant was collected for cytokine or lactate measurements and cells were collected for subsequent applications and analysis.

## Murine bone marrow derived dendritic cell (BMDCs) culture

Bone marrow cells were isolated from tibiae and femurs of adult transgenic *CES1/Es1e$^{lo}$/Rag$^{-/-}$* mice or *Rag$^{-/-}$* mice and were cultured for 7 days in RPMI-1640 containing: L-glutamine, 25 mM HEPES, 10% FBS, 1% penicillin-streptomycin, β-mercaptoethanol and mGM-CSF (20ng/ml). Cells were cultured at density of $5x10^5$/ml, medium were refreshed at day 3 and day 6, then after 7 days of culture in mGM-CSF, cells were collected and seeded in 24 well plate at density of $1x10^6$/ml and stimulated with 100 ng/mL LPS or 10 Zymosan particles/cell or 10 ng/mL Pam3Cys or left unstimulated for 24 hours then supernatants were collected for cytokines analysis.



## T cell transfer colitis model.

We applied the T cell transfer model as follows; CD4$^+$CD45Rb$^{high}$ cells were isolated from spleens of C57BL/6 WT mice by magnetic bead depletion using dynabeads™ sheep anti-rat IgG (ThermoFisher), anti-CD11b (Biolegend), anti-CD45R (Sony) and anti-CD8a (Biolegend) followed by fluorescence-activated cell sorting using anti-CD45RB-FITC and anti-CD4-PE/Cy5 (BD Bioscience). Ten to fourteen weeks old male and female *CES1/Es1e$^{lo}$/Rag$^{-/-}$* mice or *Rag$^{-/-}$* mice received intraperitoneally $4.5 \times 10^5$ CD4$^+$CD45Rb$^{high}$ cells; mice that did not receive T cells transfer served as control groups. Body weight was assessed three times a week then daily starting from week 4 until sacrifice. Animals losing> 20% from their highest weight or showing sickness behaviour were euthanized. *Rag$^{-/-}$* mice were sacrificed at end of week 5 while *CES1/Es1e$^{lo}$/Rag$^{-/-}$* mice and no T cell transfer mice were scarified at end of week 7.

## Cytokine measurements

Cytokines were measured in supernatants using either enzyme-linked immunosorbent assay (ELISA) kits (R&D systems) or cytometric bead array (CBA); mouse inflammation kit (BD bioscience) or human inflammatory cytokine kit (BD bioscience) according to the manufacturer's protocol. Samples were analyzed using Biotek Synergy HT (Agilent) or flow cytometry (Fortessa) respectively.

## Flowcytometry analysis

MoDCs surface markers staining: following MoDCs culture, cells were collected and washed in PBS, stained for live/dead™ fixable near-IR dead cell stain (Thermofisher) for 30 minutes, then washed in FACS Buffer and stained for another 30 minutes for CD209-Percp-Cy5.5 (clone 9E9A8, Biolegend), CD1b-BV421 (clone M-T101, Becton Dickinson), CD86-FITC (clone 2331(FUN-1), Becton Dickinson), MHCII-AlexaFlour700 (clone LN3, eBioscience), CD14-PE-CY7 (clone 16A1 , Biolegend).

T cells intracellular cytokines staining: following mMoDCs - T cells co-culture, cells were harvested and plated in supplemented RPMI-1640 medium containing phorbol 12-myristate 13-acetate (PMA, 100ng/ml) and ionomycin (1µg/ml) for 2 hours then brefeldin-A (10µg/ml) was added for extra 2 hours. Afterwards, cells were harvested and washed in PBS and stained for live/dead™ fixable near-IR dead cell stain (Thermofisher), then washed in FACS Buffer and stained for CD3-BV421 (clone UCHT1, Biolegend), then were fixed and permeabilized using FIX & PERM Cell Permealization kit (ThermoFisher), stained for IL17A-Percp (Clone 41802, R&D systems) IFNγ-FITC (clone B27, Biolegend) FOXP3-AlexaFlour647 (clone 2-6D, Biolegend). All samples were acquired using a FACS Fortessa (BD Biosciences) and analyzed using FlowJo software (Treestar Inc., Ashland, OR).

## Phagocytosis assay

Phagocytosis assay was performed using pHrodo™ Green E. coli BioParticles™ Conjugate (Invitrogen) according to manufacture protocol. In brief, following MoDCs culture, cells were collected, washed and re-plated in RPMI-1640 medium supplemented with 10% FBS, 100 U/mL penicillin/streptomycin and 2mM L-Glutamine in 96 well plates at density of $5x10^4$ cells/well, and incubated for 1 hour at 37C, 5% CO2 with pHrodo E.coli particle as indicated per manufacture protocol. Control samples were cultured without pHrodo E.coli particles (negative control) at 37C, 5% CO2 or with pHrodo E.coli particles at 4C (control for non specific particles adhesion to the outer cell surface without true phagocytosis). Afterwards, cells were washed in FACS buffer and acquired immediately using a FACS Fortessa (BD Biosciences) and analyzed using FlowJo software (Treestar Inc., Ashland, OR). Amount of phagocytosed particles were quantified as geometric mean of intensity of FITC green signal per viable cells.

## MoDCs T cell co-culture assay

$CD14^+$ monocytes were isolated from PBMCs and differentiated to mMoDCs as

described above in presence of DMSO or 2.5μM or 10μM WWL113. Meanwhile autologous $CD4^+$ T cells from same donors were isolated from the $CD14^-$ fraction using $CD4^+$ T cell isolation kit (Miltenyi Biotec) through negative selection, then cultured for 6 days in RPMI-1640 medium that contains 5ng/ml recombinant human IL7 (R & D systems). Afterwards, mMoDCs were co-cultured with autologous T cells for 3 days (DCs to T cells ratio; 1:5) in RPMI-1640 medium supplemented with 10% FBS, 100 U/mL penicillin/streptomycin and 2mM L-Glutamine in 96 well plate at T cell concentration of $1x10^5$/well. Samples with only T cell cultured in medium containing IL7 (5ng/ml) or co-cultured with imMoDCs, served as control samples. After 3 days of culture, cells are harvested for intracellular cytokines staining as described above.



## RNA isolation, transcriptomic analysis and quantitative real-time PCR (RT-qPCR).

RNA was isolated from MoDCs using RNeasy Plus Mini Kit (Bioline ISOLATE II) and according to the manufacturer's protocol. RNA sequencing was performed on the NovaSeq 6000 in a 150bp paired ended fashion to a depth of 40M reads. Reads were subsequently aligned in a paired ended fashion using STAR (v2.7.9a) [25], whereupon post-alignment processing was performed using SAMtools (v1.15.1) [26]. Finally, the mapped reads were assigned to genes using Subread (v2.0.1) [27]. Quality control was performed using FastQC (v.0.11.9) [28] and MultiQC (v1.11) [29]. Raw reads were subsequently imported in R (v4.2.2) using Bioconductor (v3.16) package DESeq2 (v1.38.1) where we conducted pairwise comparative analyses. Gene set enrichment analyses were conducted against the Kyoto Encyclopedia of Genes and Genomes (KEGG) [30] using the fgsea (v1.24.0). Visualizations were made using ggplot2 (v3.34.0) [31] and pheatmap (v1.0.12) [32].

For *CES1* qPCR analysis, complementary DNA (cDNA) was synthesized by random hexamer primers (Promega), oligo dT primers (Invitrogen), revertaid (Fermentas), deoxynucleotide triphosphates (Thermofisher Scientific), riboblock RNAse inhibitor (Fermenta) and 5x RT-buffer (Fermentas). RT-qPCR was conducted on cDNA products with SensiFAST SYBR No-ROX (GC Biotech) by the Biorad CFX 96. The genes amplified by RT-qPCR were *CES1*, *cyclophilin* and *TBP*. The LinRegPCR software was used to analyse the expression levels of *CES1* gene. The geometric means of the housekeeping genes *cyclophilin* and *TBP* were used to normalize gene expression.

Primers sequence (forward sequence – reverse sequence);
*CES1* (GGAACAGACGACACTGTCAAA – GCTCCAGCATCTCTGTGGTT),
*cyclophilin* (ACGGCGAGCCCTTGG - TTTCTGCTGTCTTTGGGACCT)
and *TBP* (TCTCATGTACCCTTGCCTCC - GTGCACAAATAATGCCCCTT).

### Lactate measurement

A master mix was prepared by combining 130 µL of 0.5M glycine-0.4M hydrazine buffer (pH 9.0) and 20 µL of 27mM nicotinamide adenine dinucleotide (NAD) [33]. Then, 5 µL of the sample supernatant was added to the master mix, and 20 µL of Milli-Q water. To measure lactate levels in the sample, a standard solution was prepared of concentrations that range from 2.5 mM to 250 µM. The fluorescence was measured at a wavelength of 340 nm (excitation) and 450 nm (emission) every 2 minutes at 37 °C using the CLARIOstar microplate reader. After 6 cycles, 25 µL of a start solution (5 mg/mL L-lactate dehydrogenase diluted 1:50 in 0.5M glyzine-0.4 hydrazine buffer) was added to the wells, and fluorescence was measured every 2 minutes for up to 45 minutes.

### Oxygen consumption and extracellular acidification rate

A 96-well Seahorse plate was coated with 25 µg/ml of CelTak (Corning, Life Sciences) for 30 minutes at RT. The wells were washed with aquadest and left to dry in ambient air. The plate was then stored at 4°C. MoDCs differentiated in the presence of 10 µM WLL113 or DMSO were collected by centrifugation and resuspended at a density of 1.5x106 cells/ml in modified RPMI 1640 medium (without NaHCO3 and phenol red) containing 5.5 mM glucose and 2 mM glutamine as substrates and supplemented with 0.1% BSA and 20 mM HEPES (pH 7.4). The cells were then added to the pre-coated 96-well Seahorse plate by adding 55 µl per well. After 5 minutes of incubation at RT, the Seahorse plate was centrifuged at 1500 rpm for 2 minutes to induce adhesion of the cells to the bottom of the pre-coated wells. 120 µl of pre-warmed incubation medium was then carefully added to the wells and, after a pre-incubation of 10 min at 37C, the plate was loaded to the Seahorse XF96 analyzer (Agilent Technologies). After another equilibration period of about 20 min, the measurement of basal respiration and acidification was started. Prior to transfer of the cells to the Seahorse apparatus, the injection ports of the Seahorse cartridge were filled with 25 µl of the following solutions (all diluted in medium without BSA): port A – 25 µM oligomycin; port B – 20 µM FCCP; port C – 25 µM antimycine + 10 µM rotenone. All measurement times were put at 2 min, and the number of measurements was 6 times for the basal rate, 3 times after port A injection, 2 times after port B injection and 3 times after port C injection. Mixing times were put at 1 min or 2 min (after FCCP injection). A waiting period of 30 sec between mixing and measurement was also included in the protocol. After completion of the Seahorse run, most of the supernatant in the wells was removed by suction and the cells were fixed by addition of 4% paraformaldehyde (in PBS). After 15 min at RT, the fixative was decanted and after one wash with DNA staining buffer (5 mM EDTA-NaOH pH 8.0, 5 mM $Na_2SO4$ and 0.0001% Triton X-100), 75 µl of staining buffer containing Hoechst 33324 (5 µg/ml)

was added to all wells to determine the DNA content of each well. Samples were read after 24 h of incubation with Hoechst 33324. Calf thymus DNA (1 mg/ml) was used as reference for the Hoechst staining. The Wave software (version 2.3.0) was used for analysis. The oxygen consumption rate (OCR) under basal and uncoupled conditions was corrected for non-mitochondrial respiration, as determined after antimycine plus rotenone addition.

### Metabolomics analysis

Freshly isolated Human CD14$^+$ monocytes were pretreated with 10 μM WLL113 or DMSO for 1 hour prior to differentiation to MoDCs as described above. Cells pellets were collected, snap frozen and stored in liquid nitrogen in 2 ml tubes. Metabolites measurements was performed by the metabolomics core facility at the Amsterdam UMC using ultra-high-pressure liquid chromatography as described previously [34]. The HPLC system consisted of an acquity binary HPLC pump, a vacuum degasser, a column temperature controller, and an auto sampler (Waters, Milford, MA, USA). The column temperature was maintained at 30C. The metabolite extract was injected onto a SeQuant 100 x 2.1 mm ZIC-cHILIC column, 3μm particle diameter (Merck, Darmstadt, Germany). Impact II QTOF (Bruker Daltoniks) mass spectrometer was used in the negative and/or positive electrospray ionization mode. In both the negative and positive ionization mode, mass spectra of the metabolites were obtained by continuous scanning from m/z 50 to m/z 1200 with a resolution of 50000 FHMW. List of measured metabolites are provided in **Supplementary table S1**.



### Statistical analysis

Statistical analyses were performed with GraphPad Prism version 9.0 (GraphPad Software Inc.). Differences between groups was assessed with the Student T-test in. For comparisons in multiple groups one-way ANOVA was used. .* $p \leq 0.05$, ** $p \leq 0.01$, *** $p \leq 0.001$ were considered significant.

## Results

### CES1 expression peaks early during MoDCs differentiation and following LPS stimulation.

In order to explore the relevance of CES1 to the DCs differentiation and function, we first aimed to explore the temporal expression of *CES1* during monocytes to DCs differentiation. RNA expression was analyzed in freshly isolated blood CD14$^+$ monocytes and temporally throughout 5 days of differentiation to immature DCs with IL4 and GM-CSF cytokines mix. In accord with previous reports [35], *CES1* was

expressed in freshly isolated CD14$^{+}$ monocytes early during differentiation and upregulated (up to 13 fold) at day 1 during the differentiation protocol. Interestingly, this early peak of *CES1* expression was completely abrogated to extremely low values around day 3 and remain very low afterwards up till complete differentiation to imMo-DCs. Following LPS stimulation of imMo-DCs, *CES1* expression levels remained low at early time point (3 hours), however strong upregulation was noted at late time point (24 hours) as a part of the late LPS response (**Figure 1A**).

## CES1 inhibition promote differentiation of MoDCs with stronger inflammatory phenotype.

To further explore the potential role of CES1 upregulation in MoDCs, we aimed to inhibit CES1 during monocytes to DCs differentiation using WWL113, a CES1 specific inhibitor, and examined the phenotype of the generated MoDCs afterwards (**Figure 1B**). During MoDCs differentiation in presence of concentration range of WWL113 (0.15-10μm), the generated imMoDCs were stimulated with LPS and secreted inflammatory cytokines were measured in the supernatant. IL6, IL8, IL10 and TNF secretion were increased in a dose dependent manner (**Figure 1C**). Flow cytometry analysis of DCs differentiation and activation markers were performed and represented as geometric mean of intensity (geoMFI) of markers of interest among viable imMoDCs or mMoDCs. Both CD1b and CD209 are known markers of DCs differentiation, but in the presence of 10μm WWL113 CD1b expression was absent. However CD209 was significantly upregulated. Interestingly CD86, also a known DCs activation marker, was upregulated in imMoDCs, most noticed in 10μm condition, even without LPS stimulation (**Figure 1D**). We next used LPS stimulation to mature the imMoDCs in culture. Following LPS maturation, both CD86 and MHCII expression were relatively higher in WWL113 treated conditions (**Figure 1E**), while CD1b and CD209 remain stable (data not shown). Collectively, pharmacological inhibition of CES1 during MoDCs differentiation have modulated MoDCs phenotype with primed inflammatory properties.

## Human *CES1* transgenic overexpression in murine bone marrow derived dendritic cells (BMDCs) mediates attenuated inflammatory response to TLR ligands.

We next aimed to examine the effect of *CES1* overexpression on the inflammatory response of BMDCs. For that purpose, we made use of transgenic human *CES1*/*Es1e*$^{lo}$ mice, which overexpress human *CES1* under *CD68* promotor [36], this allows for high CES1 expression specifically in mononuclear myeloid cells. BMDCs were generated from both transgenic and wild type mice strains and both are stimulated with multiple TLR ligands (LPS, zymosin and Pam3Cys).

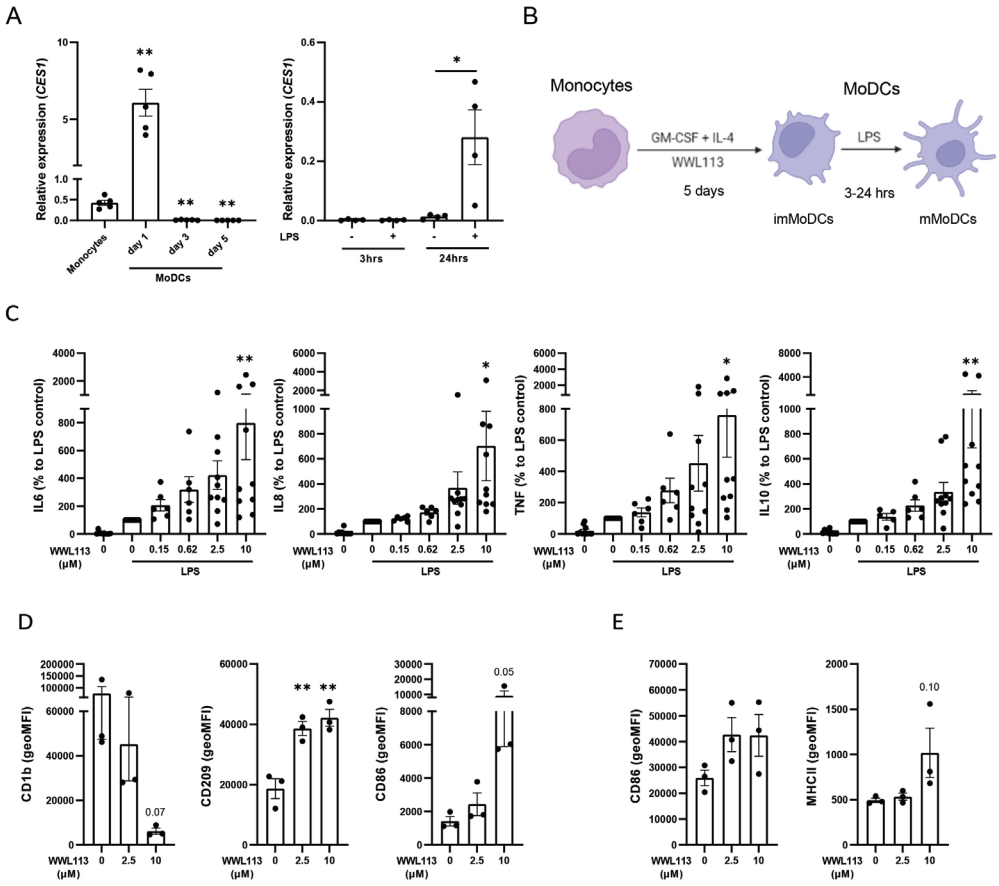


**Figure 1. CES1 inhibition promotes differentiation of monocytes derived dendritic cells (MoDCs) with stronger inflammatory phenotype.** (**A**) Quantitative PCR analysis of CES1 temporal expression upon MoDCs differentiation and following LPS stimulation. (**B**) Experimental design of CES1 pharmacological inhibition with WLL113 during MoDCs differentiation. (**C**) IL6, IL8, TNF and IL10 protein secretion were measured with CBA in supernatant of 24 hours LPS stimulated MoDCs that were previously generated under CES1 inhibition (WWL113 treatment) as demonstrated in (**B**). (D-E) CD1b, CD209, CD86 and MHCII geometric mean of intensity as measured by flow cytometry in imMoDCs (**D**) or mMoDCs (**E**) following differentiation under WLL113 treatment as demonstrated in (**B**). MoDCs; monocytes derived dendritic cells, imMoDCs; immature monocytes derived dendritic cells, mMoDCs; mature monocytes derived dendritic cells. Statistical testing was performed using one way annova or student t test; * $p \leq 0.05$, ** $p \leq 0.01$. SEM; standard error of the mean.

IL6 secretion was significantly lower in transgenic BMDCs compared to WT BMDCs for the all 3 tested TLR ligands. TNF secretion demonstrated the same pattern that reached statistical significance for Pam3Cys. IL10 secretion followed similar pattern to less extent for both LPS and zymosan stimulation, but was not statistically significant. Lastly, CCL2 secretion did not differ between transgenic and WT BMDCs except for

PamCys that was significantly upregulated in transgenic BMDCs (**Figure 2**). We then wondered whether these *in vitro* observations has a translational impact *in vivo*. Therefore we performed a T cell transfer colitis experiment, in which wild type T cells are adoptively transferred to *Rag*$^{-/-}$ mice that lack T and B cells in order to establish a T cell mediated colon inflammation, in which endogenous DCs play a critical role to drive T cell activation and disease pathology (**Figure S1A**). We noted that *CES1/Es1e*$^{lo}$*/Rag*$^{-/-}$ mice were more resistant to develop colitis and survived longer compared to *Rag*$^{-/-}$ mice controls, which might reflect a relatively lesser capacity of CES1 over expressing DCs to drive the T cell mediated colitis (**Figure S1B**). Collectively, this indicates a relatively less inflammatory response of CES1 over expressing BMDCs, the opposite effect to what we observed earlier with pharmacological inhibition of CES1 in human MoDCs.

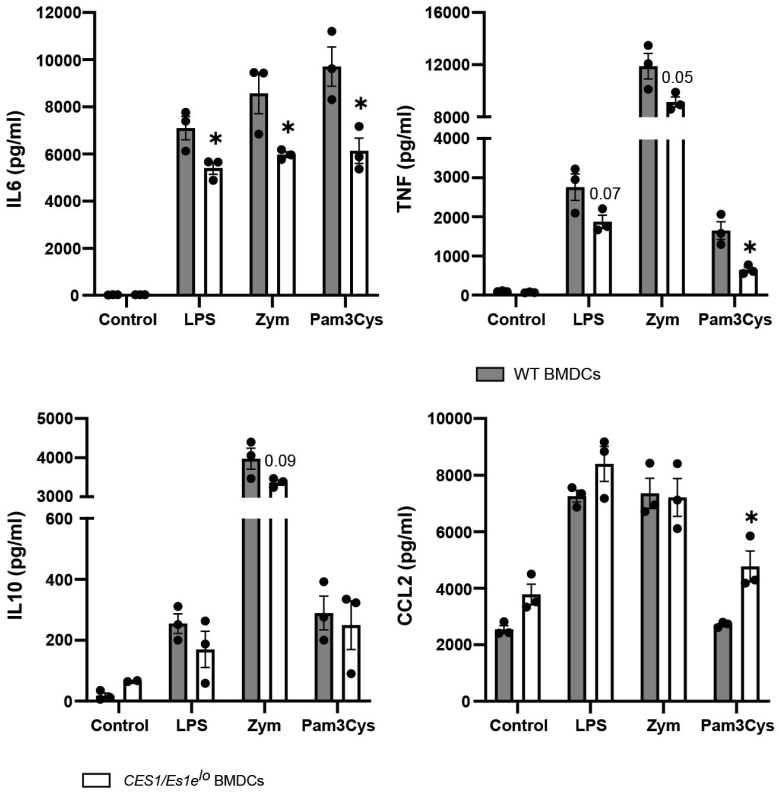


**Figure 2. Human *CES1* transgenic overexpression in murine bone marrow derived dendritic cells (BMDCs) mediates attenuated inflammatory response to TLR ligands.** IL6, TNF, IL10 and CCL2 protein secretion quantified with CBA assay in supernatant of BMDCs in response to multiple TLR agonists (LPS, zymosin and Pam3Cys). BMDCs generated from *CES1/Es1e*$^{lo}$transgenic mice overexpressing human *CES1* under *CD68* promotor (white bars) are compared to WT mice (grey bars). Statistical testing was performed using student t test; * $p \leq 0.05$. SEM; standard error of the mean.

## Human MoDCs generated under CES1 inhibition have more phagocytic capacity and promote Th17 differentiation.

Next, we wondered whether the observed DCs phenotype generated under CES1 pharmacological inhibition, may have an impact on DCs functional properties. Therefore, we investigated the potential impact on MoDCs phagocytic and T cell differentiation capacity. MoDCs differentiated under DMSO, 2.5 or 10µm WWL113 treatment, as shown in (**Figure 1B**), were incubated with FITC-labelled E.coli and the amount of internalized E.coli was assessed using flow cytometry, as a quantification of geoMFI of FITC, to reflect DCs phagocytic capacity. WLL113 treated MoDCs demonstrated higher phagocytic capacity, which was significantly evident in 10µm dose, both in imMoDCs and mMoDCs (**Figure 3A-B**). Furthermore, in order to assess T cell skewing property, mMoDCs were differentiated and co-cultured with autologous $CD4^+$ T cells isolated from same donor, then intracellular IL17, IFNγ and IL10 expression were assessed within T cell using flow cytometry. Following MoDCs – T cell co-culture, there was an increased expression of IL17 among T cells in a dose dependent manner (**Figure 3C-D**), while no change was noted in both IL10 and IFNγ expression (**Figure S2**). Collectively, the distinctive inflammatory phenotype of the MoDCs, differentiated under CES1 inhibition, was also accompanied by higher phagocytic capacity and preferential capacity to drive Th17 skewing.

## Transcriptomic analysis of MoDCs generated under CES1 inhibition demonstrates modulation of multiple metabolic and inflammatory pathways.

To explain the changes driven by CES1 inhibition, we aimed to study the transcriptomic profile of the generated DCs under WWL113 treatment, using RNA-sequencing. We followed the same experimental layout as in (**Figure 1B**) to generate imMoDCs treated with either DMSO, 2.5 or 10µm WWL113 for 5 days, then imMoDCs were subjected to 3 hours of LPS stimulation prior to transcriptomic analysis. When we compared DMSO treated to WWl113 treated conditions, regardless of the dose, we could identify 2339 significantly differentially expressed genes (DEGs), where 801 DEGs were upregulated, while 1538 DEGs were downregulated (**Figure 4A**). In order to examine to what extent the WLL113 driven DEGs changes were dose dependent, the effect sizes of DEGs were compared using Wald statistics. WWL113 (2.5µm) was compared to DMSO treatment on the x-axis, while WWL113 (2.5µm) was compared to WWL113 (10µm) treatment on the y-axis (**Figure S3A**). We could observe that most of the significantly DEGs were shared between the 2 comparisons, indicating a dose dependent effect of the WWL113 treatment. Furthermore, gene set enrichment analysis (GSEA) with functional annotation using the Kyoto Encyclopedia of Genes and Genomes (KEGG) pathways analysis has shown significant positive enrichment in response to WWL113 treatment for 146 pathways.

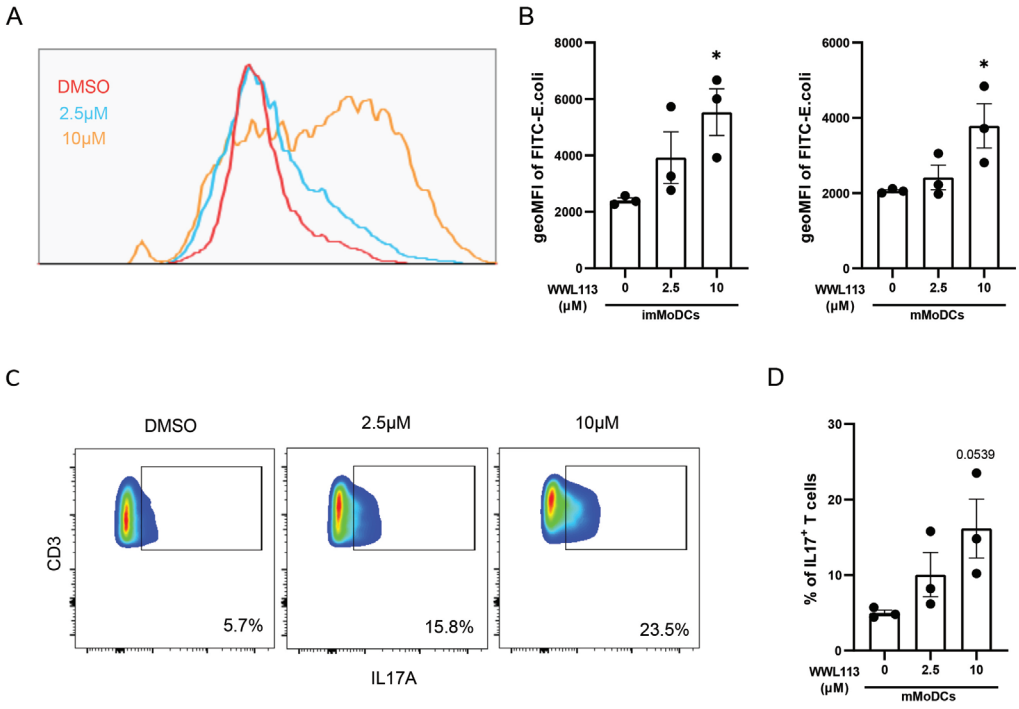


**Figure 3. Human MoDCs generated under CES1 inhibition have more phagocytic capacity and promote Th17 differentiation.** (**A**-**B**) The amount of phagocytosed E.coli as measured by geometric mean of intensity of FITC labelled E.coli following incubation with MoDCs. (**A**) The overlay histogram compares MoDCs differentiated under either DMSO or WWL113 (2.5μM and 10μM) as experimental design shown in Figure 2B. (**B**) FITC labelled E.coli geoMFI is quantified in both imMoDCs and mMoDCs. (**C**-**D**) Flow cytometry analysis of IL17 expression in T cells following co-culture with mMoDCs generated under either DMSO or WWL113 (2.5μM and 10μM). (**C**) FACS plots demonstrate IL17 expression among alive $CD3^+$ T cells. (**D**) Frequency of $IL17^+$ T cells among total $CD3^+$ T cells is quantified. Statistical testing was performed using one way annova test; * $p \leq 0.05$. SEM; standard error of the mean.

When we examined the top positively enriched pathways, as represented by normalized enrichment score (NES), we could identify multiple inflammation or metabolism related pathways. Among the 146 pathways, there were 31 and 26 pathways for inflammation and metabolism respectively (**Figure S3C**). Given the function of the CES1 enzyme, we further focused on the metabolism related pathways. Among the 26 metabolism related pathways, we could identify some pathways (**Figure S3C**) that have a direct impact on DCs inflammatory phenotype switch, including the citric cycle (TCA cycle) (**Figure S4**), oxidative phosphorylation, glycolysis / gluconeogenesis (**Figure S5**), pentose phosphate (**Figure S6**), and biosynthesis of amino acids and purine metabolism pathways.

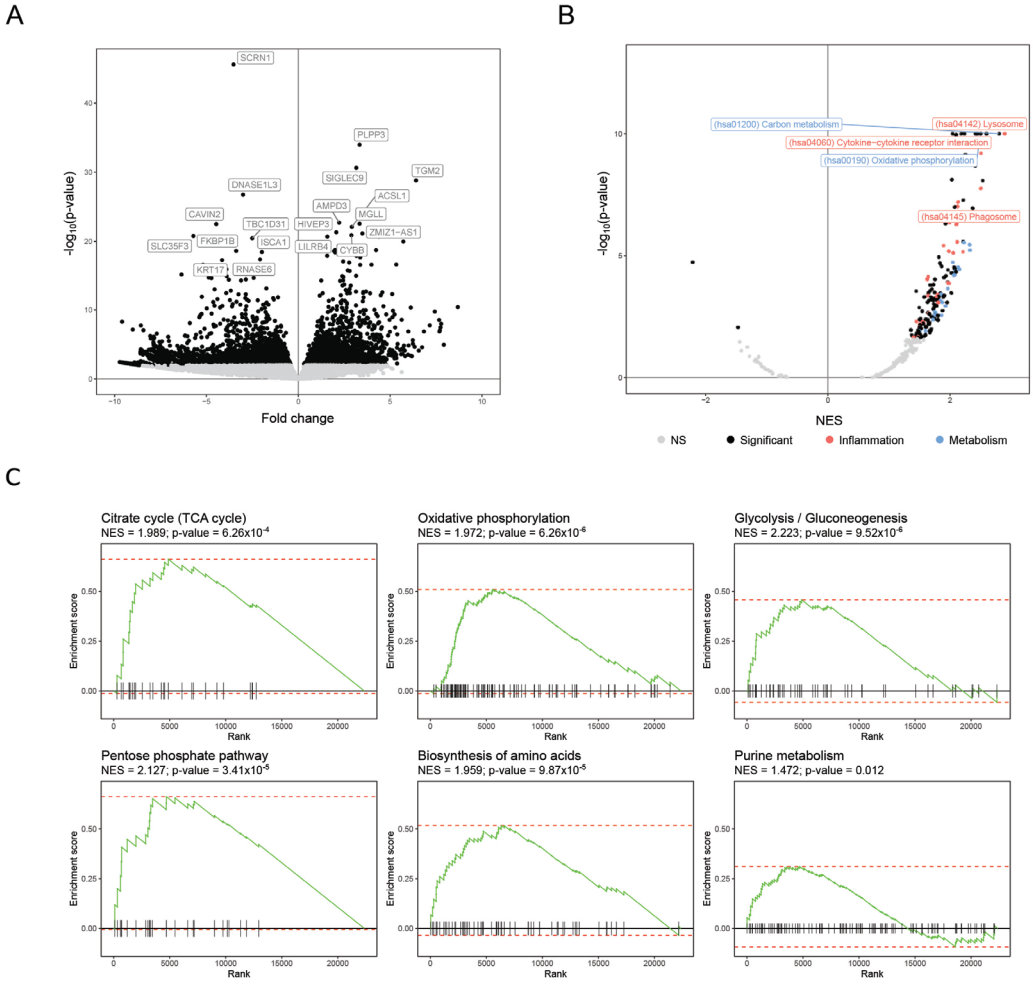


**Figure 4. Transcriptomic analysis of MoDCs generated under CES1 inhibition demonstrates modulation of multiple metabolic and inflammatory pathways.** RNA sequencing data analysis of human CD14$^{+}$ monocytes derived DCs (MoDCs), differentiated in presence of DMSO or WWL113 (2.5μM and 10μM), following 3 hours of LPS stimulation (n=3 healthy donors). (**A**) Volcano plot highlight top 10 differentially up or down regulated genes, comparing DMSO and WWL113 treated MoDCs. (**B**) Gene set enrichment analysis (GSEA) with functional annotation using Kyoto Encyclopedia of Genes and Genomes (KEGG) pathways was performed, volcano plot shows positively and negatively enriched pathways, inflammation and metabolism related pathways are highlighted. (**C**) Enrichment scores of citrate cycle (TCA cycle), oxidative phosphorylation, glycolysis / gluconeogenesis, pentose phosphate, biosynthesis of amino acids and purine metabolism pathways are shown.

## CES1 inhibition promotes a glycolytic DCs phenotype and impairs mitochondrial respiration capacity.

Our transcriptomic data revealed modulation of multiple energy metabolism pathways. Given the key role of DCs energy metabolism in determining DCs cellular functions and promoting phenotype switch, we aimed to further assess the functional metabolic profile of DCs differentiated under CES1 pharmacological inhibition. Therefore, following the same experimental layout as in (**Figure 1B**), we assessed lactate production as well as, glycolytic and mitochondrial respiratory capacities of WWL113 treated DCs. Lactate production was increased in response to LPS maturation, reflecting the glycolytic shift that characterizes the inflammatory DCs phenotype of MoDCs. Interestingly, WWL113 treatment resulted in significantly increased lactate production as compared to DMSO control for both imMoDcs and mMoDCs (**Figure 5A**), reflecting an increased glycolytic activity. Next, we used Seahorse technology to assess the extracellular acidification rate (ECAR) and oxygen consumption rate (OCR). These were measured under basal conditions, and again after oligomycin addition to block mitochondrial ATP synthesis. The difference in ECAR mainly reflecting glycolytic lactate formation [25] caused by oligomycin (delta oligo) is a good indicator of the mitochondrial contribution to cellular ATP production (**Figure 5B**). The delta oligo was not significantly different in the 3 donors tested (**Figure 5C**). Similarly, mitochondrial respiration was assessed under basal, oligomycin-inhibited and uncoupled (FCCP) conditions. With FCCP present, the maximal respiratory capacity of the mitochondria is measured. In both imMoDCs and mMoDCs, WWL113 treated DCs showed similar rates as the control cells under all 3 conditions. (**Figure 5D-E**). In another experiment, following differentiation of imMoDCs in presence of DMSO or WWL113 as shown in (**Figure 1B**), we repeated the same measurements, but with addition of WWL113 acutely during the respirometry assay. The acute WWL113 treatment of imMoDCs during the assay demonstrated significant reduction of delta oligo following oligomycin addition (**Figure S7A-B**), as well as maximal respiratory capacity under uncoupled conditions (**Figure S7C-D**). This indicates a significant reduction of mitochondrial ATP synthesis induced by WWL113. Collectively, functional metabolic profiling of MoDCs demonstrated modulated mitochondrial respiration and glycolytic activity of WWL113 treated DCs that was more evident during acute treatment.

## Metabolomic analysis of MoDCs generated under CES1 inhibition shows distinctive metabolic profile with depletion of multiple amino acids.

Given the observed DCs functional metabolic changes in response to WWL113 treatment, we performed metabolomics profiling of MoDcs generated under WWL113 treatment as described in (**Figure 1B**).

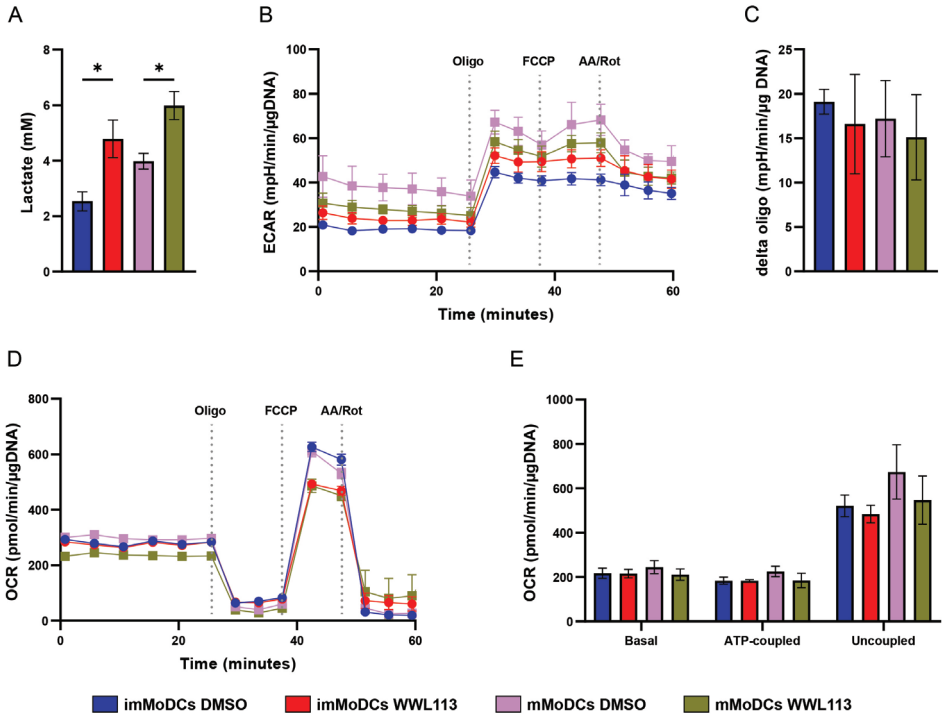


**Figure 5. CES1 inhibition promotes a glycolytic DCs phenotype with increased lactic acid production.** Lactate levels, oxygen consumption rate (OCR) and extracellular acidification rate (ECAR) of MoDCs differentiated in presence of DMSO or 10µM WWL113 (n=3-4 healthy donors) are measured, experimental set up is the same as shown in figure 1B, imMoDCs represent MoDCs following 5 days of differentiation, this is furthered stimulated with LPS for 24 hours to generate mMoDCs, WWL113 treatment is only applied during imMoDCs differentiation part. OCR and ECAR were measured with Seahorse XF96 analyzer. (**A**) Lactate levels were measured in the supernatant of DMSO and WWL113 treated imMoDCs and mMoDCs. (**B-C**) ECAR are measured for both imMoDcs and mMoDCs under basal conditions and after addition of 25 µM oligomycin, 25 µM FCCP and 25 µM antimycine combined with 10 µM rotenone, a representative donor (n=6 technical replicates) is shown in (**B**) and delta oligo (the difference between basal ECAR and ECAR after oligomycin addition; a measurement of the glycolytic flux) is shown for 3 donors in (**C**).(**D-E**) OCR are measured for both imMoDcs and mMoDCs under basal conditions and following 25 µM oligomycin, 25 µM FCCP and 25 µM Antimycine combined with 10 µM rotenone. Uncoupled conditions indicate the maximal mitochondrial respiratory capacity, a representative donor (n=6 technical replicates) is shown in (**D**). Quantification of OCR levels under basal conditions, after oligomycin addition (ATP-coupled), and after FCCP addition (uncoupled) are shown for 3 donors in (**E**). Results are illustrated as mean ± SEM; standard error of the mean. Statistical testing was performed using student t test; * $p \leq 0.05$, DMSO and WWL113 treated conditions are compared.

Principal component analysis (PCA) has demonstrated a distinguishable clustering between WWL113 and DMSO treated conditions, in imMoDCs (**Figure 6A**) and to less extent in mMoDcs (**Figure 6C**). Among the analyzed 122 metabolites, 26 metabolites were significantly changed, of which 13 metabolites were decreased, while 13 metabolites were increased in WWL113 treated imMoDCs compared to DMSO (**Figure 6B**). On the other hand, following LPS maturation, WWL113 treated DCs and displayed significant changes of 42 metabolites, with 3 metabolites being increased and 39 metabolites being decreased in WWL113 treated mMoDCs (**Figure 6D**). In order to understand the relevance of these metabolomics changes, we performed pathway analysis of the most significantly changed metabolites, which demonstrated changes in pathways involved in amino acids synthesis and metabolism such as, arginine, proline, alanine, aspartate and glutamate, along with energy metabolism pathways, such as TCA cycle, pyruvate metabolism and penthouse phosphate pathway (PPP) metabolism (**Figure 6E**). Purine and pyrimidine metabolism pathways were also positively enriched (**Figure 6E**). When we compared the whole list of human amino acids between WWL113 and DMSO treated MoDCs, we observed a striking reduction of majority of amino acids in WWL113 treated imMoDCs and mMoDCs (**Figure 6F**). We further validated the changed intermediate metabolites of the TCA cycle, and identified decreased levels of succinate, citrate and pyruvate, meanwhile, glucose 6-phosphate and malate were increased (**Figure 7**). These changed TCA intermediates reflects the CES1 mediated impaired mitochondrial respiration capacity (**Figure 5D-E, H-I**). Collectively, these data underscore that CES1 mediates TCA cycle activity which modulates DCs inflammatory reactivity and maturation.

**> Figure 6. Metabolomic analysis of MoDCs generated under CES1 inhibition shows distinctive metabolic profile with depletion of multiple amino acids.** Concentration of 122 metabolites are measured by ultra-high-pressure liquid chromatography within both imMoDCs and mMoDCs, differentiated in presence of DMSO or 10μM WWL113 (n=6 healthy donors), experimental set up is the same as shown in figure 1B, imMoDCs represent MoDCs following 5 days of differentiation, this is furthered stimulated with LPS for 24 hours to generate mMoDCs. (**A,C**) Principal component analysis (PCA) of imMoDCs (**A**) and mMoDCs (**C**) are shown. (**B,D**) Volcano plots show changed metabolites in imMoDCs (**B**) and mMoDCs (**D**), color codes represent comparison of 10μM WWL113 treated to DMSO treated conditions. (**E**) Pathway analysis depicts impact of metabolic pathways that are enriched in WWL113 compared to DMSO-pretreated MoDCs. On the x-axis pathway impact scores are shown, while the y-axis shows -log (p-value) retrieved from pathway enrichment analysis. Pathway impact scores are illustrated in the volume of the circles, the colors of the circles are associated with the p-values, a more intense color indicates a higher p-value and thus more significantly changed metabolites in a particular pathway. (**F**) Heat maps compare amino acids concentrations between DMSO and 10μM WWL113 treated samples in both imMoDCs and mMoDCs,

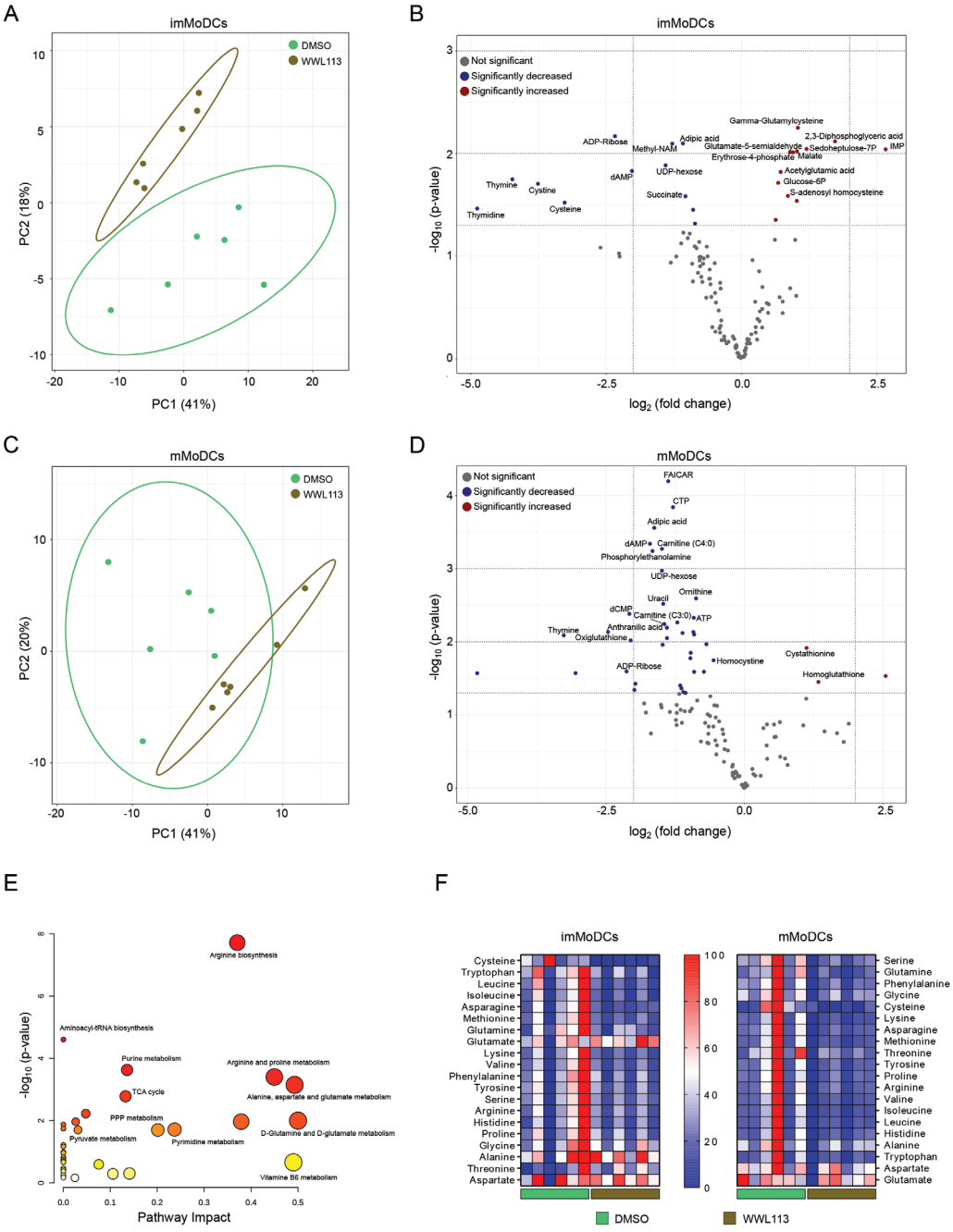
A
imMoDCs
DMSO
WWL113
PC2 (18%)
PC1 (41%)
B
imMoDCs
Not significant
Significantly decreased
Significantly increased
-log10 (p-value)
log2 (fold change)
Gamma-Glutamylcysteine
2,3-Diphosphoglyceric acid
ADP-Ribose
Adipic acid
Methyl-NAM
Glutamate-5-semialdehyde
Sedoheptulose-7P
IMP
Erythrose-4-phosphate
Malate
dAMP
UDP-hexose
Acetylglutamic acid
Thymine
Cystine
Glucose-6P
Succinate
S-adenosyl homocysteine
Thymidine
Cysteine
C
mMoDCs
DMSO
WWL113
PC2 (20%)
PC1 (41%)
D
mMoDCs
Not significant
Significantly decreased
Significantly increased
-log10 (p-value)
log2 (fold change)
FAICAR
CTP
Adipic acid
dAMP
Carnitine (C4:0)
Phosphorylethanolamine
UDP-hexose
Ornithine
Uracil
dCMP
Carnitine (C3:0)
ATP
Thymine
Anthranilic acid
Oxiglutathione
Cystathionine
Homocystine
ADP-Ribose
Homoglutathione
E
-log10 (p-value)
Pathway Impact
Arginine biosynthesis
Aminoacyl-tRNA biosynthesis
Purine metabolism
Arginine and proline metabolism
TCA cycle
Alanine, aspartate and glutamate metabolism
PPP metabolism
D-Glutamine and D-glutamate metabolism
Pyruvate metabolism
Pyrimidine metabolism
Vitamine B6 metabolism
F
imMoDCs
mMoDCs
Cysteine
Tryptophan
Leucine
Isoleucine
Asparagine
Methionine
Glutamine
Glutamate
Lysine
Valine
Phenylalanine
Tyrosine
Serine
Arginine
Histidine
Proline
Glycine
Alanine
Threonine
Aspartate
Serine
Glutamine
Phenylalanine
Glycine
Cysteine
Lysine
Asparagine
Methionine
Threonine
Tyrosine
Proline
Arginine
Valine
Isoleucine
Leucine
Histidine
Alanine
Tryptophan
Aspartate
Glutamate
DMSO
WWL113

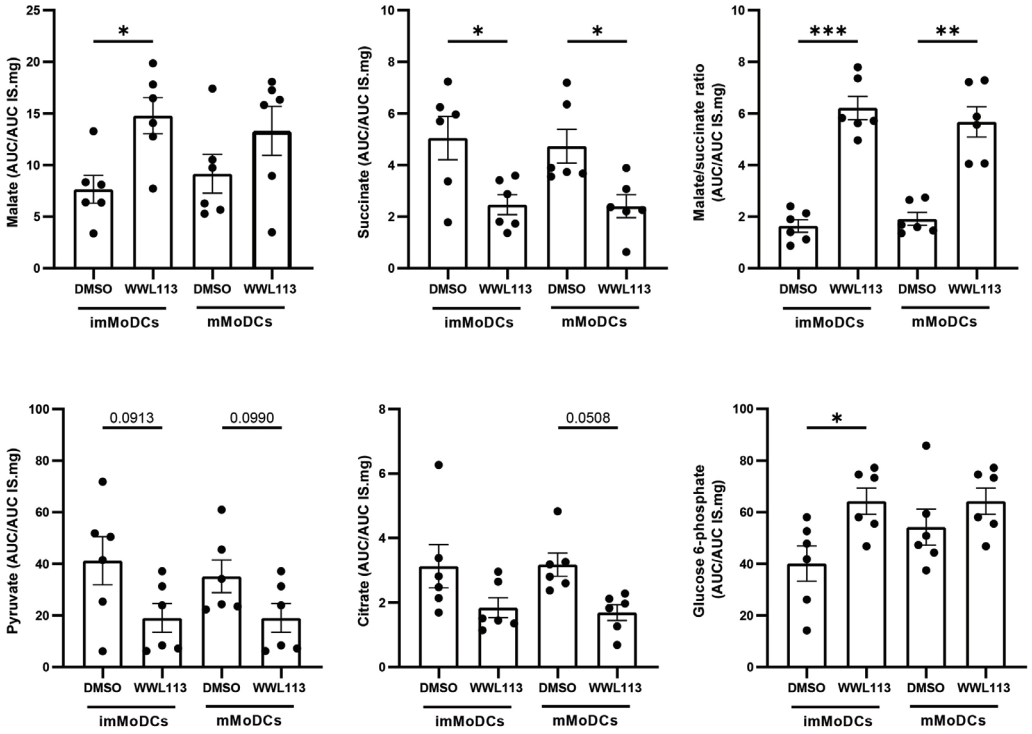


**Figure 7. Changes in TCA cycle intermediates metabolites reflect a disturbed mitochondrial respiration in MoDCs generated under CES1 inhibition.** TCA cycle metabolites (malate, succinate, pyruvate, citrate and glucose 6-phosphate) levels and malate/succinate ratio within both imMoDCs and mMoDCs (n=6) are shown, as measured by ultra-high-pressure liquid chromatography, the area under the curve (AUC) of each metabolite was corrected for by an internal standard (AUC IS) to estimate the concentrations. The internal standard used was the sum of AMP, ADP and ATP (TAN). Both 10um WWL113 and DMSO treated MoDCs were compared, results are illustrated as mean ± SEM; standard error of the mean. Statistical testing was performed using student t test; * p ≤ 0.05, **p ≤0.01, *** p ≤0.001.

# Discussion

A functional role of CES1 has been extensively studied in context of metabolic diseases, like obesity, diabetes mellitus and atherosclerosis [19, 37, 38] , as well as drugs pharmacokinetics [39, 40] due to its well characterized activity in the metabolism of endogenous and exogenous compounds. Moreover, the notable and specific expression of CES1 in mononuclear myeloid cells compared to other immune cells [15] has prompted the development of a macrophage-targeted therapeutic platform to deliver highly potent anti-inflammatory drugs with minimal off target effects [41]. The precise function of CES1 in mononuclear myeloid cells has been largely overlooked except for its role in lipid metabolism. Most of the studies focused

on the role of CES1 in cholesterol trafficking and foamy macrophage phenotype in context of atherosclerosis and mainly limited to macrophage and THP-1 cell lines[17]. In our study, we investigate a potential role of CES1 in regulating DCs immune metabolism that can modulate DCs phenotype and function.

We observed an upregulation of CES1 expression early during MoDCs differentiation in response to GM-CSF and IL4 signaling that later fell to very low levels. This may highlight a role of CES1 in shaping DCs immune metabolism early during MoDCs differentiation. Mammalian target of rapamycin (mTOR) and peroxisome proliferator-activated receptor gamma (PPARγ) signalling are activated early in response to GM-CSF and IL4 stimulation and orchestrate the development of tolerogenic DCs phenotype, primarily by regulating lipid metabolism [42] and supporting mitochondrial biogenesis [43, 44]. CES1 and PPARγ have shown to be mechanistically related in macrophages [18] and hepatocytes [45], as genetic deletion or blocking of CES1 can reduce PPARγ signalling and decrease its downstream targets [18, 45]. Moreover, mitochondrial respiration is impaired upon CES1 pharmacological inhibition or genetic deletion in hepatoblastoma cell line [45]. Therefore, we speculate that interfering with CES1 during DCs differentiation may have an impact on DCs metabolic profile as well as phenotype and functions. In our study, upon CES1 inhibition, the generated MoDCs exhibited stronger inflammatory phenotype and higher CD209 expression. CD209 is a type II transmembrane lectin receptor that plays important role in DCs adhesion, migration and T cell activation functions [46]. Previous reports show that enhancing PPARγ signalling in differentiating DCs is associated with less CD209 expression and altered DCs immunogenicity [47]. Whether observed effects following CES1 inhibition in DCs is mediated by altered PPARγ signalling is not conclusive and warrant further mechanistic investigations. Conversely, Scheaffer et al has shown an anti-inflammatory effect of blocking CES1 in THP-1 monocytes and macrophage via regulating prostaglandin metabolism [48]. In contrary to our results, these finding are generated in THP-1 cell line which might show differences in CES1 expression and regulation compared to primary cells. Furthermore, CES1 might play a differential role in DCs compared to macrophages and monocytes that can be cell type and context dependent.

Alternatively, transgenic expression of high levels of human CES1 in murine BMDCs promoted less inflammatory response, following different TLRs agonists' stimulation. This anti-inflammatory effect seems to mount a protective effect for *CES1* transgenic mice in T cell transfer colitis. However, in our T cell transfer colitis experiment, *CES1* transgenic mice also had low blood esterase background, unlike control mice. Therefore, these dereferences in blood esterase activities prompt

further confirmation of our findings in normal esterase background mice. Recent reports exploring the role of CES1 in *in vivo* models of inflammatory diseases have demonstrated contradicting results. While some reports demonstrated a protective role in LPS induced lung inflammation [20] and alcohol induced steatohepatitis [22] murine models, other reports showed pro-inflammatory role in LPS induced sepsis model [49]. However, caution should be taken when interpreting results from *in vivo* studies and immortalized cell line due to the large differences in CES enzymes expression and functions between species. Mice have more than 20 isoform of CES enzyme, while humans have only 3 well characterized isoforms so far [13, 14]. Nomenclature of CES enzymes and their orthologues was also quite challenging [50]. Furthermore, expression pattern of same orthologue can be different among species. While *CES1* is highly expressed in human macrophages, the murine orthologue *ces1d* show minimal expression in murine peritoneal macrophages which express other isoforms of CES enzymes [38]. Collectively, more *in vivo* studies are required, preferable using humanized transgenic *CES1* mice, to explore the potential role of CES1 in different inflammatory diseases.

The enhanced inflammatory phenotype of MoDCs, generated under CES1 inhibition, was associated with enhanced phagocytic capacity and increased T cell polarization towards Th17 phenotype. Metabolic adaptions of DCs are closely linked to their functional activities. Specific deletion of mTOR in inflammatory lung DCs modulate fatty acid oxidation to promote Th17 polarization [51], another report shows enhanced DCs Th1/17 skewing capacity upon increased free fatty acids [52]. Therefore CES1 inhibition allow for metabolic adaption of DCs that modulates not only DCs phenotype but also their key functions. This might be of clinical significance, as local ovarian cancer infiltration of Th17 cells is associated with favorable disease outcome. This is mediated by DCs that is programed to instruct stronger Th17 skewing [53]. Such approach is of therapeutic importance in DCs cancer vaccines design and showed efficacy and safety in early clinical trials [54].

Furthermore, our transcriptomic and metabolomics analysis identified positive enrichment of multiple inflammatory and metabolic pathways in WWL113 treated MoDCs. Among most relevant and significantly modulated metabolic pathways, are energy production related pathways, like glycolysis, TCA cycle, oxidative phosphorylation and gluconeogenesis. In our experimental setup, WWL113 treatment promoted differentiation of a glycolytic DCs phenotype, which secrete higher quantities of lactic acid. Functional metabolic analysis using seahorse respirometry did not detect significant effect on mitochondrial respiration. However treating MoDCs acutely demonstrated significant reduction of MoDCs mitochondrial

ATP production. Therefore we hypothesize that the effect of WWL113 treatment is the strongest early during DCs differentiation and has a long lasting effect on DCs that might be less evident to detect by seahorse respirometry later in a fully differentiated DCs. However the effect is clearly demonstrated with higher lactate levels. A recent report shows similar effect on mitochondrial respiration in hepatocytes following WWL113 acute treatment [45]. This collectively suggests a model where CES1 inhibition compromises mitochondrial respiration which induces cellular metabolic shift towards glycolytic respiration. In support of this model, metabolomics analysis revealed decreased levels of TCA cycle intermediates, while both malate and glucose 6-phosphate increased in CES1 treated MoDCs. Strikingly, intracellular amino acids levels are all decreased. However reasons behind this striking observations are not clear. This can be explained by consumption of amino acids to support high energy demands and proteins synthetic functions of the generated inflammatory DCs [55]. Moreover, perturbation of amino acids availability has shown to directly interfere with TCA cycle in MoDCs [56].



To sum up, our study uncovers the significance of CES1 in DC differentiation by playing a role to meet the metabolic demands of DCs, which in turn modulate their phenotype and functions. Even though, we didn't fully explore the mechanisms involved, we demonstrate a distinctive metabolic profile that underlies the modulated DCs phenotype and functions. Further studies are required to investigate the potential mechanistic link between the early CES1 upregulation during MoDCs differentiation and the key PPAR-γ and mTOR signalling pathways that orchestrates early DCs differentiation. Moreover, future studies should also focus on the naturally occurring DCs as they show different metabolic profile compared to *in vitro* generated MoDCs [57]. Our findings imply that specific manipulating of CES1 activity in DCs might have a functional impact of clinical significance to DCs vaccine designs and inflammatory diseases.

**Author Contributions:** Management of the study, laboratory, and writing of the manuscript: A.M.I.E.; lab experiments: A.M.I.E., J.L.; study design: A.M.I.E., A.J.V.; bioinformatics analysis: A.Y.F.L.Y.; metabolomics data analysis: M.G.; supervision: W.J.d.J. and A.J.V.; reviewing and editing: W.J.d.J. and A.J.V. All authors have read and agreed to the published version of the manuscript.

**Funding and acknowledgement:** This work was supported by the European Union's Horizon 2020 research and innovation program under grant agreement no. ITN-2014-EID-641665. WJ was funded by a grant from the Dutch Economic Affairs Top Sector

Life Sciences and Health (LSH)—Top Consortia for Knowledge and Innovation's (TKI), grant no. TKI-LSH T2017, and the European Crohn's and Colitis Organization (ECCO) Pioneer Grant, 2018. We would like to thank the metabolomics core facility at the Amsterdam UMC for performing mass spectrometry metabolites measurements and preliminary analysis.

# References


1. Qian, C. and X. Cao, *Dendritic cells in the regulation of immunity and inflammation.* Semin Immunol, 2018. **35**: p. 3-11.
2. Ganguly, D., et al., *The role of dendritic cells in autoimmunity.* Nat Rev Immunol, 2013. **13**(8): p. 566-77.
3. Morante-Palacios, O., et al., *Tolerogenic Dendritic Cells in Autoimmunity and Inflammatory Diseases.* Trends Immunol, 2021. **42**(1): p. 59-75.
4. O'Neill, L.A. and E.J. Pearce, *Immunometabolism governs dendritic cell and macrophage function.* J Exp Med, 2016. **213**(1): p. 15-23.
5. Thwe, P.M., et al., *Cell-Intrinsic Glycogen Metabolism Supports Early Glycolytic Reprogramming Required for Dendritic Cell Immune Responses.* Cell Metab, 2017. **26**(3): p. 558-567 e5.
6. Perrin-Cocon, L., et al., *Toll-like Receptor 4-Induced Glycolytic Burst in Human Monocyte-Derived Dendritic Cells Results from p38-Dependent Stabilization of HIF-1alpha and Increased Hexokinase II Expression.* J Immunol, 2018. **201**(5): p. 1510-1521.
7. Everts, B., et al., *Commitment to glycolysis sustains survival of NO-producing inflammatory dendritic cells.* Blood, 2012. **120**(7): p. 1422-31.
8. Basit, F., et al., *Human Dendritic Cell Subsets Undergo Distinct Metabolic Reprogramming for Immune Response.* Front Immunol, 2018. **9**: p. 2489.
9. Sim, W.J., P.J. Ahl, and J.E. Connolly, *Metabolism Is Central to Tolerogenic Dendritic Cell Function.* Mediators Inflamm, 2016. **2016**: p. 2636701.
10. Malinarich, F., et al., *High mitochondrial respiration and glycolytic capacity represent a metabolic phenotype of human tolerogenic dendritic cells.* J Immunol, 2015. **194**(11): p. 5174-86.
11. Adamik, J., et al., *Distinct metabolic states guide maturation of inflammatory and tolerogenic dendritic cells.* Nat Commun, 2022. **13**(1): p. 5184.
12. Palsson-McDermott, E.M. and L.A.J. O'Neill, *Targeting immunometabolism as an anti-inflammatory strategy.* Cell Res, 2020. **30**(4): p. 300-314.
13. Wang, D., et al., *Human carboxylesterases: a comprehensive review.* Acta Pharm Sin B, 2018. **8**(5): p. 699-712.
14. Lian, J., R. Nelson, and R. Lehner, *Carboxylesterases in lipid metabolism: from mouse to human.* Protein Cell, 2018. **9**(2): p. 178-195.
15. Elfiky, A.M.I., et al., *A BET Protein Inhibitor Targeting Mononuclear Myeloid Cells Affects Specific Inflammatory Mediators and Pathways in Crohn's Disease.* Cells, 2022. **11**(18).
16. Capece, D., et al., *Enhanced triacylglycerol catabolism by carboxylesterase 1 promotes aggressive colorectal carcinoma.* J Clin Invest, 2021. **131**(11).
17. Crow, J.A., et al., *Inhibition of carboxylesterase 1 is associated with cholesteryl ester retention in human THP-1 monocyte/macrophages.* Biochim Biophys Acta, 2008. **1781**(10): p. 643-54.
18. Mangum, L.C., et al., *Silencing carboxylesterase 1 in human THP-1 macrophages perturbs genes regulated by PPARgamma/RXR and RAR/RXR: down-regulation of CYP27A1-LXRalpha signaling.* Biochem J, 2018. **475**(3): p. 621-642.
19. Wei, E., et al., *Loss of TGH/Ces3 in mice decreases blood lipids, improves glucose tolerance, and increases energy expenditure.* Cell Metab, 2010. **11**(3): p. 183-93.
20. Szafran, B.N., et al., *Carboxylesterase 1d Inactivation Augments Lung Inflammation in Mice.* ACS Pharmacol Transl Sci, 2022. **5**(10): p. 919-931.
21. Lavalett, L., et al., *Alveolar macrophages from tuberculosis patients display an altered inflammatory gene expression profile.* Tuberculosis (Edinb), 2017. **107**: p. 156-167.

22. Xu, J., et al., *Carboxylesterase 1 Is Regulated by Hepatocyte Nuclear Factor 4alpha and Protects Against Alcohol- and MCD diet-induced Liver Injury.* Sci Rep, 2016. **6**: p. 24277.
23. Dominguez, E., et al., *Integrated phenotypic and activity-based profiling links Ces3 to obesity and diabetes.* Nat Chem Biol, 2014. **10**(2): p. 113-21.
24. Jaatinen, T. and J. Laine, *Isolation of mononuclear cells from human cord blood by Ficoll-Paque density gradient.* Curr Protoc Stem Cell Biol, 2007. **Chapter 2**: p. Unit 2A 1.
25. Dobin, A., et al., *STAR: ultrafast universal RNA-seq aligner.* Bioinformatics, 2013. **29**(1): p. 15-21.
26. Li, H., et al., *The Sequence Alignment/Map format and SAMtools.* Bioinformatics, 2009. **25**(16): p. 2078-9.
27. Liao, Y., G.K. Smyth, and W. Shi, *The Subread aligner: fast, accurate and scalable read mapping by seed-and-vote.* Nucleic Acids Res, 2013. **41**(10): p. e108.
28. Simon Andrews, B.I. *A quality control tool for high throughput sequence data*. 2019 2023]; Available from: https://www.bioinformatics.babraham.ac.uk/projects/fastqc/.
29. Ewels, P., et al., *MultiQC: summarize analysis results for multiple tools and samples in a single report.* Bioinformatics, 2016. **32**(19): p. 3047-8.
30. Laboratories, K. *KEGG Database*. 1995 [cited 2023; Available from: https://www.genome.jp/kegg/kegg1.html.
31. H, W. *ggplot2: Elegant Graphics for Data Analysis. Springer-Verlag New York*. . 2016 [cited 2023; Available from: https://ggplot2.tidyverse.org.
32. Kolde, R. *Implementation of heatmaps that offers more control over dimensions and appearance.* 2019 [cited 2023; Available from: https://CRAN.R-project.org/package=pheatmap.
33. Gilglioni, E.H., et al., *Improved oxygenation dramatically alters metabolism and gene expression in cultured primary mouse hepatocytes.* Hepatol Commun, 2018. **2**(3): p. 299-312.
34. van Weeghel, M., et al., *Profiling of intracellular metabolites produced from galactose and its potential for galactosemia research.* Orphanet J Rare Dis, 2018. **13**(1): p. 146.
35. Markey, G.M., *Carboxylesterase 1 (Ces1): from monocyte marker to major player.* J Clin Pathol, 2011. **64**(2): p. 107-9.
36. Iqbal, A.J., et al., *Human CD68 promoter GFP transgenic mice allow analysis of monocyte to macrophage differentiation in vivo.* Blood, 2014. **124**(15): p. e33-44.
37. Quiroga, A.D., et al., *Deficiency of carboxylesterase 1/esterase-x results in obesity, hepatic steatosis, and hyperlipidemia.* Hepatology, 2012. **56**(6): p. 2188-98.
38. Jones, R.D., et al., *Carboxylesterases are uniquely expressed among tissues and regulated by nuclear hormone receptors in the mouse.* Drug Metab Dispos, 2013. **41**(1): p. 40-9.
39. Her, L. and H.J. Zhu, *Carboxylesterase 1 and Precision Pharmacotherapy: Pharmacogenetics and Nongenetic Regulators.* Drug Metab Dispos, 2020. **48**(3): p. 230-244.
40. Song, Y.Q., et al., *Carboxylesterase inhibitors from clinically available medicines and their impact on drug metabolism.* Chem Biol Interact, 2021. **345**: p. 109566.
41. Ghiboub, M., et al., *Selective Targeting of Epigenetic Readers and Histone Deacetylases in Autoimmune and Inflammatory Diseases: Recent Advances and Future Perspectives.* J Pers Med, 2021. **11**(5).
42. Szatmari, I., et al., *PPARgamma regulates the function of human dendritic cells primarily by altering lipid metabolism.* Blood, 2007. **110**(9): p. 3271-80.
43. Wculek, S.K., et al., *Metabolic Control of Dendritic Cell Functions: Digesting Information.* Front Immunol, 2019. **10**: p. 775.
44. Zaccagnino, P., et al., *An active mitochondrial biogenesis occurs during dendritic cell differentiation.* Int J Biochem Cell Biol, 2012. **44**(11): p. 1962-9.

45. Li, G., et al., *Interfering with lipid metabolism through targeting CES1 sensitizes hepatocellular carcinoma for chemotherapy.* JCI Insight, 2023. **8**(2).

46. Svajger, U., et al., *C-type lectin DC-SIGN: an adhesion, signalling and antigen-uptake molecule that guides dendritic cells in immunity.* Cell Signal, 2010. **22**(10): p. 1397-405.

47. Zhu, W., et al., *PPAR-gamma agonist pioglitazone regulates dendritic cells immunogenicity mediated by DC-SIGN via the MAPK and NF-kappaB pathways.* Int Immunopharmacol, 2016. **41**: p. 24-34.

48. Scheaffer, H.L., et al., *Inactivation of CES1 Blocks Prostaglandin D(2) Glyceryl Ester Catabolism in Monocytes/Macrophages and Enhances Its Anti-inflammatory Effects, Whereas the Pro-inflammatory Effects of Prostaglandin E(2) Glyceryl Ester Are Attenuated.* ACS Omega, 2020. **5**(45): p. 29177-29188.

49. Zhou, Q., et al., *Pig Liver Esterases Hydrolyze Endocannabinoids and Promote Inflammatory Response.* Front Immunol, 2021. **12**: p. 670427.

50. Holmes, R.S., et al., *Recommended nomenclature for five mammalian carboxylesterase gene families: human, mouse, and rat genes and proteins.* Mamm Genome, 2010. **21**(9-10): p. 427-41.

51. Sinclair, C., et al., *mTOR regulates metabolic adaptation of APCs in the lung and controls the outcome of allergic inflammation.* Science, 2017. **357**(6355): p. 1014-1021.

52. Stelzner, K., et al., *Free fatty acids sensitize dendritic cells to amplify TH1/TH17-immune responses.* Eur J Immunol, 2016. **46**(8): p. 2043-53.

53. Cannon, M.J., et al., *Modulation of p38 MAPK signaling enhances dendritic cell activation of human CD4+ Th17 responses to ovarian tumor antigen.* Cancer Immunol Immunother, 2013. **62**(5): p. 839-49.

54. Block, M.S., et al., *Th17-inducing autologous dendritic cell vaccination promotes antigen-specific cellular and humoral immunity in ovarian cancer patients.* Nat Commun, 2020. **11**(1): p. 5173.

55. Brombacher, E.C. and B. Everts, *Shaping of Dendritic Cell Function by the Metabolic Micro-Environment.* Front Endocrinol (Lausanne), 2020. **11**: p. 555.

56. Kakazu, E., et al., *Plasma amino acids imbalance in cirrhotic patients disturbs the tricarboxylic acid cycle of dendritic cell.* Sci Rep, 2013. **3**: p. 3459.

57. Minarrieta, L., et al., *Dendritic cell metabolism: moving beyond in vitro-culture-generated paradigms.* Curr Opin Biotechnol, 2021. **68**: p. 202-212.

# Supplementary figures and tables

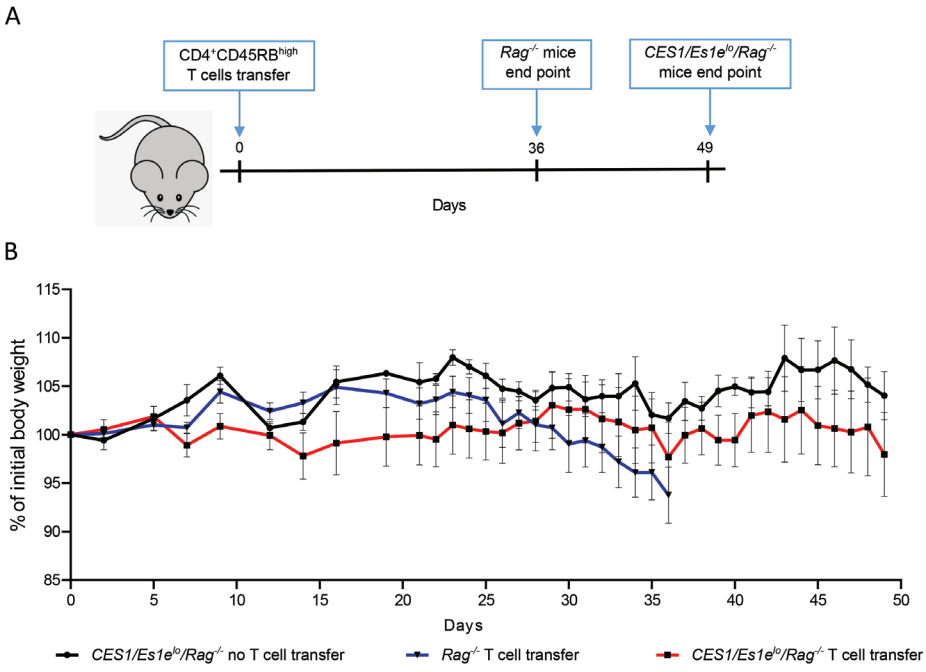


**Figure S1. Transgenic human *CES1* mice are less susceptible to T cell transfer induced colitis.** (**A**) A schematic of the T cell transfer colitis model experimental design. (**B**) Weight changes are indicated as percentage of initial body weight, both *Rag*$^{-/-}$ and *CES1/Es1e*$^{lo}$*/Rag*$^{-/-}$ mice are compared for body weight and survival, both were sacrificed upon reaching human end point at day 36 and 49 respectively.

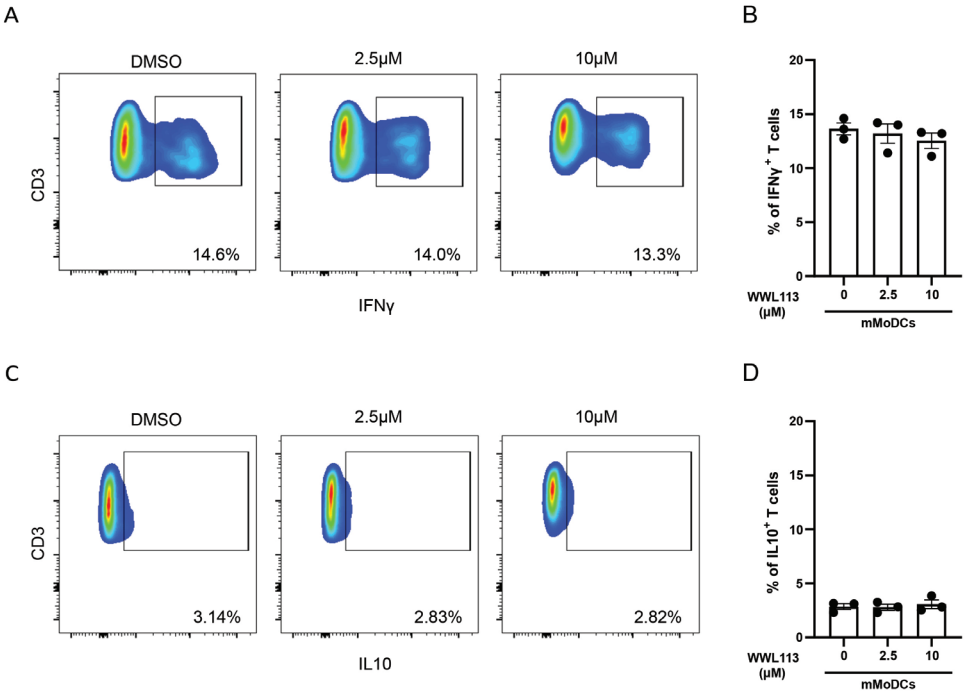


**Figure S2. Human MoDCs generated under CES1 inhibition have no impact on Th1 or Tregs differentiation.** Flow cytometry analysis of IFNγ and IL10 expression in T cells following co-culture with mMoDCs generated under either DMSO or WWL113 (2.5μM and 10μM). (**A**) FACS plots demonstrate IFNγ expression among alive $CD3^+$ T cells. (**B**) Frequency of $IFN\gamma^+$ T cells among total $CD3^+$ T cells is quantified. (**C**) FACS plots demonstrate IL10 expression among alive $CD3^+$ T cells. (**D**) Frequency of $IL10^+$ T cells among total $CD3^+$ T cells is quantified.

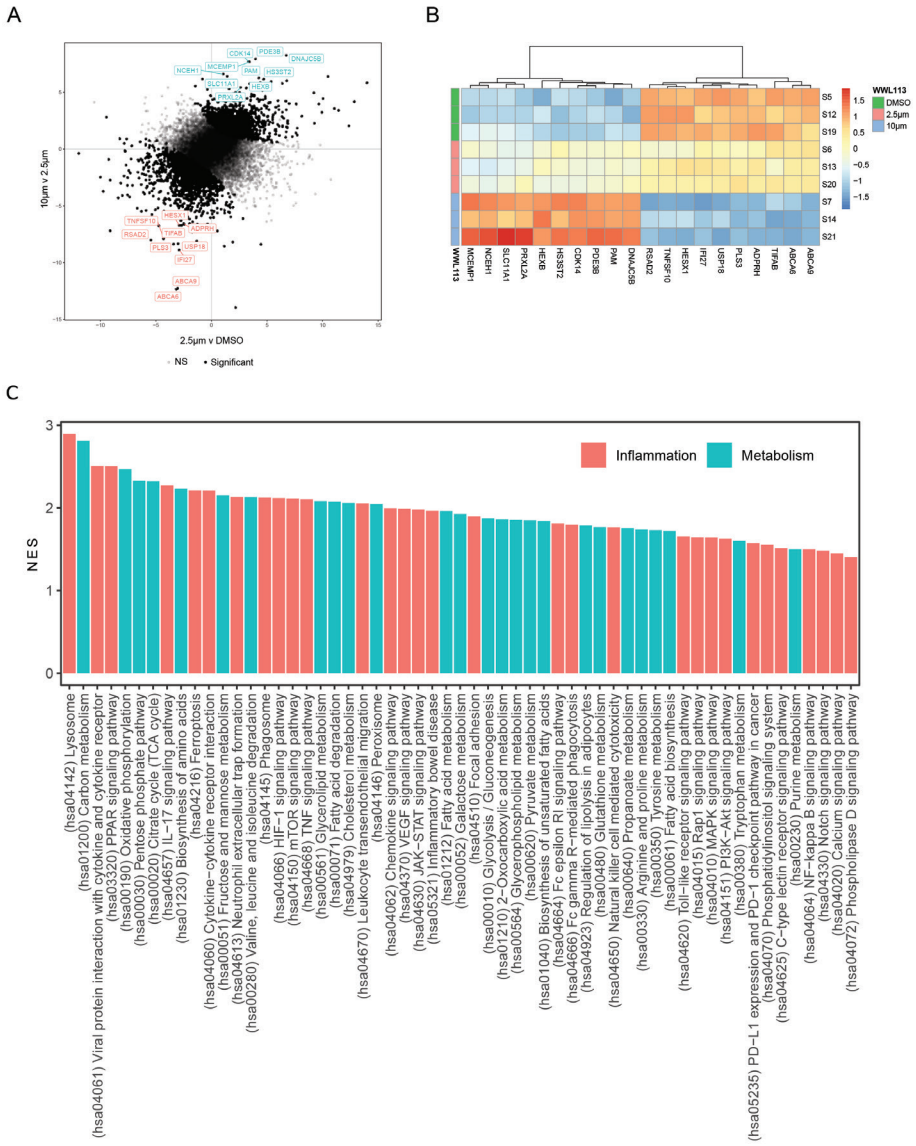


**Figure S3. Transcriptomic analysis of top deferentially expressed genes and pathways in MoDCs generated under CES1 inhibition.**RNA sequencing data analysis of human CD14⁺ monocytes derived DCs (MoDCs) differentiated in presence of DMSO or WWL113 (2.5μM and 10μM) following 3 hours of LPS stimulation (n=3 healthy donors). (**A**) Comparison of the Wald statistic obtained from DESeq2 when comparing 2.5μM WWL13 with DMSO, and 10μM WWL13 with DMSO on the x- and y-axes, respectively. The top 10 up- and downregulated genes (DEGs) in dose dependent manner are highlighted and further demonstrated in heat map (**B**), comparing WWL113 vs. DMSO (n = 3) in MoDCs following LPS stimulation. (**C**) Gene set enrichment analysis (GSEA) of inflammation and metabolism related pathways with functional annotation using Kyoto Encyclopedia of Genes and Genomes (KEGG) pathways, are shown. Both inflammation and metabolism related pathways are differentiated by color code, normalized enrichment scores (NES) are plotted.

A

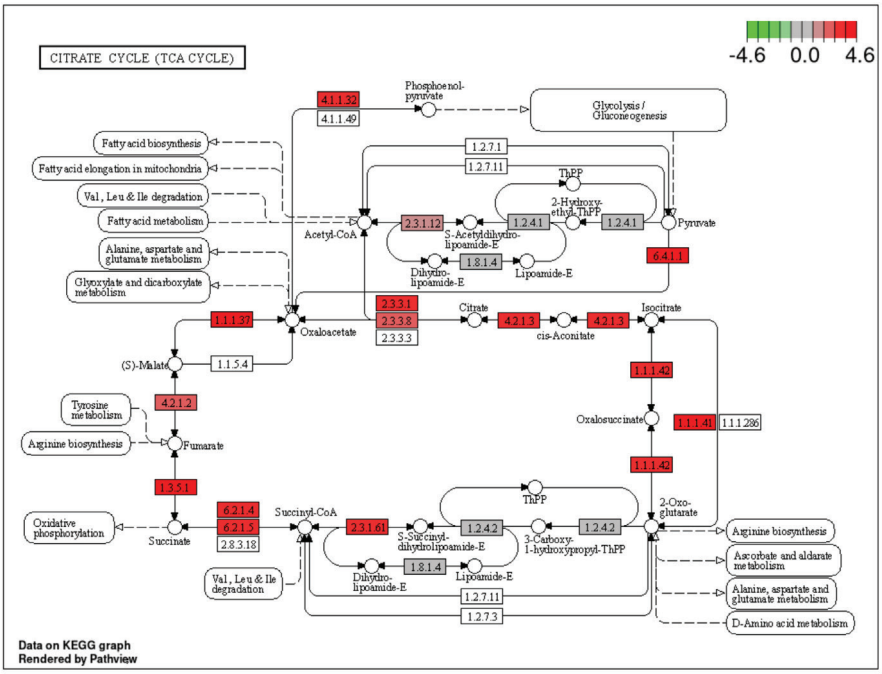


B

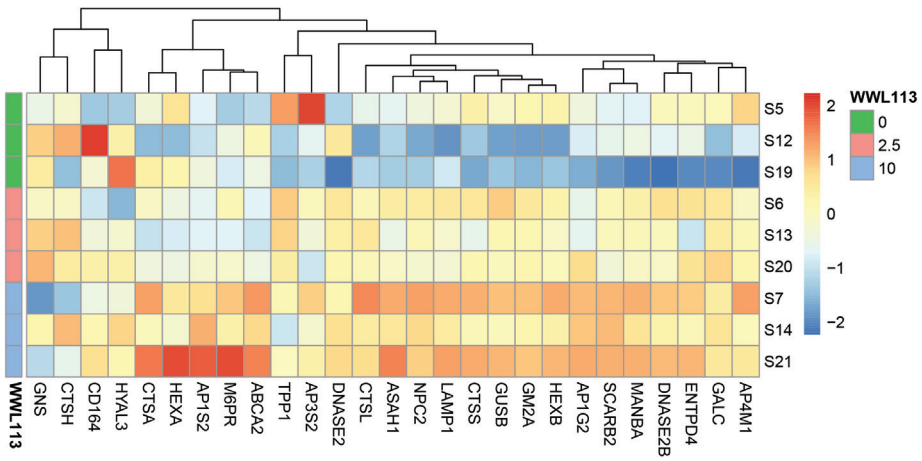


**Figure S4. Transcriptomic analysis of top deferentially expressed TCA cycle related genes.** (**A**) The KEGG TCA cycle pathway with colors representing the effect size obtained from interaction analysis. RNA sequencing analysis of MoDCs differentiated in presence of WWL113 or DMSO (n = 3) are compared following 3 hours of LPS stimulation. (**B**) Heat map of top differentially expressed genes in the TCA cycle pathway compares WWL113 vs. DMSO (n = 3) conditions, both 2.5μM and 10μM WWL113 doses are shown.

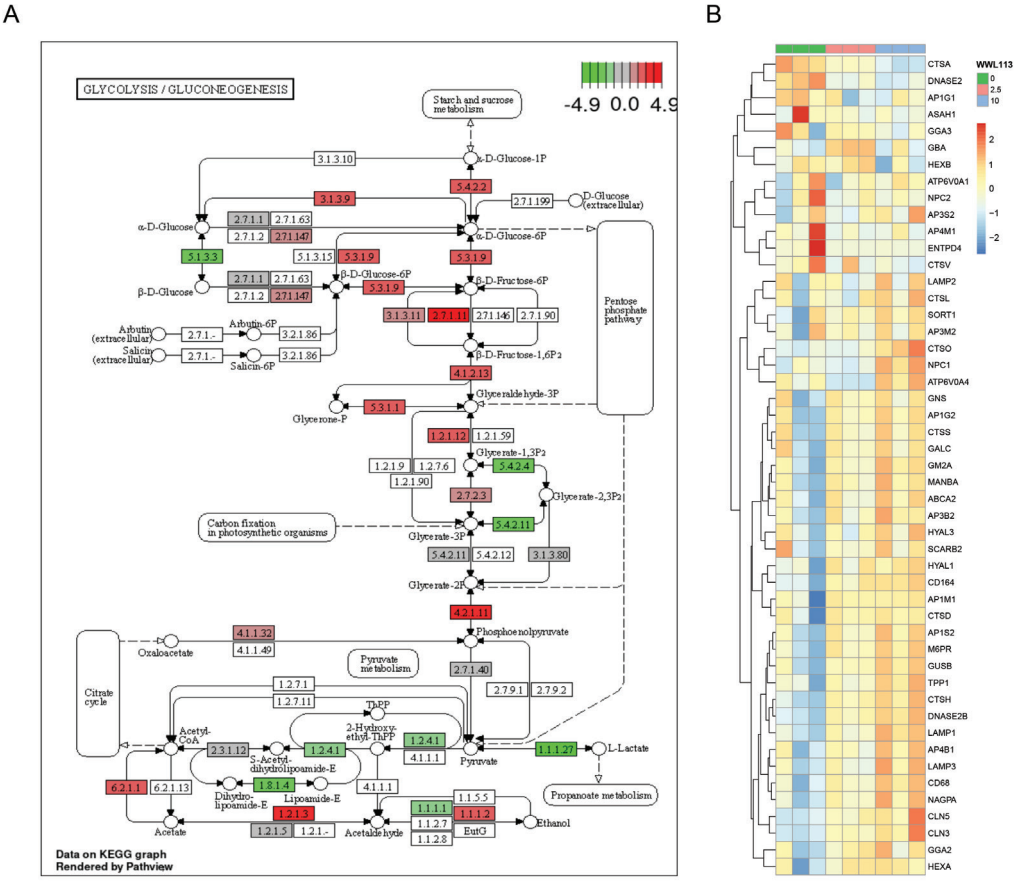


**Figure S5. Transcriptomic analysis of top deferentially expressed glycolysis / gluconeogenesis related genes.** (**A**) The KEGG glycolysis / gluconeogenesis pathway with colors representing the effect size obtained from interaction analysis. RNA sequencing analysis of MoDCs differentiated in presence of WWL113 or DMSO (n = 3) are compared, following 3 hours of LPS stimulation. (**B**) Heat map of top differentially expressed genes in glycolysis / gluconeogenesis pathway compares WWL113 vs. DMSO (n = 3) conditions, both 2.5μM and 10μM WWL113 doses are shown.

A

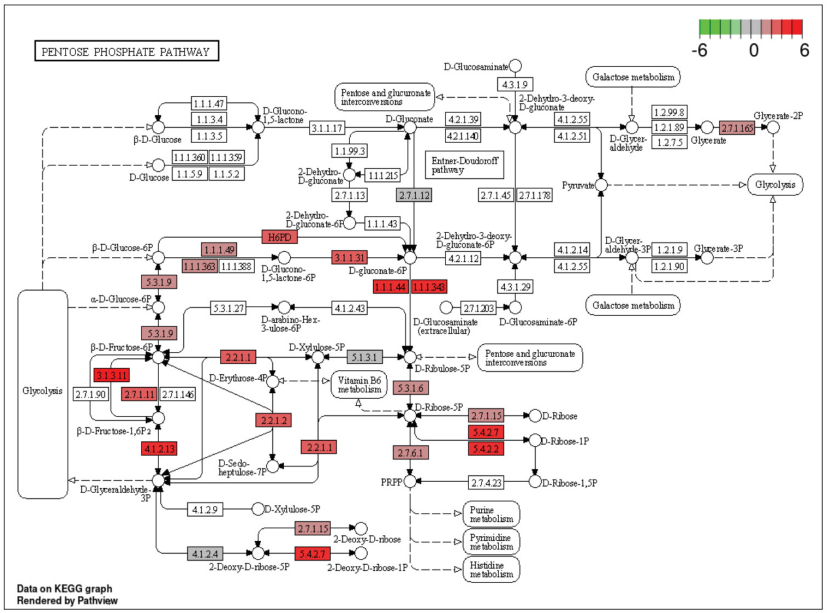


B

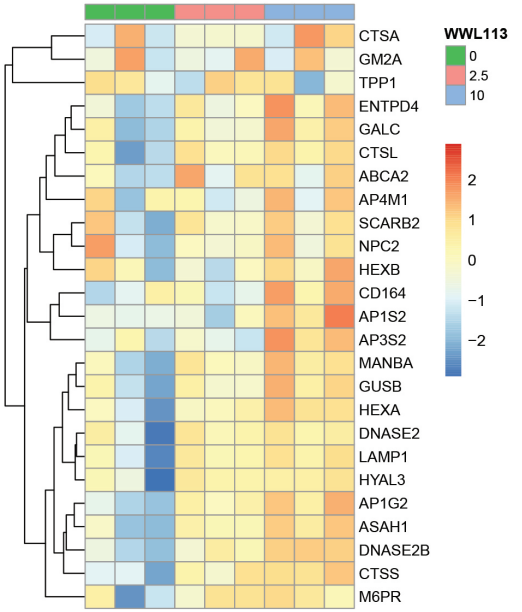


**Figure S6. Transcriptomic analysis of top deferentially expressed pentose phosphate pathway related genes.** (**A**) The KEGG pentose phosphate pathway with colors representing the effect size obtained from interaction analysis. MoDCs differentiated in presence of WWL113 or DMSO (n = 3) are compared, following 3 hours of LPS stimulation. (**B**) Heat map of top differentially expressed genes in the glycolysis / gluconeogenesis pathway compares WWL113 vs. DMSO (n = 3) conditions, both 2.5μM and 10μM WWL113 doses are shown.

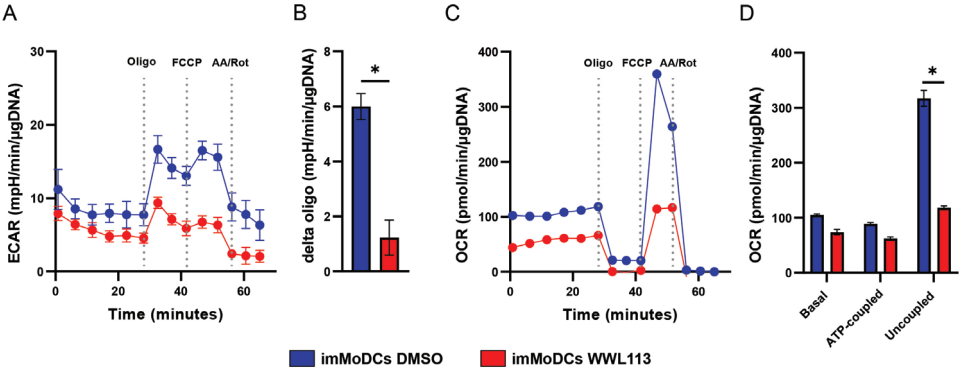


**Figure S7. CES1 inhibition impairs MoDCs mitochondrial respiration capacity and induce switch towards glycolysis.** Oxygen consumption rate (OCR) and extracellular acidification rate (ECAR) are measured in imMoDCs, differentiated in presence of DMSO or 10µM WWL113 (n=3 healthy donors), then treated acutely with DMSO or 10µM WWL113 during the Seahorse XF96 assay. (**A**) Representative donor of measured ECAR (n=4-6 technical replicates) and (**B**) delta oligo of 3 donors are shown. (**C**) Representative donor of measured OCR (n=4-6 technical replicates) and (**D**) quantification of OCR levels under basal conditions, after oligomycin addition (ATP-coupled), and after FCCP addition (uncoupled) of 3 donors are shown. Results are illustrated as mean ± SEM; standard error of the mean. Statistical testing was performed using student t test; * $p \leq 0.05$, DMSO and WWL113 treated conditions are compared.

**Table S1: list of measured analytes in mass spectrometry metabolomics analysis.**

| Analyte | Formula | Analyte | Formula | Analyte | Formula |
|---|---|---|---|---|---|
| 2-Hydroxyglutarate | C5H8O5 | Cystathionine | C17H16O5 | Isoleucine | C6H13NO2 |
| 2-Hydroxyglutarate | C5H8O5 | Cysteine | C3H7NO2S | Lactate | C3H6O3 |
| 2-Hydroxyglutarate | C5H8O5 | Cystine | C6H12N2O4S2 | Leucine | C6H13NO2 |
| 2-phosphoglyceric acid | C3H7O7P | dAMP | C10H14N5O6P | Lysine | C6H14N2O2 |
| 2,3-Diphosphoglyceric acid | C3H8O10P2 | dCMP | C9H14N3O7P | Malate | C4H6O5 |
| 3-phosphoglyceric acid | C3H7O7P | Dihydroxyacetone-P | C3H7O6P | Methionine | C5H11NO2S |
| 6-Phosphogluconolactone | C6H11O9P | Erythrose-4-phosphate | C4H9O7P | Methyl-NAM | C7H8N2O |
| Acetylglutamic acid | C7H11NO5 | FAD | C27H33N9O15P2 | Nicotinamide | C6H6N2O |
| Adenine | C5H5N5 | FAICAR | C10H15N4O9P | Ornithine | C5H12N2O2 |
| Adenosine | C10H13N5O4 | Folic acid | C19H19N7O6 | Oxiglutathione | C20H32N6O12S2 |
| Adenylthiomethylpentose | C11H15N5O3S | Fructose-1,6-diphosphate | C6H14O12P2 | Phenylalanine | C9H11NO2 |
| Adipic acid | C6H10O4 | Fumarate | C4H4O4 | Phosphoenolpyruvate | C3H5O6P |
| ADP | C10H15N5O10P2 | Gamma-Glutamylcysteine | C8H14N2O5S | Phosphorylethanolamine | C2H8NO4P |
| ADP-Ribose | C15H23N5O14P2 | GDP | C10H15N5O11P2 | Phosphoserine | C3H8NO6P |
| AICAR | C9H15N4O8P | Gluconate | C6H12O7 | Proline | C5H9NO2 |
| Alanine | C3H7NO2 | Gluconate-6P | C6H13O10P | Pyridoxal | C8H9NO3 |
| Allantoin | C4H6N4O3 | Glucose | C6H12O6 | Pyroglutamic acid | C5H7NO3 |
| Alpha-Ketoglutarate | C5H6O5 | Glucose-6P | C6H13O9P | Pyruvate | C3H4O3 |
| Aminoadipic acid | C6H11NO4 | Glutamate | C5H9NO4 | Ribose | C5H10O5 |

**Table S1: Continued**

| Analyte | Formula | Analyte | Formula | Analyte | Formula |
|---|---|---|---|---|---|
| AMP | C10H14N5O7P | Glutamate-5-semialdehyde | C5H9NO3 | Ribose-5P | C5H11O8P |
| Anthranilic acid | C7H7NO2 | Glutamine | C5H10N2O3 | S-adenosyl homocysteine | C14H20N6O5S |
| Arginine | C6H14N4O2 | Glutathione | C10H17N3O6S | S-adenosyl methionine | C15H23N6O5S |
| Argininosuccinate | C10H18N4O6 | Glyceraldehyde-3P | C3H7O6P | Sedoheptulose-7P | C7H15O10P |
| Asparagine | C4H8N2O3 | Glycerate | C3H6O4 | Serine | C3H7NO3 |
| Aspartate | C4H7NO4 | Glycerophosphocholine | C8H20NO6P | Succinate | C4H6O4 |
| ATP | C10H16N5O13P3 | Glycerophosphoinositol | C9H19O11P | Taurine | C2H7NO3S |
| beta-Alanine | C3H7NO2 | Glycine | C2H5NO2 | Threonine | C4H9NO3 |
| Betaine | C5H11NO2 | GMP | C10H14N5O8P | Thymidine | C10H14N2O5 |
| Carnitine | C7H15NO3 | Guanine | C5H5N5O | Thymine | C5H6N2O2 |
| Carnitine (C2:0) | C9H17NO4 | Guanosine | C10H13N5O5 | Tryptophan | C11H12N2O2 |
| Carnitine (C3:0) | C10H19NO4 | Hexose-P | C6H13O9P | Tyrosine | C9H11NO3 |
| Carnitine (C4:0) | C11H21NO4 | Hexose-P | C6H13O9P | UDP | C9H14N2O12P2 |
| Carnitine (C6:0) | C13H25NO4 | Hexose-P | C6H13O9P | UDP-HexNac | C17H27N3O17P2 |
| Carnosine | C9H14N4O3 | Hexose-P | C6H13O9P | UDP-HexNac | C17H27N3O17P2 |
| CDP-choline | C14H26N4O11P2 | Hippuric acid | C9H9NO3 | UDP-HexNac | C17H27N3O17P2 |
| CDP-ethanolamine | C11H20N4O11P2 | Histidine | C6H9N3O2 | UDP-hexose | C15H24N2O17P2 |
| Citric acid | C6H8O7 | Homocystine | C8H16N2O4S2 | UDP-hexose | C15H24N2O17P2 |
| Citrulline | C6H13N3O3 | Homocystine | C8H16N2O4S2 | UMP | C9H13N2O9P |

**Table S1: Continued**

| Analyte | Formula | Analyte | Formula | Analyte | Formula |
|---|---|---|---|---|---|
| CMP | C9H14N3O8P | Homoglutathione | C11H19N3O6S | Uracil | C4H4N2O2 |
| Creatine | C4H9N3O2 | Hydroxyphenyllactic acid | C9H10O4 | Uric acid | C5H4N4O3 |
| Creatine-P | C4H10N3O5P | Hypoxanthine | C5H4N4O | Uridine | C9H12N2O6 |
| Creatinine | C4H7N3O | IMP | C10H13N4O8P | Valine | C5H11NO2 |
| CTP | C9H16N3O14P3 | Inosine | C10H12N4O5 | Xanthine | C5H4N4O2 |

5

# Chapter 5

## Targeting Bromodomain 2 of BET Proteins in Inflammatory Bowel Disease

**Ahmed M. I. Elfiky**, Patricia H. P. van Hamersveld, Olaf Welting, Inmaculada Rioja, Sigrid E. M. Heinsbroek, Matthew J. Bell,Wouter J. de Jonge

## Abstract

Inflammatory bowel disease (IBD) is chronic intestinal inflammation of multifactorial complex aetiology. T cells have been identified as the main culprits behind the pathogenesis of these disorders, and as such, they have become the main target for treatment. Bromodomain and extra terminal domain (BET) inhibitors have demonstrated potent anti-inflammatory activity in both *in vitro* and *in vivo* models of inflammation mediated diseases. However efficacy in preclinical models of inflammatory bowel disease (IBD) is inconclusive. Bromodomain 2 (BD2) selective inhibition is shown to be more specific to inflammatory response therefore can mitigate potential off target effects of pan BET inhibition including gastrointestinal toxicity and thus improves the tolerability and therapeutic efficacy in the complex pathology of IBD. In the current study, we aim to investigate the efficacy of GSK620, a specific BD2 inhibitors, along with I-BET151, a pan BET inhibitor, in T cell transfer colitis preclinical model of IBD. We applied our intervention in therapeutic manner following establishment of active colon inflammation for 3 weeks. We demonstrated only modest clinical efficacy of both GSK620 and I-BET151 treatment, only improving weight loss. Both inhibitors significantly reduced circulating inflammatory cytokines (IL12, IL6, IFNγ and TNFα), indicating efficient systemic anti-inflammatory activity. However local intestinal inflammatory cytokines did not improve except at low dose (1mg/kg) GSK620 treatment that shows trends towards reduced colon IFNγ and TNFα. In conclusion, GSK620 and I-BET151 are efficient to reduce systemic inflammatory response in preclinical model of IBD. However, this is not translated to significant reduction of intestinal inflammation.


**Keywords**: BD2, BET, IBD.

## Introduction

Bromodomain and extra terminal domain (BET) proteins are group of epigenetic readers that bind acetylated histone residues to facilitate genes transcription [1]. BET inhibition demonstrates strong pro-apoptotic and anti-inflammatory proprieties in multiple preclinical models of cancer and inflammatory diseases [1, 2]. However multiple adverse events are reported in clinical trials attributable to their wide range of activities [3].

BET proteins family contains 4 members, BRD2, BRD3, BRD4 and BRDT. Structurally they share common 2 bromodomains, BD1 and BD2, while each individual protein has an extra distinctive terminal domain [1]. Mechanistic studies show that BD1 is sufficient to anchor BET protein to acetylated histone residue [4]. Furthermore, distinctive functional roles of BD1 and BD2 during homeostasis and inflammation are identified. While BD1 allows for BET protein localization within chromatin and permits genes expression for homeostatic cellular functions, BD2 is essential for recruitment and binding of transcription factors during activated cellular states. Therefore specifically targeting BD2 would interfere with inflammatory signalling meanwhile maintaining other homeostatic cellular transcriptional programs essential for cell survival. BD2 inhibition has shown efficacy in ameliorating inflammation in preclinical models of rheumatoid arthritis, psoriasis and non-alcoholic fatty liver disease (NAFLD) with similar efficacy to standard therapies [5]. In collagen induced arthritis rat model, GSK620 (BD2 inhibitor) shows similar efficacy to the pan-BET inhibitor I-BET151 [5]. On the other hand, specific BD2 inhibition has demonstrated better safety profile. ABBV-744 (BD2 inhibitor) exhibits less haematological and gastrointestinal toxicities compared with pan-BET inhibitor [6]. RVX-208, another BD2 inhibitor is extremely well tolerated, with safety data exceeding 2700 patient years [7]. Collectively, targeting BD2 might be a very promising and safer therapeutic strategy to benefit from BET inhibitors therapeutic potentials in inflammatory diseases meanwhile minimizing their clinically limiting wide range of toxicities.

Despite efficiency of pan-BET inhibitors in multiple preclinical models of immune mediated inflammatory diseases [8], the outcome in inflammatory bowel disease (IBD) is uncertain. Contradictory results were obtained from T cell mediated murine colitis model [9, 10]. The proposed anti-inflammatory efficacy maybe hampered by the known gastrointestinal toxicity of pan-BET inhibitors [11]. Therefore, we hypothesize that selective inhibition of BD2 domain might allow for potent anti-inflammatory effect while mitigating gastrointestinal toxicity resulting in resolution of colonic inflammation. In the current study, we aim to evaluate the effect of pan-BET inhibitor (I-BET151) and BD2 selective inhibitor (GSK620) in T cell transfer colitis model of IBD.

# Materials and Methods

## Mice

C57BL/6NCrl wild type female mice were purchased from Charles River laboratories and our own in-house bred female RAG1$^{-/-}$ were used. All animal studies were ethically reviewed and carried out in accordance with European Directive 2010/63/EEC, the guidelines of the Ethical Animal Research Committee of the University of Amsterdam, and the GSK Policy on the Care, Welfare and Treatment of Animals.

## T cell transfer colitis model

30female C57BL/6NCrl mice (donors) 8-12 weeks old are sacrificed, spleens are harvested and CD4$^{+}$CD45RB$^{high}$ were isolated as following; splenocytes were negatively enriched through dynabeads™ sheep anti-rat IgG (ThermoFisher), anti-CD11b (Biolegend), anti-CD45R (Sony), and anti-CD8a (Biolegend), then CD4$^{+}$CD45RB$^{high}$ were sorted by fluorescence-activated cell sorting using anti-CD45RB-FITC and anti-CD4-PE/Cy5 (BD Bioscience). CD4$^{+}$CD45RB$^{high}$ T cells are suspended in PBS and administered intraperitoneally to 66 female RAG1$^{-/-}$ mice (approx. 300, 000 cells per mouse in 100 ul PBS), meanwhile 6 mice did receive PBS only to serve as control group for the colitis. After three weeks of transfer, colon inflammation was confirmed by endoscopy. Transfer mince were randomized into 5 groups, each consists of 11 mice and received daily intraperitoneal injections of either vehicle or I-BET151 or GSK620 (1 or 3 or 10 mg/kg) respectively for 3 weeks. Non-transfer control mice received vehicle. All mice were treated for 3 weeks until they were sacrificed at end of the 6$^{th}$ week. Body weight was measured three times a week and then daily after the start of compounds treatment until sacrifice.

Following sacrifice; blood, colon and spleen were harvested. Blood was collected into EDTA tubes and placed on roller for minimum 5 minutes, centrifuged at 12500 rpm for 10 min, plasma decanted into Eppendorf tube and stored frozen (-80oC) until required. Spleen and Colon were weighed, colon length was measured and colon density (weight / length ratio) was calculated. Colon then was opened, cut longitudinally, rolled using "Swiss roll" technique and fixed in 10% buffered formalin for histology. Small parts of terminal colon (minimum 2 pieces of 30 mg) and spleen were weighed and snap frozen for later RNA and / or protein expression analysis. The swiss rolls were processed, cut and stained with H/E for histopathological scoring according to parameters indicated in table S1.

## Mice colon and serum cytokines measurement

Frozen colon tissue was homogenized on ice in lysis buffer (150 mM NaCl, 15 mM Tris, 1 mM MgCl·6H2O, 1 mM CaCl2, 1% Triton) with added protease inhibitor

cocktail (Roche Applied Science), pH 7.4, diluted 1:1 with PBS. Blood was collected via cardiac puncture following mice sacrifice, allowed to clot at room temperature, then centrifuged and serum was collected. In colon tissue lysates or serum, protein concentrations of IL6, IL10, TNFα, IFNγ, IL12 and MCP-1 were measured with a mouse inflammation kit by BD cytometric bead assay (BD Bioscience) according to the manufacturer's protocol. Colon protein expression was normalized to total protein per sample as measured by BCA Protein Assay Kit (Pierce).

### Quantitative real time PCR

RNA was isolated using RNeasy mini kit (Qiagen) following the manufacturer's protocol. Complementary DNA (cDNA) was synthesized using deoxynucleotide triphosphates (Thermo Fisher Scientific), Random primers (Promega), Oligo dT primers (Invitrogen), Revertaid, and Ribolock (both Fermentas). Quantitative PCR was performed using SensiFAST SYBR No-ROX (GC Biotech) and were run on a LightCycler 480 II (Roche Applied Science) to analyze expression levels of murine TNFα, IL1β, IL6, IL10 and IL12b using LinRegPCR software. For normalization, murine 36B4, NONO and EEF2 were used as reference genes. Primers (Sigma) are listed in table S2.



## Results

### Pan-BET and BD2 inhibitors ameliorate systemic inflammation but only show modest clinical efficacy.

In order to investigate the potential therapeutic benefits of selective targeting of BD2 over nonspecific BET inhibition, we made use of T cells transfer colitis model as detailed in methods. After 3 weeks of treatment with either GSK620 or I-BET151 following established intestinal inflammation, we assessed different clinical parameters of the model. We observed improvement of weight loss in mice groups treated with I-BET151 and low doses of GSK620 (1 and 3 mg/kg) respectively that reaches statistical significance for I-BET151 and 3 mg/kg GSK620 (Figure 1A, B). However other clinical parameters of the model only showed modest improvement. Colon density, a measure of colon edema, did not improve in any of treatment groups (Figure 1C). Meanwhile spleen weight corrected for individual mice weight did not show significant change from vehicle treated control group, only modest improvement was observed in GSK620 treated groups at both low (3 mg/kg) and high (10mg/kg) doses, yet not statistically significant (Figure 1D). Blinded histo-pathogical examination of the mice colon sections were done to objectively assess colon inflammation. Among all treatment groups, only low dose GSK620 did demonstrate a trend towards improved total histology scores (Figure 1E), largely

attributable to improved crypts loss and hyperplasia scores (**Figure S1**). However it did not reach statistical significance. Collectively clinical efficacy of both I-BET151 and GSK620 was modest in T cell transfer colitis model.

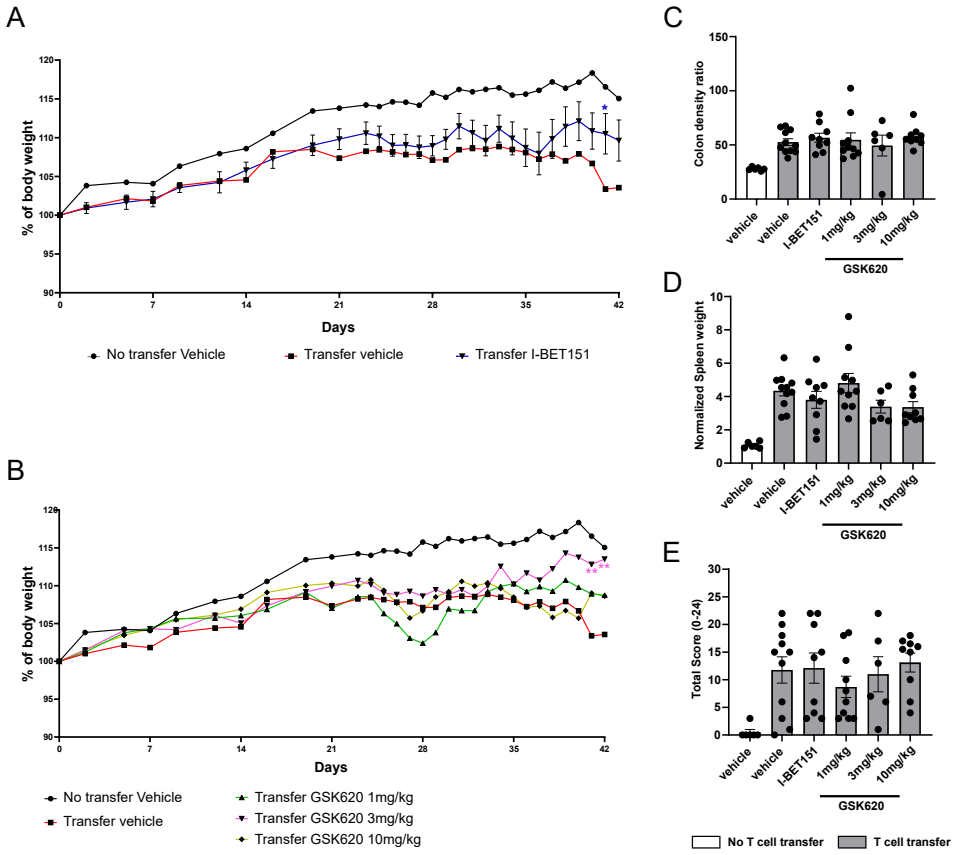


**Figure 1. GSK620 and I-BET151 show modest clinical efficacy in T cell transfer colitis model.** T cell transfer model; mice received $CD4^{+}CD45RB^{high}$ T cells to induce colitis at day 0, then after 3 weeks treatment start for another 3 weeks. Weight curve data are indicated as percentage of initial body weight for (**A**) I-BET151 and (**B**) GSK620 respectively. (**C**) Colon density (weight mg / length cm ratio) and (**D**) normalized spleen weight (spleen weigh mg / total mouse weight gm ratio) were measured at sacrifice. (**D**) Colon histopathology scores were graded from 0 to 24 points by an experienced pathologist. 4 parameters were scored goblet cell loss, crypt loss, crypt hyperplasia and submucosal inflammation, each scored from 0-3 and the total score was calculated using this formula (goblet cell loss + 2 x Crypt loss + 2 x crypt hyperplasia + 3 x submucosal inflammation). Data are represented as mean with SEM, *P ≤ 0.05, **P ≤ 0.01, *** P ≤ 0.001.

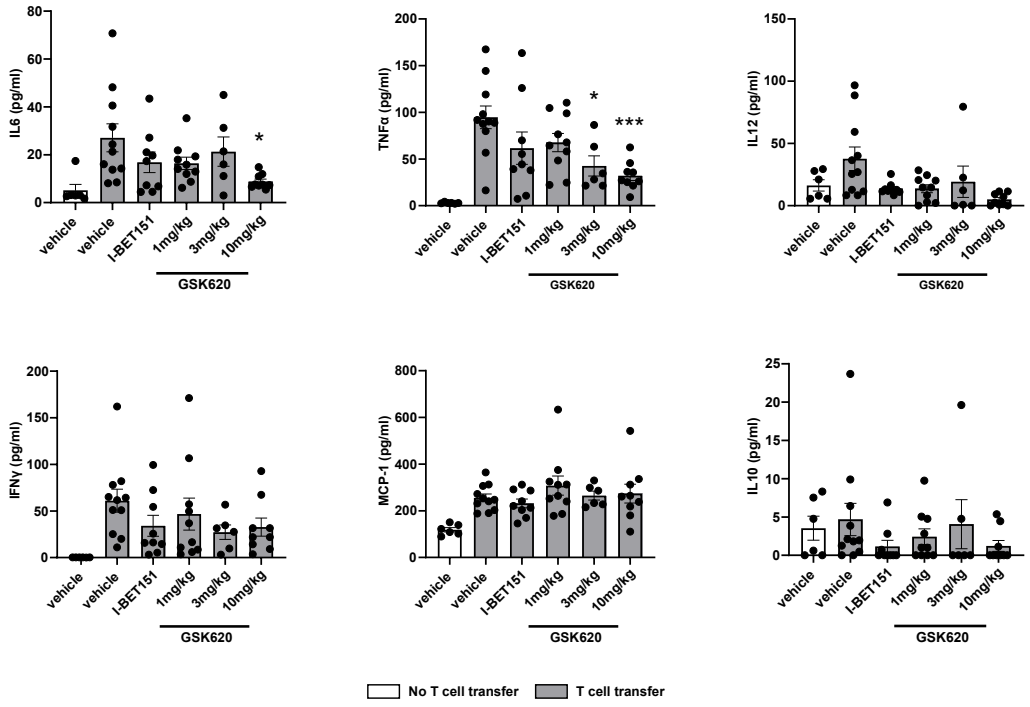


**Figure 2. GSK620 and I-BET151 significantly reduced circulating inflammatory cytokines in T cell transfer colitis model.** Mice blood serum was collected at sacrifice, IL6, IL12, IL10, MCP-1, TNFα and IFNg cytokines were measured using mouse inflammation CBA kit. Data are represented as mean with SEM, *P ≤ 0.05, **P ≤ 0.01, *** P ≤ 0.001.

## Low dose BD2 inhibitor shows modest superior effect on intestinal inflammatory cytokines compared to pan-BET inhibitor.

Despite modest clinical efficacy, both I-BET and GSK620 significantly reduced multiple circulating inflammatory cytokines, including IL12, IL6, IFNγ and TNFα to variable degrees but not MCP-1 (**Figure 2**). Moreover no effect was observed on IL10 levels, however most of IL10 values were below detection limit making them less reliable. While both inhibitors showed similar effects towards serum cytokines, only low dose (1 mg/kg) GSK620 demonstrated a trend towards improved colon inflammatory cytokines particularly IFNγ and TNFα at protein levels (**Figure 3A**) and IL6 and TNFα at *mRNA* expression levels (**Figure 3B**). Moreoevr, Colon *IL10* RNA expression remain unchanged across all groups except at low dose GSK620 treatment, that lead to slight upregulation of *IL10,* yet not statistically significant (**Figure 3B**) . Collectively both inhibitors demonstrated significant systemic anti-inflammatory efficacy however that did not translate to a successful resolution of colitis.

## Discussion and concluding remarks

In this study, we were not able to demonstrate a sufficient clinical efficacy of GSK620 in a T cell driven preclinical model of IBD. Despite apparent effect on reducing systemic inflammation, local intestinal inflammation seems to be ongoing. This can be explained by a potential gastrointestinal toxicity of GSK620, which is largely elusive. Of particular relevance to IBD, BET inhibition is associated with significant gastrointestinal toxicity [11] which may explain the unfavourable clinical efficacy despite efficient systemic anti-inflammatory effect of different BET inhibitors. Despite that GSK620 is well characterized and has shown superior affinity to BD2 over BD1 of few hundred folds in *in vitro* assays [5], this degree of selectivity might not be sufficient to avoid un-desirable adverse effects *in vivo*. Recently, more specific inhibitor with more than 5000 fold selectivity towards BD2 is reported [12]. Moreover multiple other BD2 selective inhibitors are developed, including ABBV-744 [6], GSK973 [13] and GSK046 [14]. ABBV-744 is reported to have less gastrointestinal toxicity [6]. In this context, ABBV-744 might be interesting candidate to investigate in IBD. However, more specific inhibitors are expected to be available soon therefore screening of potential BD2 inhibitor candidates in *ex vivo* organoid models for potential toxicity on intestinal epithelium will be highly helpful for better selection of suitable drug candidates with highly favourable outcome in IBD.

In conclusion, BD2 inhibition might be a very interesting approach to harness the potential anti-inflammatory benefits of BET inhibition in IBD given specificity is improved and gastrointestinal toxicity are mitigated.

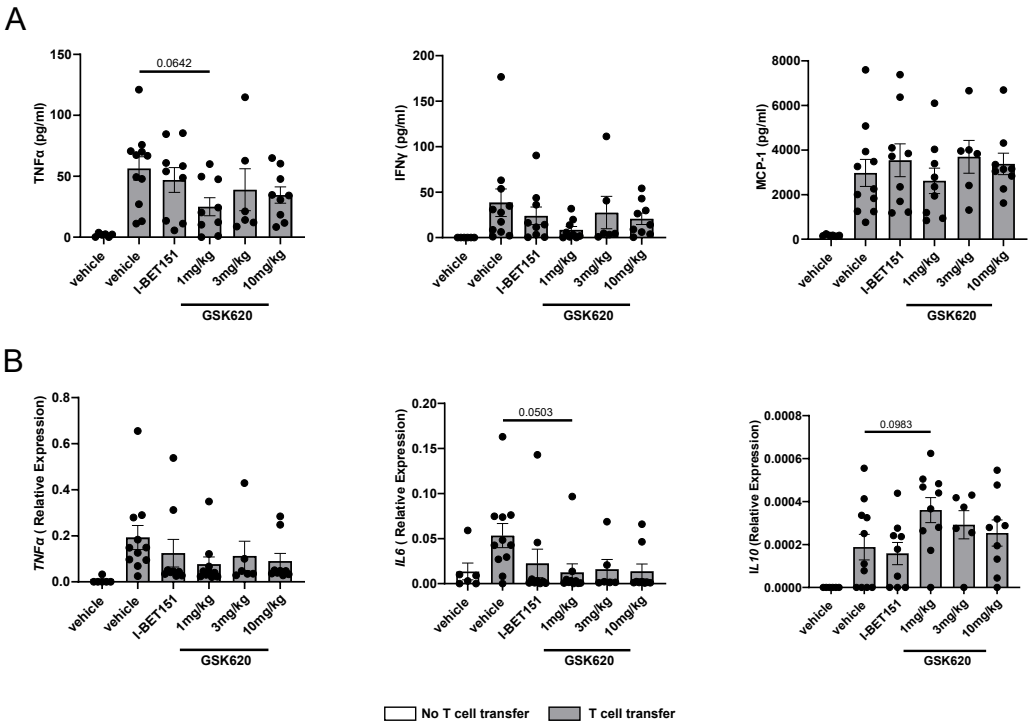


**Figure 3. Intestinal inflammatory cytokines are only modestly affected by GSK620 and I-BET151.** (**A**) Protein levels of TNFα, IFNγ, and MCP-1 in colon homogenates were quantified using mouse inflammation CBA kit, normalized for total protein levels. (**B**) mRNA levels of *TNFa, IL10 and IL6* in colon homogenates were measured and normalized to geometric mean of reference genes (mNONO, mEEF2 and m36B4). Data are represented as mean with SEM, *P ≤ 0.05, **P ≤ 0.01, *** P ≤ 0.001.

# References


1. Taniguchi, Y., *The Bromodomain and Extra-Terminal Domain (BET) Family: Functional Anatomy of BET Paralogous Proteins.* Int J Mol Sci, 2016. **17**(11).
2. Wang, N., et al., *The BET family in immunity and disease.* Signal Transduct Target Ther, 2021. **6**(1): p. 23.
3. Sun, Y., et al., *Safety and Efficacy of Bromodomain and Extra-Terminal Inhibitors for the Treatment of Hematological Malignancies and Solid Tumors: A Systematic Study of Clinical Trials.* Front Pharmacol, 2020. **11**: p. 621093.
4. Tyler, D.S., et al., *Click chemistry enables preclinical evaluation of targeted epigenetic therapies.* Science, 2017. **356**(6345): p. 1397-1401.
5. Gilan, O., et al., *Selective targeting of BD1 and BD2 of the BET proteins in cancer and immunoinflammation.* Science, 2020. **368**(6489): p. 387-394.
6. Faivre, E.J., et al., *Selective inhibition of the BD2 bromodomain of BET proteins in prostate cancer.* Nature, 2020. **578**(7794): p. 306-310.
7. Nicholls, S.J., et al., *Efficacy and safety of a novel oral inducer of apolipoprotein a-I synthesis in statin-treated patients with stable coronary artery disease a randomized controlled trial.* J Am Coll Cardiol, 2011. **57**(9): p. 1111-9.
8. Kulikowski, E., B.D. Rakai, and N.C.W. Wong, *Inhibitors of bromodomain and extra-terminal proteins for treating multiple human diseases.* Med Res Rev, 2021. **41**(1): p. 223-245.
9. Schilderink, R., et al., *BET bromodomain inhibition reduces maturation and enhances tolerogenic properties of human and mouse dendritic cells.* Mol Immunol, 2016. **79**: p. 66-76.
10. Cheung, K., et al., *BET N-terminal bromodomain inhibition selectively blocks Th17 cell differentiation and ameliorates colitis in mice.* Proc Natl Acad Sci U S A, 2017. **114**(11): p. 2952-2957.
11. Bolden, J.E., et al., *Inducible in vivo silencing of Brd4 identifies potential toxicities of sustained BET protein inhibition.* Cell Rep, 2014. **8**(6): p. 1919-1929.
12. Rianjongdee, F., et al., *Discovery of a Highly Selective BET BD2 Inhibitor from a DNA-Encoded Library Technology Screening Hit.* J Med Chem, 2021. **64**(15): p. 10806-10833.
13. Preston, A., et al., *GSK973 Is an Inhibitor of the Second Bromodomains (BD2s) of the Bromodomain and Extra-Terminal (BET) Family.* ACS Med Chem Lett, 2020. **11**(8): p. 1581-1587.
14. Preston, A., et al., *Design and Synthesis of a Highly Selective and In Vivo-Capable Inhibitor of the Second Bromodomain of the Bromodomain and Extra Terminal Domain Family of Proteins.* J Med Chem, 2020. **63**(17): p. 9070-9092.

# Supplementary tables and figures

**Table S1. Histology inflammation score (T cell transfer colitis model).**

| Item / Score | 0 | 1 | 2 | 3 |
|---|---|---|---|---|
| Goblet cell loss | 0% | <10% | 10-50% | > 50% |
| Crypt loss | Normal | <10% decrease in density | >10% decrease in density | --- |
| Crypt hyperplasia | None | slightly increased crypt length | 2 to 3 times increase in crypt length | >3 times increase in crypt length |
| Submucosal infiltrate | None | individual infiltrating cells | infiltrates | large infiltrates |

Total score = goblet cell loss score + 2 x crypt loss score + 2 x crypt hyperplasia score + 3 x submucosal inflammation score.

**Table S2. qPCR primers**

| Gene | Forward sequence | Reverse sequence |
|---|---|---|
| *36B4* | CCAGCGAGGCCACACTGCTG | ACACTGGCCACGTTGCGGAC |
| *NONO* | AAAGCAGGCGAAGTTTTCATTC | ATTTCCGCTAGGGTTCGTGTT |
| *EEF2* | TGTCAGTCATCGCCCATGTG | CATCCTTGCGAGTGTCAGTGA |
| *TNFα* | TGGAACTGGCAGAAGAGGCACT | CCATAGAACTGATGAGAGGGAGGC |
| *IL1β* | GCCCATCCTCTGTGACTCAT | AGGCCACAGGTATTTTGTCG |
| *IL6* | GAGTTGTGCAATGGCAATTCTG | TGGTAGCATCCATCATTTCTTTGT |
| *IL10* | TGTCAAATTCATTCATGGCCT | ATCGATTTCTCCCCTGTGAA |
| *I L12b* | AGACCCTGCCCATTGAACTG | CGGGTCTGGTTTGATGATGTC |

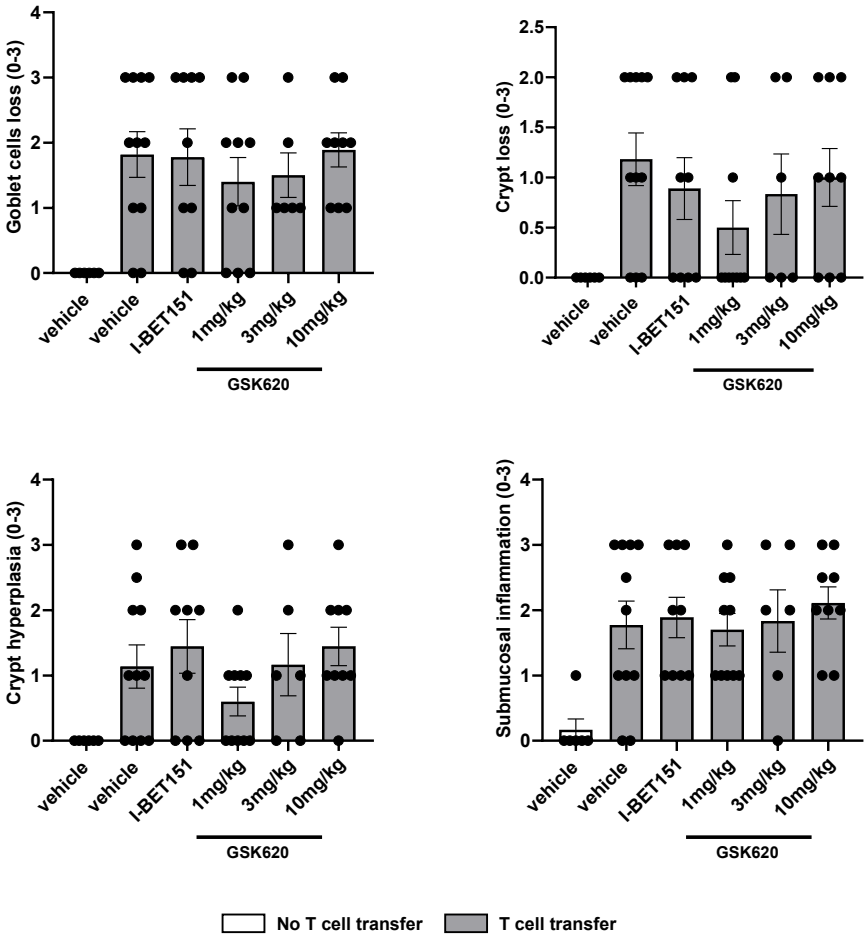


**Figure S1. Histopathological scoring parameters.** Individual histopathological scores of goblet cell loss, crypt loss, crypt hyperplasia and submucosal inflammation are shown. Data are represented as mean with SEM.

6

# Chapter 6

## Single-cell characterization identifies systemic inflammation-associated differences in cellular composition and behavior as a result of vedolizumab treatment in Crohn's disease

Andrew Y.F. Li Yim[†], Ishtu L. Hageman[†], Vincent Joustra[†], **Ahmed M. I. Elfiky**, Mohammed Ghiboub, Evgeni Levin Jan Verhoeff, Caroline Oostveen-Verseijden, Iris Admiraal-van den Berg, Marcel M.A.M. Mannens, Marja E. Jakobs, Susan B. Kenter, Alex T. Adams, Jack Satsangi, Geert R. D'Haens, Wouter J. de Jonge, and Peter Henneman

[†] Equally Contributing First authors

Under submission in Journal of Clinical Investigation

## Abstract

**Background & Aims:** Vedolizumab (VDZ) is a monoclonal antibody approved for treating Crohn's disease (CD) by abrogating the gut-homing behavior of various leukocytes. Despite its efficacy, non-response to VDZ is common in clinical practice. Here, we performed an observational case-control study to interrogate the differences between responders and non-responders to VDZ during treatment.

**Methods:** CD patients on VDZ treatment were classified as steroid-free responder or non-responder based on endoscopic- (≥3 drop in Simple Endoscopic Score for Crohn's Disease (SES-CD)), biochemical (≥50% reduction in C-reactive protein (CRP) and fecal calprotectin) and/or clinical response criteria (≥3 point drop in Harvey-Bradshaw Index (HBI)) during which peripheral blood was collected. Peripheral blood mononuclear cells (PBMCs) were isolated from a cohort of four responders and four non-responders which were then subjected to single-cell RNA-sequencing (scRNAseq) and mass cytometry by time of flight (CyTOF) analyses.

**Results:**The most prominent differences between responders and non-responders were observed in the T and myeloid compartment, which were more and less abundant, respectively, among non-responders. T cells from non-responders generally presented lower expression of inhibitors of the NFκB signaling pathway. Abundance-wise, a lower concentration of plasmacytoid dendritic cells (pDCs) was observed among non-responders, which could be correlated with a higher abundance of pDCs in lesional tissue based on a public dataset. Classical monocytes presented a different transcriptome, with non-responders presenting lower expression of genes involved in wound-healing and cytokine-cytokine receptor signaling.

**Conclusions:** Non-response to VDZ during treatment is associated with differences in abundance and expression of the T and myeloid compartment.


**Keywords:** single-cell RNA-sequencing, scRNAseq, cytometry by time of flight, CyTOF, vedolizumab, therapy response, T cell, pDC, classical monocytes.

# Introduction

Crohn's disease (CD) is an incurable, chronic, inflammatory condition of the gastrointestinal tract characterized by a relapsing-remitting transmural inflammation of the digestive tract belonging to the family of inflammatory bowel diseases (IBD). Current treatments for CD include the use of monoclonal antibodies that target mediators of inflammation with the goal of ameliorating the inflammatory phenotype and/or maintaining a state of clinical and endoscopic remission. One such monoclonal antibody is vedolizumab (VDZ), which was approved for use in CD patients in 2014 by the United States Food and Drug Administration as well as the European Medicines Agency [1].

VDZ targets the gut homing receptor complex integrin α4β7 (also known as lymphocyte Peyer's patch adhesion molecule 1; LPAM-1) [2,3], which prevents it from binding mucosal vascular addressin cell adhesion molecule 1 (MAdCAM-1), a molecule expressed exclusively by the intestinal endothelial cells. By preventing integrin α4β7 from binding MAdCAM-1, the attachment and stabilization of circulating immune cells that express integrin α4β7 to high endothelial venules in the gut is destabilized, thereby abrogating gut-homing capabilities [4–6]. While VDZ has traditionally been discussed within the context of the T cell lineage [7–10], more recent studies suggest that the myeloid [11,12] as well as B cells [13] are affected by VDZ treatment as well. Despite the advances VDZ therapy has provided patient care, the efficacy or therapy response rate is reported to be approximately between 30% to 45% [1,14–16] with a recent meta-analysis indicating that loss of response towards VDZ among CD patients was estimated at 47.9 per 100 person-years [17]. To date, we have no proper understanding why only a subgroup of patient responds to therapy, nor do we have a prognostic biomarker for predicting response to VDZ therapy. To better understand how response to VDZ manifests, we conducted an exploratory case-control study to characterize the immune cell composition of peripheral blood mononuclear cells (PBMCs) from CD patients on VDZ treatment. Here, we compared the composition between responders and non-responders using single-cell RNA-sequencing (scRNAseq) and cytometry by time of flight (CyTOF).



# Methods

## Sample collection and preparation

Blood samples were obtained from patients included in the EPIC-CD study, which is a multi-center consortium with the goal of identifying prognostic biomarkers at the level of peripheral blood (PBL) DNA methylation capable of predicting response

to adalimumab, infliximab, vedolizumab, and ustekinumab prior to treatment in CD patients [18]. For the current study, 8 VDZ-treated CD patients (4 responders and 4 non-responders) were sampled for peripheral blood at a median of 26 weeks into treatment during routine care at the AmsterdamUMC hospital, location AMC, Amsterdam, Netherlands (**Table 1**). Patients were labeled as steroid-free responder to VDZ if they presented endoscopic- (≥3 drop in Simple Endoscopic Score for Crohn's Disease (SES-CD)), biochemical (≥50% reduction in C-reactive protein (CRP) and fecal calprotectin), and/or clinical response criteria (≥3 point drop in Harvey-Bradshaw Index (HBI)) relative to their baseline measurements. Immediately after collecting peripheral blood, peripheral blood mononuclear cells (PBMC) were isolated by means of Ficoll (GE Healthcare) separation and IMDM medium (Gibco) supplemented with 10% DMSO and 50% FBS (Serana). Isolated PBMCs were stored overnight at -80 C whereupon they were transferred to liquid nitrogen until cohort completion.

## Single-cell RNA-sequencing analysis

Samples were removed from the cryostat and thawed on ice. Thawed PBMCs were washed and then labelled using the hashtag oligo (HTO) antibodies for multiplexing purposes whereupon the oligo-tagged PBMC suspensions were then mixed and distributed across 6 GEM-wells on the Chromium controller (10X Genomics). Single-cell barcoded partitions were prepared using 10X chemistry v3 where after separate sequencing libraries were prepared for HTOs and the actual mRNA after size-selection. Libraries were sequenced on the Illumina HiSeq4000 in a 150 bp paired-ended fashion at the Core Facility Genomics, Amsterdam UMC. The mRNA libraries were sequenced on 150M reads per GEM-well, whereas the HTO libraries were sequenced to a depth of 50M reads per GEM-well. Raw data was imported and analyzed in R. A detailed overview as well as the data analyses can be found in the **Supplementary Information.**

## Mass cytometry by time-of-flight

Concurrent with the single-cell RNA-sequencing analyses, mass cytometry by time of flight (Cy-TOF) was performed on a separate aliquot of the PBMC samples. Here, we measured the cell-surface expression of 37 proteins with a particular focus on the T cell lineage. Acquisition was performed on the Fluidigm Helios system. Sample was diluted in $H_2O$ and supplemented with 10% v/v of EQ Four Element Calibration beads (Fluidigm). Staining, barcoding, data acquisition, and analyses were performed in R and are described in **Supplementary Information**. An overview of all the antibodies used and their clones can be found in **Supplementary Table 1.**

### Flow cytometry of the plasmacytoid dendritic cells

In addition to using an aliquot of PBMCs of the same patients analyzed for scRNAseq and CyTOF, an additional two patients (1 responder and 1 non-responder) were included in the flow cytometry analyses. Upon thawing, PBMCs were washed in PBS and stained for a live/dead cell viability marker (LifeScience, Amsterdam, the Netherlands). Cells were subsequently stained for surface markers in FACS buffer (0.5% BSA, 0.01% NaN3 in PBS) using the following antibodies: CD11c-PerCP Cy5.5 (clone: S-HCL-3, BioLegend), HLA-DR-Alexa Fluor 700 (clone: LN3, eBioscience), CD123-FITC (clone: 6H6, BioLegend), CD1C-PE-Cy7 (clone: L161, BioLegend), pan-lineage (CD3/CD19/CD20/CD56)-APC (clones: UCHT1;HIB19;2H7;5.1H11, BioLegend), CD14-BD Horizon V500 (clone: M5E2, Becton Dickinson) and CD16-PE (clone: 3G8, Becton Dickinson). Acquisition was performed on the BD LSR Fortessa™, where plasmacytoid DCs (pDCs) were identified as (T/B/NK) Lin-HLA-DR+CD14-CD16-CD11c-CD123+. Analysis was performed using FlowJo (Treestar) and R. The gating strategy can be found in the **Supplementary Information.** An overview of all antibodies and their clones used can be found in **Supplementary Table 2.**

### RNA-sequencing of the classical monocytes

Akin to the flow cytometric analyses, PBMCs were washed in PBS and stained for a live/dead cell viability marker (LifeScience, Amsterdam, the Netherlands) alongside the antibodies mentioned above. Cell sorting was conducted on the SH800 Cell Sorter (Sony). Classical, intermediate, and non-classical monocytes were identified as (T/B/NK) $Lin^{-}HLA\text{-}DR^{+}CD14^{++}CD16^{-}$, $HLA\text{-}DR^{+}CD14^{++}CD16^{+}$, and $HLA\text{-}DR^{+}CD14^{+}CD16^{+}$, respectively. The classical monocytes were sorted out and were subsequently processed for RNA sequencing. Due to low input material, classical monocytes mRNA was converted into cDNA using the Ovation RNA-seq System V2 kit (NuGEN; Agilent, Santa Clara, United States), whereupon sequencing libraries were prepared using the Ovation Ultralow System V2 kit (NuGEN; Agilent, Santa Clara, United States) and thereafter sequenced in a 150 bp paired-ended fashion on the Illumina NovaSeq6000 to a depth of 40 million reads at the Amsterdam UMC Core Facility Genomics. The data analyses can be found in the **Supplementary Information.**



## Results

### Cohort assembly

CD patients on VDZ treatment were followed at the AmsterdamUMC, location AMC as part of routine care. All included patients provided informed consent and the sampling was in accordance with the institutional ethics committee (METC reference number: NL53989.018.15). Response to treatment in the EPIC-CD consortium was

defined as endoscopic- (≥50% drop in simple endoscopic score for Crohn's Disease (SES-CD)) in combination with biochemical (≥50% reduction in C-reactive protein (CRP) and fecal calprotectin or an absolute CRP < 5.0 µg/g and fecal calprotectin < 250 µg/g) and/or clinical response (≥3 point drop in Harvey-Bradshaw Index (HBI)) in the presence of measurable drug serum concentrations and in the absence of corticosteroid usage. For this study, we selected a cohort of 8 CD patients at a median of 14 weeks into VDZ treatment, which were classified as responder (N = 4) and non-responder (N = 4) (**Methods**, **Table 1**,and **Figure 1**).

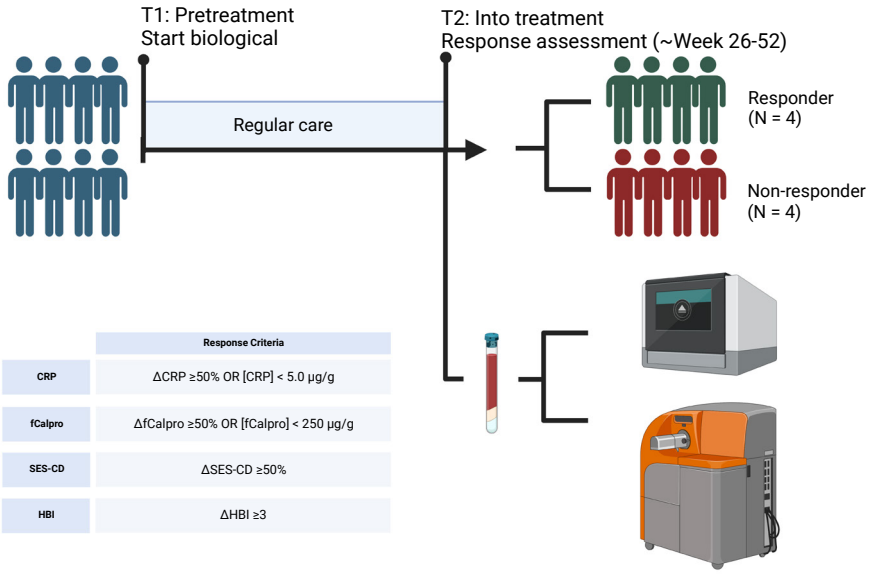


**Figure 1. Sampling strategy.** Peripheral blood samples were obtained from 4 CD patients that responded to VDZ and 4 CD patients that did not respond to VDZ. Response was defined based the Harvey Bradshaw Index (HBI), C-reactive protein (CRP), fecal calprotectin (fCalpro), and simple-endoscopic score CD (SES-CD). From peripheral blood, peripheral blood mononuclear cells (PBMCs) were isolated which were subsequently used for single-cell RNA-sequencing and mass cytometry by time of flight (CyTOF) using the Chromium controller (10X Genomics) and CyTOF3-Helios systems (Fluidigm), respectively. Created with BioRender.

## ITGA4 expression is detected on all PBMCs

Single-cell RNA-sequencing (scRNAseq) and mass cytometry by time of flight (CyTOF) provided transcriptional and proteomic profiles of 15,981 and 16,000 (subsampled from 1,783,641) cells, respectively. Cells were annotated to 31 known cell types (**Figure 2A-B**) using a combination of automatic and manual curation based on canonical markers (**Figure 2C-D**). We observed general agreement between the two experiments (r = 0.73; **Figure 2E**).

**Table 1. Patient characteristics scRNAseq and CyTOF analyses.** Overview of the demographics of the included patients.

| | Responders (N = 4) | Non-responders (N = 4) |
|---|---|---|
| Female, N (%) | 3 (75) | 4 (100) |
| Age, years, median (IQR) | 40 (29-60) | 48 (33-68) |
| Disease duration, years, median (IQR) | 10.5 (7.5-18.5) | 7 (4.5-23) |
| Ethnic background, N (%) | | |
| - Caucasian | 3 (75) | 1 (25) |
| C-reactive protein, mg/L, median (IQR) | 9.8 (5.1-22.7) | 2.2 (1.1-2.9) |
| Faecal calprotectin, µg/g, median (IQR) | 187 (111-NA) | 393 (276-NA) |
| Disease location, n (%) | | |
| - Ileal disease (L1) | 3 (75) | 1 (25) |
| - Colonic disease (L2) | - | - |
| - Ileocolonic disease (L3) | 1 (25) | 3 (75) |
| Disease behavior, N (%) | | |
| - Non structuring/penetrating (B1) | 1 (25) | 2 (50) |
| - Stricturing (B2) | 2 (50) | 2 (50) |
| - Penetrating (B3) | 1 (25) | - |
| - Perianal disease (p) | 1 (25) | - |
| Previous IBD-related surgery, N (%) | 2 (50) | 1 (25) |
| Concomitant medication, N (%) | | |
| - Immunomodulators | - | - |
| - Prednisone | - | - |
| Previous biological treatment, N (%) | | |
| - Immunomodulators | 3 (75) | 1 (25) |
| - Anti-TNF (ADA or IFX) | 1 (25) | 3 (75) |
| Smoking, N (%) | | |
| - Never | 1 (25) | 1 (25) |
| - Active | - | 3 (75) |
| - Former | 3 (75) | - |

Interrogation of the protein expression of integrin $\alpha_4$ as well as its encoding gene *ITGA4* were measurably expressed in all cell types (**Figure 2F-G**)**.** By contrast, gene expression of *ITGB7* was notably muted, with the plasma cells presenting the highest expression. Nonetheless, our observations confirm that genes encoding integrin $\alpha_4\beta_7$ expression are active in many cell types and is hence not solely restricted to the T cells.

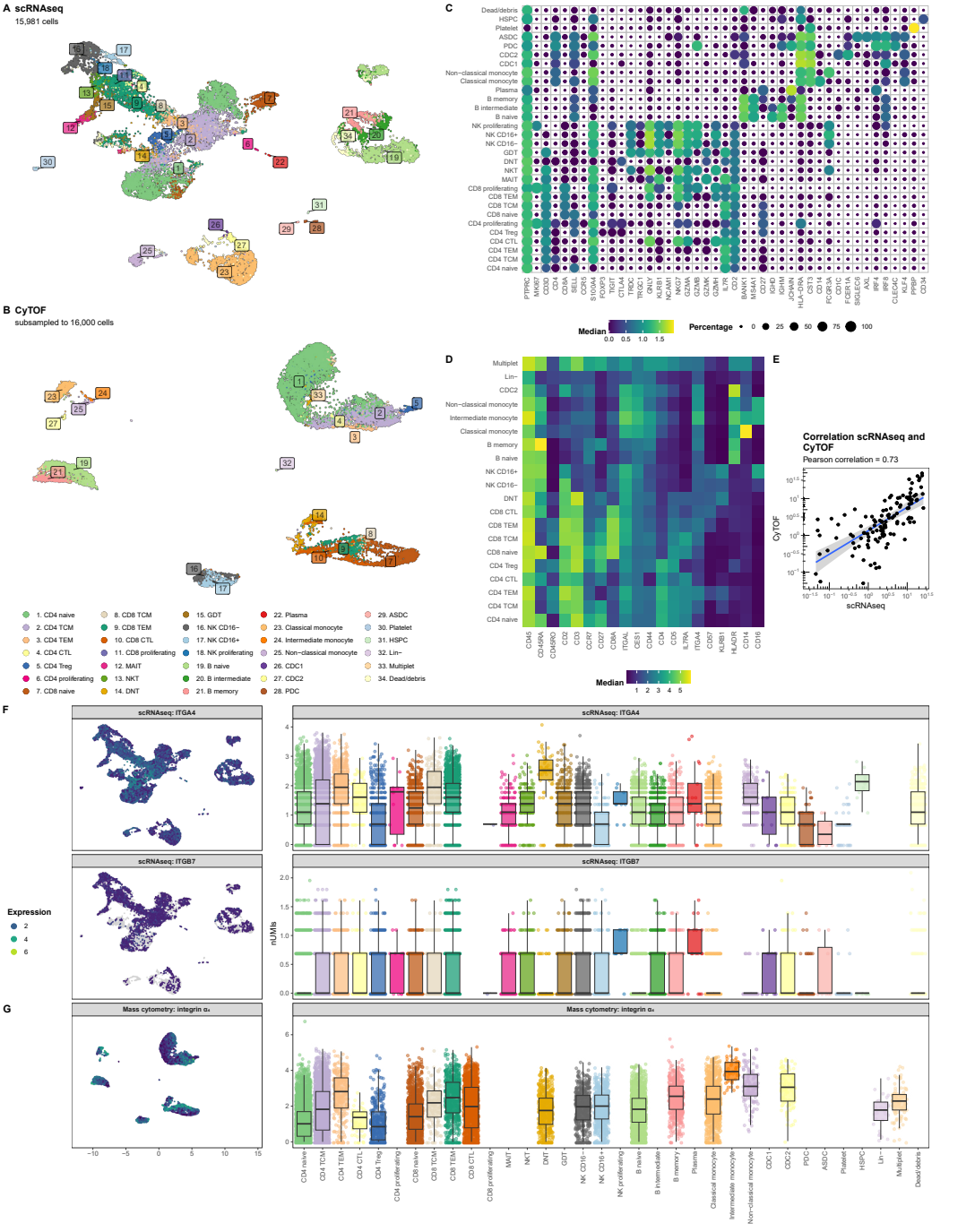
A scRNAseq
15,981 cells
B CyTOF
subsampled to 16,000 cells
C
Median
Percentage
D
Median
E
Correlation scRNAseq and CyTOF
Pearson correlation = 0.73
CyTOF
scRNAseq
F
scRNAseq: ITGA4
scRNAseq: ITGB7
Expression
nUMIs
G
Mass cytometry: integrin α4

**< Figure 2. *ITGA4* is expressed by all cell types.** Uniform manifold approximation and projection (UMAP) visualization of the PBMCs from CD patients on VDZ that respond (R; N = 4) and that do not respond (NR; N = 4) colored by the cellular identity as obtained through (**A**) single-cell RNA-sequencing (scRNAseq) and (**B**) mass cytometry by time of flight (CyTOF). Visualization of the marker expression used to annotate the PBMCs at the level of (**C**) gene expression through a dotplot where size and color intensity represent the percentage cells with measurable expression and the median expression, respectively, and (**D**) protein expression through a heatmap with the color representing the median expression. (**E**) Scatterplot representing the percentage cell types per sample relative to all PBMCs for scRNAseq on the X-axis and CyTOF on the Y-axis colored by lineage show general agreement between the scRNAseq and CyTOF experiment. UMAP (left) and boxplot (right) visualization of the gene expression for (**F**) ITGA4, ITGB7, as well as (**G**) the protein expressionfor integrin $\alpha_4$ per cell type shows that gene and protein expression of ITGA4 can be found on all celltypes, whereas ITGB7 expression is more muted.

## Circulating T cells from VDZ non-responders express lower inhibitors of the NFκB signaling pathway

Differential abundance analysis of both the scRNAseq and CyTOF data indicated concordant differences between responders and non-responders (**Figure 3A-C** and **Supplementary Table 3**). Overall, we observed a significantly lower and higher concentration of myeloid (p-value = 4.6E-03) and T cells (p-value = 0.029), respectively, among the non-responders (**Figure 3D**). At a more granular level, a significantly higher proportion of CD8 T central memory (CD8 TCM) was observed through CyTOF (p-value = 0.01), which we could reproduce in direction, but not in significance, through scRNAseq (p-value = 0.89) (**Figure 3E**). At scRNAseq level, a significantly higher and lower proportion was observed for the mucosal associated invariant T cells (MAIT; p-value = 0.029) (**Figure 3F**) and plasmacytoid dendritic cells (pDCs; p-value = 0.041) (**Figure 3G**), respectively, which we were unable to reproduce using CyTOF as no markers were included for either MAIT or pDCs. As VDZ binds T cells in particular [8], we investigated whether their transcriptome presented response-associated differences (**Supplementary Table 4**). We specifically interrogated ITGA4 and ITGB7 expression but found no differences in expression for ITGB7. By contrast, ITGA4 was found to be significantly higher in non-responders when looking at CD4 TEM, CD4 Treg, CD8 TCM, and CD8 TEM (**Figure 3H**). Notably, we observed for multiple T cell subsets that genes encoding inhibitors of the NFκB signaling pathway, such as TNFAIP3 and NFKBIA, were significantly lower in expression amongst non-responders (**Figure 3H**).

## VDZ non-responders present higher concentrations of circulating plasmacytoid dendritic cells

As our CyTOF panel did not include markers for pDCs, we conducted flow cytometry analyses where we identified the (T/B/NK)Lin-HLA-DR$^+$CD11c-CD123$^+$ fraction (**Figure 4A**). Indeed, we observed a significantly lower proportion of circulatory pDCs among responders relative to the non-responders (**Figure 4B**). Comparing the transcriptome of responders with non-responders revealed no statistically significant

response-associated differences after correcting for multiple testing (**Figure 4C** and **Supplementary Table 5**). However, interrogating the expression of ITGA4 and ITGB7 specifically indicated a notably lower expression of ITGB7 amongst non-responders albeit statistically non-significant (p-value = 0.32) (**Figure 4D** and **Supplementary Table 5**). We hypothesized that the diminished circulatory pDC concentration among non-responders was due to the recruitment of pDCs into the gastrointestinal tract thereby removing them from circulation. To corroborate our hypothesis, we interrogated the publicly available single-cell transcriptomic data from CD patients' intestinal biopsies extracted from ileal lesions (involved) and adjacent non-lesional (uninvolved) tissue as published by Martin et al. [19]. Upon identifying the pDC fraction (**Figure 4E**), we found that the pDC proportion relative to the total immune fraction was suggestively higher in lesional compared to non-lesional areas (p-value = 0.067) (**Figure 4F**), indicating that the concentration pDCs are higher under inflammatory conditions, thereby supporting our hypothesis.

## Classical monocytes from VDZ non-responders present an altered transcriptome.

UMAP visualization of the monocytes indicated response-associated clustering (**Figure 5A**), which was most visible for the classical monocytes, suggesting transcriptome-wide differences. Differential expression analysis of the classical monocytes identified 30 statistically significant differentially expressed genes (DEGs) (**Figure 5B** and **Supplementary Table 6**). Notably, responders presented higher expression of several monocyte/macrophage-function related genes including genes encoding cytokines (CXCL2 [20,21], CCL3 [22–24], CCL4 [25,26]), mediators of host defense signaling (RIPK2 [27]), and macrophage scavenging receptor (MSR1 [28]), typically observed in M2-like macrophages. By contrast, complement factor D encoding gene CFD and negative regulator of NFκB signaling pathway VSTM1 [29] were higher among non-responders (**Figure 5C**). We were able to confirm differential expression for CFD and MSR1 through bulk RNA-sequencing on sorted classical monocytes (**Figure 5D** and **Supplementary Table 7**). Specifically interrogating ITGA4 and ITGB7 indicated neither significant nor visible differences in the gene expression thereof (**Figure 5E**). Gene set enrichment analysis against the KEGG data-base identified general lower expression of the cytokine-cytokine receptor signaling pathway among non-responders (**Figure 5F-G** and **Supplementary Table 8**). We were therefore interested in identifying which other PBMCs were the sender/receiver to the differentially expressed cytokines produced by the classical monocytes. Among classical monocytes derived from responders, we observed a significantly higher expression of vascular endothelial growth factor (VEGF). Notably, VEGF receptor 1-encoding FLT1 was found to be higher in both the CD4T naïve as well as the classical monocytes (**Figure 5H**), suggesting a more wound-healing phenotype in classical monocytes obtained from responders.

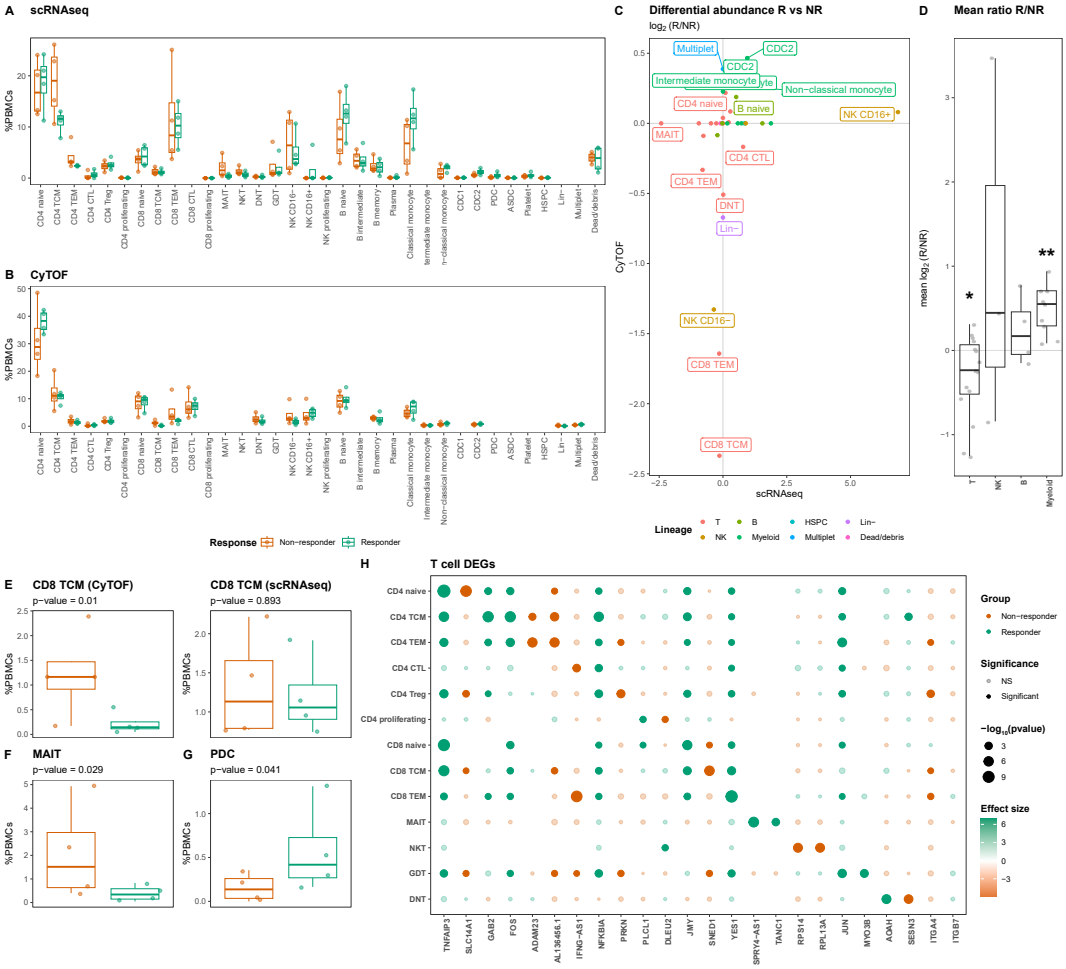


**Figure 3. T cells present response-associated differences in abundance and expression.** Boxplot visualizations of the cell type abundances relative to all measured PBMCs colored by response for (**A**) scRNAseq and (**B**) CyTOF. (**C**) Scatterplot comparing the differences in abundance based on scRNAseq on the X-axis and CyTOF on the Y-axis. Values represent $\log_2$-transformed responder: non-responder ratios per cell type and colors represent the parent lineages of each cell type. (**D**) Boxplot visualizations of the mean scRNAseq-CyTOF $\log_2$-transformed responder: non-responder ratios shows that T and myeloid cells are significantly more and less abundant amongst non-responders, respectively. Asterisks denote statistical significance using a one-sample t-test against 0. * $p<0.05$; ** $p<0.01$. Boxplot visualizations of the abundance (**E**) CD8 T central memory (CD8 TCM) in the (left) CyTOF experiment and (right) scRNAseq experiment, (**F**) mucosal associated invariant T (MAIT) cells, and (**G**) plasmacytoid dendritic cells (pDC) relative to all PBMCs. *P*-values were calculated using the t-test implementation in speckle::propeller. (**H**) Dotplot visualization representing the most significant differentially expressed genes, as well as *ITGA4* and *ITGB7* per T cell subset. Size represents statistical significance, transparency the significance threshold, and color whether the gene is upregulated in either responders (green) or non-responders (orange). A notable lower expression of *TNFAIP3* and *NFKBIA* can be observed among non-responders.

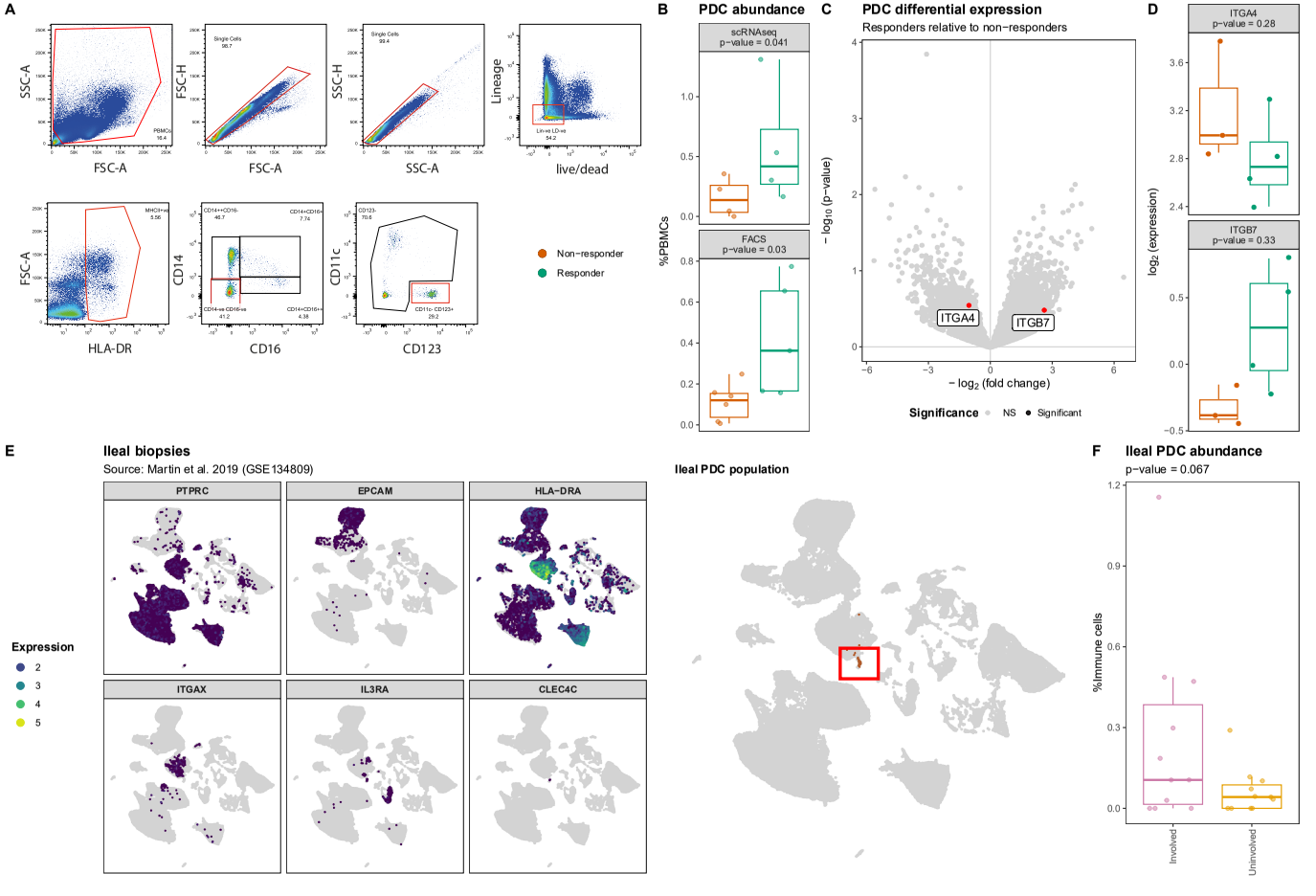
A
SSC-A
FSC-A
FSC-H
SSC-H
Lineage
live/dead
HLA-DR
CD14
CD16
CD11c
CD123
Non−responder
Responder
B
PDC abundance
scRNAseq
p−value = 0.041
FACS
p−value = 0.03
%PBMCs
C
PDC differential expression
Responders relative to non−responders
− log10 (p−value)
− log2 (fold change)
ITGA4
ITGB7
Significance
NS
Significant
D
ITGA4
p−value = 0.28
ITGB7
p−value = 0.33
log2 (expression)
E
Ileal biopsies
Source: Martin et al. 2019 (GSE134809)
PTPRC
EPCAM
HLA−DRA
ITGAX
IL3RA
CLEC4C
Expression
Ileal PDC population
F
Ileal PDC abundance
p−value = 0.067
%Immune cells
Involved
Uninvolved

**< Figure 4. Lower abundance of plasmacytoid dendritic cells in PBMCs of non-responding patients.** (**A**) Flow cytometry strategy used to identify and quantify the HLA-DR+CD14-CD16-CD11c-CD123+ pDCs where red boxes indicate selected events. (**B**) Boxplot visualizations of the pDC abundances relative to all measured PBMCs annotated with the p-value obtained through t-test. (**C**) Volcanoplot comparing pDCs from responders with non-responders where the X-axis represents the log2(fold-change) and the Y-axis the –log10(p-value). Highlighted in red are ITGA4 and ITGB7. (**D**) Boxplot visualizations of the ITGA4 and ITGB7 expression in pDCs showing visible but no statistical significant differences between responders and non-responders. P-values were calculating using the t-test implementation in speckle::propeller. (**E**) UMAP visualization of GSE134809 showing (left) the identification strategy of the PTPRC [CD45] +EPCAM-HLA-DRA+ITGAX [CD11c]-IL3RA [CD123] +CLEC4C [BDCA2] + pDCs, (right) as highlighted by the red box. (**F**) Boxplot visualization of the ileal pDC abundance relative to all immune cells colored by whether they originate from lesions (involved) or outside a lesion (uninvolved) shows that lesional pDCs are more abundant than non-lesional pDCs.

## Discussion

We demonstrate that VDZ-treated CD patients differ in cellular composition and intrinsic cellular behavior when comparing responders with non-responders. Interrogating the T cell compartment suggested a higher abundance of MAIT and CD8 TCM among non-responders. Notably, both T cells from non-responders appeared to be transcriptionally primed for NFκB signaling, a signaling pathway typically reserved for inflammation, by downregulating inhibitors thereof. The priming of the NFκB pathway would match the non-responding phenotype, where inflammation is still present despite treatment. While our results confirm that response to VDZ affects the T cell compartment, we also find response-associated differences within the myeloid compartment. We observed that the circulatory pDCs were less abundant amongst non-responders. The pDC population represents a unique cell type whose ontogeny and lineage affiliation remain under debate due to its similarity to both myeloid and lymphoid lineages [30–34]. Previously, pDCs were called "natural interferon producing cell" as they can produce large amounts of type I interferons (IFN), which typically occurs in response to viruses. This in turn activates NK and B cells [35–38], thereby bridging the innate and adaptive immune system. Remarkably, pDCs constitute only 0.4% of all measured cells when looking at all measured PBMCs in our scRNAseq experiment and only 0.12% of the immune compartment when interrogating ileal tissue from Martin et al. [19]. Despite the rarity of this cellular population, they have been implicated in multiple immune-mediated inflammatory disorders (IMIDs) [34]. Currently, an ongoing phase II clinical trial is testing the efficacy of litifilimab, a monoclonal antibody against pDC-specific binding of blood dendritic cell antigen 2 (BDCA2), in systemic [39] and cutaneous [40] lupus erythematosus, where litifilimab is thought to dampen type I IFN production [41,42].

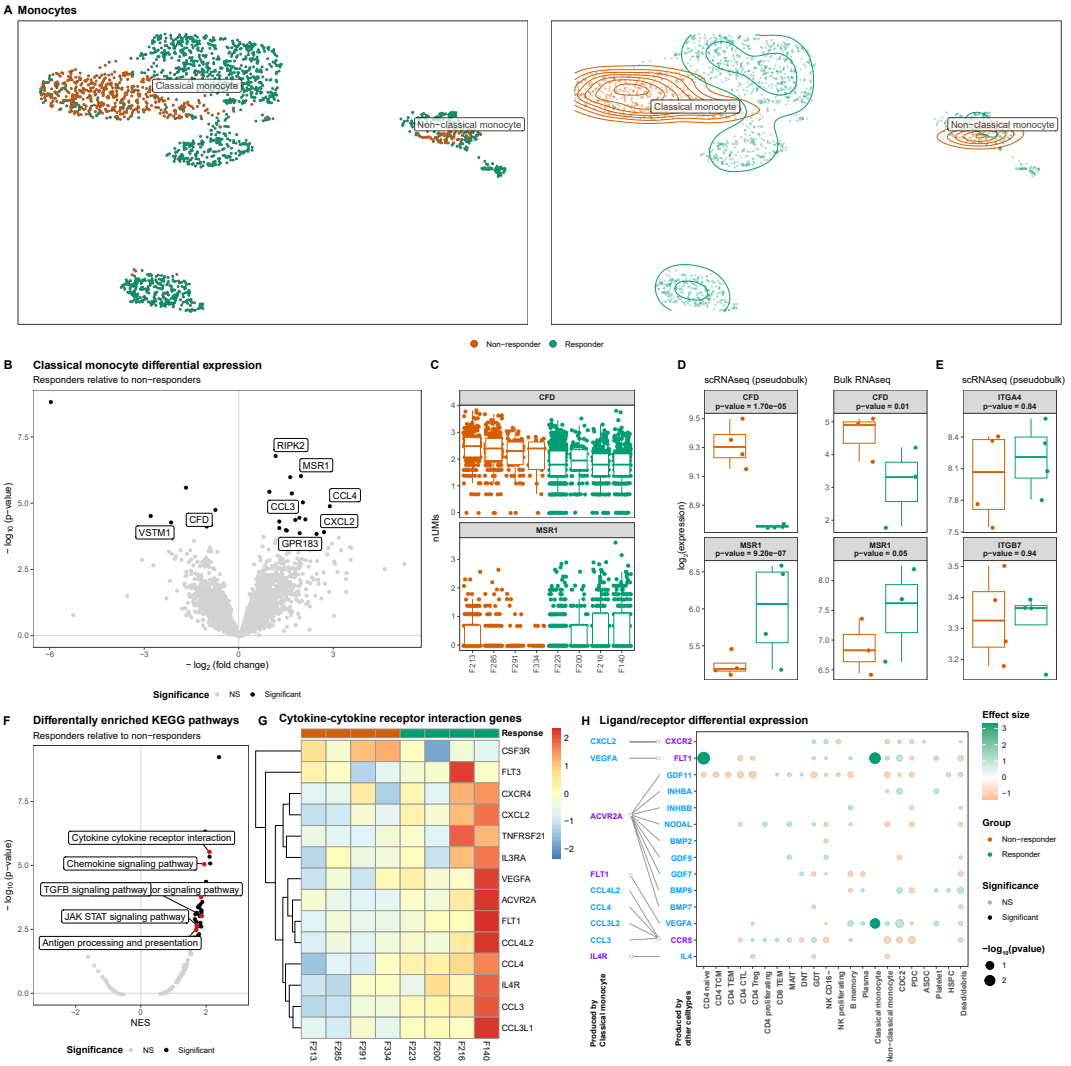


However, the association of pDCs with CD is less well documented. Previous studies have indicated that the circulatory pDC population is significantly decreased in IBD patients with active disease [43], with subsequent research by the same authors showing increased infiltration into the colonic mucosa and mesenteric lymph node (MLN) [44]. This largely corroborates our own observations, as samples were obtained during treatment and the difference between responders and non-responders is, by definition, a difference in inflammation. However, controversy exists on what role pDCs play in the pathogenesis of IBD as experiments have yielded conflicting results. It has been reported that pDCs can aggravate [45], protect [46,47], or are dispensable in the development of experimental IBD [48]. Accordingly, it remains unclear how pDCs might play a role in responsiveness towards VDZ.

**< Figure 5. Classical monocytes from non-responding patients present lower expression of cytokine-cytokine signaling.** (**A**) UMAP visualization of the monocytes colored by colored by response as dots (left) and a density plot (right) shows distinct clustering by response for the classical monocytes in particular. (**B**) Volcanoplot comparing classical monocytes from responders with non-responders where the X-axis represents the log2 (fold change) and the Y-axis the –log10(p-value). Statistically significant differences (p-valueBH-adjusted<0.05) are depicted in black. (**C**) Boxplot visualizations of CFD and MSR1 expression in classical monocytes colored by response and grouped by patient where each dot represents an individual cell. Boxplot visualizations of (**D**) CFD and MSR1, and (E) ITGA4 and ITGB7 where the Y-axis represents gene log-transformed (left) normalized pseudobulk expression from our scRNAseq experiment and (right) normalized expression obtained through bulk RNAseq analysis on classical monocytes colored and grouped by response. P-values were obtained through Wald test as implemented in DESeq2. (**F**) Volcanoplot comparing classical monocytes from responders with non-responders where the X-axis represents the normalized enrichment score (NES) and the Y-axis the –log10 (p-value). Statistically significant differences (p-valueBH-adjusted<0.05) are depicted in black with pathways of interest highlighted in red. (**G**) Heatmap visualization genes belonging to the cytokine-cytokine receptor interaction pathway. Values represent the pseudobulk expression per sample, where color is proportion to the level of expression. (**H**) Dotplot visualization of a receptor/ligand interaction analysis of the differentially expressed cytokines representing ligands and receptors are colored in blue and purple, respectively. Depicted in the dotplot are the binding partners of the cytokines found to be differentially expressed by the classical monocytes for each cell type found in PBMCs. Size of the dots represents statistical significance, transparency the significance threshold, and color whether the gene is upregulated in either responders (green) or non-responders (orange). We find that VEGFA receptor FLT1 is significantly higher expressed among the CD4 naïve and classical monocytes of responders.



Significant differences in expression were observed for the circulating classical monocytes, which presented a more scavenger-like, wound-healing phenotype amongst responders. By contrast, classical monocytes from non-responders appeared to present higher expression of CFD, a gene involved in the alternative complement pathway. Complement factor D cleaves factor B forming Bb, thereby activating the complement cascade [49]. The alternative complement pathway is an important component of the innate immune response where it is typically used as first line defense against microbes. Our results would imply that the classical monocytes from non-responders are primed at activating the alternative complement pathway. Such monocytes could potentially be recruited into the intestinal compartment, where they would differentiate into macrophages. Intestinal inflammatory macrophages are one of the few macrophages that are purported to be supplemented by the circulating monocyte population during inflammatory episodes [50–52]. We show that monocytes indeed present the capability of forming integrin α4β7, based on their gene expression, which corroborates observations by Schleier et al. who showed that monocytes indeed present functional integrin α4β7 on their surface, with VDZ abrogating their interactions with MAdCAM-1 in vitro [13]. While our observations do not indicate any difference in expression of either ITGA4 or ITGB7, we do note that the classical monocytes, alongside all other myeloid cells, were less abundant among non-responders, which we hypothesize is due to their recruitment out of circulation and into the intestinal compartment.

Taken together, it is evident that response to VDZ during treatment manifests itself at the single-cell level. While the current study provides novel insights into the diagnostic capabilities single-cell transcriptomics for elucidating response to VDZ, we appreciate the shortcomings of this study in terms of the limited sample size as well as the largely associative nature of the observations. More importantly, patient-samples taken during treatment do not hold prognostic value in predicting response to therapy. Future experiments would need to be conducted to validate the differences observed at the level of single-cell transcriptomics in a larger independent cohort to fully understand its utility as biomarker. Furthermore, to disentangle inflammation from VDZ-treatment samples would need to be included prior to the start of treatment. Moreover, it is imperative to compare our observations with CD patient cohorts treated with other inflammatory-reducing medication to understand which observations VDZ-specific and which observations are inflammation-associated. Such an approach would not only allow for the identification of prognostic biomarkers for VDZ response, but also provide potential targets that might be involved in the manifestation of drug non-response. Taken together, we demonstrate that patients on VDZ treatment present differences in the cellular heterogeneity of PBMCs. Further confirmatory studies are necessary to understand the full potential of the observed differences.

## Funding

This work was partly funded by the Helmsley Foundation as well as local funds from the Department of Human Genetics and the Tytgat Institute for Liver and Intestinal Research, AmsterdamUMC University of Amsterdam, Amsterdam, Netherlands. The study sponsors had no role in study, design, collection, analysis, or interpretation of data.

## Conflicts of interest

The following authors disclose the following within the past 5 years. ALY received speaker fees from Janssen, Johnson & Johnson and was employed by GSK. WJ received speaker fees from Janssen, Johnson & Johnson. GRD received speaker fees from Janssen, Johnson & Johnson. The remaining authors disclose no conflicts.

## Acknowledgements

We are thankful to all the participants included in the EPIC-CD study as well as the Core Facility Microscopy and Cytometry and the Core Facility Genomics located at the AmsterdamUMC for their expert assistance in the single-cell RNA-sequencing, mass cytometry, and flow cytometry experiments and analyses.

**Authors contributions †equally contributing first authors.**

Conduction of the study, laboratory, and writing of the manuscript: ALY, IH; study design: ALY, IH, VJ, WJ, PH; single-cell RNA-sequencing and analysis: ALY, IH, MJ, SK; mass cytometry analyses: JV, IH, ALY; flow cytometry analyses: ALY, IH, AE, CV, IAB; bulk RNA-sequencing and analysis: ALY, IH, AE, MJ; bioinformatics analysis: ALY, JV; patients samples collection: VJ, IH; sample preparation: IH, MG; supervision: PH, WJ, GD; reviewing and editing: WJ, GD, PH, EL, JS, AA, MM. All authors have read and agreed to the published version of the manuscript.

# References


1. Sandborn WJ, Feagan BG, Rutgeerts P, et al. Vedolizumab as Induction and Maintenance Therapy for Crohn's Disease. https://doi.org/101056/NEJMoa1215739 2013;369:711–721. Available at: https://www.nejm.org/doi/10.1056/NEJMoa1215739 [Accessed January 31, 2023].
2. Meenan J, Spaans J, Grool TA, et al. Altered expression of α4β7, a gut homing integrin, by circulating and mucosal T cells in colonic mucosal inflammation. Gut 1997.
3. Gorfu G, Rivera-Nieves J, Ley K. Role of 7 Integrins in Intestinal Lymphocyte Homing and Retention. 2009.
4. Yang Y, Cardarelli PM, Lehnert K, et al. LPAM-1 (integrin α4β7)-ligand binding: Overlapping binding sites recognizing VCAM-1, MAdCAM-1 and CS-1 are blocked by fibrinogen, a fibronectin-like polymer and RGD-like cyclic peptides. Eur J Immunol 1998.
5. Berlin C, Bargatze RF, Campbell JJ, et al. a4 Integrins Mediate Lymphocyte Attachment and Rolling under Physiologic Flow. 1995.
6. Hynes RO. Integrins: bidirectional, allosteric signaling machines. Cell 2002;110:673–687.
7. Soler D, Chapman T, Yang LL, et al. The binding specificity and selective antagonism of vedolizumab, an anti-α4β7 integrin therapeutic antibody in development for inflammatory bowel diseases. Journal of Pharmacology and Experimental Therapeutics 2009;330:864–875.
8. Arijs I, Hertogh G De, Lemmens B, et al. Effect of vedolizumab (anti-α4β7-integrin) therapy on histological healing and mucosal gene expression in patients with UC. Gut 2018;67:43–52. Available at: http://gut.bmj.com/lookup/doi/10.1136/gutjnl-2016-312293 [Accessed June 9, 2020].
9. Lord JD, Long SA, Shows DM, et al. Circulating integrin alpha4/beta7+ lymphocytes targeted by vedolizumab have a pro-inflammatory phenotype. Clinical Immunology 2018;193:24–32.
10. Habtezion A, Nguyen LP, Hadeiba H, et al. Leukocyte Trafficking to the Small Intestine and Colon. Gastroenterology 2016;150:340–354.
11. Zeissig S, Rosati E, Dowds CM, et al. Vedolizumab is associated with changes in innate rather than adaptive immunity in patients with inflammatory bowel disease. Gut 2019;68:25–39. Available at: http://www.ncbi.nlm.nih.gov/pubmed/29730603 [Accessed November 12, 2019].
12. Schleier L, Wiendl M, Heidbreder K, et al. Non-classical monocyte homing to the gut via α4β7 integrin mediates macrophage-dependent intestinal wound healing. Gut 2020;69:252–263.
13. Canales-Herrerias P, Uzzan M, Seki A, et al. Gut-associated lymphoid tissue attrition associates with response to anti-α4β7 therapy in ulcerative colitis. bioRxiv 2023:2023.01.19.524731. Available at: https://www.biorxiv.org/content/10.1101/2023.01.19.524731v1 [Accessed May 7, 2023].
14. Dulai PS, Singh S, Jiang X, et al. The real-world effectiveness and safety of vedolizumab for moderate-severe Crohn's disease: Results from the US VICTORY consortium. American Journal of Gastroenterology 2016.
15. Ungar B, Kopylov U, Yavzori M, et al. Association of Vedolizumab Level, Anti-Drug Antibodies, and α4β7 Occupancy With Response in Patients With Inflammatory Bowel Diseases. Clin Gastroenterol Hepatol 2018;16:697-705.e7. Available at: https://pubmed.ncbi.nlm.nih.gov/29223444/ [Accessed Janu-ary 31, 2023].
16. Perry C, Fischer K, Elmoursi A, et al. Vedolizumab Dose Escalation Improves Therapeutic Response in a Subset of Patients with Ulcerative Colitis. Dig Dis Sci 2021;66:2051–2058. Available at: https://link.springer.com/article/10.1007/s10620-020-06486-x [Accessed May 7, 2023].

17. Peyrin-Biroulet L, Danese S, Argollo M, et al. Loss of Response to Vedolizumab and Ability of Dose Intensification to Restore Response in Patients With Crohn's Disease or Ulcerative Colitis: A Systematic Review and Meta-analysis. W.B. Saunders; 2019:838-846.e2. Available at: https://www.sciencedirect.com/science/article/pii/S1542356518306360?via%3Dihub [Accessed October 6, 2019].

18. Joustra V, Li Yim A, Hageman I, et al. Highly stable epigenome-wide peripheral blood DNA methylation signatures accurately predict endoscopic response to adalimumab, vedolizumab and ustekinumab in Crohn's disease patients: The EPIC-CD study. In: Journal of Crohn's and Colitis.Vol 17. Copenhagen; 2023:i6–i8. Available at: https://doi.org/10.1093/ecco-jcc/jjac190.0003.

19. Martin JC, Chang C, Boschetti G, et al. Single-Cell Analysis of Crohn's Disease Lesions Identifies a Pathogenic Cellular Module Associated with Resistance to Anti-TNF Therapy. Cell 2019;178:1493-1508.e20. Available at: https://www.sciencedirect.com/science/article/pii/S0092867419308967 [Accessed October 16, 2019].

20. Pelus LM, Fukuda S. Peripheral blood stem cell mobilization: The CXCR2 ligand GROβ rapidly mobilizes hematopoietic stem cells with enhanced engraftment properties. Exp Hematol 2006;34:1010–1020.

21. Wolpe SD, Sherry B, Juers D, et al. Identification and characterization of macrophage inflammatory protein 2. Proceedings of the National Academy of Sciences 1989;86:612–616. Available at: https://www.pnas.org/doi/abs/10.1073/pnas.86.2.612 [Accessed May 7, 2023].

22. Li Y, Zheng Y, Yang L, et al. Chemokines CCL14 and CCL3 Facilitate Monocytes/Macrophage Infiltration in Multiple Myeloma Bone Marrow. Blood 2014;124:3380–3380. Available at: https://ashpublications.org/blood/article/124/21/3380/97633/Chemokines-CCL14-and-CCL3-Facilitate-Monocytes [Accessed May 7, 2023].

23. Kapellos TS, Bonaguro L, Gemünd I, et al. Human monocyte subsets and phenotypes in major chronic inflammatory diseases. Front Immunol 2019;10:2035.

24. Zhao X, Gu M, Xu X, et al. CCL3/CCR1 mediates CD14+CD16− circulating monocyte recruitment in knee osteoarthritis progression. Osteoarthritis Cartilage 2020;28:613–625. Available at: http://www.oarsijournal.com/article/S1063458420300352/fulltext [Accessed May 7, 2023].

25. Menten P, Wuyts A, Damme J Van. Macrophage inflammatory protein-1. Cytokine Growth Factor Rev 2002;13:455–481.

26. Sindhu S, Kochumon S, Shenouda S, et al. The Cooperative Induction of CCL4 in Human Monocytic Cells by TNF-α and Palmitate Requires MyD88 and Involves MAPK/NF-κB Signaling Pathways. International Journal of Molecular Sciences 2019, Vol 20, Page 4658 2019;20:4658. Available at: https://www.mdpi.com/1422-0067/20/18/4658/htm [Accessed May 7, 2023].

27. Canning P, Ruan Q, Schwerd T, et al. Inflammatory Signaling by NOD-RIPK2 Is Inhibited by Clinically Relevant Type II Kinase Inhibitors. Chem Biol 2015;22:1174–1184.

28. Gudgeon J, Marín-Rubio JL, Trost M. The role of macrophage scavenger receptor 1 (MSR1) in inflammatory disorders and cancer. Front Immunol 2022;13:6173.

29. Wang XF, En-Zhou, Li DJ, et al. VSTM1 regulates monocyte/macrophage function via the NF-κB signaling pathway. Open Medicine (Poland) 2021;16:1513–1524. Available at: https://www.degruyter.com/document/doi/10.1515/med-2021-0353/html [Accessed May 7, 2023].

30. Reizis B, Idoyaga J, Dalod M, et al. Reclassification of plasmacytoid dendritic cells as innate lymphocytes is premature. Nature Reviews Immunology 2023 23:5 2023;23:336–337. Available at: https://www.nature.com/articles/s41577-023-00864-y [Accessed May 25, 2023].

31. Ziegler-Heitbrock L, Ohteki T, Ginhoux F, et al. Reclassifying plasmacytoid dendritic cells as innate lymphocytes. Nature Reviews Immunology 2022 23:1 2022;23:1–2. Available at: https://www.nature.com/articles/s41577-022-00806-0 [Accessed January 21, 2023].
32. Musumeci A, Lutz K, Winheim E, et al. What makes a PDC: Recent advances in understanding plasmacytoid DC development and heterogeneity. Front Immunol 2019;10:1222.
33. Reizis B. Plasmacytoid Dendritic Cells: Development, Regulation, and Function. Immunity 2019;50:37–50. Available at: http://www.cell.com/article/S1074761318305752/fulltext [Accessed December 17, 2022].
34. Ye Y, Gaugler B, Mohty M, et al. Plasmacytoid dendritic cell biology and its role in immune-mediated diseases. Clin Transl Immunology 2020;9:e1139. Available at: https://onlinelibrary.wiley.com/doi/full/10.1002/cti2.1139 [Accessed October 16, 2022].
35. Bencze D, Fekete T, Pázmándi K. Type I Interferon Production of Plasmacytoid Dendritic Cells under Control. International Journal of Molecular Sciences 2021, Vol 22, Page 4190 2021;22:4190. Available at: https://www.mdpi.com/1422-0067/22/8/4190/htm [Accessed May 12, 2023].
36. Asselin-Paturel C, Trinchieri G. Production of type I interferons plasmacytoid dendritic cells and beyond. Journal of Experimental Medicine 2005;202:461–465. Available at: www.jem.org/cgi/doi/10.1084/jem.20051395 [Accessed May 12, 2023].
37. Colonna M, Trinchieri G, Liu YJ. Plasmacytoid dendritic cells in immunity. Nature Immunology 2004 5:12 2004;5:1219–1226. Available at: https://www.nature.com/articles/ni1141 [Accessed May 12, 2023].
38. Getz GS. Bridging the innate and adaptive immune systems. J Lipid Res 2005;46:619–622. Available at: http://www.jlr.org/article/S002222752033995X/fulltext [Accessed May 12, 2023].
39. Huang X, Dorta-Estremera S, Yao Y, et al. Predominant role of plasmacytoid dendritic cells in stimulating systemic autoimmunity. Front Immunol 2015;6:526.
40. Vermi W, Lonardi S, Morassi M, et al. Cutaneous distribution of plasmacytoid dendritic cells in lupus erythematosus. Selective tropism at the site of epithelial apoptotic damage. Immunobiology 2009;214:877–886.
41. Werth VP, Furie RA, Romero-Diaz J, et al. Trial of Anti-BDCA2 Antibody Litifilimab for Cutaneous Lupus Erythematosus. New England Journal of Medicine 2022;387:321–331. Available at: https://www.nejm.org/doi/full/10.1056/NEJMoa2118024 [Accessed May 25, 2023].
42. Furie RA, Vollenhoven RF van, Kalunian K, et al. Trial of Anti-BDCA2 Antibody Litifilimab for Systemic Lupus Erythematosus. New England Journal of Medicine 2022;387:894–904.
43. Baumgart DC, Metzke D, Schmitz J, et al. Patients with active inflammatory bowel disease lack immature peripheral blood plasmacytoid and myeloid dendritic cells. Gut 2005;54:228–236. Available at: www.gutjnl.com.
44. Baumgart DC, Metzke D, Guckelberger O, et al. Aberrant plasmacytoid dendritic cell distribution and function in patients with Crohn's disease and ulcerative colitis. Clin Exp Immunol 2011;166:46–54.
45. Arimura K, Takagi H, Uto T, et al. Crucial role of plasmacytoid dendritic cells in the development of acute colitis through the regulation of intestinal inflammation. Mucosal Immunology 2017 10:4 2016;10:957–970. Available at: https://www.nature.com/articles/mi201696 [Accessed May 25, 2023].
46. Mizuno S, Kanai T, Mikami Y, et al. CCR9+ plasmacytoid dendritic cells in the small intestine suppress development of intestinal inflammation in mice. Immunol Lett 2012;146:64–69.
47. Rahman T, Brown AS, Hartland EL, et al. Plasmacytoid dendritic cells provide protection against bacterial-induced colitis. Front Immunol 2019;10:608.

48. Sawai CM, Serpas L, Neto AG, et al. Plasmacytoid dendritic cells are largely dispensable for the pathogenesis of experimental inflammatory bowel disease. Front Immunol 2018;9:2475.
49. Barratt J, Weitz I. Complement Factor D as a Strategic Target for Regulating the Alternative Complement Pathway. Front Immunol 2021;12:3595.
50. Bain CC, Scott CL, Uronen-Hansson H, et al. Resident and pro-inflammatory macrophages in the colon represent alternative context-dependent fates of the same Ly6Chi monocyte precursors. Mucosal Immunol 2013;6:498–510.
51. Bain CC, Schridde A. Origin, Differentiation, and Function of Intestinal Macrophages. Front Immunol 2018;9:2733.
52. Bain CC, Mowat AM. The monocyte-macrophage axis in the intestine. Cell Immunol 2014;291:41–48.

# Supplementary information (SI Appendix)

# Materials and methods

## General bioinformatic data analyses

Data was imported and analyzed using the R statistical environment (v4.2)[1] using several packages obtained from the Bioconductor (v3.16)[2]repository. The analytical workflow was orchestrated by Snakemake (v7.14.0)[3]. Visualizations were typically created using the *tidyverse* (v1.3.1)[4], *ggplot2* (v3.4.2)[5], *ggrastr* (1.0.1), *ggrepel* (0.9.3), *cowplot* (v1.1.1), *viridis* (v0.6.3)[6], *pheatmap* (v1.0.12).

## Single-cell RNA-sequencing analysis

Samples were removed from the cryostat and thawed on ice. Thawed PBMCs were washed and then labelled using the BioLegend TotalSeq-B cell hashtag oligo (HTO) antibodies for multiplexing purposes per manufacturer's protocol at 1 U per 1 million cells[7]. An aliquot of the tagged PBMCs was assessed for viability using the Countess II FL Automated Cell Counter indicating that over 80% of the cells were viable. The resulting oligo-tagged cell suspensions were then mixed and distributed across 6 GEM-wells on the Chromium controller (10X Genomics) whereupon the single-cell barcoded partitions were prepared using 10X chemistry v3. Separate sequencing libraries were prepared for HTOs and the actual mRNA after size-selection and the libraries were sequenced on the Illumina HiSeq4000 in a 150 bp paired-ended fashion at the Core Facility Genomics, Amsterdam UMC. The mRNA libraries were sequenced on 150M reads per GEM-well, whereas the HTO libraries were sequenced to a depth of 50M reads per GEM-well. Raw reads were aligned and unique molecular identifier (UMI) count matrices were generated using Cellranger (v7.0.0). Subsequent import, sample-wise demultiplexing, processing, and analysis was done in Seurat (v4.3.0)[8]. Cells that were identified as multiplets, based on the presence of an equal number of different HTOs, or that did obtain sufficient HTO signal were removed as they could not be assigned to a unique donor. Subsequent quality control included identifying dead cells based on mitochondrial read content (>75%) and a low number of unique genes, which were annotated accordingly[9]. UMI counts were normalized using SCTransform[10], whereupon the cells were annotated by mapping our data onto a reference PBMC CITE-seq experiment of 162,000 annotated cells using a weighted nearest neighbor approach[11,12]. A subsequent manual curation using canonical markers confirmed the identity of the different cell types. T cells were identified based on the expression of *CD3D*, *CD2*, *CD7*, and *IL7R*. Natural killer (NK) cells were identified based on the expression of *CD2*, *CD7*, *GNLY* and *NKG7*, while lacking *CD3D*, B-cells

were identified based on the expression of *MS4A1* and *BANK1* positive. Monocytes were identified based on the expression of *CST3* and *CD14* or *FCGR3A*. Conventional dendritic cells (cDC) were identified on expression of *CD1C*, *CST3*, *FCER1A* and *HLA-DRA*. Smaller cell populations not belonging to the lineages were identified as well, namely the thrombocytes (*CST3* and *PPBP* positive), hematopoietic stem and progenitor cells (HSPCs; *CD34* positive), and erythroblasts (*HBA1*, *HBA2*, *HBQ1*, and *HBB* positive)[13]. Differential abundance analyses were conducted by comparing the proportions using a t-test as implemented in the *speckle* (v0.99.7)[14] package where we omitted cell types that were represented by 10 cells or less. Differential expression analyses were performed by pseudobulk[15] approaches to account for cells coming from the same donor using the *DESeq2* (v1.36.0)[16] package. Gene set overrepresentation analyses were performed using Wald statistic as input for *fgsea* (v1.22.0)[17] against the Kyoto Encyclopedia for Genes and Genomes (KEGG) gene sets[18].

## Mass cytometry by time-of-flight analysis

An overview of the antibody mass cytometry panel (including metal tag and supplier) is listed in **Supplementary Table S1**.Cryopreserved PBMCs were thawed, washed with PBS, and resuspended in RPMI medium, whereupon they were fixed with 1.6% PFA, labeled using the Cell-ID 20-Plex Pd Barcoding Kit (Fluidigm) for multiplexing purposes. Celular viability was assessed through live/dead staining using 5µM Cisplatin in PBS at room temperature. Cisplatin signal was quenched by washing with Cell Staining Buffer (CSB; Fluidigm), whereupon cells were permeabilized by Maxpar Barcode Perm Buffer (Fluidigm) and incubated with mass tag barcodes in permeabilization buffer. The cells were then stained for cell-surface targets in the presence of Human TruStain FcX™ Fc Receptor Blocking Solution (Biolegend). Antibody concentrations were optimized for staining 3M cells per 100 µL of CSB for 30 minutes at room temperature. For intracellular staining, cells were washed and incubated with antibodies for intracellular markers (CES1 and CTLA4), whereupon the cells were stained with goat anti-rabbit antibody, AF647 (Invitrogen) as a secondary staining for CES1. After washing with CSB, antibodies were fixed with 1.6% PFA, washed and incubated overnight with $^{191/193}$Ir DNA intercalator (1:4000) diluted in Fix-and-Perm Buffer (Fluidigm). Cells were subsequently washed before data acquisition was performed on the CyTOF3-Helios (Fluidigm). After data acquisition, raw .FCS files were imported in R. Signal intensities and sample acquisition rates were reviewed for stability over time and events gated based on the condition that the flow was stable, excluding calibration beads, and within the 90th percentile of all Gaussian parameters. Live CD45$^+$ cells were selected through sequential gating as described before. Cells were clustered in an unsupervised manner using the FlowSOM-package, where initial SOM-clustering was set to 300 clusters, using

markers listed in **Supplementary Table S1**. The 300 clusters were subsequently manually metaclustered according to their phenotypic lineages, whereafter cells were annotated. Expression values were then arcsinh-transformed with cofactor 5, whereafter UMAP dimensionality reduction was conducted using the *uwot* (0.1.14). Cells were subsampled to 16,000 cells to approximately match the number of cells identified through scRNAseq.

## Flow cytometry analysis

This protocol is identical to the one implemented in Elfiky *et al.*[19]. An overview of the antibody flow cytometry panel (including metal tag and supplier) is listed in **Supplementary Table S2**.Cryopreserved PBMCs were thawed, washed with PBS and stained for a live/dead cell viability marker (LifeScience, Amsterdam, the Netherlands). Cells were stained for surface markers in FACS buffer (0.5% BSA, 0.01% NaN3 in PBS) using the following antibodies: CD11c-PerCP Cy5.5 (clone: S-HCL-3, BioLegend), HLA-DR-Alexa Fluor 700 (clone: LN3, eBioscience), CD123-FITC (clone: 6H6, BioLegend), CD1C-PE-Cy7 (clone: L161, BioLegend), pan-lineage (CD3/CD19/CD20/CD56)-APC (clones: UCHT1;HIB19;2H7;5.1H11, BioLegend), CD14-BD Horizon V500 (clone: M5E2, Becton Dickinson) and CD16-PE (clone: 3G8, Becton Dickinson). Doublets were excluded and live single cells identified using the forward scatter height (FSC-H) versus the forward scatter area (FSC-A) and the side scatter height (SSC-H) versus side scatter area (SSC-A). Live cells were identified using the live/dead marker. Classical monocytes were defined as $Lin^{-}HLA{-}DR^{+}CD14^{++}CD16^{-}$, intermediate monocytes as $Lin^{-}HLA{-}DR^{+}CD14^{++}CD16^{+}$, and non-classical monocytes as $Lin^{-}HLA\text{-}DR^{+}CD14^{+}CD16^{+}$. Conventional dendritic cells (cDCs) were defined as $Lin^{-}HLA\text{-}DR^{+}CD11c^{+}CD1c^{+}$ and plasmacytoid DCs (pDCs) as $Lin^{-}HLA\text{-}DR^{+}CD11c^{-}CD123^{+}$. Fluorescence minus one (FMO) was used for gating and median fluorescence intensity was determined to quantify cell surface expression.

## RNA-sequencing analysis classical monocytes

PBMCs were subjected to flow cytometric sorting where classical monocytes were identified as $Lin^{-}HLA{-}DR^{+}CD14^{++}CD16^{-}$. Libraries were prepare using XXX kit due to low input material, whereupon sequencing was performed in a 150 bp paired ended fashion on the Illumina NovaSeq6000 to a depth of 40M reads. Quality control of the raw reads was done using FastQC (v0.11.8)[20] and MultiQC (v1.0)[21]. Raw reads were aligned to the human genome (GRCh38) using STAR (v2.7.0) and annotated using the Ensembl (v95) annotation[22]. Post-alignment processing was performed through SAMtools (v1.9)[23], after which reads were counted using the featureCounts function found in the Subread package (v1.6.3)[24]. Differential expression (DE) analysis was performed using *DESeq2* (v1.36.0)[16].

# References


1. R Development Core Team. *R: A language and environment for statistical computing*. Vienna, Austria: R Foundation for Statistical Computing; 2008. Available at: http://www.r-project.org/.
2. Gentleman RC, Carey VJ, Bates DM, et al. Bioconductor: open software development for computational biology and bioinformatics. Genome Biol 2004;5:R80. Available at: https://doi.org/10.1186/gb-2004-5-10-r80.
3. Köster J, Mölder F, Jablonski KP, et al. Sustainable data analysis with Snakemake. F1000Research 2021 10:33 2021;10:33. Available at: https://f1000research.com/articles/10-33 [Accessed May 26, 2023].
4. Wickham H, Averick M, Bryan J, et al. Welcome to the tidyverse. J Open Source Softw 2019;4:1686.
5. Wickham H. *ggplot2: Elegant Graphics for Data Analysis*. New York, NY: Springer-Verlag New York; 2009. Available at: http://ggplot2.org.
6. Garnier, Simon, Ross, et al. viridis(Lite) - Colorblind-Friendly Color Maps for R. 2023. Available at: https://sjmgarnier.github.io/viridis/.
7. Stoeckius M, Zheng S, Houck-Loomis B, et al. Cell Hashing with barcoded antibodies enables multiplexing and doublet detection for single cell genomics. Genome Biol 2018;19:224. Available at: https://genomebiology.biomedcentral.com/articles/10.1186/s13059-018-1603-1 [Accessed May 30, 2019].
8. Butler A, Hoffman P, Smibert P, et al. Integrating single-cell transcriptomic data across different conditions, technologies, and species. Nat Biotechnol 2018;36:411–420. Available at: https://www.ncbi.nlm.nih.gov/pubmed/29608179.
9. Luecken MD, Theis FJ. Current best practices in single-cell RNA-seq analysis: a tutorial. Mol Syst Biol 2019;15:e8746. Available at: http://msb.embopress.org/lookup/doi/10.15252/msb.20188746.
10. Hafemeister C, Satija R. Normalization and variance stabilization of single-cell RNA-seq data using regularized negative binomial regression. Genome Biol 2019;20:296. Available at: https://genomebiology.biomedcentral.com/articles/10.1186/s13059-019-1874-1 [Accessed October 27, 2020].
11. Stuart T, Butler A, Hoffman P, et al. Comprehensive Integration of Single-Cell Data. Cell 2019;177:1888-1902.e21.
12. Hao Y, Hao S, Andersen-Nissen E, et al. Integrated analysis of multimodal single-cell data. Cell 2021;184:3573-3587.e29.
13. Franzén O, Gan LM, Björkegren JLM. PanglaoDB: A web server for exploration of mouse and human single-cell RNA sequencing data. Database 2019;2019.
14. Phipson B, Sim CB, Porrello ER, et al. propeller: testing for differences in cell type proportions in single cell data. Bioinformatics 2022;38:4720–4726. Available at: https://academic.oup.com/bioinformatics/article/38/20/4720/6675456 [Accessed May 7, 2023].
15. Squair JW, Gautier M, Kathe C, et al. Confronting false discoveries in single-cell differential expression. Nature Communications 2021 12:1 2021;12:1–15. Available at: https://www.nature.com/articles/s41467-021-25960-2 [Accessed August 9, 2022].
16. Love MI, Huber W, Anders S. Moderated estimation of fold change and dispersion for RNA-seq data with DESeq2. Genome Biol 2014;15:550. Available at: http://genomebiology.biomedcentral.com/articles/10.1186/s13059-014-0550-8.
17. Sergushichev AA. An algorithm for fast preranked gene set enrichment analysis using cumulative statistic calculation. bioRxiv 2016:060012. Available at: https://www.biorxiv.org/content/10.1101/060012v1 [Accessed May 19, 2019].

18. Kanehisa M, Sato Y, Kawashima M, et al. KEGG as a reference resource for gene and protein annotation. Nucleic Acids Res 2016;44:D457–D462.

19. Elfiky AMI, Hageman IL, Becker MAJ, et al. A BET Protein Inhibitor Targeting Mononuclear Myeloid Cells Affects Specific Inflammatory Mediators and Pathways in Crohn's Disease. Cells 2022;11.

20. Andrews S. FastQC: a quality control tool for high throughput sequence data. Available at: http://www.bioinformatics.babraham.ac.uk/projects/fastqc.

21. Ewels P, Magnusson M, Lundin S, et al. MultiQC: summarize analysis results for multiple tools and samples in a single report. Bioinformatics 2016;32:3047–3048. Available at: https://www.ncbi.nlm.nih.gov/pubmed/27312411.

22. Cunningham F, Allen JE, Allen J, et al. Ensembl 2022. Nucleic Acids Res 2022;50:D988–D995. Available at: https://academic.oup.com/nar/article/50/D1/D988/6430486 [Accessed May 7, 2023].

23. Li H, Handsaker B, Wysoker A, et al. The Sequence Alignment/Map format and SAMtools. Bioinformatics 2009;25:2078–2079. Available at: internal-pdf://0894036185/pmcid-PMC3348047.ris.

24. Liao Y, Smyth GK, Shi W. The Subread aligner: fast, accurate and scalable read mapping by seed-and-vote. Nucleic Acids Res 2013;41:e108.

# Supplementary Tables

**Supplementary Table 1. Marker panel mass cytometry**. The cell-surface exposed markers assayed in the mass cytometry experiment annotated by the metal, target protein, alternative names, uniport identifier, and notes.

| Target | Alternative name | Uniprot | Metal | Pre/post-fixation | Manufacturer |
|---|---|---|---|---|---|
| CD45 | CD45 | P08575 | 89Y | Post | Fluidigm |
| ITGA4 | CD49D | P13612 | 141Pr | Post | Fluidigm |
| ITGAL | CD11A | P20701 | 142Nd | Post | Fluidigm |
| CD5 | | P06127 | 143Nd | Post | Fluidigm |
| CCR5 | CD195 | P51681 | 144Nd | Pre | Fluidigm |
| CD4 | | P01730 | 145Nd | Post | Fluidigm |
| CD8A | | P01732 | 146Nd | Post | Fluidigm |
| CD7 | | P09564 | 147Sm | Post | Fluidigm |
| CCR10 | GPR2 | P46092 | 148Nd | Pre | R&D |
| IL2RA | CD25 | P01589 | 149Sm | Post | Fluidigm |
| TNR4 | CD134;OX40L | P43489 | 150Nd | Post | Fluidigm |
| CD2 | | P06729 | 151Eu | Post | Fluidigm |
| TNR6 | CD95;FAS | P25445 | 152Sm | Post | Fluidigm |
| HAVR2 | TIM3 | Q8TDQ0 | 153Eu | Post | Fluidigm |
| CD14 | | P08571 | 154Sm | Post | Fluidigm |
| PDCD1 | CD279 | Q15116 | 155Gd | Post | Fluidigm |
| CXCR3 | CD183 | P49682 | 156Gd | Pre | Fluidigm |
| CCR4 | CD194 | P51679 | 158Gd | Pre | Fluidigm |
| CCR7 | CD197 | P32248 | 159Tb | Post | Fluidigm |
| CD28 | | P10747 | 160Gd | Post | Fluidigm |
| CTLA4 | CD152 | P16410 | 161Dy | Post | Fluidigm |
| CD69 | CLEC2C | Q07108 | 162Dy | Post | Fluidigm |
| A4B7 | vedolizumab | | 171Yb | Pre | Takeda |
| KLRB1 | CD161 | Q12918 | 164Dy | Post | Fluidigm |
| CD45RO | | | 165Ho | Post | Fluidigm |
| CD44 | | P16070 | 166Er | Post | Fluidigm |
| CD27 | | P26842 | 167Er | Post | Fluidigm |
| CCR9 | | P51686 | 168Er | Pre | Fluidigm |

| | | | | | |
|---|---|---|---|---|---|
| CD45RA | | | 169Tm | Post | Fluidigm |
| CD3 | | P04234 | 170Er | Post | Fluidigm |
| CD57 | | | 172Yb | Post | Fluidigm |
| **Target** | **Alternative name** | **Uniprot** | **Metal** | **Pre/post-fixation** | **Manufacturer** |
| TNR9 | CD137;4-1BB | Q07011 | 173Yb | Post | Fluidigm |
| HLADR | | | 174Yb | Post | Fluidigm |
| CES1 | | | 175Lu | Post | Thermo Scientific |
| IL7RA | CD127 | P16871 | 176Yb | Post | Fluidigm |
| CD16 | | P08637 | 209Bi | Post | Fluidigm |
| Barcodes | | | 103-110Pd | Post | Fluidigm |
| Iridium | | | 191-193Ir | Post | Fluidigm |
| Cisplatin | | | 194-195Pt | Pre | Fluidigm |

**Supplementary Table 2. Marker panel flow cytometry**. The cell-surface exposed markers assayed in the flow cytometry experiment alongside the antibody and clone.

| **Target** | **Fluorophore** | **Manufacturer** | **Clones** |
|---|---|---|---|
| Lineage (CD3, CD19, CD20, CD3, CD56) | APC | BioLegend | UCHT1, HIB19, 2H7, 5.1H11 |
| HLA-DR | Alexa Fluor 700 | eBioscience | LN3 |
| CD14 | BD Horizon V500 | Becton Dickinson | M5E2 |
| CD16 | PE | Becton Dickinson | 3G8 |
| CD11c | PerCP Cy5.5 | BioLegend | S-HCL-3 |
| CD123 | FITC | BioLegend | 6H6 |
| CD1c | PE-Cy7 | BioLegend | L161 |
| Live/dead | APC H7/C7 | | |

**Supplementary Table 1. Continued**

**Supplementary Table 3-8,** will be available online after manuscript acceptance.

**Supplementary Table 3. PBMC differential abundance analysis.** Results of the differential abundance analysis on the major lineages as conducted using the propeller function in speckle. Columns represent the cell type, the mean proportion for all samples ("BaselineProp.Freq"), non-responders only ("PropMean.Non.responder"), and responders only ("PropMean.Responder"), the ratio responder/non-responder ("PropRatio"), the associated T statistic ("Tstatistic") as well as the *p*-values ("P.Value" and "FDR"). Tabs separate the results from scRNAseq and CyTOF analyses.

**Supplementary Table 4. T cell scRNAseq pseudobulk differential gene expression analysis.** Results of the differential expression analysis performed on PDCs using DESeq2. Columns represent the gene, the average expression ("baseMean"), the $\log_2$ (fold change) ("log2FoldChange"), the associated standard error ("lfcSE"), the Wald statistic ("stat") as well as the *p*-values ("pvalue" and "padj"). Each tab represents a different T cell subset.

**Supplementary Table 5. pDC scRNAseq pseudobulk differential gene expression analysis.** Results of the differential expression analysis performed on PDCs using DESeq2. Columns represent the gene, the average expression ("baseMean"), the $\log_2$ (fold change) ("log2FoldChange"), the associated standard error ("lfcSE"), the Wald statistic ("stat") as well as the *p*-values ("pvalue" and "padj").

**Supplementary Table 6. Classical monocytes scRNAseq pseudobulk differential gene expression analysis.** Results of the differential expression analysis performed on classical monocytes using DESeq2. Columns represent the gene, the average expression ("baseMean"), the $\log_2$ (fold change) ("log2FoldChange"), the associated standard error ("lfcSE"), the Wald statistic ("stat") as well as the *p*-values ("pvalue" and "padj").

**Supplementary Table 7. Classical monocytes bulk RNAseq gene expression analysis.** Results of the differential expression analysis performed on classical monocytes using DESeq2. Columns represent the gene and Ensembl ID, the average expression ("baseMean"), the $\log_2$ (fold change) ("log2FoldChange"), the associated standard error ("lfcSE"), the Wald statistic ("stat") as well as the *p*-values ("pvalue" and "padj").

**Supplementary Table 8. Classical monocytes scRNAseq pseudobulk KEGG gene set enrichment analysis**. Gene set enrichment analysis as performed by fgsea.

Columns represent the gene set (“Pathway”), the *p*-values (“pvalue” and “FDR”), the $\log_2$ standard error (“log2err”), the enrichment score (“ES”), the normalized enrichment score (“NES”), and the total number of genes in the gene set (“size”).

# 7

# Chapter 7

## General discussion and future perspectives

## Current status of IBD medications

Inflammatory bowel disease (IBD) is a chronic immune mediated disease that affects the gastrointestinal tract and entails two major subtypes, crohn's disease (CD) and ulcerative colitis (UC) [1]. It affects approximately around 0.3% of general population [2] and compromises a large economic burden, given the debilitating natural course of the disease, co-morbidities, associated socioeconomic impact, costly medications and significantly high rates of primary or secondary treatment failure [3, 4].

Immunomodulatory medications are the mainstay of treatment that include not only the nonspecific immunosuppressive agents, like steroids, but also targeted biologic therapies. The most recently introduced biologics anti-TNF (infliximab, adalimumab), anti-$\alpha_4\beta_7$ integrin (vedolizumab), and anti-IL12p40 (ustekinumab) have revolutionized the IBD care, achieving successful remission in patients who used to be resistant to traditional immunosuppressants [5, 6]. Despite effectiveness in subsets of patients, rates of primary or secondary non-response to these novel medications remain substantially high, with almost 40-50% of patients reporting treatment failure and progression of the disease [1]. Drug discontinuation due to intolerable adverse effects is also reported. This represents a significant unmet clinical need that requires development of novel medications with better safety profile and effectiveness. Multiple leads are currently at different stages of clinical development including inhibitors of Janus kinases, receptor interacting protein, phosphodiesterase 4, IκB kinase, integrins, S1P, CCR9, CXCR4, and NLRP3 [7]. Moreover, with the expanding range of the current and upcoming biologics in IBD care, more research is needed to understand determinants of response to each and every biologic, and to enable a more personalized and effective approach towards clinical care [8].

### Promises and limitations of non-specific epigenetic therapies as anti-inflammatory drugs

IBD pathogenesis is a very elusive topic that remains challenging to fully understand. Multiple facets seem to be involved including genetics, epigenetics and environmental factors. Recent research points to a significant role of epigenetics in IBD pathogenesis [9]. This sparks our interest to explore the potential of targeting epigenetics as a promising therapeutic strategy in IBD drug development. As we discussed in chapter 1, inhibitors of histone deacetylase (HDAC) enzymes and bromodomains and extra terminal domain (BET) have shown potent anti-inflammatory activities in *in vitro* and *in vivo* models of inflammatory mediated diseases including IBD [10, 11]. Histone organization is a key determinant of gene expression. The dynamic fluctuation between open euchromatin and closed

heterochromatin states is mediated by histone tail modifications; methylation, phosphorylation, acetylation, ubiquitylation, and sumoylation. Histone acetylation is associated with an open euchromatin state and regulated by opposing actions of two groups of enzyme families; histone acetyltransferases (HAT) and histone deacetylases (HDAC) that add or remove acetyl groups to lysine residues of histone tails respectively [12]. Global HDACs pharmacological inhibition demonstrates clinical efficacy in murine models of IBD [13-15]. Moreover, BET proteins belongs to a group of epigenetic readers (BRD2, BRD3, BRD4 and BRDT) that recognize acetylated lysine residues on histone tails and allow for recruitment of transcription factors necessary for gene expression [16]. Efficacy of BET pan inhibitors in multiple preclinical models of inflammatory mediated diseases are well documented [11], however results from IBD preclinical models are inconclusive [17-19].

Despite the early development of these inhibitors, clinical trials raised a number of safety concerns due to their wide range of toxicities including serious cardiac arrhythmias, gastrointestinal toxicity and bone marrow suppression [20, 21]. This is not completely surprising given the lack of specificity of these inhibitors that target large families of epigenetic enzymes involved in multiple cellular functions. The wide range of therapeutic benefits of theses nonspecific inhibitors sparked enthusiasm towards early development into clinical trials despite lack of selectivity and incomplete understanding of the molecular mechanisms underlying their potent therapeutic effects. This largely hindered the progress towards translating the beneficial effects of these epigenetic therapies to clinical practice, with less encouraging results coming back from clinical trials. In order to overcome this limitation, 2 main strategies are followed to enhance specificity of these medications and improve their safety profile. As we detailed in chapter 1, the first strategy is to develop drug delivery platforms that target nonspecific potent inhibitors to inflammatory immune cells. The second strategy is to identify novel epigenetic targets that are more specific to inflammatory responses through performing more mechanistic studies to understand the epigenetic modulators of inflammation and subsequently develop class-, isoform-, or domain-specific inhibitors towards epigenetic targets of interest. In the current thesis, we further explore translational aspect of some of these novel and more specifically targeted epigenetic medicines in IBD.



## Mononuclear myeloid cells (MMCs) targeted epigenetic therapies

MMCs including monocytes, macrophage and dendritic cells (DCs) play a major role in IBD pathogenesis, given the importance of an aberrant innate immune response in fueling active intestinal inflammation [22]. Specific targeting of these cell populations with potent epigenetic enzymes inhibitors may help to utilise

the anti-inflammatory benefits of theses inhibitors, while minimizing their toxicity profile. As we introduced in chapter 1, esterase sensitive motif (ESM) technology is a MMCs targeted drug delivery technology that allows an ESM tagged drug to be hydrolyzed and retained in carboxylesterase 1 (CES1) expressing cells [23]. CES1 enzyme is mainly expressed in hepatocytes and MMCs, and to much less extent in adipose tissue [24]. This may be quite concerning for a potential limiting hepatotoxicity of this therapeutic technology. However, phase 1 clinical trials of ESM tagged HDAC inhibitors demonstrated no observed hepatic toxicities, while specific drug accumulation in peripheral blood monocytes was noted. Moreover, intolerable adverse effects commonly seen with pan HDAC inhibitors were absent [25, 26]. Despite high CES1 expression in hepatocytes, drug accumulation within hepatocytes seems to be negligible, possibly due to intrinsic properties of hepatocytes that may continuously pump out the hydrolyzed drug outside of the cell. However, the exact mechanisms underlying the lack of liver toxicity warrant further investigation. To that extent, ESM tagged epigenetic compounds seem to be very promising therapeutic strategy to be investigated in IBD.

In chapter 2 and 3; we explored the extent of CES1 expression in healthy and IBD patients in locally inflamed tissues and peripheral blood, as this determines where the drug will be retained the most. In peripheral blood of CD patients, CES1 is exclusively expressed in monocytes and DCs. Among monocyte subsets, CES1 expression is highest in classical monocytes in healthy donors and conversely, in non-classical monocytes in CD patients. This may be reflective of a preferential trafficking of CES1-expressing classical monocytes to the locally inflamed colon in CD patients where classical monocytes are recruited to support intestinal inflammation [27, 28]. Moreover, this exclusive CES1 expression in MMCs was confirmed in CD patients' colon biopsies as well as immune cells retrieved from locally inflamed fistulae tracts of CD patients, a common CD complication that does not respond well to standard biologic therapies. Interestingly, we found that the majority of $CD68^{+}$ macrophages in inflamed intestinal mucosa express CES1, unlike non-inflamed mucosa where less CES1-expressing macrophages were identified. Capece *et al*, have shown that CES1 expression is increased downstream of NF-κB signaling [29], and therefore is upregulated by inflammatory stimuli. In chapter 2 and 4, we extend this observation to MMCs, as we show that *CES1* is significantly increased in response to LPS in *in vitro* DCs culture. Similarly, reanalyzing RNAseq data from Bujko *et al.* shows the greatest *CES1* expression in peripheral blood monocytes and the $CD14^{+}CD11c^{+}HLA\text{-}DR^{int}$ immature macrophages in contrast to more mature macrophages subsets and DCs in non-inflamed intestinal environment. This is associated with co-expression of *S100A12*, a known inflammatory IBD biomarker

that is highly expressed in inflammatory macrophages and can endogenously activate TLR4 and subsequently the NF-κB signaling pathway [30, 31]. In contrast, in the IBD inflamed tissue environment, CES1 expression is high among most of the macrophages and DCs subsets isolated from CD inflamed fistulae tract mucosa as we demonstrated in chapter 3. This link between CES1 expression and inflammatory cues is particularly interesting in clinical application of ESM technology in IBD as ESM tagged drugs are preferentially retained in the CES1-expressing cells. MMCs are diverse cell populations that play a major role in intestinal homeostasis in health and disease. They play opposing roles to fuel intestinal inflammation or maintain tolerance respectively depending on the predominant MMCs subsets and enriched cues within the local intestinal environment [22]. Therefore, preferential targeting of the deleterious MMCs subsets while sparing the homeostatic subsets is beneficial for successful therapeutic outcome in IBD.

As demonstrated in chapter 1, the esterase sensitive motif (ESM) coupled to the drug of interest is sensitive to hydrolysis specifically by CES1 enzyme, therefore the drug is hydrolyzed and retained intracellularly in CES1-expressing cells. Accordingly, using less potent ESM tagged drugs at low doses allows for negligible effect in all tissues except for CES1-expressing cells where compound gradually builds up to reach therapeutic levels. We made use of an ESM tagged HDAC inhibitor (ESM-HDAC528) and BET inhibitor (ESM-iBET; GSK3361191), developed by GSK to explore their therapeutic potential in IBD. As demonstrated in chapter 2, we utilized monocytes as a CES1-expressing *in vitro* model to show that ESM-HDAC528 is capable of building up intracellularly compared to non-hydrolysable HDAC800 control. Despite both drugs having same biochemical potency, ESM-HDAC528 potently inhibited IL-6 and TNF-α in monocytes at doses 1000 times lower than the non-hydrolysable HDAC800 control. This augmented anti-inflammatory therapeutic efficacy is reflective of CES1 assisted ESM-HDAC528 accumulation. How these *in vitro* findings are recapitulated *in vivo* was evident in a phase 1 clinical trial [25], addressing the pharmacokinetics and safety of ESM-HDAC391, another ESM tagged HDAC inhibitor developed by GSK. ESM-HDAC391 selectively accumulated in blood monocytes compared to lymphocytes and granulocytes. Despite the short half-life of the drug, 21-30 minutes, a sustained inhibition of inflammatory cytokines (TNFα, IL-6, IL-1β and IFN-γ) was evident up to 12 hours following drug administration. This was accompanied by enhanced total protein acetylation selectively within monocytes, a direct effect of unopposed HATs activity due to HDAC inhibition. Interestingly, these sustained pharmacodynamic effects were still evident just prior to dosing, after 7 days of once daily treatment in the absence of any measurable plasma drug concentrations, reflecting a sustained cumulative effect of repeated dosing [25]. In a preclinical

murine model of rheumatoid arthritis, ESM-HDAC inhibitor (CHR-4487) achieved clinical efficacy at doses as low as 1, 3 and 10 mg/kg compared to 100mg/kg for SAHA, a conventional pan-HDAC inhibitor [23].

These apparent *in vitro* and *in vivo* enhanced therapeutic effects, and high tolerability of ESM tagged HDAC inhibitors in phase 1 clinical trials were encouraging to explore therapeutic potential of this approach in the complex pathology of IBD. As we demonstrated in chapter 2, ESM-HDAC528 showed a moderate clinical efficacy in preclinical murine models of IBD. Selective targeting of the drug was evident by preferential increased global acetylation in blood monocytes as shown earlier in *in vivo* human clinical trials [25, 26]. In a T cell transfer colitis model, ESM-HDAC528 attenuated colon inflammation and reduced serum and colon inflammatory cytokines. Selective targeting of DCs in this model might be responsible for the achieved therapeutic benefits. HDAC inhibitors can modulate DCs functions, compromising T cell stimulatory activity and Th1 polarization [32]. DCs play a key role in this model to promote a T cell mediated colon inflammation [33, 34]. Alternatively, in a DSS-induced colitis model, the clinical benefits were modest, only improving selected end point parameters of the model. However, intestinal macrophage differentiation was compromised in the colon, while peritoneal macrophages showed less LPS-induced cytokine responses. The observed discrepancy between the outcomes of the two colitis models may be attributed to their different predominant mechanisms driving inflammation. Moreover, the inconclusive outcome in the DSS colitis model, despite selective and effective targeting of blood monocytes and tissue macrophages, can be attributed to the universal targeting of all MMCs subsets in our murine models, including anti-inflammatory subsets that play a role in limiting colon inflammation in the DSS model. To this point, it is important to note that ESM tagged drugs are only sensitive to hydrolysis by human CES1 enzyme and not murine CES enzymes. Our *in vivo* studies were conducted in transgenic mice over expressing human *CES1* under *CD68* promotor [35] which allows for universally high human *CES1* expression in all murine MMCs subsets. Unlike in human, transgenic CES1 expression in mice was not responsive to inflammatory cues. Therefore, due to discrepancy between CES1 dynamics in human vs transgenic murine systems, translating *in vivo* finding from murine studies to human should be done with care.

Another ESM tagged epigenetic drug investigated in chapter 3 was ESM-iBET (GSK3361191). Similar to ESM-HDAC528, we demonstrated that ESM-iBET was superior to non-hydrolysable iBET control (GSK3235220) at inhibiting inflammatory cytokine production in CES1-expressing monocytes. This superior potency was also evident in our monocyte transcriptomic analysis. BET inhibition can exert toxic effect

on intestinal epithelial cells [36]. This effect seems to be predominant over the anti-inflammatory benefits in the complex gastrointestinal inflammatory environment, as BET inhibition is reported to aggravate intestinal inflammation in DSS-induced colitis model [18]. Our mass cytometry analysis of CD intestinal biopsies demonstrated that the majority of $EpCAM^+$ epithelial cells did not express CES1, which is interesting for application of ESM-iBET in IBD to mitigate the potential iBET toxicity on intestinal epithelial cells while targeting inflammatory MMCs. Furthermore, our transcriptomic analysis of ESM-iBET treated monocytes showed efficient targeting of multiple inflammatory pathways relevant to IBD pathogenesis, including TNF, JAK-STAT, NF-kB, NOD2, and AKT signaling pathways. Among these pathways, TNF and JAK-STAT are targets of currently available IBD biologics in the clinic. Unlike current therapies, ESM-iBET can target multiple CD-relevant inflammatory pathways simultaneously in MMCs. This may in turn improve responses rate for a wider range of patients compared to current therapies that aim to target a specific cytokine or pathway component, which can only be beneficial in patients in which this particular pathway is predominantly driving inflammation. However, clinical trials should be conducted to explore whether this approach is of clinical benefit, as in a complex *in vivo* environment, cell types other than MMCs, such as intestinal lymphocytes, epithelial, and stromal cells, contribute to intestinal inflammation.

### CES1 regulation by inflammatory cues in DCs.

Despite high expression of CES1 in MMCs, little is known about a potential role of CES1 in modulating MMCs phenotype and inflammatory response. Most of the studies of CES1 functions in macrophages focused on role of CES1 in cholesterol trafficking and foamy macrophage phenotype [37, 38]. In chapter 2, we demonstrated that CES1 expressing macrophages were more enriched in inflammatory CD intestinal environment, in line with earlier report that shows CES1 upregulation downstream of NFκB signaling [29]. In chapter 3, we further investigated CES1 dynamics in DCs and observed strong *CES1* upregulation early during *in vitro* monocytes derived dendritic cells (MoDCs) differentiation in response to GMCSF and IL4 and later in response to LPS stimulation. When we pharmacologically blocked CES1 early during MoDCs differentiation, the resulting DCs were characterized by a more inflammatory phenotype, enhanced phagocytic capacity and stronger ability to support Th17 induction. In contrary, an attenuated inflammatory phenotype was observed in DCs overexpressing human CES1 in transgenic murine model. Metabolic adaptions of DCs are closely linked to their phenotype and functional activities [39]. A switch towards glycolytic energy metabolism is a metabolic prerequisite of inflammatory MoDCs phenotype [40-42]. Alternatively tolerogenic DCs are largely dependent on mitochondrial respiration [43]. Our metabolomics analysis and functional respirometry investigations revealed

altered metabolic profile of CES1 inhibitor treated MoDCs. We noted a higher lactic acid production, a compromised mitochondrial respiration, a long with modulated TCA cycle intermediates. A recent report shows similar effect on mitochondrial respiration in hepatocytes following CES1 inhibition [44]. Our study highlighted a role of CES1 to support metabolic demands of differentiating DCs that can be a target to modulate DCs phenotype and function. However, a full mechanistic understanding of the pathways involved was not covered in our study and requires further investigations. We alternatively focused on exploring potential clinical translation of our findings. We demonstrated that human CES1 overexpression in a CD68 specific manner conferred a protective effect against colitis development in a T cell transfer colitis model. However, our results need further validation in a normal esterase background mice, due to discrepancies in blood esterase background between our *CES1/Es1e*$^{lo}$/*Rag*$^{-/-}$ transgenic mice and *Rag*$^{-/-}$ control mice. Previous *in vivo* studies demonstrated anti-inflammatory role of CES1 in LPS induced lung inflammation and alcohol induced steatohepatitis murine models [45, 46]. However, further *in vivo* studies need to make use of human *CES1* transgenic mice due to discrepancies between human and murine CES enzyme expression and distribution. Alternatively, inflammatory DCs phenotype with Th17 supporting activity, associated with blocking CES1 may be of therapeutic benefit in cancer vaccine development. Th17 infiltration and expansion within ovarian cancer tissue, supported by DCs, is shown to be predictive of a favourable disease outcome [47, 48].

## Exploring applications of more specific epigenetic druggable targets in IBD.

To harness the translational benefits of targeting epigenetics in inflammatory diseases, additional mechanistic studies were conducted to identify novel epigenetic targets that are more specific to inflammatory responses; bromodomain 2 (BD2) was among the identified druggable targets. As detailed in chapter 1, the BET proteins family members (BRD2, BRD3, BRD4 and BRDT) structurally share 2 common bromodomains; BD1 and BD2. While BD1 anchors the BET protein to acetylated histone residues and allows for homeostatic gene expression, BD2 is essential for induced gene expression during activated cellular states [49]. These functional distinctive roles encouraged development of BD2 selective inhibitors that can specifically interfere with induced gene expression during inflammatory response, meanwhile limiting the wide range of toxicities associated with pan BET inhibitors. In chapter 5, our T cell transfer colitis study investigating clinical efficacy of BD2 inhibitor (GSK620A) and pan BET inhibitors iBET151 demonstrated a significant reduction of serum inflammatory cytokines. However, this efficient anti-inflammatory systemic effect did not translate into sufficient clinical efficacy which was unexpectedly modest. The

best outcome was observed at low dose (1 mg/kg) BD2 inhibitor treatment. Unlike pan-BET inhibitor, low dose BD2 inhibitor demonstrated reduced local inflammatory cytokines in the colon, associated with a mild reduction of intestinal inflammation. The modest clinical efficacy of pan BET inhibition confirms our earlier study in same model [17]. Moreover, in a DSS induced colitis model, the effect of pan BET inhibition was deleterious [18]. BET inhibitors have a known toxicity on intestinal epithelial cell which might explain the modest outcome in our model [36]. An earlier study using another BD2 inhibitor (ABBV-744) demonstrated less gastrointestinal toxicity compared to pan BET inhibitor [50]. However, whether the BD2 inhibitor used in our study demonstrates gastrointestinal toxicity was not investigated. Moreover, selective targeting of BD2 over BD1 at the indicated doses should be confirmed, as multiple epigenetic inhibitors appear to be less selective than proposed due to the challenging drug design of a selective inhibitor over structurally similar protein members in the same family [51]. BD2 inhibitors showed promising clinical efficacy in preclinical models of other inflammatory diseases, equivalent to standard therapies [49]. However, to harness the therapeutic potential of BET inhibition in the context of IBD, BD2 inhibitor candidates need to be prescreened within *in vitro* or *ex vivo* organoid / intestinal epithelial models to exclude any potential gastrointestinal toxicity prior to selection for further investigations in *in vivo* preclinical IBD models. This will help to refine selection of the best drug candidate for development in IBD.

## Towards better characterization of response to current IBD biologics therapies.



Multiple biologic therapies are currently available for IBD, however response rates remain unsatisfactoryly high for most of the therapeutics [1]. Despite understanding the molecular mechanisms of these medications, mechanisms behind clinical efficacy are unclear and therefore patient response to a particular biologic is highly unpredictable, with lack of reliable prognostic biomarkers [8]. In chapter 6, we explored the potential of single cell omics analysis to investigate response to vedolizumab (VDZ), an anti-integrin $\alpha_4\beta_7$ that interferes with immune cells trafficking into gut. However, while earlier reports atributes VDZ efficacy to an effect mainly exerted on T cell trafficking into gut, a growing evidence points to an effect on myeloid cells and B cells as well. In our study, we observed that changes of cellular composition predominantly affected the myeloid cell compartment, as circulating classical monocytes and plasmacytoid DCs (pDCs) were less abundant in non-responders. Previous studies have showed significantly decreased circulating pDCs in IBD patients, attributable to increased trafficking to intestinal inflamed tissues [52, 53]. However, the exact role that pDCs play in IBD pathogenesis is controversial, as in preclinical disease models, pDCs were reported to aggravate, protect or even have negligible impact on intestinal inflammation [54-56]. However, drug non-

responsiveness is associated with ongoing active inflammation which may explain the lower abundance of pDCs, reflecting active disease state. Alternatively, lower circulating classical monocyte abundance was observed in non-responders and was associated with a phenotype primed at activating the alternative complement pathway compared to a more scavenger-like, wound-healing phenotype in responders. This discrepancy of monocytes abundance and phenotype is indicative of an effect of VDZ on resolution of active inflammation. Whether these findings are specific to VDZ response or indicative of inflammation resolution regardless of treatment is inconclusive as our study lacks comparison to other medications. Moreover, we cannot imply any prognostic value of these observations given the lack of control samples prior to start of treatment and small sample size. However, our study provided novel insights into the capabilities of single-cell transcriptomics and mass cytometry for elucidating response to VDZ. Larger studies with bigger sample size, control samples prior to treatment start and other medications comparison arms are needed to better understand response to biologics and identify potential prognostic biomarkers that can refine personalized medicine practices in IBD and biologic prescriptions.

## Conclusion and future perspectives

Clinical care of IBD is in enormous need of novel, effective and safe therapeutic options to tackle the high rate of non-responsiveness to current medications. Epigenetic medicines are increasingly developed in multiple clinical domains, due to their wide range of clinical benefits attributable to nonspecific targeting of multiple cellular functions, however, this comes with a cost of many adverse events as well [20, 21]. While the first wave of epigenetic medicines lacked specificity, recently developed medicines attempt to tackle this problem. In the current thesis we discussed applications of new targeted epigenetic medicines in the treatment of IBD, that is more specific for inflammation and therefore aim to achieve clinical efficacy taking into consideration an improved safety profile.

We investigated the potential of targeting MMCs epigenome using ESM technology in IBD. We demonstrated augmented potency of ESM tagged HDAC and BET inhibitors in *in vitro* models of CES1-expressing cells, validating the CES1 assisted targeting of these medicines to MMCs. Moreover, we demonstrated selective CES1 expression in MMCs within peripheral blood and inflamed tissue of IBD patients and highlighted the potential benefits of this approach in preclinical models of IBD. We highlighted a role of CES1 in shaping DCs metabolic profile which in turn modulates

DCs inflammatory phenotype. The selective targeting of MMCs allows for focusing drug beneficial effects in cells relevant to the disease pathology therefore limiting its toxicities. Despite preclinical data supporting this approach, it is hard to predict *in vivo* efficacy to ameliorate inflammation in the complex gut inflamed environment, where contributions of other inflammatory cells, epithelial and stromal cells to the pathology is substantial. Murine studies are difficult to predict the potential efficacy in humans given the discrepancies between naturally occurring human CES1 and transgenic human CES1 expression and dynamics in murine models. Therefore, preclinical animal studies should not be a prerequisite for moving forwards to clinical trials. IBD human *ex vivo* models might be an alternative, including culture of inflamed tissue retrieved cells and more complex gut organoid cultures.

Targeting epigenetic elements specific to inflammation is an alternative approach in epigenetic medicine development. In the current thesis, we investigated BD2 as an interesting target in IBD, however screening of potential BD2 inhibitors candidates in intestinal organoids might be beneficial to ensure selectivity and lack of gastrointestinal toxicity prior to further development in IBD. Furthermore, better understanding of mechanisms and predictors of drugs response in IBD is essential to achieve better drug selection for candidate patients. We highlighted the benefits of single cell omics methods to achieve that goal, towards a better personalized medicine practice in IBD.

In conclusion, our thesis provides an insight to the translational potential of different epigenetic targeted medicines in IBD and highlights the endeavors of improving selectivity of epigenetic targeting to harness therapeutic benefits for the growing plethora of these medicines, while improving their safety profile and extending their application to inflammation mediated diseases.

# References


1. Yeshi, K., et al., *Revisiting Inflammatory Bowel Disease: Pathology, Treatments, Challenges and Emerging Therapeutics Including Drug Leads from Natural Products.* J Clin Med, 2020. **9**(5).
2. Ng, S.C., et al., *Worldwide incidence and prevalence of inflammatory bowel disease in the 21st century: a systematic review of population-based studies.* Lancet, 2017. **390**(10114): p. 2769-2778.
3. The Lancet Gastroenterology, H., *The economic burden of inflammatory bowel disease.* Lancet Gastroenterol Hepatol, 2023. **8**(5): p. 391.
4. van Linschoten, R.C.A., et al., *Systematic review: societal cost of illness of inflammatory bowel disease is increasing due to biologics and varies between continents.* Aliment Pharmacol Ther, 2021. **54**(3): p. 234-248.
5. Torres, J., et al., *ECCO Guidelines on Therapeutics in Crohn's Disease: Medical Treatment.* J Crohns Colitis, 2020. **14**(1): p. 4-22.
6. Raine, T., et al., *ECCO Guidelines on Therapeutics in Ulcerative Colitis: Medical Treatment.* J Crohns Colitis, 2022. **16**(1): p. 2-17.
7. Li, Y., et al., *Target-Based Small Molecule Drug Discovery Towards Novel Therapeutics for Inflammatory Bowel Diseases.* Inflamm Bowel Dis, 2021. **27**(Suppl 2): p. S38-S62.
8. Vieujean, S. and E. Louis, *Precision medicine and drug optimization in adult inflammatory bowel disease patients.* Therap Adv Gastroenterol, 2023. **16**: p. 17562848231173331.
9. Xu, J., et al., *New Insights Into the Epigenetic Regulation of Inflammatory Bowel Disease.* Front Pharmacol, 2022. **13**: p. 813659.
10. Glauben, R. and B. Siegmund, *Molecular basis of histone deacetylase inhibitors as new drugs for the treatment of inflammatory diseases and cancer.* Methods Mol Biol, 2009. **512**: p. 365-76.
11. Jahagirdar, R., et al., *RVX-297, a BET Bromodomain Inhibitor, Has Therapeutic Effects in Preclinical Models of Acute Inflammation and Autoimmune Disease.* Mol Pharmacol, 2017. **92**(6): p. 694-706.
12. Araki, Y. and T. Mimura, *The Histone Modification Code in the Pathogenesis of Autoimmune Diseases.* Mediators Inflamm, 2017. **2017**: p. 2608605.
13. Glauben, R., et al., *Histone hyperacetylation is associated with amelioration of experimental colitis in mice.* J Immunol, 2006. **176**(8): p. 5015-22.
14. Friedrich, M., et al., *HDAC inhibitors promote intestinal epithelial regeneration via autocrine TGFbeta1 signalling in inflammation.* Mucosal Immunol, 2019. **12**(3): p. 656-667.
15. Ali, M.N., et al., *The HDAC Inhibitor, SAHA, Prevents Colonic Inflammation by Suppressing Pro-inflammatory Cytokines and Chemokines in DSS-induced Colitis.* Acta Histochem Cytochem, 2018. **51**(1): p. 33-40.
16. Wang, N., et al., *The BET family in immunity and disease.* Signal Transduct Target Ther, 2021. **6**(1): p. 23.
17. Schilderink, R., et al., *BET bromodomain inhibition reduces maturation and enhances tolerogenic properties of human and mouse dendritic cells.* Mol Immunol, 2016. **79**: p. 66-76.
18. Wienerroither, S., et al., *Regulation of NO synthesis, local inflammation, and innate immunity to pathogens by BET family proteins.* Mol Cell Biol, 2014. **34**(3): p. 415-27.
19. Cheung, K., et al., *BET N-terminal bromodomain inhibition selectively blocks Th17 cell differentiation and ameliorates colitis in mice.* Proc Natl Acad Sci U S A, 2017. **114**(11): p. 2952-2957.
20. Sun, Y., et al., *Safety and Efficacy of Bromodomain and Extra-Terminal Inhibitors for the Treatment of Hematological Malignancies and Solid Tumors: A Systematic Study of Clinical Trials.* Front Pharmacol, 2020. **11**: p. 621093.

21. Subramanian, S., et al., *Clinical Toxicities of Histone Deacetylase Inhibitors.* Pharmaceuticals (Basel), 2010. **3**(9): p. 2751-2767.
22. Hegarty, L.M., G.R. Jones, and C.C. Bain, *Macrophages in intestinal homeostasis and inflammatory bowel disease.* Nat Rev Gastroenterol Hepatol, 2023.
23. Needham, L.A., et al., *Drug targeting to monocytes and macrophages using esterase-sensitive chemical motifs.* J Pharmacol Exp Ther, 2011. **339**(1): p. 132-42.
24. Lian, J., R. Nelson, and R. Lehner, *Carboxylesterases in lipid metabolism: from mouse to human.* Protein Cell, 2018. **9**(2): p. 178-195.
25. Furze, R.C., et al., *Phase 1 and preclinical profiling of ESM-HDAC391, a myeloid-targeted histone deacetylase inhibitor, shows enhanced pharmacology and monocytopaenia.* Br J Clin Pharmacol, 2022. **88**(12): p. 5238-5256.
26. Ossenkoppele, G.J., et al., *A phase I first-in-human study with tefinostat - a monocyte/macrophage targeted histone deacetylase inhibitor - in patients with advanced haematological malignancies.* Br J Haematol, 2013. **162**(2): p. 191-201.
27. Jones, G.R., et al., *Dynamics of Colon Monocyte and Macrophage Activation During Colitis.* Front Immunol, 2018. **9**: p. 2764.
28. Thiesen, S., et al., *CD14(hi)HLA-DR(dim) macrophages, with a resemblance to classical blood monocytes, dominate inflamed mucosa in Crohn's disease.* J Leukoc Biol, 2014. **95**(3): p. 531-41.
29. Capece, D., et al., *Enhanced triacylglycerol catabolism by carboxylesterase 1 promotes aggressive colorectal carcinoma.* J Clin Invest, 2021. **131**(11).
30. Realegeno, S., et al., *S100A12 Is Part of the Antimicrobial Network against Mycobacterium leprae in Human Macrophages.* PLoS Pathog, 2016. **12**(6): p. e1005705.
31. Sidler, M.A., S.T. Leach, and A.S. Day, *Fecal S100A12 and fecal calprotectin as noninvasive markers for inflammatory bowel disease in children.* Inflamm Bowel Dis, 2008. **14**(3): p. 359-66.
32. Brogdon, J.L., et al., *Histone deacetylase activities are required for innate immune cell control of Th1 but not Th2 effector cell function.* Blood, 2007. **109**(3): p. 1123-30.
33. Toribio-Fernandez, R., et al., *Lamin A/C deficiency in CD4(+) T-cells enhances regulatory T-cells and prevents inflammatory bowel disease.* J Pathol, 2019. **249**(4): p. 509-522.
34. Rossini, V., et al., *CX3CR1(+) cells facilitate the activation of CD4 T cells in the colonic lamina propria during antigen-driven colitis.* Mucosal Immunol, 2014. **7**(3): p. 533-48.
35. Iqbal, A.J., et al., *Human CD68 promoter GFP transgenic mice allow analysis of monocyte to macrophage differentiation in vivo.* Blood, 2014. **124**(15): p. e33-44.
36. Bolden, J.E., et al., *Inducible in vivo silencing of Brd4 identifies potential toxicities of sustained BET protein inhibition.* Cell Rep, 2014. **8**(6): p. 1919-1929.
37. Mangum, L.C., et al., *Silencing carboxylesterase 1 in human THP-1 macrophages perturbs genes regulated by PPARgamma/RXR and RAR/RXR: down-regulation of CYP27A1-LXRalpha signaling.* Biochem J, 2018. **475**(3): p. 621-642.
38. Crow, J.A., et al., *Inhibition of carboxylesterase 1 is associated with cholesteryl ester retention in human THP-1 monocyte/macrophages.* Biochim Biophys Acta, 2008. **1781**(10): p. 643-54.
39. O'Neill, L.A. and E.J. Pearce, *Immunometabolism governs dendritic cell and macrophage function.* J Exp Med, 2016. **213**(1): p. 15-23.
40. Everts, B., et al., *Commitment to glycolysis sustains survival of NO-producing inflammatory dendritic cells.* Blood, 2012. **120**(7): p. 1422-31.

41. Perrin-Cocon, L., et al., *Toll-like Receptor 4-Induced Glycolytic Burst in Human Monocyte-Derived Dendritic Cells Results from p38-Dependent Stabilization of HIF-1alpha and Increased Hexokinase II Expression.* J Immunol, 2018. **201**(5): p. 1510-1521.

42. Thwe, P.M., et al., *Cell-Intrinsic Glycogen Metabolism Supports Early Glycolytic Reprogramming Required for Dendritic Cell Immune Responses.* Cell Metab, 2017. **26**(3): p. 558-567 e5.

43. Sim, W.J., P.J. Ahl, and J.E. Connolly, *Metabolism Is Central to Tolerogenic Dendritic Cell Function.* Mediators Inflamm, 2016. **2016**: p. 2636701.

44. Li, G., et al., *Interfering with lipid metabolism through targeting CES1 sensitizes hepatocellular carcinoma for chemotherapy.* JCI Insight, 2023. **8**(2).

45. Xu, J., et al., *Carboxylesterase 1 Is Regulated by Hepatocyte Nuclear Factor 4alpha and Protects Against Alcohol- and MCD diet-induced Liver Injury.* Sci Rep, 2016. **6**: p. 24277.

46. Szafran, B.N., et al., *Carboxylesterase 1d Inactivation Augments Lung Inflammation in Mice.* ACS Pharmacol Transl Sci, 2022. **5**(10): p. 919-931.

47. Block, M.S., et al., *Th17-inducing autologous dendritic cell vaccination promotes antigen-specific cellular and humoral immunity in ovarian cancer patients.* Nat Commun, 2020. **11**(1): p. 5173.

48. Cannon, M.J., et al., *Modulation of p38 MAPK signaling enhances dendritic cell activation of human CD4+ Th17 responses to ovarian tumor antigen.* Cancer Immunol Immunother, 2013. **62**(5): p. 839-49.

49. Gilan, O., et al., *Selective targeting of BD1 and BD2 of the BET proteins in cancer and immunoinflammation.* Science, 2020. **368**(6489): p. 387-394.

50. Faivre, E.J., et al., *Selective inhibition of the BD2 bromodomain of BET proteins in prostate cancer.* Nature, 2020. **578**(7794): p. 306-310.

51. Rianjongdee, F., et al., *Discovery of a Highly Selective BET BD2 Inhibitor from a DNA-Encoded Library Technology Screening Hit.* J Med Chem, 2021. **64**(15): p. 10806-10833.

52. Baumgart, D.C., et al., *Aberrant plasmacytoid dendritic cell distribution and function in patients with Crohn's disease and ulcerative colitis.* Clin Exp Immunol, 2011. **166**(1): p. 46-54.

53. Baumgart, D.C., et al., *Patients with active inflammatory bowel disease lack immature peripheral blood plasmacytoid and myeloid dendritic cells.* Gut, 2005. **54**(2): p. 228-36.

54. Sawai, C.M., et al., *Plasmacytoid Dendritic Cells Are Largely Dispensable for the Pathogenesis of Experimental Inflammatory Bowel Disease.* Front Immunol, 2018. **9**: p. 2475.

55. Mizuno, S., et al., *CCR9+ plasmacytoid dendritic cells in the small intestine suppress development of intestinal inflammation in mice.* Immunol Lett, 2012. **146**(1-2): p. 64-9.

56. Arimura, K., et al., *Crucial role of plasmacytoid dendritic cells in the development of acute colitis through the regulation of intestinal inflammation.* Mucosal Immunol, 2017. **10**(4): p. 957-970.

A

# Appendix

# English summary

In this thesis, we explored the potential of novel approaches for targeting immune epigenome in inflammatory bowel disease (IBD). We investigated cell specific as well as epigenetic enzymes domain-specific drug targeting. These approaches aim to develop more tolerable and effective epigenetic therapies for inflammation mediated diseases.

In **Chapter 1,** we explained some of the known mechanisms by which epigenetic enzymes, such as histone acetylases (HATs), histone deacetylases (HDACs), DNA methylases, and bromodomain-containing proteins (BCPs), regulate chromatin remodeling and their impact on health and disease. We provided a comprehensive overview of the most recent progress in developing inhibitors that specifically target certain classes, isoforms, or domains of HDACs or BCPs. Additionally, we discussed innovative strategies for delivering epigenetic targeted drugs to specific immune cells. The advantages and disadvantages of these approaches were examined, with a focus on their therapeutic potential in inflammation mediated diseases, including IBD. Lastly, we proposed valuable avenues for future research to enhance safety, avoid unintended adverse effects associated with earlier non-specific epigenetic therapies and guide the application of these approaches in the context of inflammation mediated diseases.

In **Chapter 2,** we investigated the therapeutic potential of delivering a pan-HDAC inhibitor specifically to mononuclear myeloid cells (MMCs) in murine models of IBD. Using esterase sensitive motif (ESM) technology; a specific drug delivery platform that allows an ESM tagged drug to be hydrolyzed and retained in MMCs by the activity of their carboxylestarse-1 enzyme (CES1). CES1 is known to be expressed in MMCs, hepatocytes and to less extent in adipocytes. By incorporating an ESM tag into a pan-HDAC inhibitor, referred to as ESM-HDAC528, we demonstrated the specific hydrolysis and subsequent retention of ESM-HDAC528 within CES1-expressing monocytes, macrophages and dendritic cells. This in turn was associated with markedly enhanced ability to reduce inflammatory cytokines compared to HDAC800; a non ESM tagged HDAC inhibitor of same biochemical potency. In preclinical IBD murine models, we observed an improvement of colitis in both T cell transfer and to less extent in dextran sulfate sodium (DSS)-induced colitis models. Furthermore, ESM-HDAC528 specifically targeted blood monocytes, impaired monocytes into macrophages differentiation in the colon and reduced the inflammatory response of peritoneal macrophages. In human IBD patients, CES1 expressing macrophage were more abundant in inflamed compared to non-inflamed colon tissue. Collectively,

we presented ESM-HDAC inhibitor as a promising drug candidate of potential therapeutic relevance in IBD.

In **Chapter 3,** we employed single cell mass cytometry analysis to explore CES1 expression in IBD patients in both peripheral blood and locally inflamed tissues at single cell level. We demonstrated exclusive CES1 expression among MMCs in blood and intestinal biopsies of crohn's disease (CD) patients, regardless of treatment response status. We further identified different MMCs subsets in CD fistulae tracts, a common difficult to treat CD complication, and showed specific and high CES1 expression among these subsets. Using ESM drug design technology, we demonstrated enhanced ability of ESM tagged BET inhibitor (ESM-iBET; GSK3361191) to inhibit inflammatory cytokines in CES1-expressing monocytes in both PBMCs or purified $CD14^{+}$ monocytes compared to iBET (GSK3235220). Moreover, our monocytes transcriptomic analysis identified a potent inhibitory effect of ESM-iBET on multiple pathways of potential therapeutic relevance to CD including; TNF, JAK-STAT, NF-kB, NOD2, and AKT signaling pathways, with superior potency over iBET. Collectively, chapter 2 and 3 discuss MMCs targeted HDAC or BET inhibition as an interesting therapeutic strategy in IBD.

In **Chapter 4,** we highlighted a role of CES1 enzyme in modulating DCs differentiation, phenotype and function. Using pharmacological inhibitor of CES1 or transgenic overexpression in murine system, we showed that CES1 inhibition promoted DCs differentiation with stronger inflammatory phenotype, higher phagocytic capacity and ability to support Th17 polarization. Alternatively, human CES1 overexpression in murine MMCs promoted less inflammatory cytokines secretion in bone marrow derived DCs (BMDCs), in response to TLRs ligands and conferred a resistance to colitis development in T cell transfer IBD model. Our transcriptomic analysis revealed an impact of CES1 inhibition on multiple inflammatory and metabolic pathways in DCs. Functional metabolic analysis showed impaired oxidative phosphorylation meanwhile increased lactic acid production, and modulated tricarboxylic acid (TCA) cycle intermediates, reflecting a predominant glycolytic metabolic profile. Collectively, this chapter reports a role of CES1 in DCs inflammatory response through modulating their metabolic profile.



In **Chapter 5**, we explored the therapeutic potential of selective bromodomain 2 (BD2) targeting of BET proteins in preclinical model of IBD. Using T cell transfer colitis model, we explored the clinical efficacy of both pan-BET inhibitor (I-BET151) and BD2 inhibitor (GSK620). We demonstrated modest clinical improvement when treatments are applied in therapeutic approach, following establishment of colon

inflammation. Both inhibitors reduced systemic inflammation, manifested by significantly reduced circulating IL12, IL6, IFNγ and TNFα. However local intestinal inflammation remained persistently high, and only non-significantly decreased in low dose GSK620 treatment, which was accompanied by slightly improved colon histology inflammation scores. Collectively, *in vivo* BD2 specific inhibition using GSK620 only demonstrated limited clinical efficacy.

In **Chapter 6**, we explored the capabilities of single cell transcriptomic and mass cytometry technologies to identify determinants of response to vedolizumab in CD patients. Comparing PBMCs from responders and non-responders to vedolizumab after 14 weeks into treatment, we identified differences in cellular composition and intrinsic cellular behavior of both T and myeloid cells compartments. A significant reduction of circulating plasmacytoid DCs was noted, along with altered classical monocytes transcriptome, demonstrating less wound healing and cytokine-cytokine receptors signaling genes expression among non-responders. Alternatively, T cell compartment demonstrated lower expression of inhibitors of the NFκB signaling pathway among non-responders. Collectively, this study demonstrates the use of multi-omics technologies to understand responsiveness to IBD therapies for better personalized medicine practices.

# Nederlandse samenvatting

In dit proefschrift hebben we het potentieel onderzocht van nieuwe benaderingen voor het aanpakken van het immuun-epigenoom bij inflammatoire darmziekten (IBD). We onderzochten zowel celspecifieke als epigenetische enzymen, domeinspecifieke medicijntargeting. Deze benaderingen zijn gericht op het ontwikkelen van beter verdraagbare en effectieve epigenetische therapieën voor ontsteking gemedieerde ziekten.

In **Hoofdstuk 1,** hebben we enkele van de bekende mechanismen uitgelegd waarmee epigenetische enzymen, zoals histonacetylasen (HAT's), histondeacetylasen (HDAC's), DNA-methylasen en broom-domein-bevattende eiwitten (BCP's), de remodellering van chromatine reguleren en impact hebben op gezondheid en ziekte. We hebben een uitgebreid overzicht gegeven van de meest recente vooruitgang in de ontwikkeling van remmers die zich specifiek richten op bepaalde klassen, isovormen of domeinen van HDAC's of BCP's. Daarnaast bespraken we innovatieve strategieën voor het afleveren van epigenetische gerichte medicijnen aan specifieke immuuncellen. De voor- en nadelen van deze benaderingen werden onderzocht met de nadruk op hun therapeutisch potentieel bij ontstekingsgemedieerde ziekten, waaronder IBD. Ten slotte hebben we waardevolle wegen voorgesteld voor toekomstig onderzoek om de veiligheid te verbeteren, onbedoelde nadelige effecten te vermijden die verband houden met eerdere niet-specifieke epigenetische therapieën en de toepassing van deze benaderingen te begeleiden in de context van ontstekingsgemedieerde ziekten.

In **Hoofdstuk 2** hebben we het therapeutisch potentieel van het toedienen van een pan-HDAC-remmer specifiek aan mononucleaire myeloïde cellen (MMC's) onderzocht in muriene modellen van IBD. Met behulp van esterase-gevoelige motief (ESM) technologie; een specifiek medicijnafgifteplatform waarmee een ESM-gelabeld medicijn kan worden gehydrolyseerd en vastgehouden in MMC's door de activiteit van hun carboxylesterase-1-enzym (CES1). Van CES1 is bekend dat het tot expressie wordt gebracht in MMC's, hepatocyten en in mindere mate in adipocyten. Door een ESM-tag op te nemen in een pan-HDAC-remmer, aangeduid als ESM-HDAC528, hebben we de specifieke hydrolyse en daaropvolgende retentie van ESM-HDAC528 aangetoond in monocyten, macrofagen en dendritische cellen die CES1 tot expressie brengen. Dit ging op zijn beurt gepaard met een aanzienlijk verbeterd vermogen om inflammatoire cytokines te verminderen in vergelijking met HDAC800; een niet-ESM-gelabelde HDAC-remmer met dezelfde biochemische potentie. In preklinische IBD-muizenmodellen zagen we een verbetering van colitis in zowel T-celtransfer als in mindere mate in door dextraansulfaatnatrium (DSS) geïnduceerde colitismodellen. Bovendien richtte ESM-HDAC528 zich specifiek

op bloedmonocyten, verstoorde de differentiatie van monocyten tot macrofagen in de dikke darm en verminderde de ontstekingsreactie van peritoneale macrofagen. Bij menselijke IBD-patiënten waren macrofagen die CES1 tot expressie brachten meer aanwezig in ontstoken dan in niet-ontstoken darmweefsel. Gezamenlijk presenteerden we de ESM-HDAC-remmer als een veelbelovend kandidaat-geneesmiddel met potentiële therapeutische relevantie bij IBD.

In **Hoofdstuk 3** hebben we single cell mass cytometry analyse gebruikt om CES1-expressie bij IBD-patiënten te onderzoeken in zowel perifeer bloed als lokaal ontstoken weefsel, op het niveau van een enkele cel. We hebben exclusieve CES1-expressie aangetoond bij MMC's in bloed- en darmbiopten van patiënten met de ziekte van Crohn (CD), ongeacht de status van de respons op de behandeling. We identificeerden verder verschillende MMC-subsets in CD-fistelkanalen, een veelvoorkomende moeilijk te behandelen CD-complicatie, en vertoonden specifieke en hoge CES1-expressie in deze subsets. Met behulp van ESM-technologie voor het ontwerpen van geneesmiddelen hebben we een verbeterd vermogen aangetoond van ESM-gelabelde BET-remmer (ESM-iBET; GSK3361191) om inflammatoire cytokines te remmen in monocyten die CES1 tot expressie brengen in zowel PBMC's als gezuiverde CD14+ monocyten in vergelijking met iBET (GSK3235220). Bovendien identificeerde onze transcriptomische analyse van monocyten een krachtig remmend effect van ESM-iBET op meerdere routes van potentiële therapeutische relevantie voor CD, waaronder; TNF, JAK-STAT, NF-kB, NOD2 en AKT signaleringsroutes, met superieure potentie ten opzichte van iBET. Gezamenlijk bespreken hoofdstuk 2 en 3 MMC's gerichte HDAC- of BET-remming als een interessante therapeutische strategie bij IBD.

In **hoofdstuk 4,** hebben we de rol van het CES1-enzym in het moduleren van differentiatie, fenotype en functie van DC's benadrukt. Met behulp van een farmacologische remmer van CES1 of transgene overexpressie in de muis, toonden we aan dat CES1-remming de differentiatie van DC's bevorderde met een sterker inflammatoir fenotype, een hoger fagocytisch vermogen en het vermogen om Th17-polarisatie te ondersteunen. Bovendien bevorderde menselijke CES1-overexpressie in muriene MMC's minder secretie van inflammatoire cytokines in beenmerg afgeleide DC's (BMDC's), als reactie op TLR's-liganden en verleende het een weerstand tegen de ontwikkeling van colitis in het IBD-model voor T-celoverdracht. Onze transcriptomische analyse onthulde een impact van CES1-remming op meerdere inflammatoire en metabolische routes in DC's. Functionele metabole analyse toonde verminderde oxidatieve fosforylering aan met tegelijkertijd een verhoogde melkzuurproductie en gemoduleerde tricarbonzuur (TCA) cyclustussenproducten die een overheersend glycolytisch metabolisch profiel weerspiegelen. Gezamenlijk

rapporteert dit hoofdstuk een rol van CES1 in de ontstekingsreactie van DC's door hun metabolische profiel te moduleren.

In **Hoofdstuk 5** onderzochten we het therapeutisch potentieel van selectieve broomdomein 2 (BD2) targeting van BET-eiwitten in een preklinisch model van IBD. Met behulp van het T-celtransfermodel hebben we de klinische werkzaamheid van zowel pan-BET-remmer (I-BET151) als BD2-remmer (GSK620) onderzocht. We hebben een bescheiden klinische verbetering aangetoond wanneer behandelingen worden toegepast in een therapeutische benadering, na het ontstaan van darmontsteking. Beide remmers verminderden de systemische ontsteking, wat zich uitte in een significant verminderde circulatie van IL12, IL6, IFNy en TNFα. Lokale darmontsteking bleef echter aanhoudend hoog en nam slechts niet-significant af bij behandeling met een lage dosis GSK620, wat gepaard ging met licht verbeterde scores voor histologische ontsteking van de dikke darm. Gezamenlijk vertoonde in vivo BD2-specifieke remming met behulp van GSK620 slechts een beperkte klinische werkzaamheid.

In **Hoofdstuk 6** onderzochten we de mogelijkheden van single cell transcriptomics en mass cytometry technologieën om determinanten van respons op vedolizumab bij coeliakiepatiënten te identificeren. Door PBMC's van responders en non-responders op vedolizumab na 14 weken behandeling te vergelijken, identificeerden we verschillen in cellulaire samenstelling en intrinsiek cellulair gedrag van zowel T- als myeloïde celcompartimenten. Er werd een significante vermindering van circulerende plasmacytoïde DC's opgemerkt, samen met een veranderd klassiek monocytentranscriptoom, wat aantoont dat er minder wondgenezing en cytokine-cytokinereceptoren signalering genenexpressie bij non-responders.
Verder vertoonde het T-celcompartiment een lagere expressie van remmers van de NFKB-signaalroute bij non-responders. Gezamenlijk demonstreert deze studie het gebruik van multi-omics-technologieën om inzicht te krijgen in de reactie op IBD-therapieën voor betere therapie op maat: personalised medicine.

# List of publication

(* denotes first or co-first author)

**Elfiky AMI***, Hageman IL*, Becker MAJ, Verhoeff J, Li Yim AYF, Joustra VW, Mulders L, Fung I, Rioja I, Prinjha RK, Smithers NN, Furze RC, Mander PK, Bell MJ, Buskens CJ, D'Haens GR, Wildenberg ME, de Jonge WJ. A BET Protein Inhibitor Targeting Mononuclear Myeloid Cells Affects Specific Inflammatory Mediators and Pathways in Crohn's Disease. Cells. 2022 Sep 12;11(18):2846. doi: 10.3390/cells11182846. PMID: 36139421; PMCID: PMC9497176.

**Elfiky AMI***, Ghiboub M, Li Yim AYF, Hageman IL, Verhoeff J, de Krijger M, van Hamersveld PHP, Welting O, Admiraal I, Rahman S, Garcia-Vallejo JJ, Wildenberg ME, Tomlinson L, Gregory R, Rioja I, Prinjha RK, Furze RC, Lewis HD, Mander PK, Heinsbroek SEM, Bell MJ, de Jonge WJ. Carboxylesterase-1 Assisted Targeting of HDAC Inhibitors to Mononuclear Myeloid Cells in Inflammatory Bowel Disease. J Crohns Colitis. 2022 May 10;16(4):668-681. doi: 10.1093/ecco-jcc/jjab176. PMID: 34633041; PMCID: PMC9089418.

Ghiboub M*, **Elfiky AMI***, de Winther MPJ, Harker NR, Tough DF, de Jonge WJ. Selective Targeting of Epigenetic Readers and Histone Deacetylases in Autoimmune and Inflammatory Diseases: Recent Advances and Future Perspectives. J Pers Med. 2021 Apr 23;11(5):336. doi: 10.3390/jpm11050336. PMID: 33922725; PMCID: PMC8145108.

**Elfiky A***, Bonifacius A, Pezoldt J, Pasztoi M, Chaoprasid P, Sadana P, El-Sherbeeny N, Hagras M, Scrima A, Dersch P, Huehn J. *Yersinia Pseudotuberculosis* Modulates Regulatory T Cell Stability via Injection of Yersinia Outer Proteins in a Type III Secretion System-Dependent Manner. Eur J Microbiol Immunol (Bp). 2018 Nov 28;8(4):101-106. doi: 10.1556/1886.2018.00015. PMID: 30719325; PMCID: PMC6348704.

## Manuscripts under submission

**Elfiky AMI***, Lopez J, Ghiboub M, Li Yim AYF, Verhoeven AJ, de Jonge WJ. Carboxylesterase 1 mediates a distinctive metabolic profile of dendritic cells to attain an inflammatory phenotype.

Li Yim AYF*, Hageman IL*, Joustra V*, **Elfiky AMI**, Ghiboub M, Levin E, Verhoeff J, Oostveen-Verseijden C, Admiraal I, Mannens MMAM, Jakobs ME, Kenter SB, Adams AT, Satsangi J, D'Haens GR, de Jonge WJ, Henneman P. A single cell case-control study of peripheral blood mononuclear cells from vedolizumab responding and non-responding Crohn's disease patients during treatment.

Achten R*, Thijs J, van der Wal M, van Luijk C, Bakker D, Knol E, van Luin M, El Amrani M, Delemarre E, **Elfiky AMI**, de Boer J, van Wijk F, de Graaf M, de Bruin-Weller M. Ocular surface disease in moderate-to-severe atopic dermatitis patients and the effect of biological therapy.

# Contributing authors and affiliation

**Wouter J. de Jonge**
Tytgat Institute for Liver and Intestinal Research, Amsterdam Gastroenterology Endocrinology Metabolism Research Institute, Amsterdam University Medical Centers, University of Amsterdam, Amsterdam, The Netherlands.

Department of Surgery, University of Bonn, Bonn, Germany.

**Menno P. J. de Winther**
Department of Medical Biochemistry, Amsterdam University Medical Centers, University of Amsterdam, Amsterdam, The Netherlands.

Department of Medicine, Institute for Cardiovascular Prevention (IPEK), Munich, Germany.

**David F. Tough**
GSK, Stevenage, United Kingdom.

**Andrew Y.F. Li Yim**
Tytgat Institute for Liver and Intestinal Research, Amsterdam Gastroenterology Endocrinology Metabolism Research Institute, Amsterdam University Medical Centers, University of Amsterdam, Amsterdam, The Netherlands.

GSK, Medicines Research Centre, Stevenage, United Kingdom.

**Mohammed Ghiboub**
Tytgat Institute for Liver and Intestinal Research, Amsterdam Gastroenterology Endocrinology Metabolism Research Institute, Amsterdam University Medical Centers, University of Amsterdam, Amsterdam, The Netherlands.

GSK, Medicines Research Centre, Stevenage, United Kingdom.

**Ishtu L. Hageman**
Tytgat Institute for Liver and Intestinal Research, Amsterdam Gastroenterology Endocrinology Metabolism Research Institute, Amsterdam University Medical Centers, University of Amsterdam, Amsterdam, The Netherlands.

**Ivan Fung**
Tytgat Institute for Liver and Intestinal Research, Amsterdam Gastroenterology Endocrinology Metabolism Research Institute, Amsterdam University Medical Centers, University of Amsterdam, Amsterdam, The Netherlands.

**Marte A J Becker**
Tytgat Institute for Liver and Intestinal Research, Amsterdam Gastroenterology Endocrinology Metabolism Research Institute, Amsterdam University Medical Centers, University of Amsterdam, Amsterdam, The Netherlands.

**Vincent W Joustra**
Department of Gastroenterology and Hepatology, Amsterdam University Medical Centers, Amsterdam Gastroenterology Endocrinology Metabolism (AGEM), University of Amsterdam, Amsterdam, The Netherlands.

**Christianne J Buskens**
Department of Surgery, Amsterdam UMC, University of Amsterdam, 1081 HV Amsterdam, The Netherlands.

**Lieven Mulders**
Department of Gastroenterology and Hepatology, Amsterdam University Medical Centers, Amsterdam Gastroenterology Endocrinology Metabolism (AGEM), University of Amsterdam, Amsterdam, The Netherlands.

**Olaf Welting**
Tytgat Institute for Liver and Intestinal Research, Amsterdam Gastroenterol- ogy Endocrinology Metabolism Research Institute, Amsterdam University Medical Centers, University of Amsterdam, Amsterdam, The Netherlands.

**Anje A. te Velde**
Tytgat Institute for Liver and Intestinal Research, Amsterdam Gastroenterol- ogy Endocrinology Metabolism Research Institute, Amsterdam University Medical Centers, University of Amsterdam, Amsterdam, The Netherlands.

**Matthew Bell**
GSK, Stevenage, United Kingdom.

**Nicholas N Smithers**
GSK, Stevenage, United Kingdom.

**Jan Verhoeff**
Department of Molecular Cell Biology & Immunology, Amsterdam Infection & Immunity Institute and Cancer Center Amsterdam, Amsterdam University Medical Centers, Amsterdam, The Netherlands.

Tytgat Institute for Liver and Intestinal Research, Amsterdam Gastroenterol- ogy Endocrinology Metabolism Research Institute, Amsterdam University Medical Centers, University of Amsterdam, Amsterdam, The Netherlands.

**Manon de Krijger**
Tytgat Institute for Liver and Intestinal Research, Amsterdam Gastroenterol- ogy Endocrinology Metabolism Research Institute, Amsterdam University Medical Centers, University of Amsterdam, Amsterdam, The Netherlands.

**Patricia H P van Hamersveld**
Tytgat Institute for Liver and Intestinal Research, Amsterdam Gastroenterol- ogy Endocrinology Metabolism Research Institute, Amsterdam University Medical Centers, University of Amsterdam, Amsterdam, The Netherlands.

**Iris Admiraal**
Tytgat Institute for Liver and Intestinal Research, Amsterdam Gastroenterol- ogy Endocrinology Metabolism Research Institute, Amsterdam University Medical Centers, University of Amsterdam, Amsterdam, The Netherlands.

**Shafaque Rahman**
Tytgat Institute for Liver and Intestinal Research, Amsterdam Gastroenterol- ogy Endocrinology Metabolism Research Institute, Amsterdam University Medical Centers, University of Amsterdam, Amsterdam, The Netherlands.

**Juan J Garcia-Vallejo**
Department of Molecular Cell Biology & Immunology, Amsterdam Infection & Immunity Institute and Cancer Center Amsterdam, Amsterdam University Medical Centers, Amsterdam, The Netherlands.

**Manon E Wildenberg**
Tytgat Institute for Liver and Intestinal Research, Amsterdam Gastroenterol- ogy Endocrinology Metabolism Research Institute, Amsterdam University Medical Centers, University of Amsterdam, Amsterdam, The Netherlands.

**Laura Tomlinson**
GSK, Stevenage, United Kingdom.

**Richard Gregory**
GSK, Stevenage, United Kingdom.

**Inmaculada Rioja**
GSK, Stevenage, United Kingdom.

**Rab K Prinjha**
GSK, Stevenage, United Kingdom.

**Rebecca C Furze**
GSK, Stevenage, United Kingdom.

**Huw D Lewis**
GSK, Stevenage, United Kingdom.

**Thomas Gobbetti**
GSK, Stevenage, United Kingdom.

**Palwinder K Mander**
GSK, Stevenage, United Kingdom.

**Sigrid E M Heinsbroek**
Tytgat Institute for Liver and Intestinal Research, Amsterdam Gastroenterol- ogy Endocrinology Metabolism Research Institute, Amsterdam University Medical Centers, University of Amsterdam, Amsterdam, The Netherlands.

**Caroline Verseijden**
Tytgat Institute for Liver and Intestinal Research, Amsterdam Gastroenterol- ogy Endocrinology Metabolism Research Institute, Amsterdam University Medical Centers, University of Amsterdam, Amsterdam, The Netherlands.

**Geert R. D'Haens**
Department of Gastroenterology and Hepatology, Amsterdam University Medical Centers, Amsterdam, The Netherlands.

**Jessica Lopez**
Tytgat Institute for Liver and Intestinal Research, Amsterdam Gastroenterology Endocrinology Metabolism Research Institute, Amsterdam University Medical Centers, University of Amsterdam, Amsterdam, The Netherlands.

**Arthur J Verhoeven**
Tytgat Institute for Liver and Intestinal Research, Amsterdam Gastroenterology Endocrinology Metabolism Research Institute, Amsterdam University Medical Centers, University of Amsterdam, Amsterdam, The Netherlands.

# Portfolio

| | |
|---|---|
| **Name PhD student:** | Ahmed Elfiky |
| **PhD period:** | December 2017 – February 2022 |
| **Promotor:** | Prof. dr. Wouter J. de Jonge |
| **Copromotores:** | Dr. Matthew J. Bell, Dr. Sigrid E.M. Heinsbroek |

| PHD TRAINING | YEAR | WORKLOAD (ECTS) |
|---|---|---|
| **General courses** | | |
| Laboratory Safety | 2018 | 0.4 |
| Scientific writing in English for publication | 2020 | 1.5 |
| **Specific courses** | | |
| Laboratory Animal Science, Article 9 | 2018 | 3.9 |
| Advanced qPCR | 2019 | 0.7 |
| Medical Literature: Searching for a Systematic Review | 2019 | 0.1 |
| Bioinformatics | 2019 | 1.1 |
| Clinical Epidemiology: Systematic Reviews | 2019 | 0.7 |
| Entrepreneurship in Health and Life Sciences | 2019 | 1.5 |
| Dutch language course (UvA talen) | 2020 | 1.7 |
| Computing in R | 2021 | 0.4 |
| **Presentations** | | |
| Annual Tytgat Institute progress report | 2018-2022 | 1.0 |
| Annual IBD scientific progress report | 2018-2022 | 1.0 |
| AG&M elevator pitch | 2019-2020 | 0.5 |
| Poster prsesentation, Annual MarketsandMarkets epigenetics Congress | 2019 | 0.5 |
| Abstract published, DDW | 2020 | 0.5 |
| Poster presentation, DDW | 2021 | 0.5 |
| Poster presentation, European Congress of Immunology | 2021 | 0.5 |
| **(Inter)national conferences** | | |
| 4th International Congress on Epigenetics & Chromatin, UK. | 2018 | 0.5 |
| Annual AG&M PhD retreat, NL. | 2019-2021 | 1 |
| 4th Annual MarketsandMarkets epigenetics Congress, UK | 2019 | 0.5 |
| Digestive Disease Week, USA. | 2020 | 1 |
| Digestive Disease Week, USA. | 2021 | 1 |
| European Congress of Immunology, Serbia. | 2021 | 1 |

| | | |
|---|---|---|
| **Other** | | |
| Bi-weekly Journal Club Research group | 2017-2022 | 4 |
| Weekly research meeting MI group | 2017-2022 | 6 |
| Weekly research meeting Tytgat Institute | 2017-2022 | 6 |
| Bi-weekly Epimac consortium meeting | 2018-2021 | 2.5 |
| Annual Epimac consortium meeting | 2018-2021 | 1 |
| Weekly progress GSK meetings | 2019-2020 | 1.8 |
| Bi-weekly IBD meetings | 2017-2022 | 3.5 |
| **TEACHING** | | |
| **Tutoring, Mentoring** | | |
| Supervision Master Course Gastrointestinal and Liver Disease | 2020 | |
| **Supervising** | | |
| Master thesis, Jessica Lopez (Biomedical Sciences) | 2022 | |
| **PUBLICATIONS** | | |
| **Peer reviewed (included in this dissertation)** | | |
| – Selective Targeting of Epigenetic Readers and Histone Deacetylases in Autoimmune and Inflammatory Diseases: Recent Advances and Future Perspectives | 2021 | |
| – Carboxylesterase-1 Assisted Targeting of HDAC Inhibitors to Mononuclear Myeloid Cells in Inflammatory Bowel Disease | 2022 | |
| – A BET Protein Inhibitor Targeting Mononuclear Myeloid Cells Affects Specific Inflammatory Mediators and Pathways in Crohn's Disease | 2022 | |
| **Other publications** | | |
| Yersinia Pseudotuberculosis Modulates Regulatory T Cell Stability via Injection of Yersinia Outer Proteins in a Type III Secretion System-Dependent Manner | 2018 | |

# Acknowledgements

As my PhD journey is coming to an end, I have much gratitude to many people who were an integral part of my exciting journey; mentors, research institutes, funding agencies, colleagues, family and friends.

First, I'd like to thank the doctoral committee; Femke van Wijk, Menno de Winther, Pernette Verschure, Jeroen Guikema and Ronald Oude Elferink for reviewing the thesis and being a part of my graduation process.

## My academic and industrial mentors

I'd love to express my sincere gratitude to my promotor and co-promotors; Wouter de Jonge, Matthew Bell and Sigrid Heinsbroek for their continuous guide and support they provided all over the journey.

Wouter, I am very grateful that you gave me such opportunity to join your team and the whole EPIMAC collaboration. You have always been very supportive, flexible and caring. I enjoyed working together with you a lot. I highly appreciate the freedom you gave me to develop my projects and the guidance and significant input you have always provided. I have always admired your dedication and enthusiasm that you reflect on others. I have also enjoyed all the fun activities we had as a group that you have kindly accommodated.

Matthew, you have been tremendously supportive and caring, I am very happy that I landed in GSK under your supervision. You have made my stay in GSK and UK a great experience. I was touched by your sincere care and willingness to always provide help and support at all levels both at GSK and outside work matters. I have enjoyed our small team meetings and fun time we had.

Sigrid, it was a pleasure to have you in my supervision team. Thanks for all your guidance and support you have provided. I have always enjoyed our scientific discussions in Monday morning meetings and your guidance.

## Tytgat family

To the wonderful big Tytgat family that extends beyond the expanding group of Wouter to all other groups at S1 and S2, I am very thankful for the wonderful time and the dynamic and integrated nature of the building that permitted as much interactions between all scientists and researchers. The great times were not only limited to science but extended beyond work to the fun activities we

have organized all together. Collectively, this made my PhD journey pleasant. I'd like to thank all my colleagues; Andrew Li Yim, Florien Westendorp, Mohamed Ghiboub, Bart Meijer, Leonie Vries, Rose Willemze, Mona Edvardsen, Tanit Lizama Gabriel, Marte Becker, Daan Brinkman, Evelina Ferrantelli, Ivan Fung, Ishtu Hageman, Patricia van Hamersveld, Claire van Helsdingen, Anne ten Hove, Irini Kreulen, Manon de Krijger, Francisca Leeuwen-Hilbers, Paula Metselaar, Emmeline Peters, Jessica Lopez, Shafaque Rahman, Leonie Voerman, Job Saris, Isabelle van Thiel, Jan Verhoeff, Marileen Prins, Caroline Verseyden, Olaf Welting, Naomi Wieser, Konstantina Zafeiropoulou, Jing Zhao, Theodorus Hakvoort, Sigrid Heinsbroek, Jung-Chin Chang, Jurgen Seppen, Bruno Sovran, Lysbeth ten Bloemendaal, Ingrid Gaemers, Sofia Frigerio, Fadi Almehar, Valentina Gomez, Francesca Giugliano, Ikrame Aknouch, Gemma Pitotti, Iris Admiraal, Stan van de Graaf, Coen Paulusma, Ronald Oude Elferink, Simei Go, Jonathan van der Meer, Wouter Smit, Sigrid Heinsbroek, Pim Koelink, Ruben de Boer, Femke Mol, Roni Kunst, Isabelle Bolt, Olga Karpus, Dalia Lartey, Jianbo Zhang, Monique Appelman, Joanne Donkers, Reinout Roscam Abbing, Hsuan-Wei Chen, Yannick van Schajik, Remco Kersten, David Trampert, Jacqueline Vermeulen, Verburgt Charlotte, Anje te Velde, Rudi Waart, Esther Vogels, René van den Wijngaard, Manon Wildenberg, and Wouter de Jonge.

To our skilled and lovely technicians, Patricia, Olaf, Iris and Caroline, thanks all for your tremendous support you have provided to my projects and everyone else.

To my dear old and new PhD mates in Wouter group, Anne, Dan, Isabelle, Manon, Rose, Mo, Ishtu, Shafaque, Irini, Gemma, Charlotte, Claire, Yannick, Florine, Naomi, Konstantina, Ivan and Paula, thank you all for the wonderful time in and outside the labs.

To my student Jessica, I am very glad to work with you and thankful for your valuable input and contribution to my work. You were a very dedicated, reliable and enthusiastic person. I wish you always the best in your career.

My Dearest Shafaque, Ishtu, Francy, Gemma, Mo and Ruben, Thanks for all wonderful fun time we had together, for our trips within and outside NL, our dinners, lovely conversations and outings.

**GSK Family**

I am very thankful for the opportunity to join GSK for part of my PhD and being part of the immunology research unit. I'd like to thank the whole immunology research unit members for their tremendous support. I'd love to especially thank Rebecca, Huw and Pal for supporting my research projects and for fruitful and valuable discussions

we had, Inma for providing me opportunity to get involved in other research projects, Claire, Thomas, Laura and Richard for supporting some of my experiments.

## EPIMAC team

I'd love to extend my gratitude to all scientists and students involved in the EPIMAC consortium. I'd like to Thanks Wouter de Jonge, Menno de Winther, Peter Henneman, Anje te Velde, Mathew Bell, Palwinder Mander, Nicola (Nicky) Harker, Rab Prinjha and David F Tough. I would also thank my wonderful PhD mates Charo, Mo, Oliver and Andrew for the lovely time we had together in UK and the Netherlands. It was a pleasure to work with you all. I really enjoyed our discussions, brainstorming, occasional outings and coffee times.

## My Paranymphs

To my dearest Paranymphs; Shafaque, my PhD mate, occasional neighbor, travel buddy and dear friend, it was such a great pleasure to have you through this long journey, you have been always caring, passionate and a great friend. Mohamed, my dear Algerian friend, office mate, and Arabic speaking buddy, I have enjoyed your companionship, conversations and arguments. It's a great pleasure to have both of you by my side on ceremony day.

## My Family and Friends

To my beloved little family, my mom, sister and brother, I am overwhelmingly thankful for all love and support you have always provided. Without you, this wouldn't have been achieved. To my dad, I wish if you have lived to see this moment, however your soul shall be happy and proud now. To my Egyptian friends in Egypt, The Netherlands, and Europe, all Ahmeds, all Mohameds, Kareem and others, I am very happy with your existence in my life through different parts of my life journey, you have always been an immense source of joy, fun and warmth.

## About the author

Ahmed Elfiky was born in Egypt on 21st February 1991. He grew up in Ismailia city where he also completed his medical studies. He graduated from Faculty of Medicine, Suez Canal University in March 2015. Afterwards, he worked in primary health care unit as general practitioner for 6 month, then he did his first move to academia. He joined clinical pharmacology department as a teaching assistant staff at Faculty of Medicine, Suez Canal University. One year latter, he won a competitive scholarship from a non-profit organization based in Belgium called IMSAL to support doing a research internship in Braunschweig, Germany at Helmholtz Center for Infection Research. He joined department of experimental immunology, working under supervision of Prof. Jochen Hühn. His internship at Hühn's lab sparked his interest in immunology and immune regulation. Training in T regulatory cells focused lab, Ahmed studied the effects of yersinia pseudotuberculosis derived proteins on T regulatory cells phenotype and functions. His work was culminated with a publication in a peer reviewed journal. On December 2017, Ahmed moved to Amsterdam to start his PhD studies in Tytgat Institute for Liver and Intestinal Research at University of Amsterdam, under supervision of Prof. Wouter de Jonge. He joined an European Union funded Marie Skłodowska-Curie Industry-Academia consortium called EPIMAC, as a PhD student . He continued his studies in the immune regulation domain, focusing on inflammatory bowel disease (IBD). He investigated the therapeutic immuno-modulatory potentials of novel targeted epigenetic medicines in IBD, using multiple preclinical models of disease. He performed part of his PhD research studies in immunology research unit at GalxoSmithKline (GSK) labs in Stevenage, UK, under supervision of Dr. Matthew Bell. On July 2022, Ahmed joined Prof. Femke van Wijk's group as postdoctoral scientist at Center of Translational Immunology, Utrecht University Medical Center. He closely works with dermatology department and Regenerative Medicine Center Utrecht to investigate novel biologic therapies in atopic dermatitis, focusing on mechanisms and predictor of response and adverse effects.